



**ONR Biannual OSPRES Review and Technical Exchange  
Grant No. N00014-17-1-3016**



**Distribution Statement A. Approved for  
public release: distribution unlimited**

**May 15, 2021**

**PI:**  
Anthony Caruso  
Missouri Institute for Defense and Energy  
University of Missouri-Kansas City  
816-235-2505  
carusoan@umkc.edu

REPORT DOCUMENTATION PAGE				Form Approved OMB No. 0704-0188	
<p>The public reporting burden for this collection of information is estimated to average 1 hour per response, including the time for reviewing instructions, searching existing data sources, gathering and maintaining the data needed, and completing and reviewing the collection of information. Send comments regarding this burden estimate or any other aspect of this collection of information, including suggestions for reducing the burden, to Department of Defense, Washington Headquarters Services, Directorate for Information Operations and Reports (0704-0188), 1215 Jefferson Davis Highway, Suite 1204, Arlington, VA 22202-4302. Respondents should be aware that notwithstanding any other provision of law, no person shall be subject to any penalty for failing to comply with a collection of information if it does not display a currently valid OMB control number.</p> <p><b>PLEASE DO NOT RETURN YOUR FORM TO THE ABOVE ADDRESS.</b></p>					
1. REPORT DATE (DD-MM-YYYY) 15-05-2021		2. REPORT TYPE Technical Summary		3. DATES COVERED (From - To) Dec 2020 – May 2021	
4. TITLE AND SUBTITLE  ONR Biannual OSPRES Review and Technical Exchange Spring 2021			5a. CONTRACT NUMBER		
			5b. GRANT NUMBER N00014-17-1-3016		
			5c. PROGRAM ELEMENT NUMBER		
			5d. PROJECT NUMBER		
			5e. TASK NUMBER		
			5f. WORK UNIT NUMBER		
6. AUTHOR(S) Roy Allen, Wasekul Azad, Bidisha Barman, Jordan Berg, John Bhamidipati, Benjamin Bissen, Sadie Brasel, Deb Chatterjee, Plamen Doynov, Kalyan Durbhakula, Jay Eifler, Travis Fields, Nick Flippin, Ron Focia, Spencer Fry, Nicholas Gardner, Mohamed Hamdalla, Ahmed Hassan, Sai Indharapu, Faisal Khan, Paul Klappa, James Kovarik, Dario Labrada, Eliot Myers, Thomas Ory, Michelle Paquette, Sourov Roy, Scott Shepard, Cody Smith, Sarvenaz Sobhansarbandi, Heather Thompson, Anthony Caruso				8. PERFORMING ORGANIZATION REPORT NUMBER  OSPRES_Grant_Biannual_Review_MAY2021	
7. PERFORMING ORGANIZATION NAME(S) AND ADDRESS(ES)  University of Missouri – Kansas City 5100 Rockhill Rd. Kansas City, MO 64110				10. SPONSOR/MONITOR'S ACRONYM(S)  ONR	
9. SPONSORING/MONITORING AGENCY NAME(S) AND ADDRESS(ES)  Office of Naval Research One Liberty Drive, 875 N. Randolph Arlington, VA 22203				11. SPONSOR/MONITOR'S REPORT NUMBER(S)	
12. DISTRIBUTION/AVAILABILITY STATEMENT  Distribution Statement A. Approved for public release: distribution unlimited					
13. SUPPLEMENTARY NOTES					
14. ABSTRACT  The ONR Short Pulse Research, Evaluation and non-SWaP Demonstration for C-sUAS Study (OSPRES) (Grant Award No. N00014-17-1-3016) biannual review was held on 06MAY2021 via web conferencing. A total of 19 posters were briefed to ~80 attendees at the Distribution A level. The program objective is to execute high-risk, high-payoff efforts that mitigate, fill, or rectify one or more grand-challenge or elementary gaps or deficiencies needed to achieve a modular, scalable, and electronically steerable high power microwave (HPM) based defense system for the counter unmanned aerial system (cUAS) mission. The OSPRES HPM system and sub-system development/evaluation efforts are focused on the short-pulse high-average power space, and includes the kill chain considerations including the target and its responsivity to radiofrequency stimuli. Poster presentations covered all of the program's ongoing subprojects spanning prime power, laser alternatives, pulsed power switches, photo switches, pulse forming networks, thermal management, antenna design, RF coupling, as well as modeling and simulation for HPM engagement.					
15. SUBJECT TERMS  Pulsed Power Switches, High Power Microwaves, Pulse Forming Networks, Antennas, Arrays, RF Coupling, High Voltage					
16. SECURITY CLASSIFICATION OF:			17. LIMITATION OF ABSTRACT UU	18. NUMBER OF PAGES 67	19a. NAME OF RESPONSIBLE PERSON Anthony Caruso
a. REPORT U	b. ABSTRACT U	c. THIS PAGE U			19b. TELEPHONE NUMBER (Include area code) 816-235-2505

# 1. Table of Contents

<b>1.</b>	<b>Table of Contents</b> .....	<b>ii</b>
<b>2.</b>	<b>Administrative</b> .....	<b>iii</b>
2.1.	<i>Program Overview</i> .....	<i>iv</i>
2.2.	<i>Executive Summary</i> .....	<i>v</i>
2.3.	<i>Acknowledgment</i> .....	<i>viii</i>
2.4.	<i>Agenda</i> .....	<i>ix</i>
2.5.	<i>Attendees</i> .....	<i>x</i>
2.6.	<i>Acronyms</i> .....	<i>xi</i>
<b>3.</b>	<b>Abstracts and Q&amp;A</b> .....	<b>1</b>
3.1	<i>Development of a Modular High-Voltage Solid-State Switch with Integrated In-House Gate Driver</i> .....	<i>2</i>
3.2	<i>Advances in Optical Fiber Amplifiers</i> .....	<i>4</i>
3.3	<i>Compact Inexpensive Alternatives for Optical Source Drivers</i> .....	<i>5</i>
3.4	<i>Investigation of a Semiconductor Opening Switch-Inductive Energy Storage Topology</i> .....	<i>7</i>
3.5	<i>Semiconductor Opening Switch-Inductive Energy Storage Topology: Parametric Simulation Study</i> .....	<i>9</i>
3.6	<i>TCAD Optimization of Drift-Step Recovery Diode (DSRD) Peak Power and Risetime</i> .....	<i>10</i>
3.7	<i>Direct RF Modulation Using GaN Photoconductive Semiconductor Switches</i> .....	<i>12</i>
3.8	<i>Electrically Tunable Diode based Nonlinear Transmission lines Capable of GHz Frequency Generation</i> .....	<i>14</i>
3.9	<i>Geometric and Impedance Shifting Transmission line Transformers</i> .....	<i>16</i>
3.10	<i>A Novel Method of Cooling a Semiconductor Device through a Jet Impingement Thermal Management System: CFD Modeling and Experimental Evaluation</i> .....	<i>17</i>
3.11	<i>Heat Transfer Enhancement of a Jet Impingement Thermal Management System: A Comparison of Various Nanofluid Mixtures</i> .....	<i>19</i>
3.12	<i>Tradespace Analysis of a Phased Array of Electrically Small Antennas</i> .....	<i>20</i>
3.13	<i>Koshelev Single Element and Array Antenna Study with Comparison to Balanced Antipodal Vivaldi Antenna</i> .....	<i>22</i>
3.14	<i>Ultra-Wide-Band High-Aperture-Efficiency Shark Antenna Tradespace Study</i> .....	<i>24</i>
3.15	<i>Machine Learning for Antenna Optimization</i> .....	<i>26</i>
3.16	<i>Modeling and Verification of High-Power Electromagnetic Coupling to Nonlinear Electronic Systems using the Equivalent Circuit Approach</i> .....	<i>28</i>
3.17	<i>Predicting Electromagnetic Coupling to UAV Models</i> .....	<i>30</i>
3.18	<i>Coordinated Algorithms Framework Using the Traveling Salesman Problem for CUAS Engagements</i> .....	<i>31</i>
3.19	<i>Evaluation of Localization Uncertainty and Its Effect on Vehicle Intercept</i> .....	<i>32</i>
<b>4.</b>	<b>Discussion with Chip Grounds, Tom Hussey, and Other Attendees</b> .....	<b>34</b>
<b>5.</b>	<b>Appendix: Posters</b> .....	<b>A</b>

## 2. Administrative

## 2.1. Program Overview

### **ONR Short Pulse Research, Evaluation and non-SWaP Demonstration for C-sUAS Study**

**OSPRES Grant Goal:** address and transition technologies and capabilities that enable the OSPRES Grant Objective using the OSPRES Grant Approach, while educating the next generation of pulsed power and defense minded, stewards, and innovators.

**OSPRES Grant Objective:** to execute high-risk, high-payoff efforts that mitigate, fill, or rectify one or more grand-challenge or elementary gaps or deficiencies needed to achieve a modular, scalable, and electronically steerable high power microwave (HPM) based defense system for the counter unmanned aerial system (cUAS) mission. The OSPRES HPM system and sub-system development/evaluation efforts are focused on the short-pulse high-average power space, and includes the kill chain considerations including the target and its responsivity to radiofrequency stimuli.

**OSPRES Metrics of Success:** developed technologies and capabilities that are published in the peer review, protected as intellectual property, and/or transitioned to the OSPRES Contract effort and beyond for integration with other DoD needs or dual-commercial-use, as enabling/integratable capability(ies).

**OSPRES Grant Approach:** A fail-fast philosophy is maintained, where if a technology or capability is deemed infeasible to be demonstrated or validated during the project period-of-performance, it shall be culled, results to date and basis of infeasibility documented, and the next major gap/deficiency area addressed by that part of the project sub-team. Students whose thesis depends on following through with a full answer during the life of the award will be given special dispensation to continue their work.

**OSPRES Grant Security:** All efforts should be fundamental and publically releasable in nature when taken individually. This report has been reviewed for operational security, compilation, proprietary and pre-decisional information concerns.

## 2.2. Executive Summary

The ONR Short Pulse Research, Evaluation and non-SWaP Demonstration for C-sUAS Study (OSPRES) (Grant Award No. N00014-17-1-3016) biannual review was held on 06MAY2021 via web conferencing. A total of 19 posters were briefed to ~80 attendees at the Distribution A level. Abstract-based summaries from each poster author as well as questions and answers are provided in Section 3, opinions/questions from consultants Tom Hussey and Chip Grounds with associated discussion are provided in Section 4, and copies of each poster are provided in the Appendix.

From the PI's perspective, the following impact and path forward for each project include:

### *Prime Power (Prof. Khan and Mr. Azad)*

The Behlke HV Switch replacement design/build/demo is sufficiently mature that it should be transitioned to a commercial partner before the primary research assistant (Wazeskul Azad) graduates in summer 2021.

### *1064-nm Laser Alternative (Prof. Shepard and Ms. Thompson)*

The new fiber laser core cross sectional shapes proposed and validated analytically in Prof. Shepard's group promise ground breaking impact on volumetric power density and thermal transfer efficiency. Empirical validation via simulation and measurements is outstanding and key to keeping this effort moving forward.

### *Multi-Stage Optical Amplifier (Mr. Bhamidipati)*

Our survey indicates that there is a hole in the marketplace for both high current (120-A) and very fast rise time (<200-ps) optical drivers, separate from the OSPRES PCSS need; it is unclear whether monetary cost, volume, or both preclude commercial vendors from entering this space. With the near term measurement-based validation and the ability to meet the OSPRES PCSS metrics assessed (compared with available pico-second class, high average power lasers), we will be able to make a go/no-go decision on the continuation of this work by the Fall 2021 review.

### *Semiconductor Opening Switch Based Pulsed Power Source – Parametric Studies (Mr. Labrada, Dr. Roy)*

The drift step recovery diode (DSRD) based pulsed power team has already shown 12-kV output in <200-ps from a mechanically (not electrically) optimized configuration. The team was asked to take a step back and systematically find topological configurations and values for the components thereof, that would seek a maximum in gain and efficiency, for that parameter space. Initial results demonstrate a better understanding of the losses, and this group is encouraged to continue along this same path, with empirical validation builds along the way to ensure match to simulation.

### *Drift Step Recovery Diode (Semiconductor Opening Switch) Die Optimization (Dr. Eifler, Dr. Focia)*

The optimal dopant type and concentration as a function of depth of a stacked sub-die, as well as number of sub-die in a stack that comprises a full die, has remained elusive, mainly because of the disparity between simulation and measured values. The Eifler-Focia team are closing the simulation gaps and are beginning to find optimum points in the tradespace and parameter variation directions that yield diminishing returns. This work is progressing well and should be able to wrap up by Fall 2021.

#### *Direct RF Modulation via GaN PCSS (Ms. Thompson)*

Without a parallel market to inexpensively manufacture compensated gallium nitride, which is different from the high electron mobility based GaN used to make next generation transistors, it is not clear this work will find a home, despite its promise in comparison to Si- and SiC-based systems (much like the GaAs work for the BOSS and Sandia based switches). For now, this work will be put on pause as Ms. Thompson transitions to work full time on the fiber laser project with Prof. Shepard.

#### *Diode-Based Non-Linear Transmission Line (Mr. Gardner)*

Center frequency operation in excess of 1-GHz and peak power operation in excess of 1-MW have now been achieved. 100-MHz worth of center frequency control is shown through an external bias of -3V to +4V; the bias in the negative direction did not reach saturation. This work is moving forward well; conversion efficiency of these non-linear processes are still a fundamental limitation, but the size and weight reduction compared to other NLTL's and pulse forming networks make the D-NLTL work attractive and it will be continued. Mr. Gardner will graduate with the PhD in the Summer/Fall 2021 and we need to ensure this work carries on.

#### *Geometric Unity-Impedance Transformer (Mr. Kovarik)*

The impedance out of the PCSS line is intrinsically low (less than 10- $\Omega$ ) and requires transformation to the radiating structure, whose impedance starts at no less than 50- $\Omega$ . Mr. Kovarik has simulated, fabricated, and demonstrated a transforming line that meets the OSPRES contract needs, and is a solid Masters Thesis. This work will be transitioned and placed in the complete category for the OSPRES grant.

#### *Jet Impingement Thermal Management (Prof. Sobhansarbandi, Mr. Berg)*

The high average power of the PCSS system requires low ones-of-kW thermal transfer per cm<sup>2</sup>, a major feat for any state-of-the-art heat transfer technology/methodology. Jet impingement was rigorously studied and found to not meet the system requirements; the results have been captured by report and in the MS Thesis of Mr. Berg; this sub-effort will be sunset. In its wake is the study of nanofluids whose promise for heat transfer may be the breakthrough that all modes of flow would benefit from and apply well outside of the OSPRES program; however, at least an order of magnitude or more needs to be shown relative to the un-doped silicone fluid for this improvement to satisfy the heat transfer requirements.

#### *Patch-Based Electrically Small Antenna (ESA) Arrays Trade Study (Prof. Chatterjee, Ms. Barman)*

Combining microwave energy in the far field from an electronically steerable antenna array in the ultra-high-frequency band requires an aperture size that is deemed 'reasonable' by the end user. In most cases, this means reducing the size of a classic UHF aperture to at least 60% of its uncompressed area/state. In this work, the patch antenna tradespace is evaluated as a function of the antenna performance metrics and found to, indeed, provide competitive values for both volume and area when compared with the classic UHF array systems, for both simulated and measured values. However, before this approach can be considered for transition to the OSPRES Contract or Demonstration System, high power (high voltage) continued operation must be shown.

#### *Alternatives to Vivaldi-Based Antenna Elements (Prof. Durbhakula, Ms. Brasel, Mr. Indharapu)*

Aperture efficiency, gain, rE/V and other radiator performance metrics of interest have been studied and improved on, using well known starting points for the Koshlev, Shark, and Fractal-based ultra-wide-band (UWB) radiators. Results so far demonstrate that the state-of-the-art Vivaldi's can trade competitively with the alternative (Durbhakula design) Koshlev (when accounting for and comparing apples-to-apples). This work, and all the other antenna designs are

now to a point where a major decision has to be made for the OSPRES Contract Demo, and which of the present efforts should continue to be developed for the good of the UWB community who have different requirements than the array driven metrics set in the OSPRES program; the decision of which radiators to continue with will also account for student/workforce development.

*RF Coupling Effort (Prof. Hassan, Mr. Mohammed Hamdalla)*

The RF Coupling effort has made a major step forward by generating equivalent circuit models for generic UAV wire/PCB layouts to determine the extent to which accurate eigencurrents can be predicted; the circuits include both linear and non-linear elements. This work continues to progress well and is expected to be integrated with higher level models for an overall effects prediction capability at the OSPRES Contract and greater level.

*Modelling and Simulation Foundational Studies for HPM Engagement (Prof. Fields, Mr. Klappa, Mr. Smith)*

In a swarm or multi-threat scenario, determining the most efficient means of addressing (e.g., applying microwave energy to) each threat (i.e., the order of effecting), defines/drives the performance requirements of the effector and method of delivery (i.e., a large part of the C2 decision basis). In this work, the framework specific to the missionspace of interest is being built/adapted/tested for classical models which address the threat-strike-order, and, the sensors that are used to help make the feedback decision. This work is at its early stage and progressing well. A clean engagement level model that feeds into a campaign level model, without the cumbersome nature/features of AFSIM is where this work is headed.

### **2.3. Acknowledgment**

The investigators wish to thank Michelle Paquette, Humberto Gonzalez, and Joseph Crow for coordination of the review. Other thanks go out to the shop staff for fabrication, design, and troubleshooting support of the research as well as to our administrative support team, Leta Moler and Mallory Snyder, who work tirelessly to handle purchasing, tracking, scheduling, and an endless list of items that keep the program moving forward.

## 2.4. Agenda

Spring 2021 UMKC OSPRES Grant Review and Technical Exchange 06 MAY 2021 / Virtual / Distribution A			
Time (CST)	Presentation Title	Presenter	Topical Focus
8:50 AM	Overview	Caruso	
9:00 AM	Development of a Modular High-Voltage Solid-State Switch with Integrated In-House Gate Drive	Azad/Khan	Prime Power
9:15 AM	Advances in Optical Fiber Amplifiers	Shepard	Laser Alternatives
9:30 AM	Compact Inexpensive Alternatives for Optical Source Drivers	Bhamidipati	Laser Alternatives
9:45 AM	Investigation of Semiconductor Opening Switch-Inductive Energy Storage Topology	Labrada	Pulsed Power Switch
10:00 AM	Semiconductor Opening Switch-Inductive Energy Storage Topology: Parametric Simulation Study	Roy	Pulsed Power Switch
10:15 AM	-- Break --		
10:30 AM	TCAD Optimization of Drift-Step Recovery Diode (DSRD) Peak Power and Risetime	Eifler	Pulsed Power Switch
10:45 AM	Direct RF Modulation Using GaN Photoconductive Semiconductor Switches	Thompson	Photo Switch
11:00 AM	Electrically Tunable Diode-Based Nonlinear Transmission Lines Capable of GHz Frequency Generator	Gardner	Pulse Forming Networks
11:15 AM	Geometric and Impedance Shifting Transmission Line Transformers	Kovarik	Pulse Forming Networks
11:30 AM	A Novel Method of Cooling a Semiconductor Device through a Jet Impingement Thermal Management System: CFD Modeling and Experimental Evaluation	Berg	Thermal Management
11:45 AM	-- Break --		
12:00 PM	Heat Transfer Enhancement of a Jet Impingement Thermal Management System: A Comparison of Various Nanofluid Mixture:	Sobhansarbandi	Thermal Management
12:15 PM	Tradespace Analysis of a Phased Array of Electrically Small Antennas (ESAs)	Barman	Antenna
12:30 PM	Koshelev Single Element and Array Antenna Study with Comparison to Balanced Antipodal Vivaldi Antenn:	Durbhakula	Antenna
12:45 PM	Ultra-Wide-Band High-Aperture-Efficiency Shark Antenna Tradespace Study	Brasel	Antenna
1:00 PM	Machine Learning for Antenna Optimization	Indharapu	Antenna
1:15 PM	-- Break --		
1:30 PM	Modeling and Verification of High-Power Electromagnetic Coupling to Nonlinear Electronic Systems using the Equivalent Circuit Approach	Hassan	RF Coupling
1:45 PM	Predicting Electromagnetic Coupling to UAV Models	Hamdalla	RF Coupling
2:00 PM	Coordinated Algorithms Using the Traveling Salesman Problem for cUAS Engagements:	Smith	Modeling & Simulation
2:15 PM	Evaluation of Localization Uncertainty and Its Effect on Vehicle Intercept	Klappa	Modeling & Simulation
2:30 PM	Closing Session	Caruso/Hussey/Grounds	
3:00 PM	-- End --		

## 2.5. Attendees

<b>Name</b>	<b>Organization</b>	<b>Name (UMKC)</b>
Abdalla, Mike	ASR Corporation	Allen, Roy
Anderson, Travis	Naval Research Laboratory	Azad, Wasekul
Bailey, Zachary Ryan	University of Texas at Arlington	Barman, Bidisha
Beetner, Daryl	Missouri S&T	Battiston, Matthew
Bellinger, Steve	Radiation Detection Technologies	Berg, Jordan
Conway, Adam	Raytheon	Bhamidipati, John
Drikas, Zachary	Naval Research Laboratory	Brasel, Sadie
Eachan, Landreth	Raytheon	Caruso, Anthony
Giorgi, David	General Atomics	Chatterjee, Deb
Grounds, Chip	Consultant	Cottrell, Angela
Hara, Ken	Stanford	Crow, Joseph
Hartman, Seth	KCNSC, Honeywell	Currie, James
Hemmady, Sameer	Verus Research	Dale, Allen
Hobart, Karl	Naval Research Laboratory	Durbhakula, Kalyan
Hoff, Brad	Air Force Research Laboratory	Eifler, Jay
Hoffman, Ryan	ONR	Fields, Travis
Hunter, James	Missouri S&T	Flippin, Nicholas
Hussey, Tom	Consultant	Fry, Spencer
Johnston, Alexander Nathaniel	University of Texas at Arlington	Gardner, Nicholas
Kapadia, Rehan	University of Southern California	Gonzalez, Humberto
Khilkevich, Victor	Missouri S&T	Gunter, Connor (MU)
Kling, Matthew	Northeastern	Hamdalla, Mohamed
Koehler, Andrew	Naval Research Laboratory	Hassan, Ahmed
Koslover, Robert	SARA	Herrington, Shawn
Kunapareddy, N (Pratima)	Naval Research Laboratory	Hyde, Megan
Lamb, Barrett	SARA	Indharapu, Sai
Mankowski, John	Texas Tech University	Khan, Faisal
McGeehan, John	BAE Systems	Klappa, Paul
McMorrow, Julian		Kovarik, James
Mostrom, Mike		Labrada, Dario
Nunally, William	Applied Physics Electronics, LC	Mardikes, Michael
Peterkin, Robert	General Atomics	Myers, Eliot
Portillo, Salvador	University of New Mexico	Paquette, Michelle
Rolwes, Joseph	Leonardo DRS	Roy, Sourov
Sengupta, Somnath	Powerhouse Consulting Group	Shepard, Scott
Shelton, Jason	Sandia National Labs	Smith, Cody
Skipper, Mike	ASR Corporation	Thompson, Heather
Sullivan, Don	Raytheon	Verzella, James
Tatum, John	DSIAC/Survice	
Taylor, Alistair	Defense Science and Tech Lab	
Tschritter, Cole	University of Texas at Arlington	
Wagner, Adam	KCNSC, Honeywell	
Wetz, David	University of Texas at Arlington	
White, Will	Verus Research	

## 2.6. Acronyms

ASE: Amplified Spontaneous Emission  
BAVA: Balanced Antipodal Vivaldi Antenna  
COTS: Commercial Off The Shelf  
D-NLTL: Diode based Non-Linear Transmission Line  
DSRD: Drift Step Recovery Diode  
DUT: Device Under Test  
ECA: Equivalent Circuit Approach  
EM: Electromagnetic  
ESA: Electrically Small Antenna  
GTEM: Gigahertz Transverse Electro-Magnetic\  
HPM: High Power Microwave  
HV: High Voltage  
JI-TMS: Jet Impingement Thermal Management System  
LED: Light Emitting Diode  
LV: Low Voltage  
ML: Machine Learning  
ONR: Office of Naval Research  
PCSS: Photo-Conductive Solid State Switch  
PFN: Pulse Forming Network  
RBF: Radial Basis Function  
RF: Radio Frequency  
SHG/THG: Second/Third Harmonic Generation  
SOS-IES: Semiconductor Opening Switch – Inductive Energy Storage  
SoTA: State of the Art  
SWaP-C: Size, Weight, Power, and Cost  
TCAD: Technology Computer Aided Design  
UAS/V: Unmanned Aerial System/Vehicle  
UHF: Ultra High Frequency  
UWB: Ultra Wide Band  
WBG: Wide Band Gap  
WTA: Weapon's Target Assignment

### **3. Abstracts and Q&A**

### 3.1 Development of a Modular High-Voltage Solid-State Switch with Integrated In-House Gate Driver

*Wasekul Azad, Sourov Roy, Spencer Fry, Anthony N. Caruso, and Faisal Khan*

Power loss due to the lack of power conditioning leads to diminishing returns in the efficiency of a linear-mode photoconductive semiconductor switch (PCSS) based pulse forming network (PFN) for generating high-power microwaves (HPMs). A power conditioning scheme based on commercially available high-voltage (HV) solid-state switches (e.g., HV switches made by German manufacturer BEHLKE) can considerably reduce this power loss using a two-state switching mechanism. However, HV switches made by BEHLKE are expensive, have long lead times, require multiple ancillary supplies, and liquid cooling at a switching frequency greater than 10 kHz, therefore increasing the footprint of the overall system. Developing an in-house HV (~10-kV) switch from inexpensive commercial-off-the-shelf (COTS) MOSFETs that can be a direct and inexpensive replacement to the HV switches made by BEHLKE can be a solution to this problem. In addition, introducing modularity to the HV switch design can facilitate voltage withstanding scalability without a complete design overhaul. In this work, we have presented a 10 kV rated HV modular (two modules) switch coupled with a 10 kV rated isolated in-house gate driver. We have successfully tested the HV switch up to a DC supply voltage of 6 kV at a switching frequency up to 15 kHz. A maximum voltage imbalance close to 80 V was recorded among the voltages measured across the drain-source terminals of the series-connected MOSFETs in the HV switch, which is negligible compared to the breakdown voltage rating of 1.7 kV of an individual MOSFET. We will be able to integrate the in-house HV switch, replacing the BEHLKE-made HV switches, in the power conditioning circuit for the PCSS-based PFN once we can test the in-house HV switch at a DC supply voltage up to 10 kV and at a switching frequency close to 100 kHz. We are planning to design a modular HV switch rated for 20 kV using 3.3 kV rated COTS SiC MOSFETs and an in-house isolated gate driver to drive the switch.

#### Discussion, Questions, and Answers

**Eifler, Jay:** *Are the MOSFETs vertical or lateral integrated IC?*

**Azad, Wasekul:** We have used 1.7 kV rated SiC power MOSFETs from CREE in the HV switch design. The structure of these power MOSFETs is vertical.

**Eifler, Jay:** Thanks. Curious since I'm trying to put that model into TCAD with either spice model or TCAD model. Probably with the simple level 1 spice model.

**Azad, Wasekul:** We do use the LTSpice model in simulations that are provided by CREE.

**Grounds, Chip:** *This is 6 kv into a 9.6 kv load for 20 us. That doesn't seem to be much charge. Is that enough to charge the t-line?*

**Eifler, Jay:** I think Chip that the Si-PCSS needs voltage across it only so long due to breakdown.

**Fry, Spencer:** It's way more than needed.

**Azad, Wasekul:** The resistive load was used for characterizing the voltage balancing across the individual MOSFETs. In the case of the transmission line, the load for the HV switch will be a capacitance in the range of nano-farads. The RC time-constant is low enough to allow the switch to completely charge the transmission line within a few micro-seconds.

**Myers, Eliot:** Also, the PFTLs for a single switch is on the order of 100s of pF, which puts us into the nF range when multiples are charged in parallel.

**Grounds, Chip:** *Follow on: What is the expected charging current for the t-lines and has it been demonstrated by using the 9.6 k-ohm load?*

**Answer:** The required charging current will depend on the required charge time and the transmission line capacitance. Simulation shows that for a transmission line with a capacitance of 4 nF, and characteristic impedance of 4.4  $\Omega$ , the average charging current is approximately 500 mA at a DC supply voltage of 6 kV and a repetition rate of 50 kHz. The modular HV switch has been tested using a 9.6 k $\Omega$  resistive load up to a DC supply voltage of 6 kV and a repetition frequency of 15 kHz. The average current flowing through the switch in this operating condition is close to 100 mA. In addition, we have tested the HV switch using a 3.2 k $\Omega$  resistive load at a DC supply voltage of 4.5 kV and a repetition frequency of 20 kHz. The average current flowing through the switch in this operating condition is close to 300 mA.

**Khan, Faisal:** It will depend on line capacitance and rise time.

**Fry, Spencer:** The required current depends on the required charge time and the amount of transmission line capacitance. It can be as low as a few amps for a single 100 pf tl and 1 us charge time and 10 kV. So technically that wasn't met but 0.5 amps was met so a 2 us charge time would happen if that was the limit of the switch (it very much isn't).

## 3.2 Advances in Optical Fiber Amplifiers

*Scott R. Shepard, Heather A. Thompson, and Anthony N. Caruso*

In PCSS-based systems, one of the biggest obstacles is the cost and size of the laser required, with the primary hindrance in cost being the pump-power system. Fiber lasers utilizing ytterbium-doped optical fiber amplifiers can reduce the overall system size, but the state-of-the-art systems remain too expensive. To overcome this prohibitive cost, a pre-burst optical pumping scheme has been devised that could reduce this cost by a factor of 40. Additionally, amplified spontaneous emissions (ASE) noise must be minimized to prevent excessive PCSS heating and timing-jitter. Simulations have shown that this optical pumping scheme is able to achieve a factor of 40 in pump power cost reduction while maintaining an ASE level below our heating limit (of 640  $\mu\text{W}$ ). Moreover, we can further suppress the ASE (by 3 orders of magnitude) by exploiting gain saturation while adapting the mode diameter at each amplifier stage. Proof-of-concept experiments have been initiated and we recently measured the timing-jitter of the seed laser diode to be within  $\pm 15$  ps, with a probability of 0.9 (hence within our target objective). Future work includes the pursuit of photonic crystal fiber structures for higher powers and less optical nonlinearities.

### **Discussion, Questions, and Answers**

N/A

### 3.3 Compact Inexpensive Alternatives for Optical Source Drivers

*J. K. P. Bhamidipati, E. R. Myers, H. A. Thompson, M. M. Paquette, and A. N. Caruso*

Acute optical pulse energy requirements in PCSS-driven HPM-based defense systems have brought forth a need for picosecond lasers with auxiliary power and cooling subsystems. Typically, these are 1064 nm laser systems and are limited to Si-based switch technology and need additional second and third harmonic generation (SHG/THG) optics to accommodate wider bandgap materials like SiC and GaN-PCSS. Though these systems fulfill the switches' optical needs, they return a degraded SWaP-C<sup>2</sup> index due to their weight, volume, and cost factors, a majority of which are contributed by driver and control subsystems. State-of-the-art commercial off-the-shelf drivers are optimized to deliver either high currents or fast transients while maintaining a compact form factor, but not both. The objective of this effort is to design and implement a compact, lightweight, and inexpensive driver alternative for conventional high average power laser systems. Recent updates in the scope of work for PCSS-driven laser driver work have been presented in this report. Only GaN-PCSS was reported in previous reports as a potential candidate for experimental implementation. However, considering the device availability, cost, and long-term supply-chain viability, both non-PCSS and other PCSS switching technologies like silicon avalanche switch (SAS), GaN-FET, silicon opto diodes, and topologies such as frozen wave generators (FWG) are being considered as well. Initial test results for lateral GaN-PCSS grown over a SiC substrate showed linear conduction with a 355 nm optical trigger at 18 kV/cm electric field strength. The test needs to be repeated with a 404 nm trigger to verify the conduction mode in sub bandgap actuation. Pulse testing of Si optodiodes and GaN-PCSS will be done using a neoLase (1064 nm) and seed laser diode (404 nm), respectively, at ~1 μJ/pulse for baseline state-of-the-art data and TCAD parameter study will be completed to enhance their performance. For a non-PCSS approach, SPICE simulations will be done to validate jitter limitations and effectiveness of diode-based nonlinear transmission lines for pulse sharpening, and TCAD simulations will be performed for custom silicon avalanche switches as needed.

#### Discussion, Questions, and Answers

**Grounds, Chip:** *Does the first stage pulse width set the pulse widths for the next two stages?*

**Answer:** The first stage pulse width ideally sets the pulse width for the second stage. However, the pulse width of the second stage also depends on switch properties like conduction mode, recombination rates, and intrinsic/extrinsic carrier lifetime that directly contribute to sustained conduction and result in longer recovery times and thus longer pulse widths.

**Myers, Eliot:** *Of the topologies you're investigating, is there a clear front runner? Topologies/switches.*

**Answer:** PCSS-based technologies are the front runners due to their proven jitter specifications and controlled avalanching operation. However, they also come with drawbacks in terms of device maturity, availability, and cost factors that are driving us to comprehensively evaluate other switch technologies like SAS, GaN-FETs, and optodiodes.

**Grounds, Chip:** *Then if the first stage puts out a modulated pulse the output could be modulated?*

**Answer:** This would be a technical challenge we will be able to answer once we have some more test data sets. Our goal is to induce a controlled avalanche conduction which could completely change the output pulse from the switch that is being triggered. The modulation could be maintained under special circumstances like low repetition rates and borderline avalanche, resulting in low current gain, which can contribute to maintaining the pulse modulation initially fed in the first stage.

### 3.4 Investigation of a Semiconductor Opening Switch-Inductive Energy Storage Topology

*Dario Labrada, Sourov Roy, Michelle M. Paquette, and Anthony N. Caruso*

Circuit analysis of a semiconductor opening switch inductive energy storage (SOS-IES) topology was carried out to inform its design and implementation. State-of-the-art SOS-based sources are capable of generating hundreds-of-megawatts peak power on 50- $\Omega$  loads but suffer low volumetric power densities in the 10s-to-100s of kW/m<sup>3</sup>. The circuit topology analyzed here can lead to the development of a lightweight and high power density (>1.5 GW/m<sup>3</sup>) source. Investigating the impact of circuit parameters and topology permutation on the opening speed and peak interrupted current through the SOS devices found that the opening speed of the SOSs is inversely proportional to unit inductance but proportional to unit capacitance and initial charge; expanding the topology in series may reduce the peak output of the circuit while expanding in parallel may improve the peak output. The relationships and trends predicted in this analysis need to be confirmed via experimental data.

#### Discussion, Questions, and Answers

**Grounds, Chip:** *Does your analysis address jitter?*

**Labrada, Dario:** The analysis of the circuit presented here does not directly address jitter. Output pulse jitter would be dominated by the primary switch (SiC-FET) and its gate drive circuitry.

SOS-based sources will have jitter on the order of their primary switch; SOS's themselves do not have significant jitter (e.g., 1s-to-10s of picoseconds). The MOSFETs used as primary switches in this have greater jitter, but even this will then be defined by the jitter of the gate drive circuitry that directly controls the FET. Literature shows that gate drive circuitry can be designed with a jitter tolerance as low as 50 to 100 ps.

The jitter requirements in OSPRES are of the same order, with 50-ps as the goal and 100-ps as the requirement, meaning SOS-based sources can be arrayed.

**Landreth, Eachan:** *What is your anticipation of impact on system operation by slight (1st order) variation of reverse current? Sorry, I apologize. If the reverse current is not constant over time.*

**Fry, Spencer:** Isn't the reverse current already not constant over time?

**Labrada, Dario:** The peak magnitude of the reverse current at time of opening is what we are referring to. It will inevitably be in a sinusoidal form.

**Hussey, Tom:** *There's been considerable work in the literature on SOS pulsed power systems, much of it Russian, how do your goals differ from what they have claimed?*

**Answer:** The goals of this study are to analyze and make progress towards a circuit topology that can operate at 10s-to-100s of kHz repetition rate, fit a compact and lightweight form factor, and produce peak powers on the order of 10s-to-100s of megawatts. The literature does not present a clear cut design for such a topology.

**Conway, Adam:** *What model or model parameters did you use for the SOS?*

**Eifler, Jay:** The standard diode model with a few measured parameters. The DSRD models will be improved by either spice or TCAD models. My talk will follow sourov roy.

The extra measured parameters were taken from gen-1 Lawrence Livermore National Lab 13-stack diodes.

**Landreth, Eachan:** *Dario, in order to not spam the chatroom would you mind if we continued a conversation via e-mail?*

**Labrada, Dario:** Sure thing.

**Landreth, Eachan:** Thank you! My e-mail address is: [eachan.r.landreth@raytheon.com](mailto:eachan.r.landreth@raytheon.com).

### **3.5 Semiconductor Opening Switch-Inductive Energy Storage Topology: Parametric Simulation Study**

*S. Roy, D. Labrada, M. M. Paquette, A. N. Caruso*

The characteristics of semiconductor opening switch (SOS) current interruption and the corresponding output power for different permutations of SOS-inductive energy storage (IES) topology and the key component parameters have not yet been examined. Typically, an SOS itself could be used to pulse another SOS, achieving a pulse compression to enhance the output performance. The output can be further improved using these compression stages connected in parallel to drive a later compression stage. Our study leverages this series and parallel addition of the base SOS-IES units by performing a systematic study of the parameter space of the topology, whereas previous studies attempted to present only the best-case configurations. This study examines the effect of varying the numbers of SOS-IES units (both in series and parallel) along with the key circuit parameters such as inductance (L), capacitance (C), and bias-voltage (V) on the energy efficiency, and the peak power and rise-time of the output pulse. The results of this simulation study show that the peak power output positively correlates to increasing parallel branches and negatively correlates to the series addition of SOS-IES units. The energy efficiency decreases with the increasing number of series stages and increases with the increasing number of parallel branches; however, it saturates after a certain number of total parallel branches. It was also observed that peak power showed a positive correlation with the decreasing of all circuit parameters, L, C, and V, with the increasing number of series and parallel branches, whereas energy efficiency was only improved with the decreasing of circuit parameters, C and V. These results, while preliminary, provide us with the qualitative trends in output performance with respect to the different numbers of SOS-IES units along with the key circuit parameters, and suggests that the optimum topology should have (i) three or more parallel branches, and two or fewer series stages, and (ii) the parameters L, C, and V should all be decreased as a function of the series stages. Future work includes simulating more permutations of the SOS-IES topology wherein more than one parameter (L, C, and V) is varied at a time to confirm the trends in the obtained results.

#### **Discussion, Questions, and Answers**

**N/A**

### 3.6 TCAD Optimization of Drift-Step Recovery Diode (DSRD) Peak Power and Risetime

*Jay Eifler, Nick Flippin, Dario Labrada, and Anthony Caruso*

DSRD operation within a pulse characterization circuit is modeled and simulated using TCAD to improve modeling for predictive design and optimization. Models for carrier–carrier scattering and breakdown were added for transient simulation of DSRD performance and produced results comparable to experiment. For the DSRD doping profile used, circuit and its parasitics the minimum risetime achieved was, for all stack heights, 3 cm<sup>2</sup> in area. Overall, the peak power and risetime were relatively flat between 1-4 cm<sup>2</sup> areas and all stack heights. DSRD TCAD and SPICE models had not been accurate or predictive of experimental results and could not be used for predictive design and optimization. Silvaco™ TCAD had been used previously to model and simulate DSRD and DSRD-based pulser systems but only DC breakdown had been examined and carrier–carrier scattering was neglected. Carrier–carrier scattering for forward-biased high-power devices and Selberherr breakdown model are necessary to model DSRD operation correctly and can be used to develop more accurate SPICE models. TCAD models and simulation were tested using a pulse characterization circuit, optimal doping profile, and device thickness from prior art for a range of areas and stack heights of the DSRD. The peak power, risetime and voltage riserates were compared to in-house and published work (not known to author at outset of project) to check the validity of the model and simulation for predictive design and optimization. TCAD models reasonably predicted DSRD peak power and risetime for the correct DSRD doping profile, circuit and parasitics. Voltage per die and voltage riserate per die were within expected values for the static breakdown model used. The risetime was a minimum for an area of 3.0 cm<sup>2</sup> for the doping profile, circuit and parasitics (none) used. TCAD models and simulations can be used for predictive design of DSRD and DSRD-based pulser systems now that the models are comparable, for peak power, to experiment and published results (see poster). The TCAD model and simulation will be compared more closely to experiment, and the effects of parasitics on DSRD operation and performance will be examined.

#### Discussion, Questions, and Answers

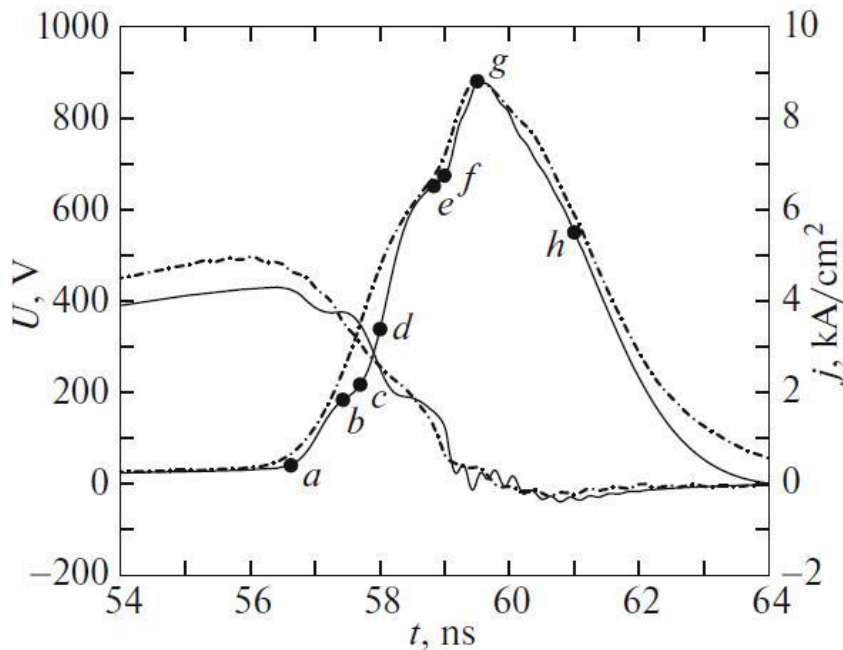
**Bellinger, Steve:** *What is your optimum area based on the results shown?*

**Eifler, Jay:** Tentatively, 1–4 cm<sup>2</sup> areas should give the best reduction in risetime, with peak power relatively constant over these areas. These results should be better matched to experiment to apply simulation results to predictive design, but the effect of parasitics can be explored immediately.

**Grounds, Chip:** *Can the TCAD work you have done on DSRDs be compared to any of the experimental work on DSRDs by UMKC so far?*

**Eifler, Jay:** I believe so. I just have to meet with the expt people and get the specifics I need. If somehow not we can run some pulse tests on DSRDs we know best.

Eifler, Jay:



Here's a result from the Russian paper in their effort. We will repeat this for our systems. (Calculated is solid, experimental dotted).

As well, this can be combined with Labrada and Roy's efforts. Either with TCAD model or a spice model developed from the TCAD and expt.

Jason Shelton also requested an offline DSRD discussion that Caruso would setup.

**Dario answers questions about Jitter:**

*Q. What is the jitter presently?*

A. Current jitter (total jitter) is 600 ps (at  $3\sigma$ ).

*Q. Is jitter too poor to steer?*

A. Yes, bad for arrayability.

*Q. Sources of jitter?*

A. Primary switch and driver are major jitter sources probably due to EMI sensitivity. Literature out there on low-jitter gate drivers. Want jitter between 50-100 ps for steering. Important to keep DSRD system at stable temperature for jitter concerns. More research on jitter is needed.

### 3.7 Direct RF Modulation Using GaN Photoconductive Semiconductor Switches

*Heather Thompson, Eliot Myers, Spencer Fry, Scott Shepard, and Anthony Caruso*

There is a need for a more compact, cost-effective RF pulse generation system for Navy afloat missions on smaller vessels and vehicles. Commonly, these systems use Si-based PCSS due to the maturity and low cost of material, but the short bandgap and theoretical material properties of Si limit the performance of these systems due to approaching the theoretical property limits of Si. To overcome this, we propose using carbon-compensated gallium nitride (GaN:C), due to its theoretical material characteristics, to improve the efficiency and reduce the amount of material, form factor, and thermal requirements of these systems. To this end, because of the fast recombination time of GaN:C, bulky pulse-forming transmission lines can be eliminated by modulating the output waveform by changing the incident laser characteristics (the rise-time, pulse-width, pulse repetition rate, and delay between pulses) to further reduce system size and design a frequency agile RF generation system. Based on the setup used in work done in the 1990's using GaAs, unipolar modulation using one GaN:C PCSS with the free-space optical delay has been demonstrated at <2 kV using the wedge laser (~1 ns rise-time). This output was then used to simulate the output that would be seen if the unipolar was manipulated to being a bipolar output pulse, to predict the output of the next planned test with GaN:C PCSS using two GaN:C devices to show bipolar RF modulation, showing that an output of hundreds-of-MHz to ones-of-GHz could be achievable with this alteration in design. Work will continue to demonstrate and evaluate the bipolar output of such a system using the neoLASE laser (70 ps pulse-width) system to allow for quicker rise time, shorter pulse width, and higher pulse repetition to be shown. Work towards a safer, more efficient, compact laser system utilizing optical fiber amplification will also be explored for its feasibility in demonstrating a cost-effective frequency agile GaN:C RF generation system.

#### Discussion, Questions, and Answers

**Grounds, Chip:** *What limited your experiment to 1 KV?*

**Thompson, Heather:** Sylgard has been used to try to prevent flashover occurring, but air bubbles are still forming in the curing process, even with utilizing a vacuum oven for this process. Moving forward, corona dope is going to be used due to the Si-PCSS team having the same problems with Sylgard and better results using this instead.

**Bellinger, Steve:** Suggests pressure cure instead of using a vacuum oven.

**Caruso, Anthony:** *For the audience – Does anyone see a clear path to the manufacture of inexpensive, compensated GaN (i.e. not the same material used to form GaN HEMTs)?*

**Conway, Adam:** How inexpensive? Bulk GaN substrates are getting cheaper and cheaper.

**Hussey, Tom:** *Assuming you get this to work as you hope, what are your expectations of laser requirements relative to Si?*

**Thompson, Heather:** Currently, I have achieved  $<1 \Omega$  on-state resistances using tens-of- $\mu\text{J}$  of incident energy per pulse, varying based on the device gap length. Efficiency in conversion of an IR laser to UVA is a concern due to the SHG/THG system used not being known for its efficiency and the setup also requiring splitting of the beam to allow for free-space optical delay between pulses, further increasing the laser requirements.

**Eifler, Jay:** I thought the laser requirements were surprisingly similar.

### 3.8 Electrically Tunable Diode based Nonlinear Transmission lines Capable of GHz Frequency Generation

*Nicholas Gardner, Dario Labrada, Plamen Doynov, and Anthony N. Caruso*

The SWAP-C capabilities of a high-power microwave (HPM) system must be optimized for use on Navy afloat missions. Diode-based nonlinear transmission lines (D-NLTLs) serve as a potential part of a solution by improving the SWAP-C capabilities of the pulse forming network (PFN) in the larger HPM system. Our goal is to fabricate D-NLTLs capable of generating GHz center frequencies at single MW peak powers capable of electrical tuning and parallelization for power scaling. The presented results included work on high voltage (HV) D-NLTLs capable of GHz frequencies and a low voltage (LV) D-NLTL capable of electrical tuning. The HV results saw two different prototypes tested: the first was a single diode line using the diode model K50F, and the second was a two-diode line utilizing two K50F diodes in a series arrangement. Both lines generated a pulse with a rising edge of ~600 ps at pulse amplitudes of ~10 kV, corresponding to max frequencies of ~1.67 GHz and peak powers of ~1.6 MW. Secondly the comparison of the 1D and 2D lines demonstrated that if sources of loss are minimized, diodes can be stacked in series to achieve higher peak powers and higher frequencies. The LV tests demonstrated that a DC bias applied to the cathode of each diode to electrically tune the center frequency, with positive bias increasing frequency and negative bias decreasing frequency. The presented results demonstrated that not only can GHz frequencies and MW powers be achieved using a D-NLTL, but the behavior of the network can also be electrically controlled. Future work will focus on studying the capability of D-NLTLs to be parallelized for power scaling as well as further HV tests to demonstrate pulses being broken into component solitons.

#### Discussion, Questions, and Answers

*Eifler, Jay: How does the D-NLTL compare to SAS for sharpening? How much sharpening from the DSRD by the D-NLTL?*

**Gardner, Nicholas:** I do not know how the SAS achieves its sharpening so I cannot comment. However, in both cases the D-NLTL decreased rise time from ~1 ns to ~600 ps, so ~400 ps of rise time reduction.

**Labrada, Dario:** So far both are successful in rise-time sharpening. DNLTL has achieved this without significant power loss, whereas with SAS we have yet to overcome the power loss.

*Labrada, Dario: Does the DNLTL need a rest period between shots, i.e. limiting PRF?*

**Gardner, Nicholas:** There is, the D-NLTL needs time for the diodes to relax back to their unbiased state. However, to this point none of the applications have run into an issue of the line being excited repeatedly to the point of the diode material not being able to relax fully.

*Nunnally, William: What is the energy efficiency = energy in to RF energy out?*

**Gardner, Nicholas:** Theoretically, 30%. Realistically we have seen around 10%.

**Conway, Adam:** *Did you do the FFT of the pulse?*

**Gardner, Nicholas:** Enough to show that energy is being sifted, but we have not reached a point where we are consistently taking that measurement. For the recent tests we have just wanted to see the frequencies and powers generated.

**Grounds, Chip:** *Have you actually generated RF energy out? Or have you shown the potential to generate RF energy at above a GHz?*

**Gardner, Nicholas:** We have generated RF energy out. In the tests where the 1D and 2D line were compared we had to isolate the line as the generated RF start a feedback loop triggering the HB continue generating pulses. We, however, have not radiated from an antenna of any sort, currently these are waveforms sent right into the scope through attenuation.

**Grounds, Chip:** *The results I saw from you earlier showed frequencies in the low hundreds of MHz range. Have you achieved RF above 1 GHz like the theory predicts?*

**Gardner, Nicholas:** Not from a waveform wide enough to be broken into component solitons. The waveform sent from the HB to the D-NLTL generated a rising edge sock-wave in the network that can be related to a max frequency in the single GHz. As far as pulses that have been broken into the sequences of solitons we are still in the 100s of MHz. With a wide enough pulse the K100F/K50F lines would generate a component soliton waveform with a separation between solitons in the low 1.0 GHz range.

**Gardner, Nicholas:** We have a max/bragg frequency in the single GHz and not yet a center frequency in the single GHz.

### **3.9 Geometric and Impedance Shifting Transmission line Transformers**

*James Kovarik and Anthony Caruso*

This poster explores methodology for using linear or tapered parallel plate transmission lines for the purposes of geometric and/or impedance transformation. Parallel plate transmission lines work naturally for geometric transformation, as a tapered transmission line can fit the shape of differing signal driving and radiating elements with ease. Parallel plate transmission line transformers can operate at a high bandwidth when transmitting high-frequency pulses. The objective presented was to create a geometric transformer between a coaxial element and a parallel plate element for a high-frequency pulse. A tapered transmission line transformer was designed and fabricated to meet this objective. The transformer was fabricated with 3D printed parts, and the goal was to maintain low attenuation across a 0.5–1.5 GHz bandwidth. The approach for meeting this goal was to design the transformer with as little impedance change as possible. The poster shows that the transformer maintained less than 1% impedance shift across its length. This resulted in low attenuation, with an input/output pulse comparison presented to demonstrate that. Future work is focused on improving this design further.

#### **Discussion, Questions, and Answers**

**N/A**

### 3.10 A Novel Method of Cooling a Semiconductor Device through a Jet Impingement Thermal Management System: CFD Modeling and Experimental Evaluation

*Jordan Berg, Roy C. Allen, and Sarvenaz Sobhansarbandi*

Laminar-flow-based cooling technologies are limited in their ability to compensate average-power dissipation  $>1 \text{ kW/cm}^2$  of the thermal load of high-power density electronics. An order-of-magnitude greater fluid flowrate and two orders greater pressure drop with a jet impingement (JI) technique is required without increasing SWaP-cost. Increased cooling performance facilitates semiconductor devices that can operate at higher average-power ( $>1 \text{ kW}$ ). High power density electronics employing jet impingement thermal management systems (JI-TMSs) have achieved 10's-of-kW of average power handling capabilities. The pump system power consumption required to produce adequate thermal compensation generates extreme pressures (100's-of-psi) to achieve optimal flow regime and cooling metrics. The utilization of novel cooling technologies which employ non-laminar flow regimes (i.e., JI-TMS) will allow for the development of a JI-TMS that is able to compensate average-power dissipation  $>1 \text{ kW}$  while maintaining the semiconductor temperature  $<80 \text{ }^\circ\text{C}$ . The results from the prototype created show that device temperature is well maintained below the desired operating temperature for 100 W of average power. The results for 200 W average power test show good agreement with the numerical data, however, the switch temperature exceeds the threshold temperature. For this reason, the current geometry will not be pursued. Based on the pressure drops incurred by the JI-TMS, the proposed cooling system is deemed unfeasible at this scale. A more optimized cooling method is being considered as the on-going work of this study.

#### Discussion, Questions, and Answers

**Nunnally, William:** *What is the ratio of the heat transfer per area of jet impingement compared to laminar flow - that is the parameter of interest?*

**Answer:** Laminar flow heat transfer coefficients are found to be on the order of 10's to several thousand  $\text{W/m}^2 \text{ K}$  (usually reaching up to 2-5 thousand for efficient (in regard to heat transfer) laminar flow devices. This differs from jet impingement or other extremely turbulent flow regimes that have been reported to reach greater than 100k  $\text{W/m}^2 \text{ K}$ . Everything else being equal, this gives a potential turbulent to laminar heat transfer performance ration of greater than 20 for optimized systems.

**Seth:** *What FLIR camera did you guys use?*

**Myers, Eliot**

I believe it is the FLIR A325SC.

**Allen, Roy:** Yes. Although resolution is limited to 320x240 pix, we also have a 4x zoom lens and leverage its capability to go from  $-20\text{C}$  up to  $350\text{C}$  depending on settings selected.

**Eifler, Jay:** *So how small of detail on the surface of the switch is that? I was wondering on the spatial resolution of that at one point.*

**Allen, Roy:** Depends on focal plane distance from aperture. We have measured the spatial temperature profile of a thin film nichrome on AlN surface mount resistor (~2 mm long) with roughly 0.05-mm resolution using said setup.

### 3.11 Heat Transfer Enhancement of a Jet Impingement Thermal Management System: A Comparison of Various Nanofluid Mixtures

*Jordan Berg, Roy C. Allen, and Sarvenaz Sobhansarbandi*

Dielectric heat transfer fluids possess thermophysical fluid properties that inhibit their ability to achieve  $>1 \text{ GW/m}^3$  cooling densities. Pure silicone fluid with viscosity of 20 centiStokes (PSF-20cSt) is  $\sim 15$  times more viscous than water, and therefore requires increased pumping power within the TMS. Increased cooling performance facilitates semiconductor devices to operate at higher average-power ( $>1 \text{ kW}$ ). Nanofluids have been shown to increase the thermal conductivity of base-fluids by 12% in comparison to the generic dielectric fluid alone; resulting in greater cooling density and decreased pumping power. The addition of nanoparticles in base-fluids results in a tradeoff between thermophysical properties, i.e., the addition of nanoparticles can increase the thermal conductivity, while also increasing viscosity of the mixture. The development of a nanofluid by entraining ceramic nanoparticles in the dielectric base-fluid will increase the nanofluid's thermal conductivity, thereby potentially improving cooling density capabilities of the TMS. In this work, several samples of varying amounts of nanofluids and surfactants were added to the PSF-20cSt. The mixtures with highest and lowest heat capacity were selected to be tested for thermal conductivity. The enhancement in heat capacity results in high convective heat transfer, while enhancement in thermal conductivity results in conductive heat transfer enhancement. The enhancement in thermophysical properties of nanoparticle-based PSF-20cSt will improve the performance of the high-power density electronics.

#### **Discussion, Questions, and Answers**

**Seth:** *Was the vendor able to explain the  $\sim 30\%$  lower heat capacity that you measured vs. their value of  $1.6 \text{ J/g } ^\circ\text{C}$ ?*

**Answer:** The vendor was contacted, and we inquired about their analysis of the specific heat capacity, as well of other testing methods they used to deduce the thermophysical properties of PSF-20cSt. The contact was unable to provide information about testing. When asked if a technical liaison was present or reachable, they said no. No further attempts to contact the vendor have been made.

## 3.12 Tradespace Analysis of a Phased Array of Electrically Small Antennas

*Bidisha Barman, Deb Chatterjee, and Anthony N. Caruso*

The primary objective is to determine the extent to which the physical aperture size of an antenna array, composed of microstrip electrically small antenna (ESA) elements, can be reduced, while maintaining performance in peak power density, bandwidth, and electronic beam steerability over the UHF range (0.4–1 GHz), compared with present-art high-power-microwave (HPM)-capable antenna arrays. The state-of-the-art includes phased arrays composed of ultra-wideband antenna elements, such as Horn, Reflector, Vivaldi, and Valentine. However, these antennas have the disadvantage of large physical aperture size. A method to reduce the overall array aperture area is to use ESAs as array elements, followed by their arrangements in suitable lattice structures (preferably, hexagonal/triangular). In this work, a new method to design wideband, coaxial probe-fed microstrip patch ESA elements, is presented. Following the design approach, single antenna elements are designed, manufactured, and experimentally validated on TMM-6 and TMM-10i substrates at 2.5–5 GHz, and are shown to yield >35% 2:1 VSWR bandwidth along with  $\approx 5$  dBi peak gain. Comparison of the proposed ESA elements, designed at the UHF range ( $f_c = 900$  MHz), with Koshelev, Shark and U-slot antennas, shows that the proposed antennas occupy the least volume, have better gain ( $\geq 5$  dBi at 900 MHz), while having comparable bandwidth ( $\approx 340$  MHz) and rE/V values ( $\approx 1$ ). Tradespace analysis of the arrays, composed of the designed ESA elements, of various size and lattice arrangements, shows that with  $\approx 36\%$  reduction in the aperture area ( $\approx 50\%$  reduction in number of elements), the gain drops by  $\approx 2.5$  dBi with no scan blindness spotted, as the main beam is steered from boresight to  $\pm 60^\circ$  in the range 640 – 990 MHz. Performance optimization of the designed ESA elements, via genetic algorithm and particle swarm optimizer, followed by testing time-domain reflectometry will be investigated soon.

### Discussion, Questions, and Answers

**Fry, Spencer:** *Does the loss in gain equate to the loss in gain that you would expect by just reducing an array by the number of elements you removed to make it hex shaped instead of square shaped?*

**Answer:** We are interpreting the question to be, whether the reduction in array gain is proportional to the number of array elements? The answer to this question is: No. Reduction in the number of elements in an array does not always translate into the equivalent proportional reduction in array gain. This is because the gain  $G^R$  is given by [1]:

$$G^R(\theta, \phi) = 4\pi\epsilon_r \frac{|U(\theta, \phi)|}{P_{in}}$$

$\epsilon_r$  being the radiation efficiency.  $U(\theta, \phi)$  is the radiation intensity – a complex term – which is array factor (number of antenna elements and current distribution) times the element pattern (the effect of mutual coupling between antenna elements is contained in the element pattern if the array is large enough). The effect of reduction in the number of elements on the input peak power

$P_{in}$  is less than the corresponding effect on the  $U(\theta, \phi)$ , which in turn affects the overall radiation property of the antenna and hence the array antenna gain.

It has been shown in the literature [2] that just by strategically exciting the antenna elements and hence controlling the array factor of an array with lesser number of elements, it is possible to achieve enhanced gain.

**Nunnally, William:** *What is the radiated power per square cm in the far field referenced to 1 m? 2.5 MW/cm<sup>2</sup> is about what the ideal atmosphere can support.*

**Answer:** The radiated power for all the arrays are:

Array	Radiating Aperture Area (m <sup>2</sup> )	Volume (m <sup>3</sup> )	Peak Gain $G^R$ (dBi)	Input peak power per element (kW)	Input peak power $P_{in}$ to array (kW)	Power density $S(\theta, \phi)$ at $R = 1$ m (W/cm <sup>2</sup> )
15 × 15 Square	4.4377	0.1185	27.76	1.2	270	1.28
183-Hex	3.0994	0.0828	26.09		219.6	0.71
139-Hex	3.1252	0.0834	25.66		166.8	0.49
114-Hex	2.8536	0.0762	25.20		136.8	0.36
80-Hex	2.9456	0.0786	24.50		96	0.22

Note: Power density,  $S(\theta, \phi) = \frac{1}{4\pi} \frac{P_{in}}{R^2} G^R(\theta, \phi)$  [3].

**Wagner, Adam:** *Why hex and not circle?*

**Answer:** So far, we have investigated square and hexagonal lattice arrangements based on the array design guidelines given in [4]. Further investigations into other lattice arrangements will be continued.

**Fry, Spencer:** *Reducing the number of elements results in less total input power, so there needs to be a balance between gain and reduction of elements when using sources.*

**Answer:** Yes, reduction in the number of array antenna elements will reduce the total input power.

## References

- [1] W.L. Stutzman and G. A. Thiele, *Antenna Theory and Design*, 3<sup>rd</sup> ed. New York, NY, USA: John Wiley & Sons, 2012.
- [2] R. Gardelli, M. Albani and F. Capolino, "Array thinning by using antennas in a Fabry–Perot cavity for gain enhancement," in *IEEE Transactions on Antennas and Propagation*, vol. 54, no. 7, pp. 1979-1990, July 2006.
- [3] R. J. Mailloux, *Phased Array Antenna Handbook*, 3<sup>rd</sup> ed. Boston, USA: Artech House, 2018. S. K. Rao and C. Oostroot, "Design Principles and Guidelines for Phased Array and Reflector Antennas," *IEEE Antennas and Propag. Mag.*, Vol. 62, No. 2, pp. 74-81, April 2020.

### 3.13 Koshelev Single Element and Array Antenna Study with Comparison to Balanced Antipodal Vivaldi Antenna

*Kalyan Durbhakula, Eliot Myers, Roy Allen, and Anthony Caruso*

Determine the extent to which physical aperture area of an antenna array, composed of antenna elements, can be reduced, while maintaining performance in peak power density, bandwidth and electronic beam steering capability over the UHF range (0.4 GHz to 1 GHz). The balanced antipodal Vivaldi antenna is considered as SOTA for its exceptional bandwidth (20:1) and power handling capabilities. Carry out detailed tradespace study to understand the radiating properties of the Koshelev antenna and to try and reduce aperture area of single element followed by antenna array. We presented the workings of the Koshelev antenna as well as a table that compares the Koshelev single element antenna metrics against the SOTA BAVA metrics obtained from an open source. The key results are as follows: 1) Optimized and improved aperture area (9.3 cm × 8.5 cm), peak gain of 4 dBi at 900 MHz, aperture efficiency of 300% at 900 MHz and a high rE/V value of 1.49 of the Koshelev single element antenna. 2) The 4 × 4 Koshelev antenna array displayed a peak gain of 15 dBi at 900 MHz with an aperture efficiency of 113% at same frequency. In summary, the optimized single element metrics of the Koshelev antenna exceed many of the target metrics as well as displayed improved performance when compared against open source BAVA. One of the future works include optimizing and/or reducing aperture area of Koshelev antenna array to obtain higher aperture efficiency values (>130%) without causing degradation to its bandwidth and rE/V.

#### Discussion, Questions, and Answers

**Grounds, Chip:** *How is aperture efficiency defined such that you can have higher than 100%?*

**Durbhakula, Kalyan:** We define aperture efficiency as a ratio of effective aperture area to physical aperture area. The effective aperture area is the ratio of the available power at the terminals of the antenna to the power flux density of a plane wave incident upon the antenna, provided the polarizations of incident wave and receiving antenna are matched. An effective aperture area equal to or higher than physical aperture area implies that the antenna has high gain over a smaller aperture area. In part, this is possible due to extended transverse length (the direction of EM wave propagation) of the antenna.

**Chatterjee, Deb:** Chip, Koshelev antenna has never been analyzed by previous authors/researchers. Kalyan is doing a thorough job here for the 1st time and as a consequence some of the issues are not very clear. We have to work on that more to give you a better answer.

**Koslover, Robert:** To Chip: You can get >100% ap efficiency because the fields extend out laterally (like a wire type antenna, such as a dipole). However, I see no advantage to this in an array, since you cannot leverage it to reduce the overall aperture area consumed by the array. And it can also reduce power handling and introduce other issues.

**Koslover, Robert:** Individual stand-alone element aperture efficiency is not a relevant figure of merit for evaluation of array performance.

**Durbhakula, Kalyan:** Dr. Koslover, thank you for your suggestions and feedback. We reported the metrics of Koshelev stand-alone element to try and draw a comparison against open source BAVA (stand-alone element) and to explore the boundaries of the Koshelev antenna. We strongly agree with your assertion that gain does not increase linearly moving from stand-alone element to an array (total number of elements\*gain of stand-alone element) primarily due to mutual coupling between fields generated by adjacent elements. We have identified few special EM techniques (various array configurations, array placements, and sub-array placements) and will shift our efforts on applying these techniques (without reducing aperture area of stand-alone element) to try and reduce the array aperture area. We will also look into field distribution plots for the Koshelev and other antennas for better analysis.

**Grounds, Chip:** *This is different than ratio of power seen at the antenna input port divided by the amount of incident energy in the physical area of the antenna?*

**Koslover, Robert:** Aperture efficiency is not power efficiency. It is directivity relative to a uniform-field ideal aperture of the same physical area. Defining that area leads to much confusion.

**Nunnally, William:** *What is the radiated power per square cm in the far field referenced to 1 m? 2.5 MW/cm<sup>2</sup> is about what the ideal atmosphere can support.*

**Durbhakula, Kalyan:** The current version of the Koshelev stand-alone antenna can accept a 20 kV peak to peak pulse, which is about 8 MW input power per element, and with an array gain of 15 dBi, the Koshelev array antenna can radiate about 32 kW/cm<sup>2</sup> at 1 m. The value is still below 2.5 MW/cm<sup>2</sup>.

### 3.14 Ultra-Wide-Band High-Aperture-Efficiency Shark Antenna Tradespace Study

*Sadie Brasel, Kalyan Durbhakula, Michelle Paquette, and Anthony Caruso*

In this presentation we explore the extent to which the physical aperture area of the Shark antenna array can be reduced, while maintaining performance in peak power density, bandwidth, and electronic beam steerability over the UHF range (0.4–1 GHz), compared with present-art high-power-microwave-capable antenna arrays. The balanced antipodal Vivaldi antenna (BAVA) is considered to be the state-of-the-art antenna element due to its exceptional 20:1 impedance bandwidth ratio as well as the ability to handle tens-of-MW input power. The BAVA design parameter space has been exhausted over the past couple of decades. In this work, we have explored the design space of Shark antenna single elements to understand their effect on the impedance bandwidth, transient gain, and radiation pattern. The design space of the novel Shark antenna is explored using electromagnetic (EM) solving tools with an objective of reducing physical aperture area while maintaining low-frequency performance, a directive radiation power, and peak gain performance. During our analysis, we have found that the low-frequency performance of the antenna is dictated primarily by the cone height and cone flare angle. Increased cone heights also result in more directive radiation patterns. Having increased distance from the cones to the backplane has been shown to have minimal effects on the bandwidth of the Shark antenna and has negative effects on the transient gain at the front of the antenna. The tradespace study has provided valuable information about how the design space of the antenna affects key performance metrics. Moving forward special EM techniques will be used to further reduce the size of the Shark antenna, such as inclusion of ground plane, dielectric loading, and capacitive loading.

#### Discussion, Questions, and Answers

**Lamb, Barrett:** *Are the efficiency numbers based on effective or physical aperture area?*

**Brasel, Sadie:** Both. The aperture efficiency is the ratio of effective aperture area to the physical aperture area.

**Caruso, Anthony:** *Sadie - how much have you improved on the original French design?*

**Answer:** Using the same cone height in the original French design, we were able to achieve a lowest cutoff frequency of 400 MHz compared to 800 MHz, by using a smaller flare angle and a ground plane. The smaller angle led to significant reduced aperture area by more than 58%. Thus, we have optimized their original design and increased the electrical size of the antenna without increasing physical size.

**Koslover, Robert:** *Sadie, please take a look at the overall aperture fields of your arrays. Although individual elements are interesting to analyze, you cannot leverage their high aperture efficiencies to shrink sizes of arrays.*

**Durbhakula, Kalyan:** Dr. Koslover, what you said is in line with our initial observations from array studies.

**Wagner, Adam:** *Is this antenna going to be used in an array? If so how do you overcome that obstacle?*

**Brasel, Sadie:** Yes, we have been able to reduce the physical aperture area of the single element which will allow for reduced area of the array.

**Koslover, Robert:** *Sadie, that is where you will run into trouble. Pushing the elements together to reduce the area will reduce the gain. You will be disappointed. You must always consider the aperture field distribution overall.*

**Brasel, Sadie:** I see. We will have to investigate further into this and try using different array placements with this in mind.

### 3.15 Machine Learning for Antenna Optimization

*Sai Indharapu, Anthony Caruso, and Kalyan Durbhakula*

To determine the extent to which a machine learning (ML) model can be applied to evaluate the performance of antenna geometries while maintaining the accuracy of conventional electromagnetic (EM) wave solvers. In general, conventional EM wave solvers are applied for optimization and performance analysis of antenna design. The main objective of this work is to evaluate ML models available in Altair Hyperstudy and study their limitations and accuracy levels when applied to antenna optimization and/or prediction. A particular ML model called Radial Basis Function (RBF) has been applied on a fractal antenna geometry for predicting reflection coefficient response. The figure below compares the response from the ML (RBF) model as well as the response from traditional solvers in FEKO and CST. A good agreement has been obtained from the ML (RBF) model over the desired frequency range (0.75 GHz to 2.5 GHz). In summary, this poster has shown that ML can be applied to predict antenna response in a short time while also maintaining accuracy levels of conventional EM wave solvers. Our immediate future work will focus on increasing the training data set size, using stochastic algorithms as additional optimization tool on trained ML models, and extending the antenna response prediction to other metrics such as gain and electric field.

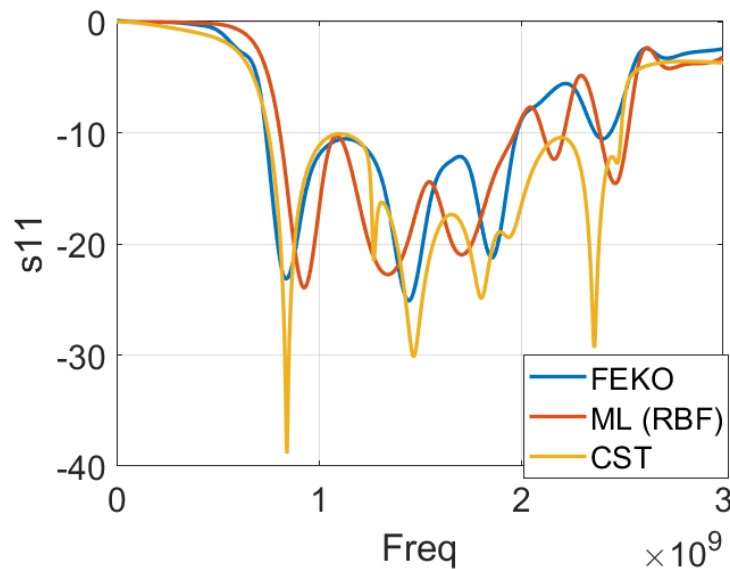


**Figure.** Reflection coefficient (S11) comparison between FEKO, CST and ML (RBF) model.

#### Discussion, Questions, and Answers

**Grounds, Chip:** *The general agreement in Fig 2 is good. How come CST and FEKO aren't closer?*

**Answer:** The feed of our fractal antenna in FEKO and CST differ slightly due to inherent type of excitations available in FEKO and CST. In FEKO, the solver requires the antenna design to have additional conductive pieces connecting transmission line and the ground plane. In CST, this is

not the case as we can use a discrete port to directly connect the transmission line and ground plane. The disagreement can be seen mainly beyond 2 GHz and we can confirm that this disagreement is due to slight change in antenna design between FEKO and CST. We will fix this issue and report a better agreement in the next monthly status report. Also, the ML model has been trained using output data from FEKO and therefore the ML (RBF) curve is in better agreement with the FEKO results than the CST results.

**Shepard, Scott:** *Any point in trying to incorporate atmospheric and terrain factors in HPM antenna design?*

**Answer:** Altair Hyperworks software currently provides propagation modeling of indoor and outdoor areas, wherein you can create or import an outdoor area and add custom environmental conditions. The propagation modeling takes the radiation pattern of HPM antenna into account and calculates metrics such as path loss, electric field etc. The atmospheric and terrain factors must be incorporated into the outdoor area through custom environmental conditions.

**Koslover, Robert:** *I want to encourage anyone in this group hoping to reduce array aperture areas by reducing element areas to rethink it. You must compute the overall array aperture field. When element fields overlap, the gain of the array falls below  $N * \text{gain of the element}$ .*

**Answer:** We will definitely re-evaluate our approach on trying to reduce array aperture area by reducing element area.

**Lamb, Barrett:** *Were step sizes the same in feko and cst?*

**Answer:** If you are talking about frequency step size over the desired frequency range (0 to 3 GHz), then I think they are not same. In FEKO, we have chosen 51 discrete frequency step sizes, whereas CST uses 1001 default step sizes. We will ensure that our future simulations maintain step size consistency between FEKO and CST to draw fair comparison.

**Lamb, Barrett:** I agree if we have over 100% efficiency it would mean the fields are overlapping trying to use the same space.

### 3.16 Modeling and Verification of High-Power Electromagnetic Coupling to Nonlinear Electronic Systems using the Equivalent Circuit Approach

*Mohamed Z. M. Hamdalla, Benjamin Bissen, Thomas Ory, Ahmed M. Hassan, and Anthony N. Caruso*

This work aims to develop a predictive tool that can quantify high-power electro-magnetic wave coupling to a device under test (DUT) that is composed of a system of wires/traces connecting linear and nonlinear loads. Coupling to such a DUT will depend on the properties of the wires and the linear/nonlinear loads. The equivalent circuit approach (ECA) provides a unique solution to this convoluted coupling problem by modeling the wires as receiving antennas that can be represented by a Thevenin equivalent circuit terminated with the linear/nonlinear load of interest. To highlight the advantages of the ECA technique, we studied a representative example composed of a square trace printed on an FR4 substrate connecting a 1 M $\Omega$  resistor and an RB886CST2R Schottky diode. We showed that the ECA could predict the optimum center frequency and the minimum pulse repetition frequency (PRF) of the incident waveform to maximize the coupled voltage to the load. We also developed an experimental setup composed of a GTEM and an arbitrary waveform generator to validate the ECA predictions. By varying the characteristics of the incident waveform, we show that certain field strength and PRF can cause the voltage to build up across the nonlinear diode, maximizing the probability of creating an effect. The computational and experimental approach presented herein can explain RF coupling to a wide range of wire/trace systems, including practical DUT.

#### Discussion, Questions, and Answers

*Eifler, Jay: So is 477 a magic frequency for a diode coupling?*

**Hassan, Ahmed:** No in this case it was the optimum frequency given a combination of factors such as the trace dimensions and the diode properties. If any of the previous factors change, this optimum frequency will also change.

*Grounds, Chip: How complicated a circuit do you think you can analyze with this technique? What would cause the limit?*

**Hassan, Ahmed:** In the next poster by Hamdalla, we show a much more complicated system, full UAV wires, modeled using ECA. The limit would be in finding a suitable equivalent circuit to match the input impedance of the DUT.

*Hussey, Tom: Have you surveyed nonlinear components that might be used to see the extent to which your results might be universal?*

**Hassan, Ahmed:** Surveying multiple nonlinear components is definitely our next step since the ECA is fast. We will definitely use this analysis of multiple nonlinear loads to generate universal guidelines.

**Hussey, Tom:** *Have you considered twisted pairs and the relative importance of common mode and differential mode coupling?*

**Hassan, Ahmed:** We did not study twisted pairs yet but we can definitely do so. The nice thing about the ECA approach is that the common and differential mode coupling are inherently included if the electronic components are accurately modeled.

### **3.17 Predicting Electromagnetic Coupling to UAV Models**

*Mohamed Z. M. Hamdalla, Anthony N. Caruso, and Ahmed M. Hassan*

In this work, we developed two computational models of the wiring and electronics of a UAV, with different computational complexity, while maintaining a good/accurate representation of the system. We used the equivalent circuit approach (ECA) to develop an equivalent circuit for each UAV model to quantify the RF coupling to one load in each system. We showed how the equivalent circuit could be updated when the UAV wires and electronics are placed in a partially open metallic enclosure. The coupling results from the equivalent circuit showed excellent agreement with the full-wave simulations at a fraction of the computational time. The developed UAV model and the corresponding equivalent circuit can be used to guide experimental RF coupling measurements of UAVs and predict the incident waveform characteristics to generate the desired coupled voltages and currents at a particular load in the UAV.

#### **Discussion, Questions, and Answers**

N/A

### 3.18 Coordinated Algorithms Framework Using the Traveling Salesman Problem for CUAS Engagements

*Cody D. Smith and Travis Fields*

This study aims to handle weapon's target assignment (WTA) during hostile unmanned arial threat engagements by developing a framework that efficiently optimizes target assignment. Path planning algorithms like the Traveling Salesman Problem and the Vehicle Routing Problem have historically been utilized for WTA. The development of an effective WTA framework will require a combination of features from several path planning algorithms. For example, the Traveling Salesman Problem with Neighborhoods to manage conditions where direct interception is not required, the Dynamic Traveling Salesman Problem where incoming hostile targets are moving, and Dubin's Paths where the vehicles in the scenario are assumed to be nonholonomic. These path planning features are combined into a framework which is termed the Coordinated Dynamic Traveling Salesman Problem with Neighborhoods. Through the construction and customization of a cost function, this framework will be used to determine sufficiently low-cost paths for WTA. Future work includes the reduction of engagement scenario assumptions, layered defense coordination, and dynamic path updating.

#### Discussion, Questions, and Answers

**Hussey, Tom:** *Is the neighborhood radius a single value for which  $P_k$  is 1 or 0 depending on whether you are inside it? Or can  $P_k$  be a function of distance of closest approach?*

**Smith, Cody:** As it stands, the current model would use a fixed radius with a probability of kill ( $P_k$ ) equal to 1. Eventually, varying  $P_k$  could be considered.

**Fields, Travis:** To add on to Cody's answer, we are working to continue to increase the realism over the next several years. And as Cody helps to get the foundation built in this space, we will be able to add in the more complex components (i.e. actual  $P_k$ ).

**Landreth, Eachan:** *Do you plan on incorporating varying weights for each threat?*

**Smith, Cody:** Yes, weighting will be considered when developing the cost functions associated with determining the costs of each path between assignments.

**Fields, Travis:** To add on to Cody's answer, an interesting aspect of different weights for different threats is the ability to model/simulate a classification system. Currently it's simply a detect-and-go type of approach. Classification requires more threat information, but it definitely add some interesting permutations to the space.

### 3.19 Evaluation of Localization Uncertainty and Its Effect on Vehicle Intercept

*Paul Klappa and Travis Fields*

Typically, ground-based defense systems depend on target range and the quality of the tracking sensor system. Range dependence is mitigated by incorporating an aerial-based defense system; however, both ground and aerial-based systems still rely on the quality of the tracking sensor. Thus, a need exists to assess the impact of tracking sensor uncertainty during an engagement. In this research, a pursuer–evader endgame simulation was developed. The engagement was used to evaluate the impact of varying tracking sensor uncertainty by comparing an evader's raw position measurements to its Kalman Filter estimates. Four tracking sensor uncertainty values were assessed where each value was representative of combined uncertainty from many sources of error. Miss distance, defined as the Euclidean distance between the pursuer and evader, was evaluated along with the time of miss distance. The Kalman Filter estimation method improved the modeling capabilities of the evading aircraft as velocity was accurately estimated along with the evader's position. When using the Kalman Filter, the average miss distance decreased in most engagements. Finally, a Kalman Filter with higher tracking uncertainty was comparable to using raw measurements from a tracking sensor with less uncertainty.

#### Discussion, Questions, and Answers

*Hussey, Tom: How smart is the evader? Can it sense the pursuer?*

**Klappa, Paul:** The evader can be considered as a “dumb” evader and does not sense anything around itself. The evader's objective is to fly due North at a fixed velocity without maneuvering.

*Conway, Adam: Is your goal to kill the evader?*

**Fields, Travis:** Get within XX distance for whatever effector/technique you want.

*Conway, Adam: Is the heading of the interceptor updated as it tries to intercept?*

**Klappa, Paul:** Yes, the heading of the pursuer updates at every time step in the simulation. This heading changes based on proportional navigation and updates the pursuer's position thereafter. The pursuer attempts to intercept the last known location of the evader. This location is based on the selected method that is used (non-Kalman Filter and Kalman Filter). In the case of the non-Kalman Filter, the pursuer attempts to intercept the raw tracking sensor measurements. In the case of the Kalman Filter method, the pursuer attempts to intercept the Kalman Filter position estimates for the evader.

**Conway, Adam:** Based on new sensor data?

**Klappa, Paul:** Yes, the new sensor data becomes available at a frequency of 10 Hz. It should be noted that the simulation runs at 450 Hz, so the heading updates first by using proportional navigation which then updates the pursuer and evader positions.

## 4. Discussion with Chip Grounds, Tom Hussey, and Other Attendees

### Grounds, Chip:

- Likes poster/pre-recording format; suggests to Zoom in on poster during presentations
- Highlights concerns about cost and robustness of lasers; what are we doing toward this end with the efforts by Shepard and Bhamidipati?
- Likes DSRD theoretical work; highlights desire to see comparison between theory and experiment, and theoretical work with respect to jitter

### Hussey, Tom:

- asks what aspects of the grant work are on the critical path? In particular, what about the laser and Behlke switch replacement?
- will send a list of more formulated questions (to follow up)

### Responses/Discussion

#### Myers, Eliot:

Re: laser

- currently looking at laser systems on order of 30-40% of total system cost (from memory)
- agrees that robustness is important: eliminate mechanical risk of free-space system
- available laser systems are not prohibitive, though fiber system but would be nice

Re: switch

-can put together a system with existing technology (problems with dealing with foreign company, still, though)

#### Caruso, Tony:

- thinks that if we transition, stakeholder would want US company to be able to deliver enough product (for both laser and switch)
- thinks Scott's work could get to high enough TRL level in ~5 years

### Dario, Tony, and Eliot discuss jitter at some length

### Hussey, Tom:

- Sandia claims good lifetime from GaAs lock-on switches if careful with multi-channel illumination (will send references)
- Mentions Russian work on semiconductor opening switches

### Sullivan, Don:

- impressed with breadth of work being done
- particularly interested in electronic circuit analysis work (to follow up with Hassan and Beetner)
- rather than large array of components at fixed site – looking at smaller system mounted in pursuer is of interest

**Conway, Adam:**

-missed Scott Shepard's talk, but interested in following up

**Giorgi, David:**

-suggests reference for fiber laser work: Larry Grimes from DEJTO, connect with Shepard

-asks what laser specs we are shooting for? Suggests that it would be useful to have a list of targets

-concerned about the efficiency of a GaN direct drive radiator (Thompson); fast recombination times/how much light to put in?

-consider comparison to Q switch microlasers

**Myers, Eliot (re: laser requirements):**

-single kHz

->100 uJ

-silicon 1064 nm

-pulse width <100 ps

**Koslover, Robert:**

-emphasizes that there is not a lot of advantage to reducing aperture areas for arrays (diminishing returns)

-suggests to focus on other areas for improvement: peak and average power handling; impedance matching; depth, weight, and cost reduction; supporting polarizations other than linear

**Skipper, Mike:**

-antenna aperture efficiency is what it is, but probably incremental improvements possible

-can help out Heather based on experience with GaAs

**Abdalla, Mike:**

-mentions time domain antenna work

**Shelton, Jason:**

-appreciated pre-recorded format for staying on track

-interested in following up on DSRDs and ECA work (Tony suggests to go through him)

**Hoffman, Ryan:**

-virtual poster session works well for creating a reference and being able to speak to work

-highlights that he believes that Grant work is only important for long-term, not demonstrator

-emphasizes the need to clarify to community what the end state is

-appreciates seeing where students go

-antenna issues always come up; wants to think of ways to explore new contributions

## 5. Appendix: Posters

# Development of a Modular High-Voltage Solid-State Switch with Integrated In-House Gate Driver

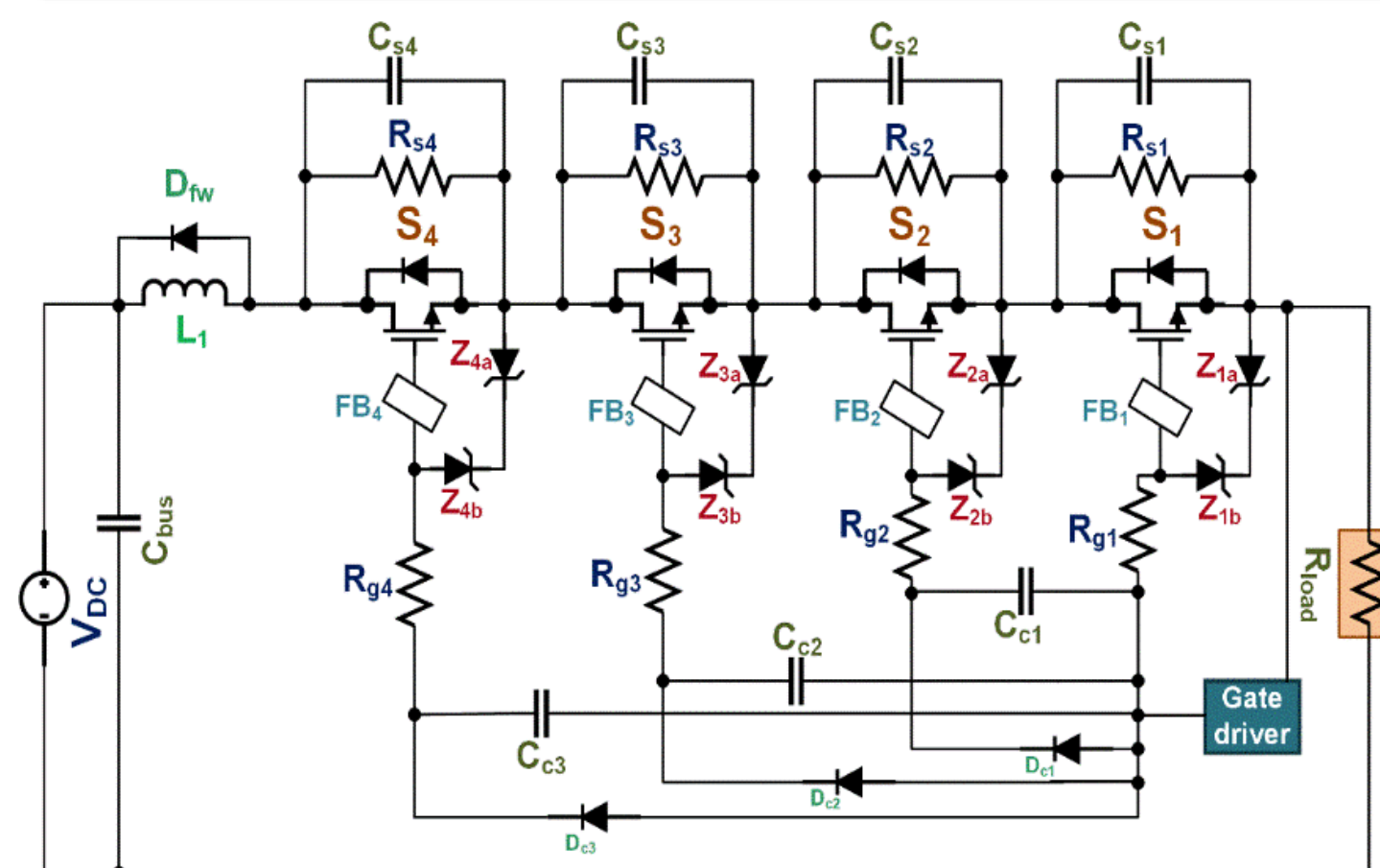
Wasekul Azad<sup>1,2</sup>, Sourov Roy<sup>1,2</sup>, Spencer Fry<sup>1,2</sup>, Anthony N. Caruso<sup>1,2</sup>, and Faisal Khan<sup>1,2</sup>

<sup>1</sup>University of Missouri-Kansas City MO, <sup>2</sup>Missouri Institute for Defense and Energy

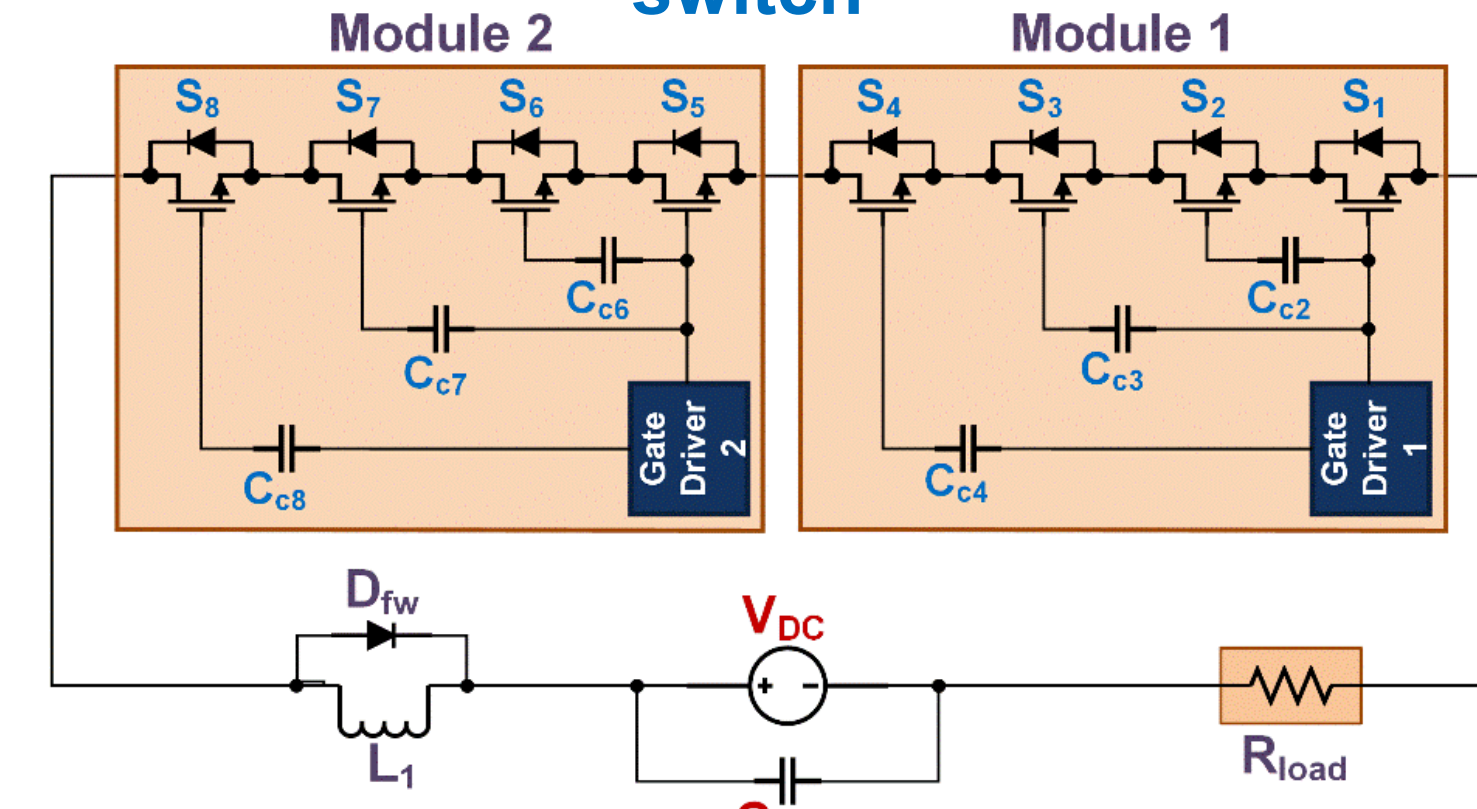
## Motivation and Objective

- Power loss due to the lack of power conditioning affects the efficiency of a linear-mode photoconductive semiconductor switch (PCSS) based pulse forming network (PFN) for generating high-power microwave (HPM).
- A two-state switching mechanism facilitated by a high-voltage (HV) switch can minimize the power loss, thereby increasing system efficiency.
- Commercially available HV switches (e.g., switches made by German manufacturer BEHLKE) are expensive, have long lead time, require liquid cooling for a switching frequency greater than 10 kHz, and are powered by multiple ancillary DC supplies.
- We are developing an in-house modular HV (~10-kV) switch from inexpensive COTS MOSFETs capable of operating up to a switching frequency of 200 kHz that can be a direct and inexpensive replacement to the HV switches made by BEHLKE
- We have introduced modularity in the HV switch design to facilitate voltage withstanding scalability of the switch without complete design overhaul.

## Schematic of the Proposed Modular HV Switch



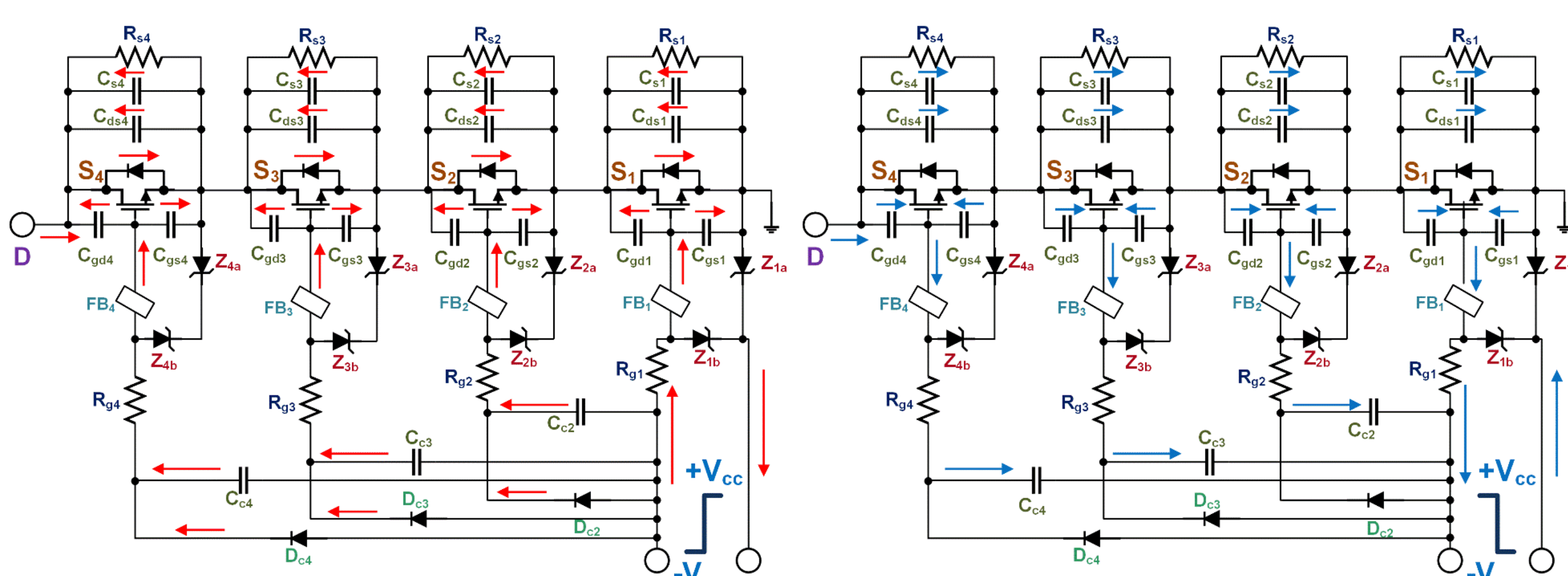
Schematic of the single gate driver-based series-connected in-house HV switch



Schematic of the modular HV switch

- Each module consists of four series-connected MOSFETs and one in-house gate driver.
- Two modules are connected in series to increase the voltage rating of the entire switch.
- 1.7 kV rated surface-mount SiC MOSFETs from CREE are used to develop the HV switch.
- The limit of the theoretical breakdown voltage of the HV MOSFET is therefore 13.6 kV.
- Coupling capacitors, snubber capacitors are used to ensure voltage balancing during turn-ON and turn-OFF transients.
- Balancing resistors are used to ensure voltage balancing during the OFF-state.

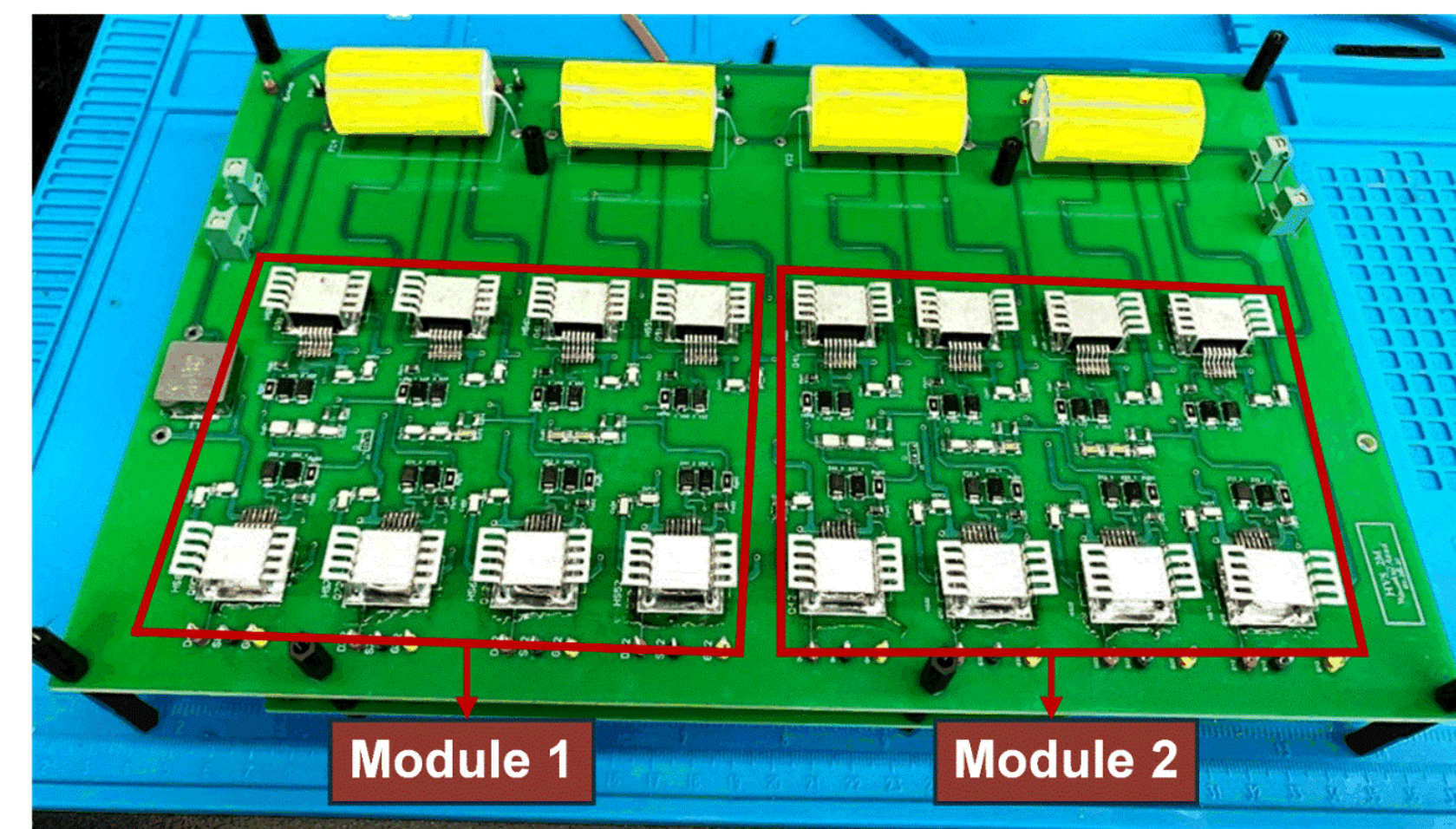
## Switching Transition Dynamics of the HV Switch



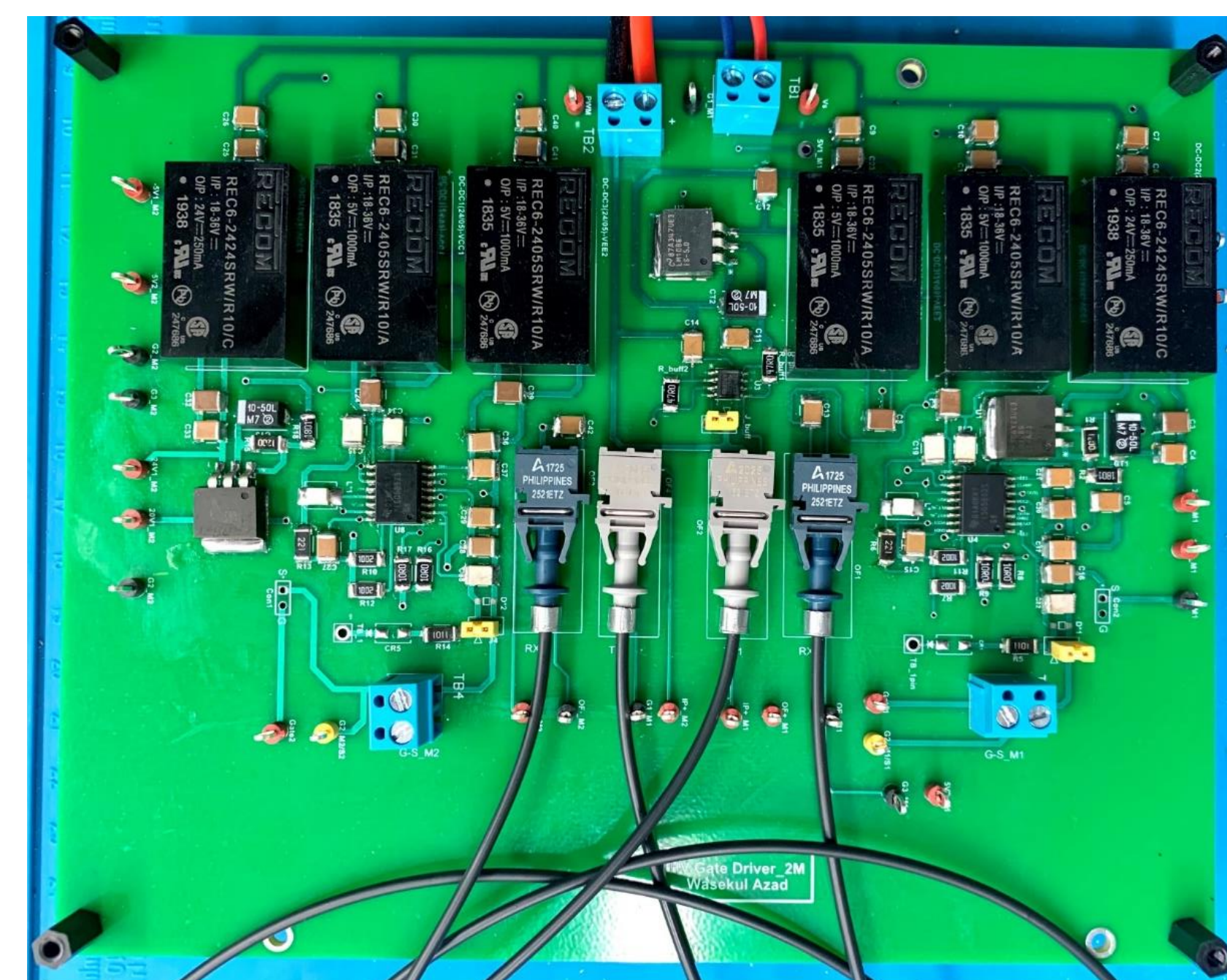
Main current paths during turn-ON transition

Main current paths during turn-OFF transition

## Fabricated In-house Modular HV Switch and HV Gate Driver Prototype



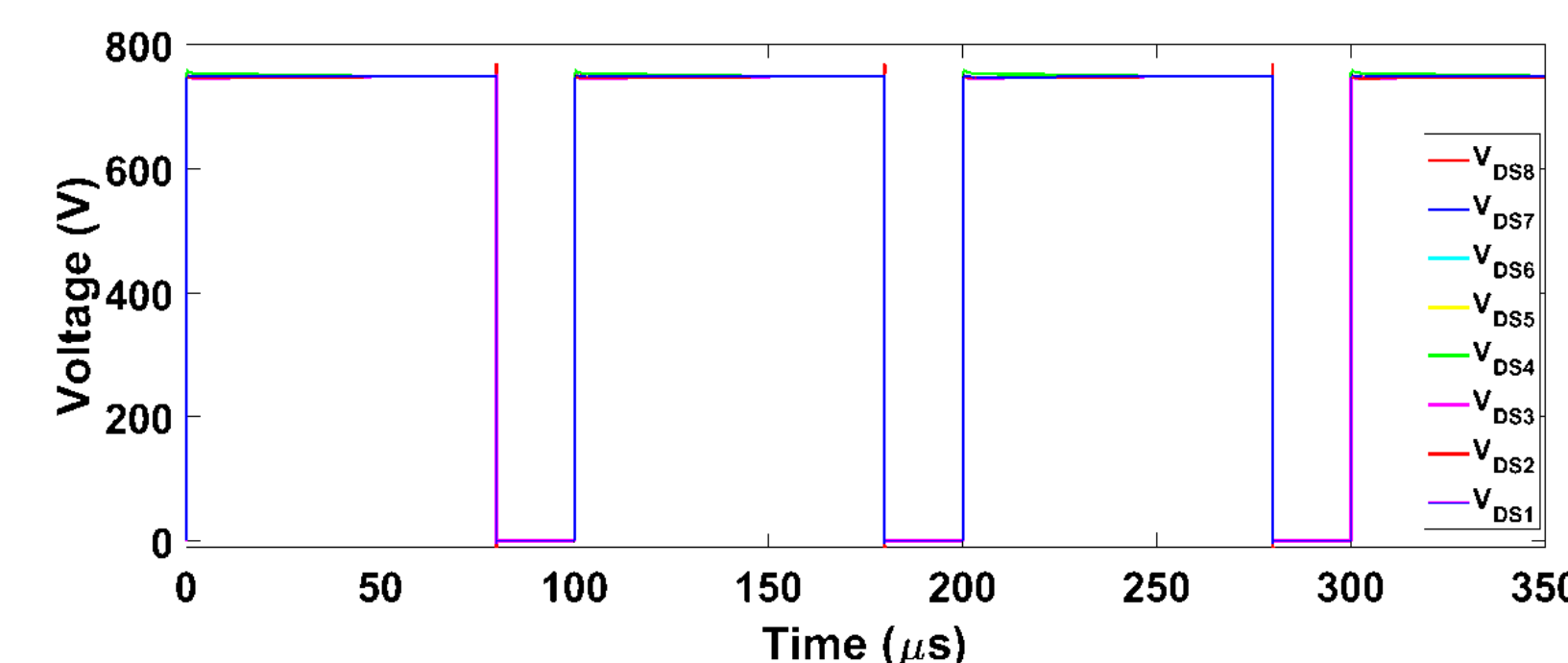
An eight-stage in-house modular HV switch (13.6 kV rated)



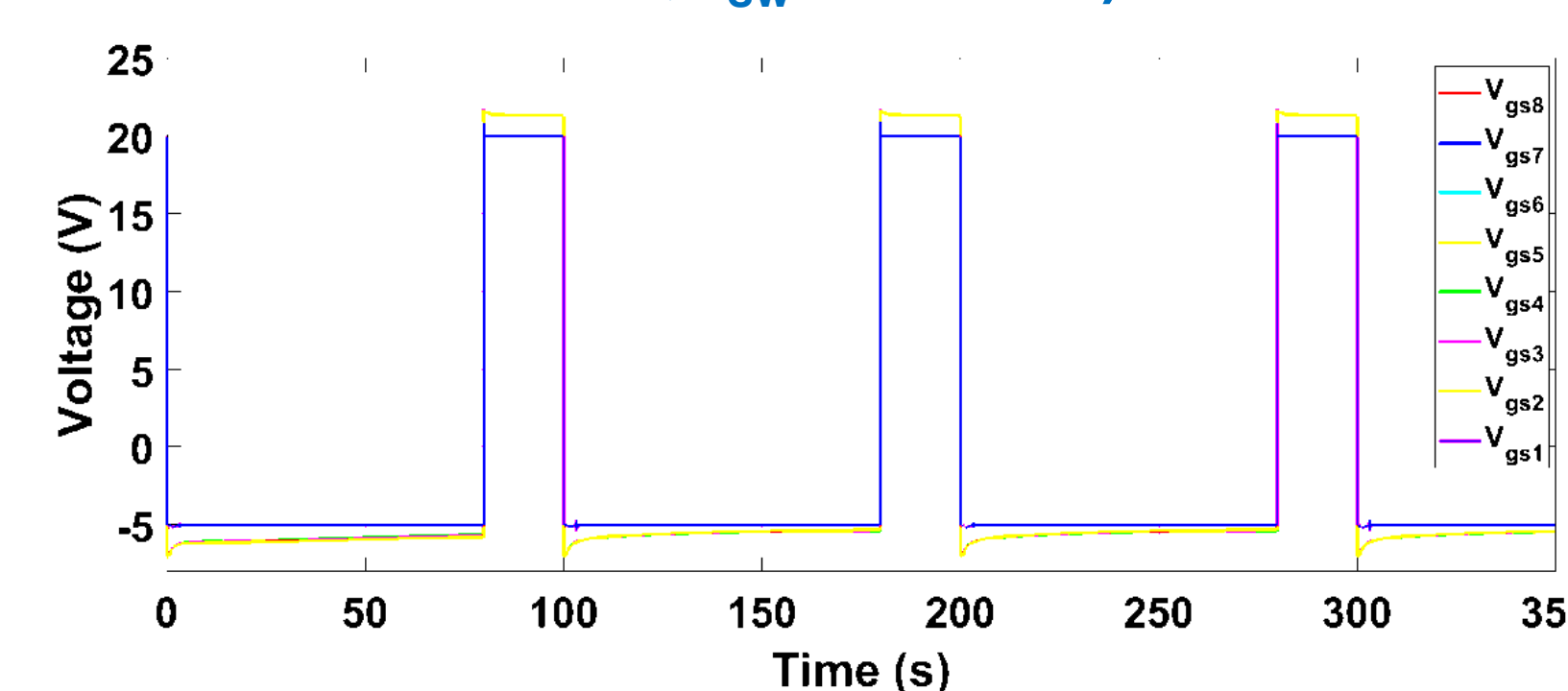
An in-house modular HV (10 kV rated) isolated gate driver

- Two parallel branches of series-connected MOSFETs are incorporated in the modular design to increase the current rating.
- Trace lengths are maintained at minimum to reduce the tray inductance.
- 10 kV rated isolated DC-DC converters are used to provide galvanic isolation for the power supplies of gate driver ICs in both modules.
- A 5.7 kV<sub>RMS</sub> rated reinforced isolated gate driver IC with 2.5 A sourcing and 5 A sinking current capability is chosen to fabricate the gate driver modules.
- Two optical fiber links for two modules have been incorporated in the gate driver board for isolation of the PWM signals.

## Simulation Results: 6 kV Excitation



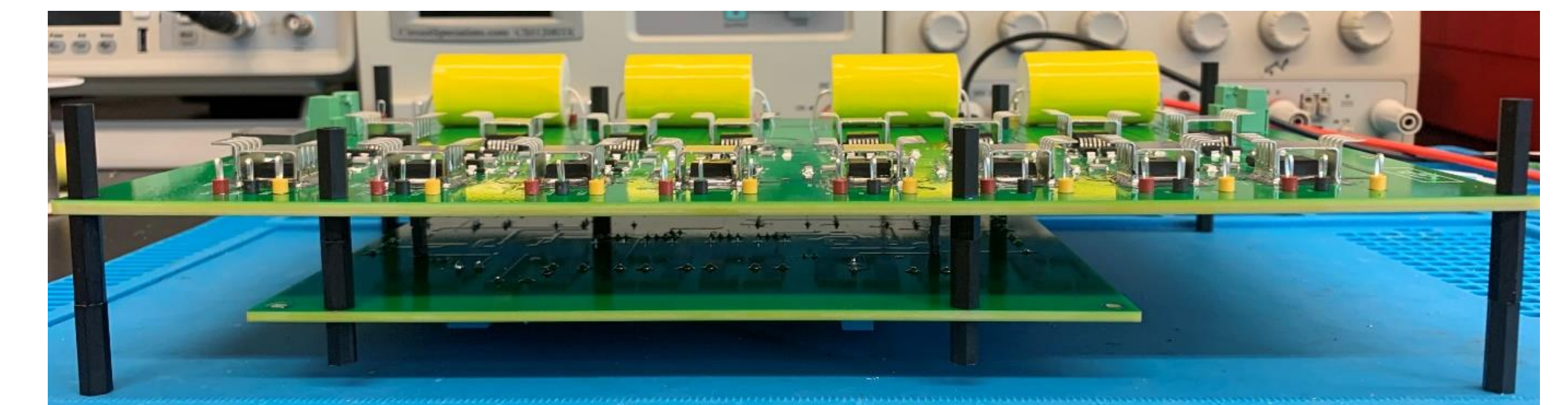
Simulated drain-source ( $V_{DS}$ ) voltages across the eight individual MOSFETs ( $V_{DC} = 6$  kV,  $f_{sw} = 20$  kHz)



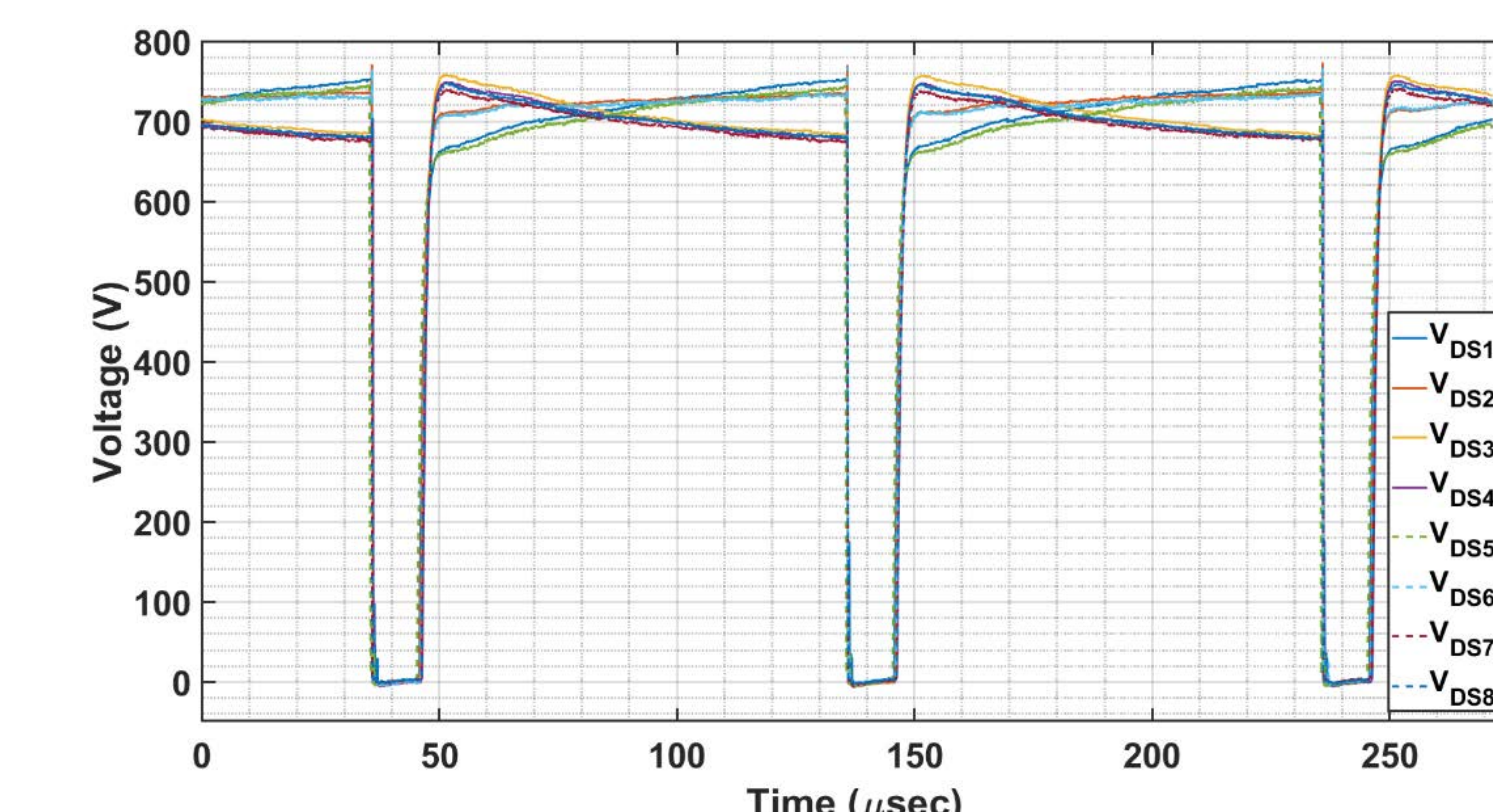
Simulated gate-source ( $V_{GS}$ ) voltages across the eight individual MOSFETs ( $V_{DC} = 6$  kV,  $f_{sw} = 20$  kHz)

- Simulation shows a maximum voltage imbalance close to 60 V among the series-connected MOSFETs.
- The lowest rise time is measured across the switch farthest from the master switch in each module and is recorded close to 13 ns.
- The master MOSFET of each module exhibits the highest rise time in simulation, close to 19 ns.
- The simulated rise time of the entire modular switch was recorded as 17.8 ns

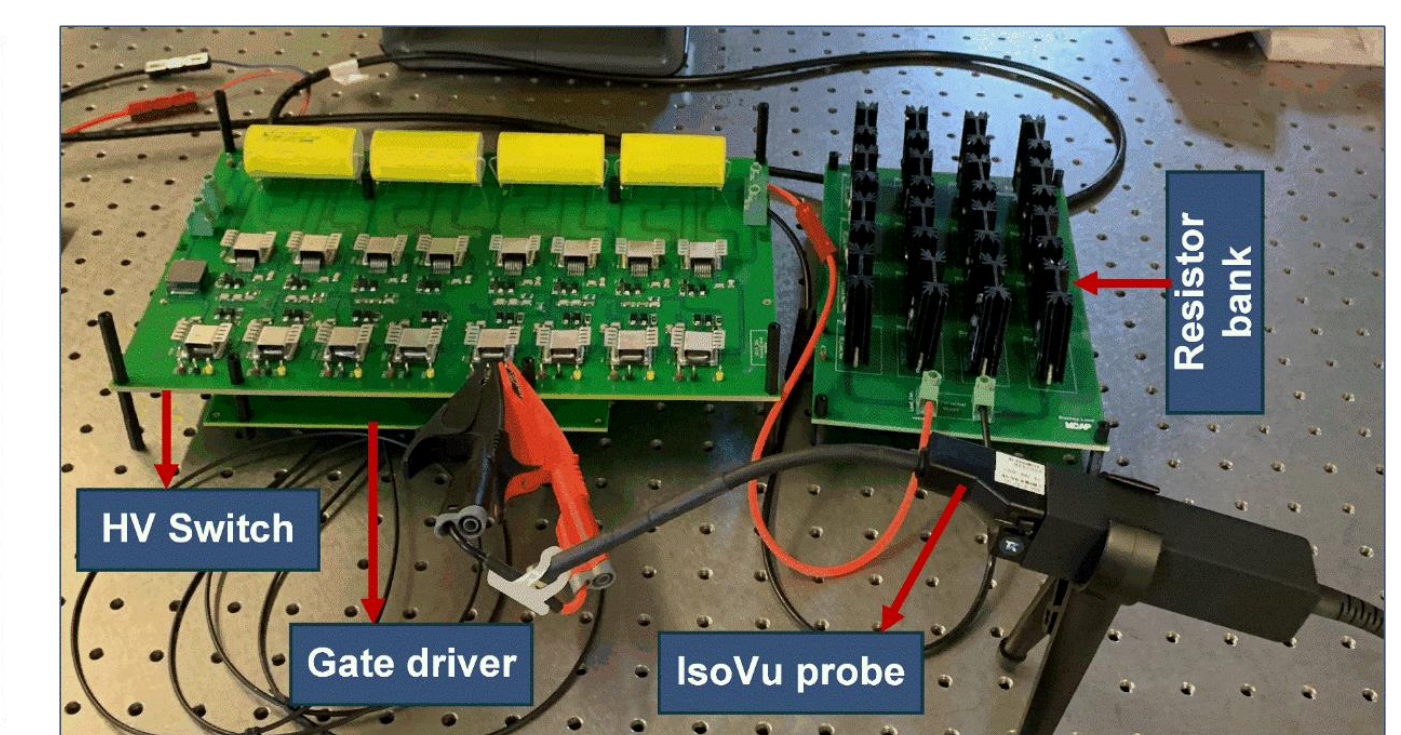
## Experimental Results: 6 kV Excitation



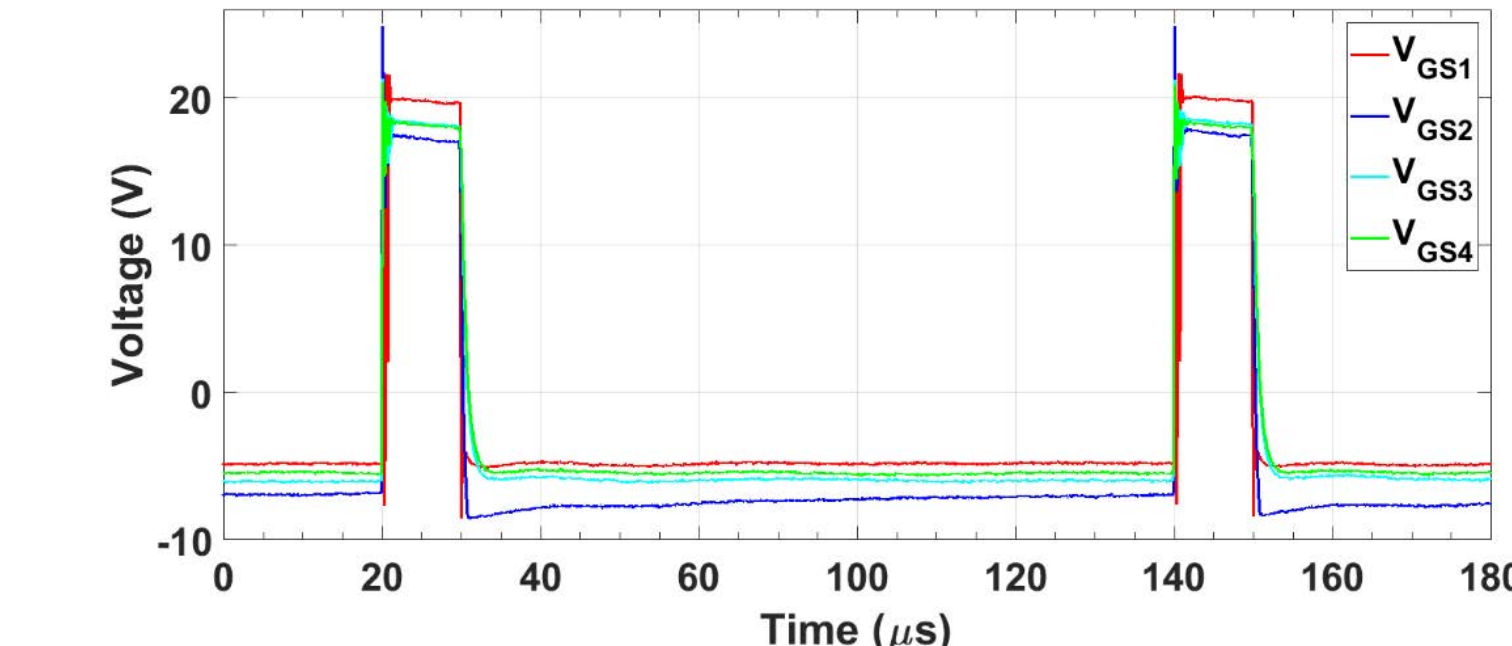
Prototype of a modular 10 kV rated HV switch compatible with negative DC power supply



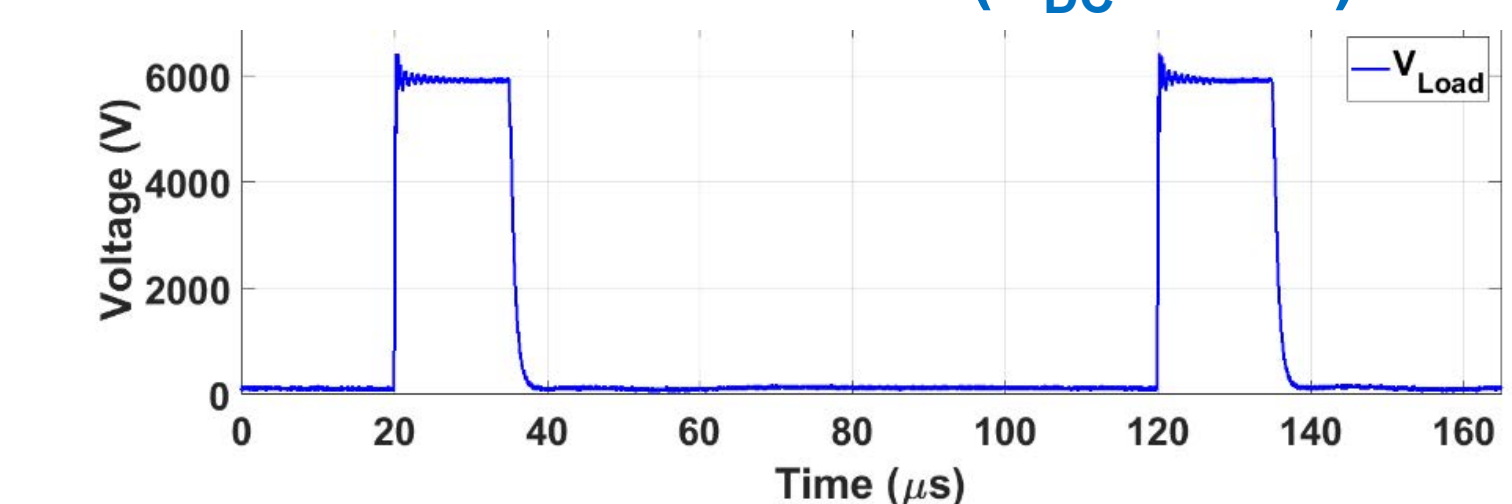
Experimental  $V_{DS}$  measured across the individual MOSFETs ( $V_{DC} = 6$  kV)



Experimental setup of the modular in-house HV switch with a 9.6 kΩ resistive load



Experimental  $V_{GS}$  measured across the individual MOSFETs ( $V_{DC} = 6$  kV)



Experimental voltage measured across the resistive load ( $V_{DC} = 6$  kV,  $f_{sw} = 10$  kHz)

- The modular HV switch has been tested up to a DC supply voltage of 6 kV at a repetition frequency up to 15 kHz with a 9.6 kΩ resistive load.
- A maximum voltage imbalance close to 80 V was recorded among the drain-source voltages across individual MOSFETs.
- The master MOSFET of each module exhibits the highest rise time, close to 52 ns.
- The lowest rise time is associated with the switch farthest from the master switch and recorded close to 41 ns.

## Summary

- An in-house modular (2 modules) 8-stage HV switch ( $\approx 10$  kV rated) has been designed, fabricated and tested up to a DC supply voltage of 6 kV and switching frequency up to 15 kHz using an in-house modular gate driver.
- A modular HV switch with a voltage rating close to 20 kV will be designed and fabricated using new COTS 3.3 kV rated SiC MOSFETs
- A gate driver with higher isolation rating ( $\approx 20$  kV) will be designed and fabricated to drive the 20 kV rated modular HV switch

## Acknowledgement

The authors wish to thank the Office of Naval Research for their support of this work under award no. N00014-17-1-3016

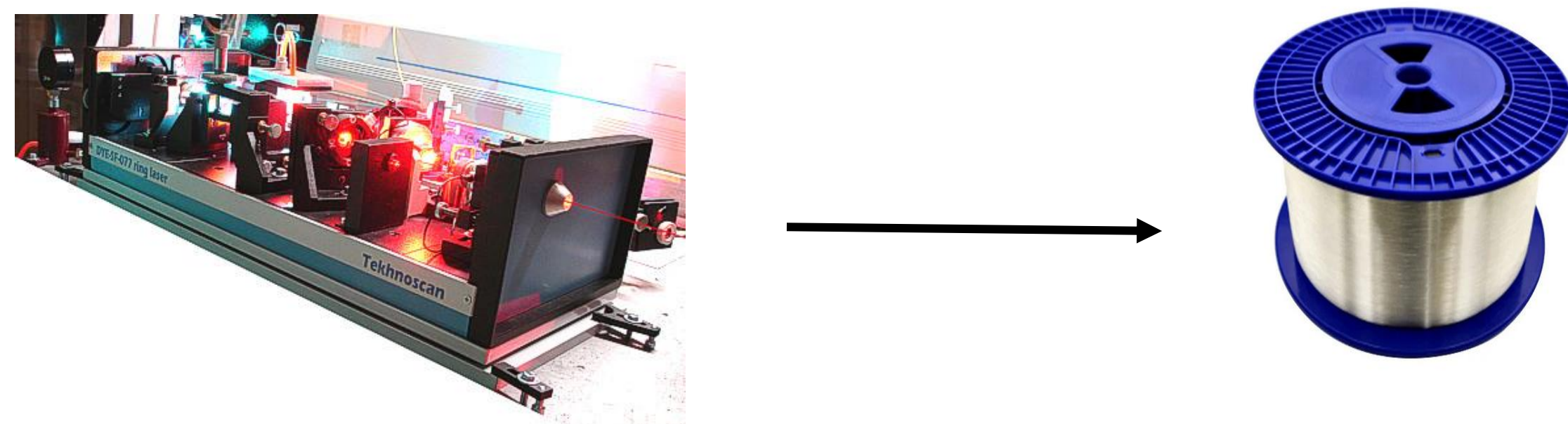
## Cost Reduced Amplifier

### Problem/Solution Space

Laser size and costs have long been the Achilles heal of photo-conductive semiconductor switch (PCSS)-based systems.

Scalable and modular systems to place on Naval vessels must be small, lightweight, have minimal cooling requirements and be monetarily inexpensive.

Fiber Lasers comprised of optical fiber amplifiers, fed by a low-power stable seed laser diode, can offer a cost-effective, low-weight and small-volume solution. Larger surface areas of active media also diminish the cooling requirements.



## Reduction in Pump Power Cost

**Goal:** Reduce the dominant laser cost, of pump power systems by a factor of two. SOTA Ytterbium-doped fiber amplifiers (optimized for LIDAR and laser cutting) are lightweight and readily cooled, but the optical pump power system costs are prohibitive by a factor of two. We devised a **pre-burst optical pumping scheme**, which for our burst profile can reduce costs by a factor of **forty**. This **breaks the pump-power cost bottleneck**.

For example: a high-performance laser of 240 μJ/pulse at 500 kHz repetition rate that was originally at \$173,000 in pump power costs could be pumped for only \$4,300.

**Risks and Challenges:** The major risk of cutting cost by pumping outside the bust time is that the amplified spontaneous emissions (ASE) noise will increase from pumping while the population inversion not dropping from pulses. The increased ASE could lead to excessive heating and timing-jitter in the PCSS.

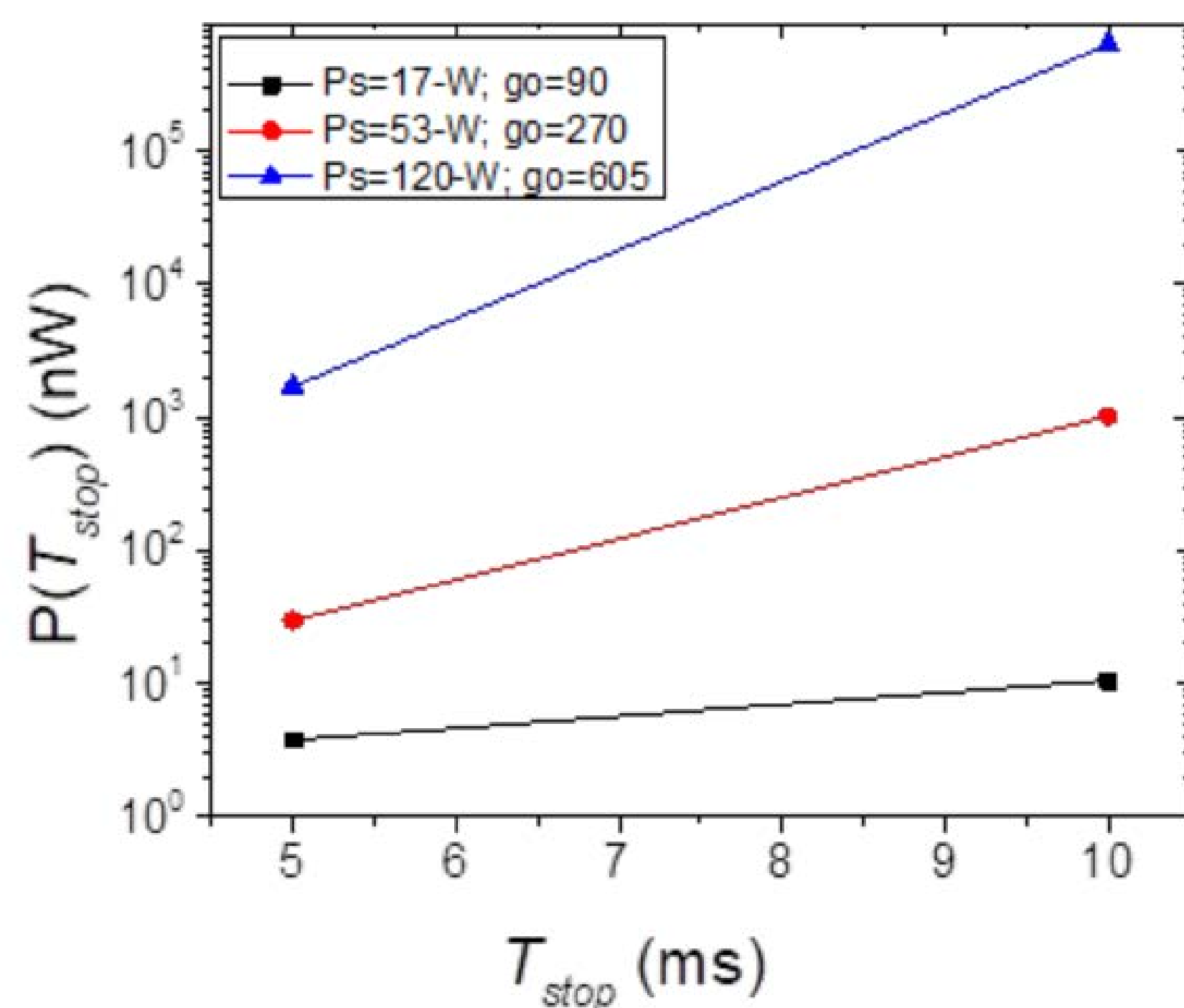
## Cost Reduced Optical Pumping Scheme

Simulations reveal that our technique can dramatically reduce optical pumping power costs, with tolerable pre-burst ASE enhancement: < 640 μW (our heat limit) in a 10 ms pre-burst pumping time.

ASE power growth during pre-burst time [5 to 10 ms].

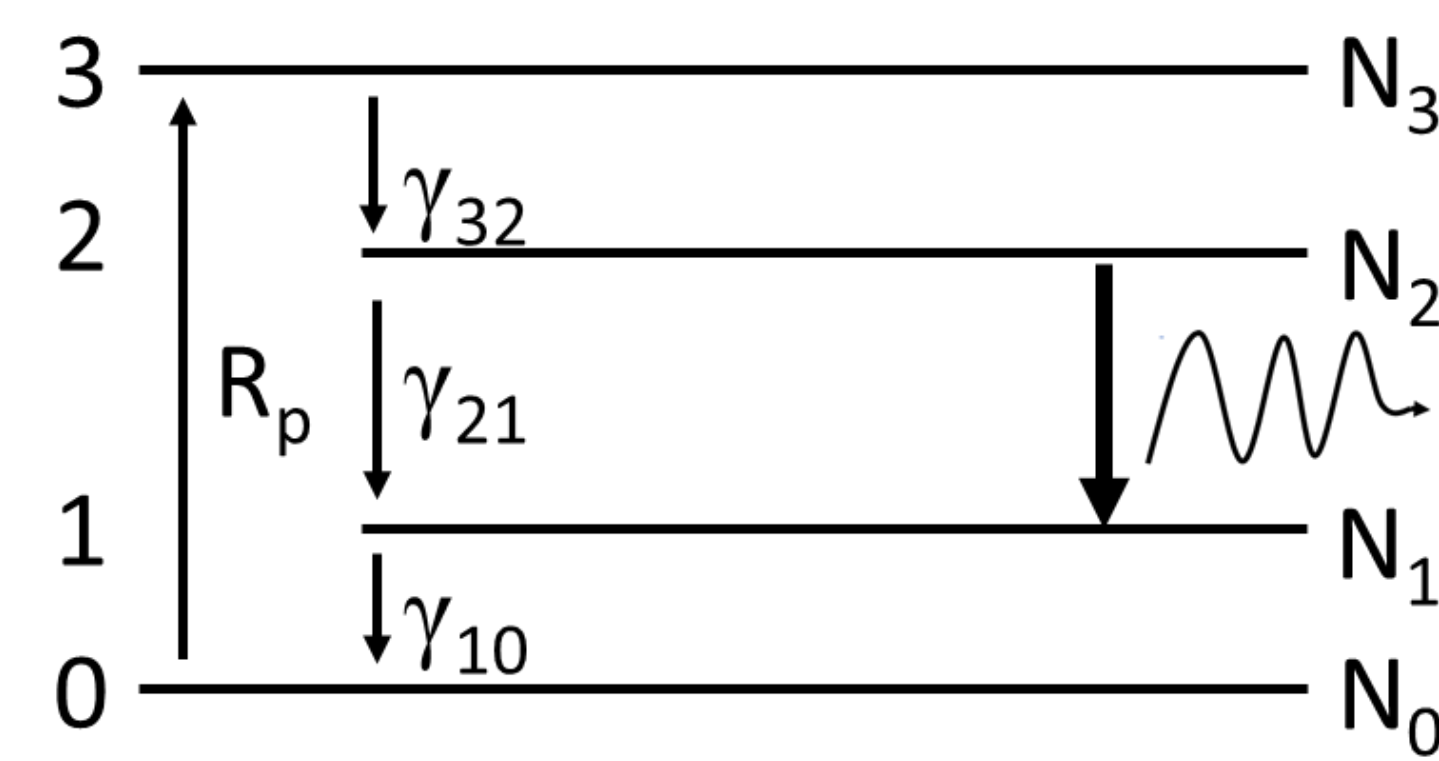
At 10 ms the 120 W system (of pumping rate  $g_0 = 650$ ) grows to 626 μW.

At 10 ms the 53 W system (of pumping rate  $g_0 = 270$ ) grows to 1.02 μW.



## Low Noise Amplifier

### Background: The Equations



the rate equations

$$\frac{d}{dt} N_2 = -\frac{N_2}{\tau_p} + 2\sigma v_g N_2 n_L + R_p$$

$$\frac{d}{dt} n_L = -\frac{n_L}{\tau_p} + 2\frac{\sigma v_g}{V} N_2 (n_L + \frac{1}{V})$$

$\gamma_{10}$  is fast  $\rightarrow N_1 \approx 0$  become

$$\frac{d}{dt} g = -\frac{g - g_0}{\tau_L} - \frac{gP}{E_{sat}}$$

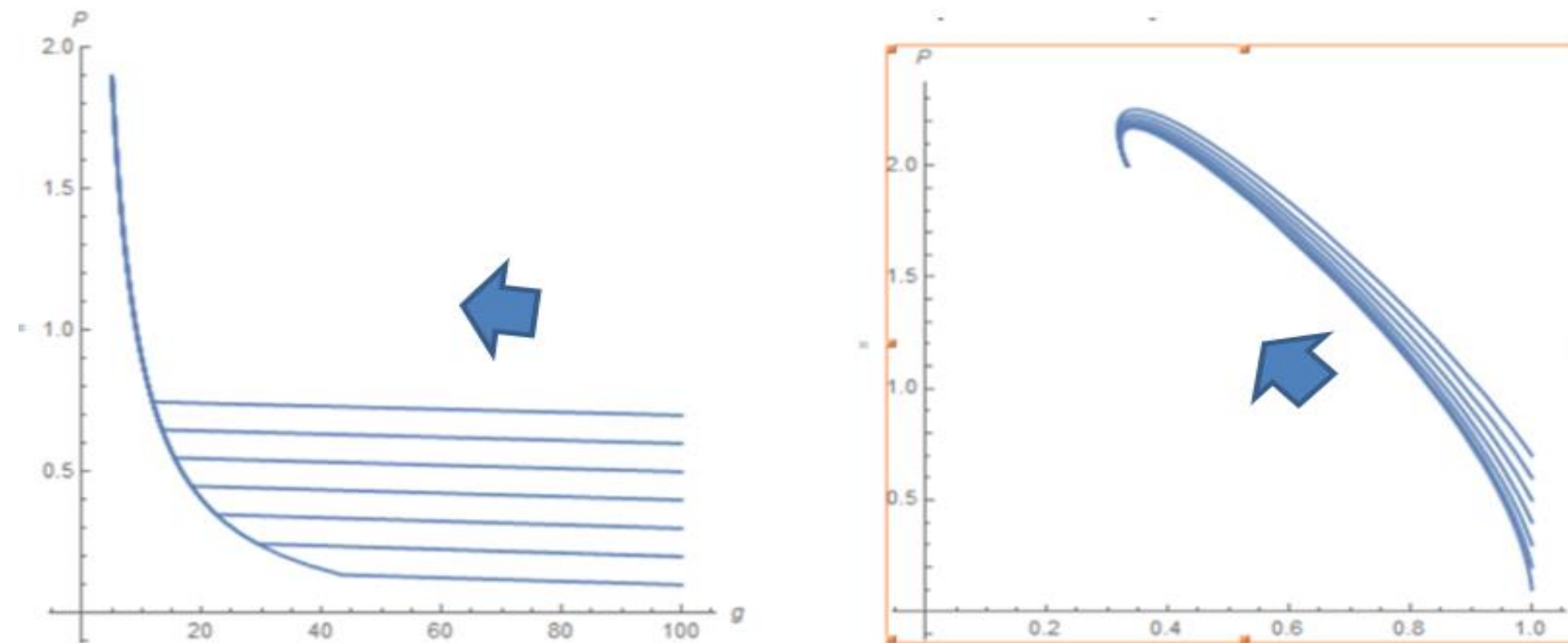
$$\frac{d}{dt} P = -\frac{1}{\tau_p} P + \frac{2g}{T_R} (P + P_{vac})$$

Constants

$g_0$  = initial gain, linearly proportional to the pumping rate/pump power  
 $\tau_p$  = Cavity loss time constant (or loss per length in fiber amp)  
 $E_{sat} = P_{sat} * T_L$ , where  $T_L = T_1 = T_{sp}$  = Spontaneous decay rate time constant and  $P_{vac} = \frac{1}{2} (h * f) BW > 1$  nW at 1064 nm is what turns into ASE

## Saturable Gain Model

SATURABLE GAIN MODEL HAS ONLY ONE STABLE CRITICAL POINT  
**P = Output Power g = Gain**

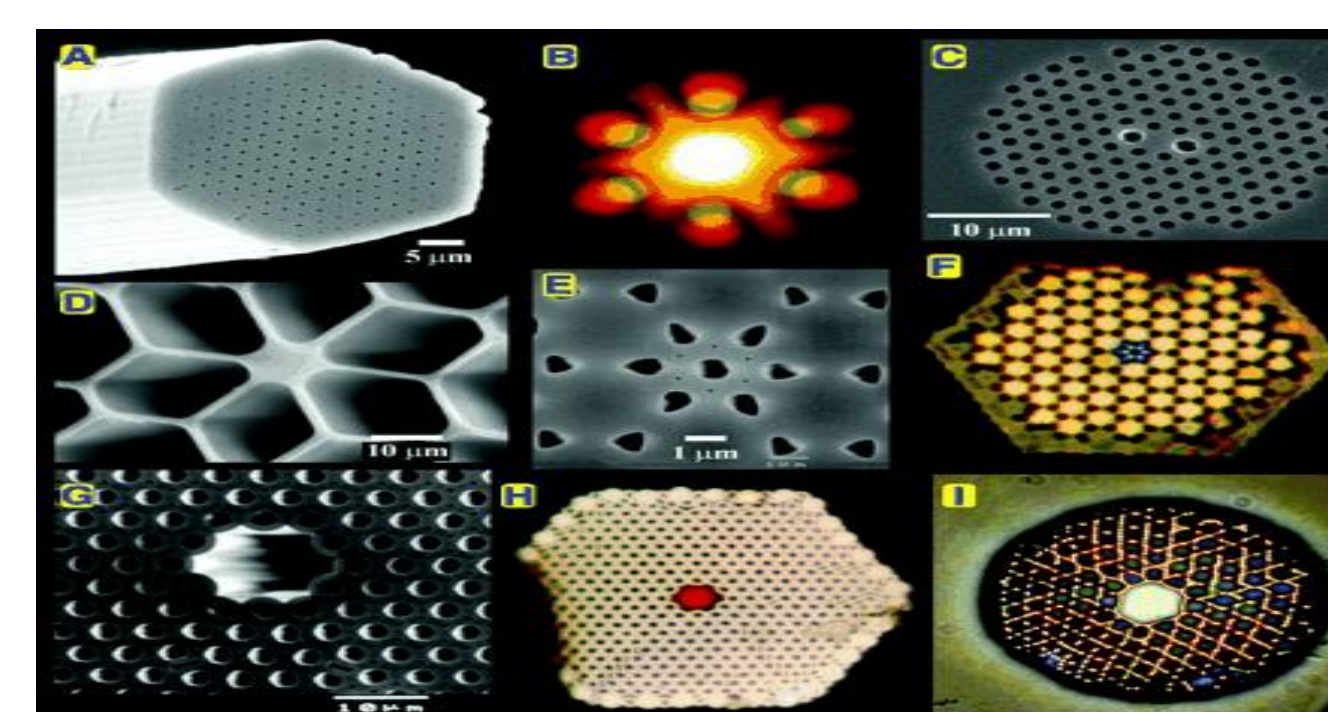


Gain and power converge to the unconditionally stable ( $g_{cp}, P_{cp}$ ).

Simulations show we can utilize this to suppress ASE by 3 orders of magnitude.

## Low Timing-Jitter Laser System

The major Risk in our solution of suppressing ASE via gain saturation (while adapting the mode diameter at each amplifier stage) is: **that gain saturation will also distort the optical pulse shape.**



But the Payoff is huge: 3 orders of magnitude. The major Challenges are: to utilize dispersion and nonlinearities to improve pulse-shape and minimize timing-jitter.

[Adding a photonic crystal fiber stage should suffice.]

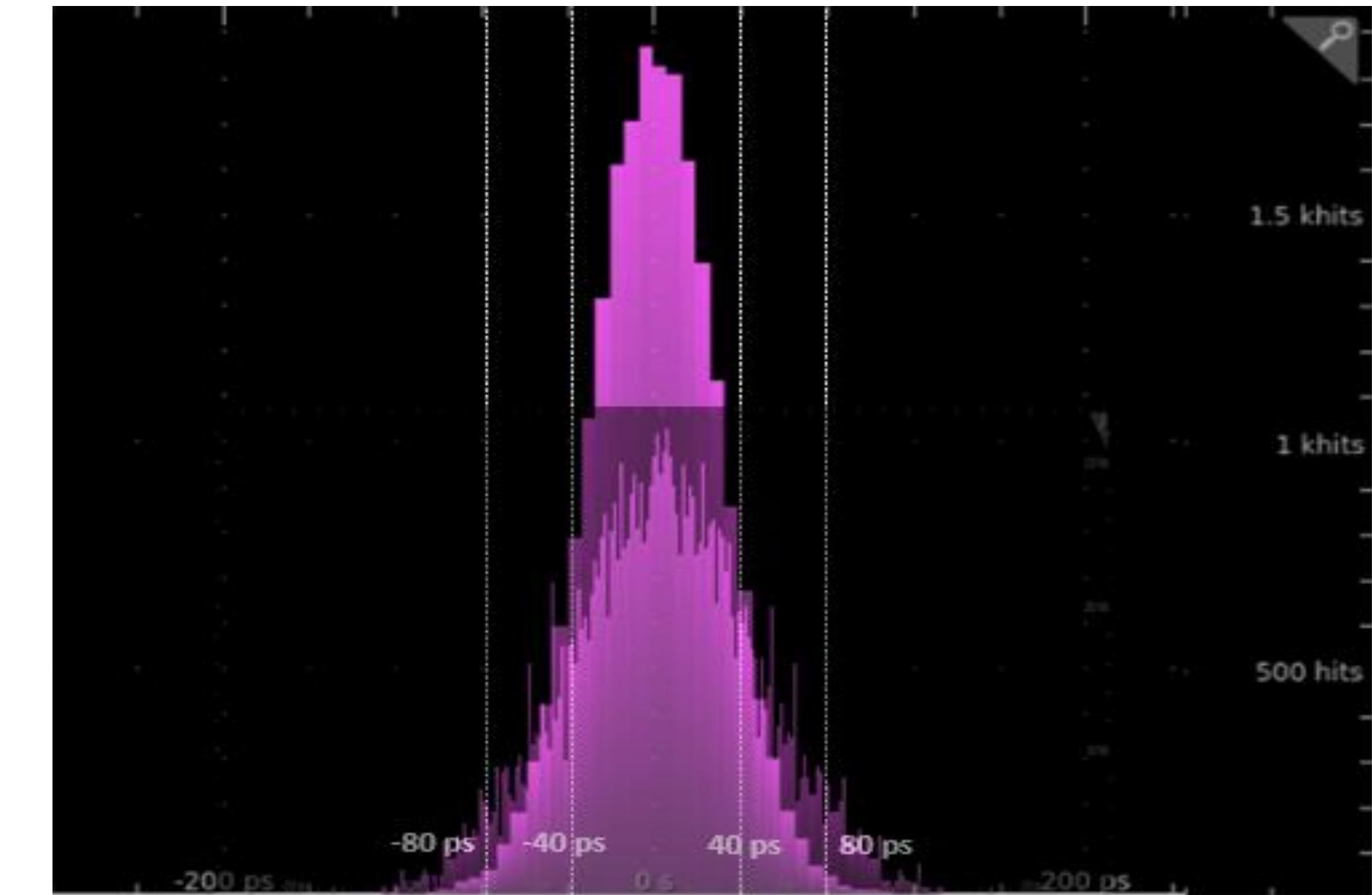
Similarly we can reduce nonlinearities (by a factor of 204) and increase surface area (by 100) in a tubular core amplifier (2.5mm OD and 100 micron thickness) with respect to 50 micron cylindrical core fiber of the same length.



## Experimental Progress

We are constructing **proof-of-concept experiments**. These utilize a low-jitter seed laser diode (of DFB = distributed feedback technology)

### TIMING JITTER OF SEED DIODE WITH WEDGE JITTER OVERLAY FOR COMPARISON



Timing jitter of the seed laser diode was measured to be +/-15 ps with a probability greater than 0.9. (in contrast to that of a wedge laser at +/-40 ps with a probability greater than 0.9). The measurements confirm DFB quality.

The fiber amplifier build/experiments are targeted for completion August 2021.

## Summary

- A **pre-burst pumping scheme** can reduce the (dominant) pump power costs by a factor of 40, with negligible ASE enhancement.
- **Gain saturation can suppress the ASE** (for a system of gain =  $8 \times 10^6$ ) by a factor of 9,525 in a staged design of different fiber cores enhancing saturation while remaining below stimulated Brillouin (SBS) and Raman (SRS) thresholds.
- Gain saturation can suppress the ASE (for a system of gain = 12,500) by a factor of 274 in a 2-stage design of different fiber cores enhancing saturation while remaining below SBS and SRS thresholds.
- We are **building** the gain = 12,500 fiber amplifier/laser design via a Yb-doped dual-clad fiber (2 meter) preamp and a (6 meter) power amp.
- **Timing jitter measurements** of our DFB seed laser diode are within spec.
- HEL (**high energy lasers**) benefit from our lower cost and lower noise amplifiers because they **combine** a large number of fiber lasers (in phase).

## Acknowledgement

This work was supported by the Office of Naval Research, Award No. N00014-17-1-3016.

## Objective

Design and implement a compact (~1.1 cu-ft), lightweight (<10–12 lbs.), and inexpensive (<\$15,000) alternative for conventional high average power optical trigger (laser) system capable of sub nanosecond pulse widths and MHz order pulse repetition rates.

## Relevance to OSPRES Objective

Provides an alternative solution for conventional laser driver subsystem(s) used in photoconductive semiconductor switch (PCSS) activation with enhanced SWaP-C<sup>2</sup> compliance and a subsequent impact on overall HPM system cost, volume, and power (optical and electrical) requirements.

## Background

Acute optical pulse energy requirements in PCSS-driven HPM-based defense systems have brought forth a need for high average-power 1064-nm picosecond lasers with ancillary optics, auxiliary power and cooling subsystems. Being bulky (>5000 cm<sup>3</sup>W<sup>-1</sup>), heavy (~125 lbs.) and expensive (>\$1000 μJ<sup>-1</sup>pulse<sup>-1</sup>) while requiring second and third harmonic generation (SHG/THG) optics to trigger WBG solids (GaN/SiC), these subsystems return a degraded SWaP-C<sup>2</sup> index. While most of the size and weight constraints arise from driver and control subsystem, a laser in this class would occupy a volume of ~10 cu-ft and provide an average power of 50 W, requiring 5.67 x 10<sup>3</sup> cm<sup>3</sup> W<sup>-1</sup>.

Despite being an established market, the existing state-of-the-art (SOTA) pulsed drivers only satisfy either the high output current (>110 Amp) requirement or fast transients (<1 ns FWHM) at ~MHz PRR while maintaining a compact form factor. This effort proposes a one-stop solution based on compact optical sources like laser diode arrays (LDAs) that is compact (<0.75cu-ft), capable of >120 A output current, <1 ns pulse widths at <200 ps rise time (t<sub>r</sub>) and >1 MHz PRR. This provides a SWaP-C<sup>2</sup> optimized solution for the driver subsystem of an LDA-based optical source by implementing a multi-stage driving circuit.

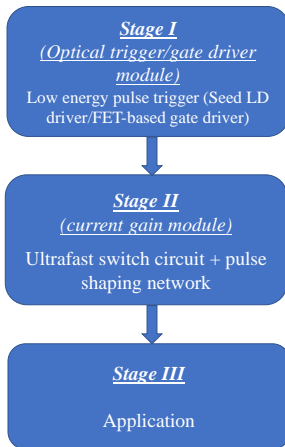


Figure: Block diagram showing different stages of implementation

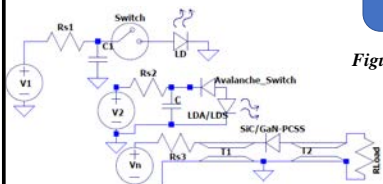
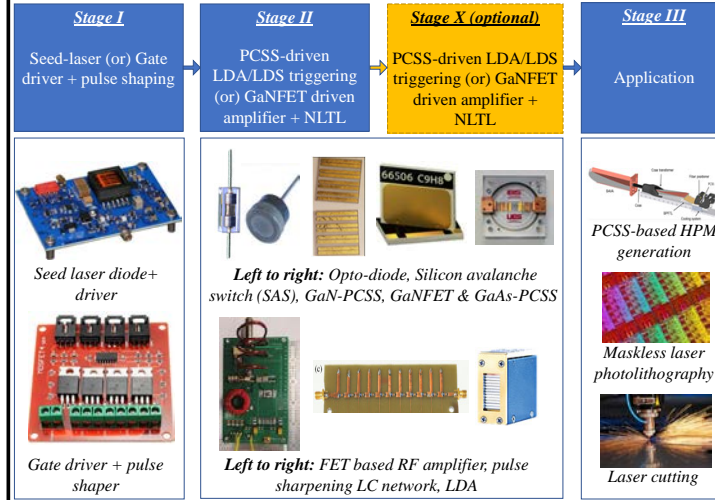


Figure: Schematic showing multi-stage current amplifying optical source driver

## Approach

### Multi-stage pulse amplification and sharpening:



## Potential Implementation Paths

Switch Tech.	SOTA	Pros	Cons
GaAs-PCSS	<ul style="list-style-type: none"> <li>&gt;10 kV hold-off</li> <li>Optically induced avalanche capable</li> <li>Sub-ns t<sub>r</sub></li> <li>~ns fall time (t<sub>f</sub>)</li> </ul>	<ul style="list-style-type: none"> <li>Electrical isolation</li> <li>Mature device tech.</li> <li>High e<sup>-</sup> mobility</li> <li>Sub-ns transients</li> </ul>	<ul style="list-style-type: none"> <li>Device degradation due to Joule heating</li> <li>Low device lifetime</li> <li>Avalanche at &gt;10kV</li> <li>COTS unavailability</li> </ul>
GaN-PCSS	<ul style="list-style-type: none"> <li>&gt;5 kV hold-off</li> <li>Sub-ns t<sub>r</sub></li> <li>ns-order t<sub>f</sub></li> </ul>	<ul style="list-style-type: none"> <li>Electrical isolation</li> <li>Sub-ns transients</li> <li>Avalanche @ 3.5kV/cm</li> </ul>	<ul style="list-style-type: none"> <li>Immature device tech.</li> <li>Expensive</li> <li>COTS unavailability</li> </ul>
Silicon Avalanche Switch (SAS)	<ul style="list-style-type: none"> <li>&gt;&gt;5 kV hold-off</li> <li>Sub-ns t<sub>r</sub></li> <li>ns-order t<sub>f</sub></li> </ul>	<ul style="list-style-type: none"> <li>Avalanche @ 1kV/ns rise rate</li> <li>Inexpensive solution</li> <li>sub-ns risetime possible</li> </ul>	<ul style="list-style-type: none"> <li>High jitter &amp; carrier lifetime</li> <li>COTS unavailability</li> </ul>
FET-run frozen wave generator	N/A	<ul style="list-style-type: none"> <li>Inexpensive</li> <li>FET implementable</li> <li>Tunable transients</li> </ul>	<ul style="list-style-type: none"> <li>Bipolar pulse – not ideal for LDA trigger</li> </ul>
GaN-FET closing switch	<ul style="list-style-type: none"> <li>2-ns t<sub>rise</sub></li> <li>&gt;900V V<sub>ds</sub></li> </ul>	<ul style="list-style-type: none"> <li>Inexpensive</li> <li>COTS availability</li> </ul>	<ul style="list-style-type: none"> <li>Need for additional pulse shaping network for current gain stage</li> </ul>
Opto-diodes & opto-couplers	<ul style="list-style-type: none"> <li>15 kV hold-off</li> <li>Integrated high gain LED</li> </ul>	<ul style="list-style-type: none"> <li>Electrical isolation</li> <li>High voltage rating</li> <li>Integrated optical source</li> </ul>	<ul style="list-style-type: none"> <li>Need &gt;100-μJ optical pulse energy</li> <li>Slow turn-off (~ 3 μs)</li> </ul>

Table I: Table showing the potential paths of implementation being considered, their state-of-the-art capabilities, as well as pros and cons.

## Implementation Challenges/Risks

### I. PCSS-based implementation:

- Negative currents due to PCSS ringing during recovery
- System interconnect design issues at >150 °C operation.

#### a) GaN-PCSS

- Unconfirmed avalanche at <50 V bias
- Unquantified compensated device parameters

#### b) GaAs-PCSS

- Poor device longevity
- Undemonstrated low field avalanching

#### c) Opto-diodes & opto-couplers

- Need for >100 μJ optical pulse energy
- Laser attenuation and thermal handling

### II. Non-PCSS based implementation:

- Limiting jitter to <10-20 ps at low voltages
- Need for pulse shaping networks as GaN-FET SOTA t<sub>r</sub> ≥ 2 ns

#### a) Silicon avalanche switch

- Need custom devices with carrier lifetime engineering

#### b) FET driven frozen wave generators (FWG)

- Need for high-speed rectifier circuit to convert bipolar output to unipolar

## Future Work

PCSS-based: Perform pulse testing of Si optodiodes and GaN-PCSS at ~1μJ/pulse for baseline SOTA data and use TCAD modeling for parametric study.

Non-PCSS-based: Perform SPICE simulations to validate jitter limitations, effectiveness of D-NLTLs for pulse sharpening and perform TCAD simulations for custom SAS as required.

## References

- J. Y. Tsao, S. Chowdhury, M. A. Hollis, D. Jena, N. M. Johnson, K. A. Jones, R. J. Kaplar, et al. 2018. "Ultrawide-Bandgap Semiconductors: Research Opportunities and Challenges." *Advanced Electronic Materials* 4 (1): 1–49. <https://doi.org/10.1002/aeml.201600501>.
- C. R. Wilson, M. M. Turner and P. W. Smith, "Pulse sharpening in a uniform LC ladder network containing nonlinear ferroelectric capacitors," *Nineteenth IEEE Symposium on Power Modulators*, 1990, pp. 204-207, doi: 10.1109/MODSYM.1990.201058
- S. Best, M. F. Rose, Z. Shotts, M. Rader and L. L. Altgiers, "Frozen Wave Generator technology as a source of constant amplitude high power high frequency radio frequency pulses," *2013 19th IEEE Pulsed Power Conference (PPC)*, 2013, pp. 1-6, doi: 10.1109/PPC.2013.6627507.
- E. A. Hirsch et al., "High-Gain Persistent Nonlinear Conductivity in High-Voltage Gallium Nitride Photoconductive Switches," *2018 IEEE International Power Modulator and High Voltage Conference (IPMHVC)*, 2018, pp. 45-50, doi: 10.1109/IPMHVC.2018.8936660.
- C. V. Reddy, K. Balakrishnan, H. Okumura, and S. Yoshida, "The origin of persistent photoconductivity and its relationship with yellow luminescence in molecular beam epitaxy grown undoped GaN", *Applied Physics Letters* 73, 244-246 (1998) <https://doi.org/proxy.library.umkc.edu/10.1063/1.106311>
- M. Zhang, R. Yang, N. Liu, and X. Wang, "Persistent photoconductivity in neutron irradiated GaN", *Journal of Semiconductors* 34, Vol 9, doi: 10.1088/1674-4926/34/9/093005

## Acknowledgement

This work was supported by the Office of Naval Research, Award No. N00014-17-1-3016.

## Objective

Analyze the circuit component value's and topology permutation's tradespace for qualitative trends in the case of a Semiconductor Opening Switch (SOS)-inductive energy storage (IES) topology. Identify parametric relationships that yield the greatest peak power output, lowest rise time, and best-case efficiency for this topology given theoretical and real-world constraints.

## OSPRES Relevance

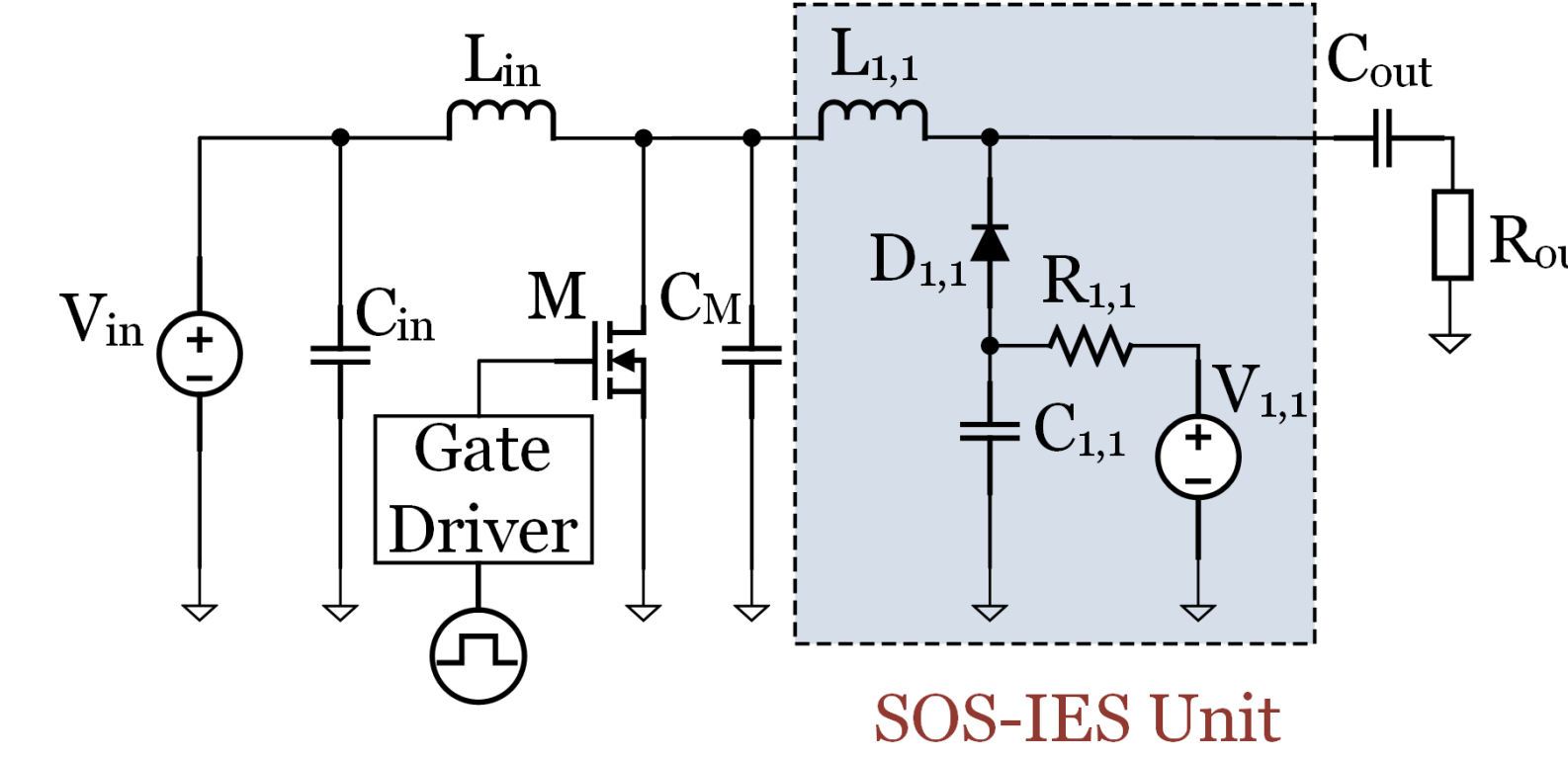
SOS-based sources can remove the need for photo-triggered switches and their laser subsystems. They are ideal for triggering sub-nanosecond rise time sharpeners (SAS, DNLTL, etc), summarily improving SWaP-C2

## Background

SOS-based pulse generators use inductive energy storage (IES) to generate nanosecond, megawatt pulses on 50-Ω loads. Certain SOS-pulse generators can produce up to ones of gigawatts in ones of nanoseconds but suffer from non-standard load impedances and low volumetric power densities (~50 kW/m<sup>3</sup>). The topology investigated in this poster has the potential to produce hundreds-of-megawatts on 50-Ω without taking up more than 2000 cm<sup>3</sup> and weighing less than 3 kg (~1.5 GW/m<sup>3</sup>). The modular topology leverages the series and parallel additions of base SOS-IES units to achieve greater output power and pulse repetition rates than alternative SOS topologies.

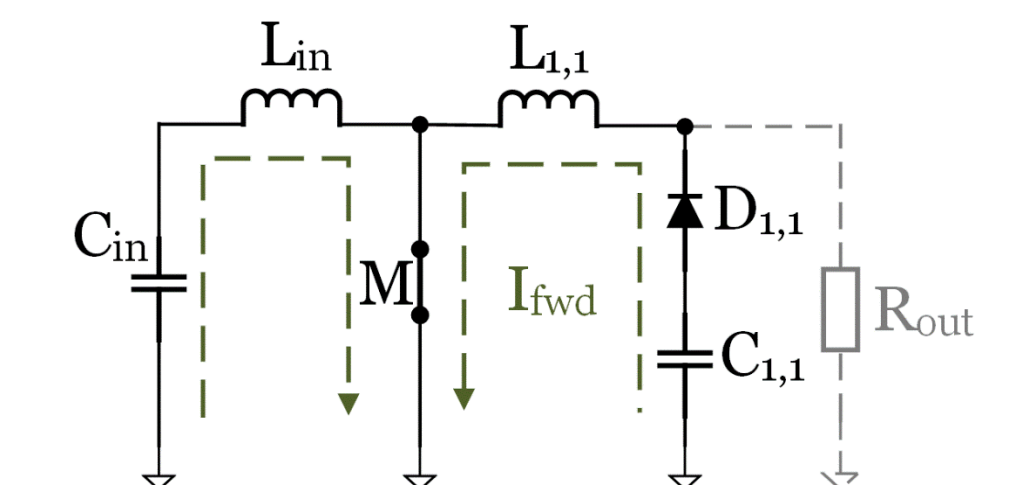
## SOS-IES Unit

The base SOS-IES unit is shown in fig. 1. It consists of an inductor ( $L_1$ ), SOS diode-assembly ( $D_1$ ), and capacitor ( $C_1$ ) charged to a bias voltage ( $V_1$ ). The circuit is trigger by a primary switch (i.e., SiC MOSFET).  $C_{out}$  is a high-pass filter to remove DC from the output.

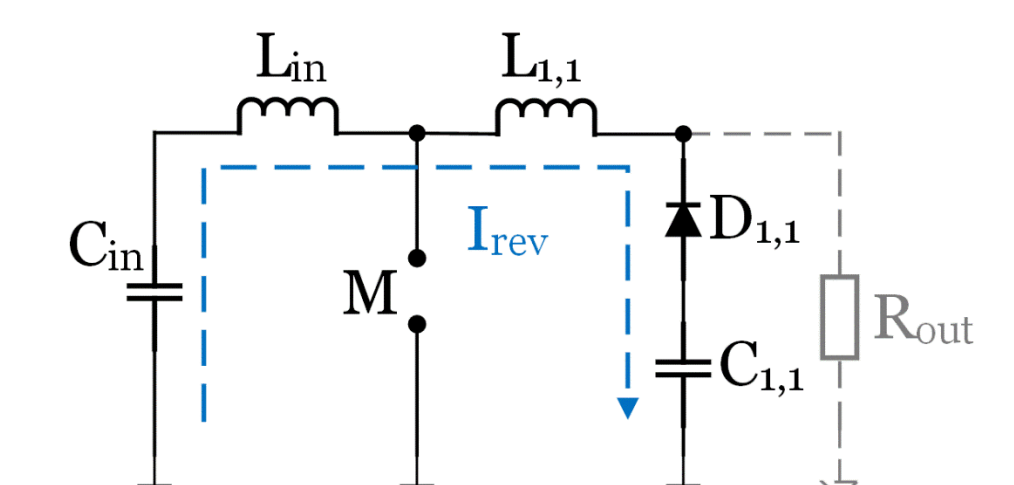


## Circuit Operation

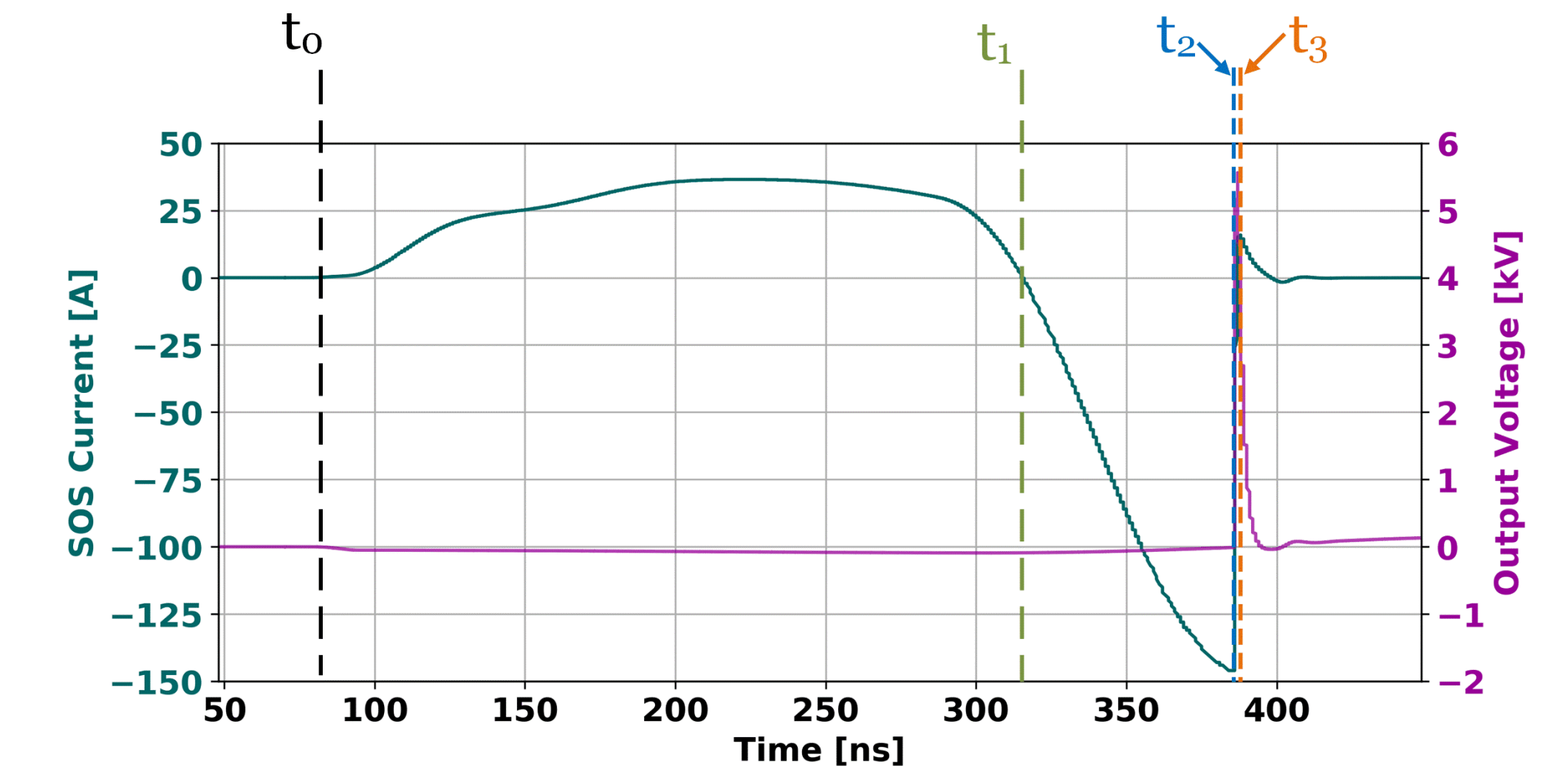
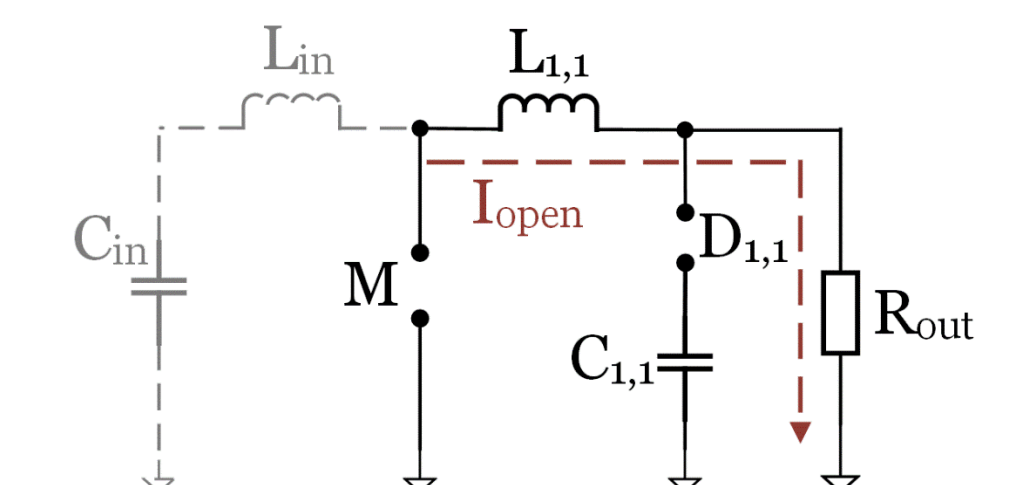
**Step 1 – ( $t_0 - t_1$ )**  
The primary switch is activated by a high gate signal, causing the unit's capacitor to discharge through the SOS, injecting excess carriers.



**Step 2 – ( $t_1 - t_2$ )**  
After some time (i.e., ~220 ns in the example below), the primary switch opens resulting in the current reversal in the SOS-IES unit and charging  $L_1$  with current.



**Step 3 – ( $t_2 - t_3$ )**  
Once the accumulated charge in the SOS has been extracted, the diode rapidly recovers to its open state. This interrupts the current in  $L_1$  resulting in a voltage pulse on the load.



## Parameter Tradespace

The values of the inductor, capacitor, and bias voltage in each unit influence the opening-speed of its SOS diode. The inductor-capacitor pair act as resonant energy stores, and the bias voltage determines the initial stored charge in the unit. Together these determine the amplitude ( $I_{fwd,n}$ ) and duration ( $t_{fwd,n}$ ) of the forward current, or charge injection period. Both the charge injection duration and total charge injected into the SOS determine the rate-of-opening. Then, because the output is a function of  $di_{rev}/dt_{open}$ , the circuit's output can be related to the unit's parameter values.

$$(1) V_{out} \approx I_{rev} R_{out} \approx L \frac{di_{rev}}{dt_{open}}$$

Conditions for shorter SOS opening time ( $t_{open}$ )<sup>[1]</sup>:

- Shorter injection duration ( $t_{fwd}$ )  $\rightarrow$  (2)  $t_{open} \propto t_{fwd}$
- Less injected charge ( $Q_{inj}$ )  $\rightarrow$  (3)  $t_{open} \propto Q_{inj}$
- Greater reverse current ( $I_{rev}$ )  $\rightarrow$  (4)  $t_{open} \propto \frac{1}{I_{rev}}$

Taking  $I_{fwd,N} \approx \frac{V_N}{Z_N}$  with (2):

$$(5) t_{open} \propto \frac{V_N}{Z_N}$$

Isolating the circuit parameters with  $Z_N = \sqrt{\frac{L_{eq}}{C_N}}$ , we get:

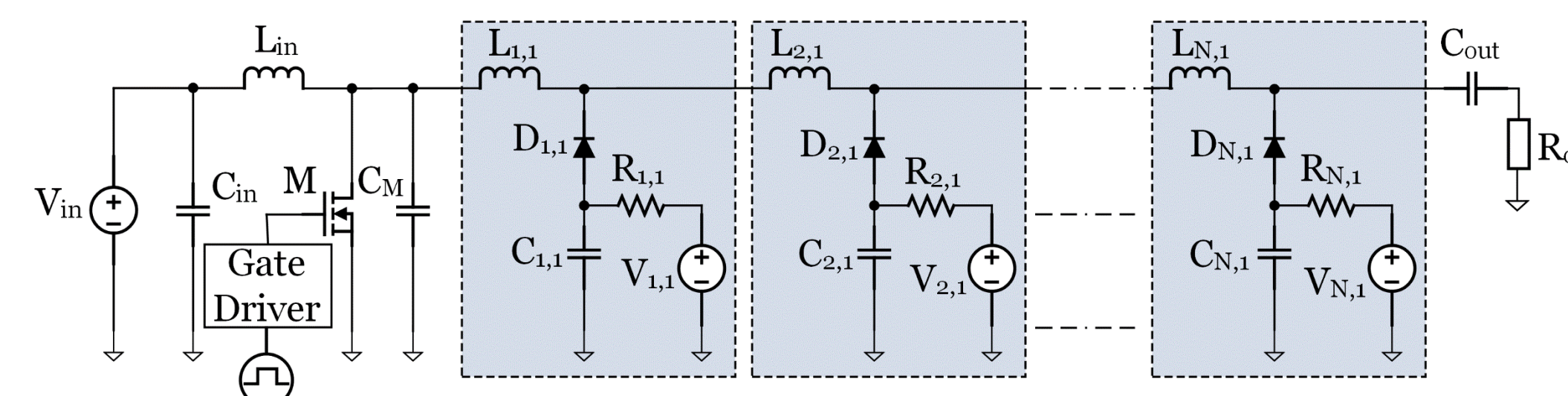
$$(6) t_{open} \propto V_N \quad (7) t_{open} \propto C_N \quad (8) t_{open} \propto \frac{1}{L_{eq}}$$

Hence, to maximize the power output of an SOS-IES unit, or combination of, via component values,  $L_{eq}$  should be increased while  $C_N$  and  $V_N$  decreased. This leads to the optimal forward current waveform.

## Topology Tradespace

### Series Addition

With the series combination of SOS-IES units, the reverse current for unit at n-stage is then driven by the unit before it. The later units also see a greater loop impedance ( $Z_{LC}$ ) during the charge injection phase due to the addition of inductance, consequently reducing  $I_{fwd,N}$ . The consequence of series addition is predicted to be a shorter  $t_{open}$  but reduced  $I_{rev}$ .



Eqns. 12-14 show how the parameter values at each unit are determined. A first order approximation for the equivalent inductance of each unit is shown in (15)

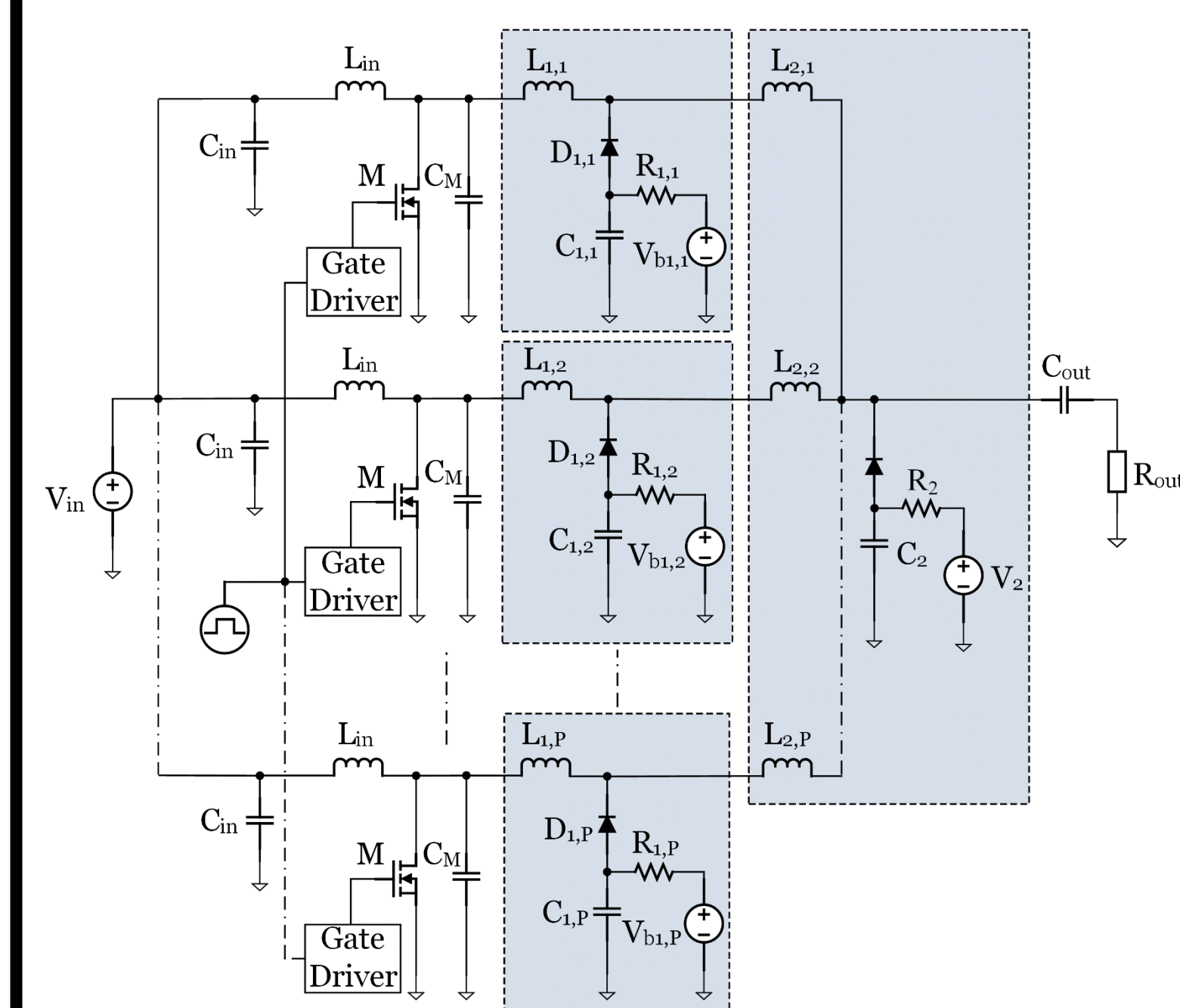
$$(12) V_N = V_1 + \Delta V(N - 1)$$

$$(13) L_N = L_1 + \Delta L(N - 1)$$

$$(14) C_N = C_1 + \Delta C(N - 1)$$

$$(15) L_{eq} = \sum_{N=1}^S L_N$$

### Parallel Addition



In the case of parallel combination of SOS-IES units, the reverse current for the final unit is equal to the prior stage's  $I_{rev}$  multiplied by the number of parallel branches. Although, the decreased equivalent inductance of the final stage (eqn. 16) means a greater  $I_{fwd,N}$  potentially increasing the final  $t_{open}$ ; the combination of this with a proportionally greater  $I_{rev}$  may produce greater power on load (see eqn. 1).

$$(16) L_{eq} = \frac{1}{P} * \sum_{N=1}^S L_N$$

## Summary

The analytical study of the proposed SOS-IES unit circuit as a function of the unit capacitance, inductance, and charge voltage, reveals the following trends:

1. SOS opening speed decreases as unit capacitance and charge voltage decreases.
  2. SOS opening speed decreases as unit inductance increases.
- In the case of series and parallel addition, first order approximations of the equivalent loop impedances for the final output units give a rough prediction of trends:
3. With series addition, inductance and capacitance should decrease in order to decrease SOS opening speed.
  4. With parallel addition, inductance and capacitance should increase in order to decrease SOS opening speed.

The simulated numerical confirmation of these trends is given in the poster of Sourov Roy

## References

- [1] T. Sugai, W. Jiang and A. Tokuchi, "Influence of forward pumping current on current interruption by semiconductor opening switch," in IEEE Transactions on Dielectrics and Electrical Insulation, vol. 22, no. 4, pp. 1971-1975, August 2015

## Objective

To select the optimal permutation of the semiconductor opening switch (SOS)-inductive energy storage (IES) and release topology and its key component parameters (see "Approach" for more information) allowing for the generation of nanosecond-scale hundreds-of-megawatts peak power output from a compact (<2000 cm<sup>3</sup>) and lightweight (<3 kg) pulsed power source.

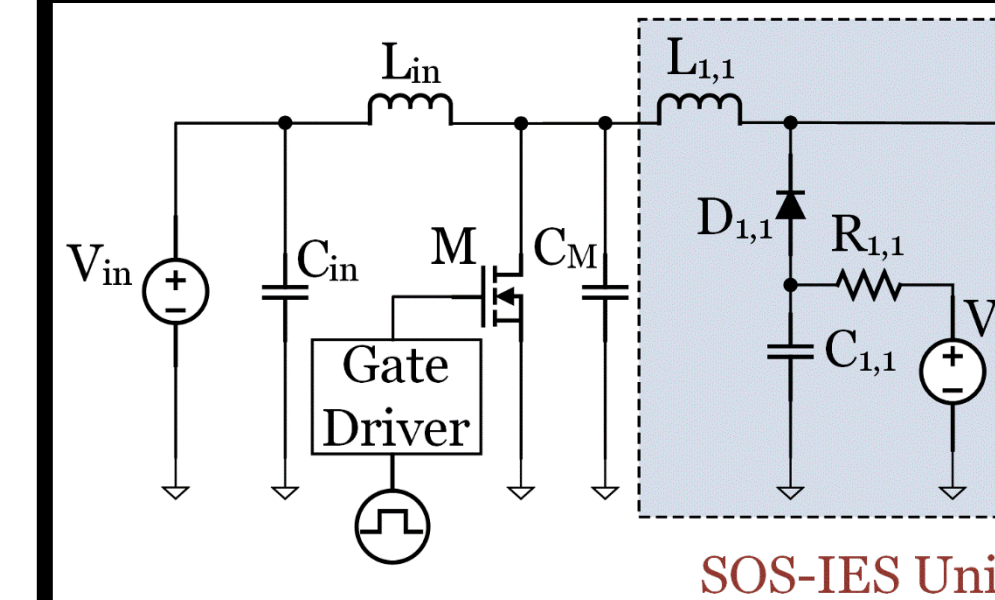
## OSPRES Relevance

SOS-based sources can remove the need for photo-triggered switches and their laser subsystems. They are ideal for triggering sub-nanosecond rise time sharpeners (SAS, D-NLTL, etc.), reducing overall cost, volume, and weight.

## Background

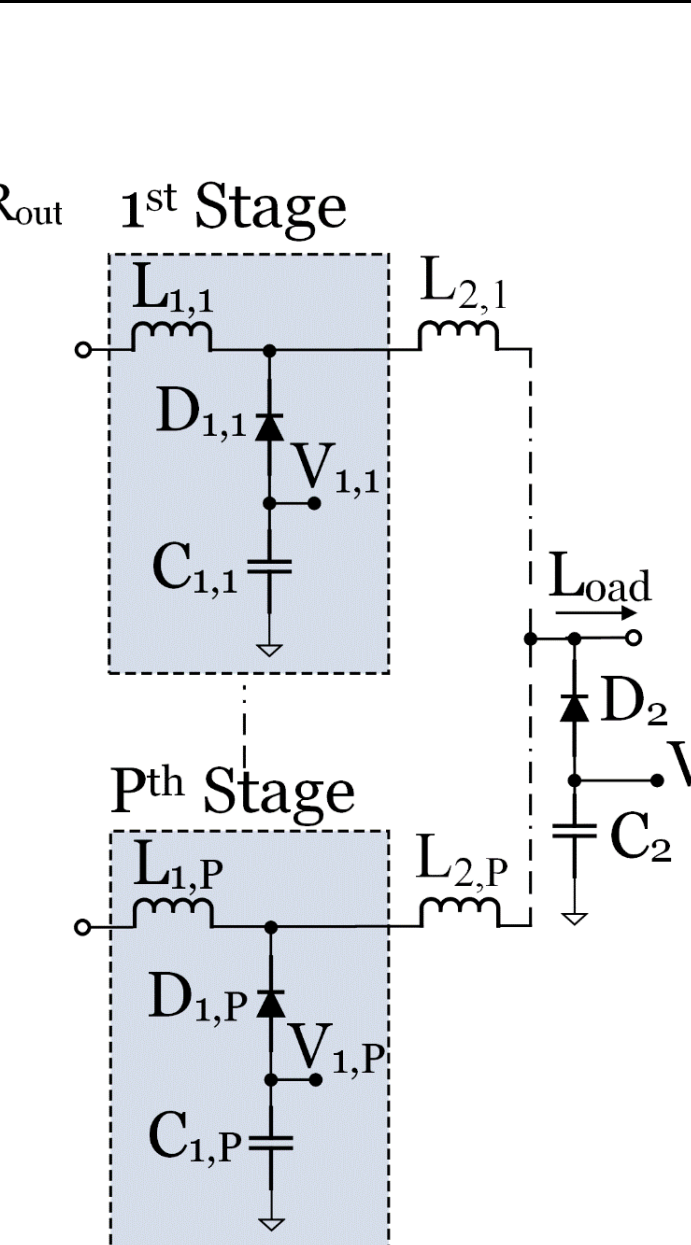
SOS-based pulse generators use IES to generate nanosecond, megawatt pulses on 50-Ω loads. Certain SOS-pulse generators can produce up to ones of gigawatts in ones of nanoseconds, but their applications are limited by the pulser's large size and weight, non-standard load impedances and lower pulse repetition frequencies (PRF). Typically, an SOS itself could be used to pulse another SOS achieving a pulse compression to enhance the output performance. The output can be further improved using these compression stages connected in parallel to drive a later compression stage [1]. The modular topology proposed in this poster leverages this series and parallel addition of the base SOS-IES units to achieve greater output power and PRF than alternative SOS topologies. This is a systematic study of the parameter space of the topology, whereas previous studies attempted to present only the best-case configurations.

## Approach



Circuit Set-up Parameters

V <sub>in</sub>	100 V
C <sub>1</sub>	100 nF
L <sub>1</sub>	100 nH
V <sub>1</sub>	50 V
T <sub>gate,on</sub>	200 ns
L <sub>s</sub>	200 nH
C <sub>in</sub>	10 μF
C <sub>M</sub>	15 nF



**Series cases**  
N = { 1, 2, 3, 4 }  
P = { 1 }

**Parallel cases**  
N = { 2 }  
P = { 1, 2, 3, 4, 5 }

According to (1)-(3), one parameter was varied at a time. Simulations for each configuration of series or parallel unit combination was carried out with respect to the varied parameter.

$$(1) \quad V_N = V_1 + \Delta V(N - 1)$$

$$(2) \quad L_N = L_1 + \Delta L(N - 1)$$

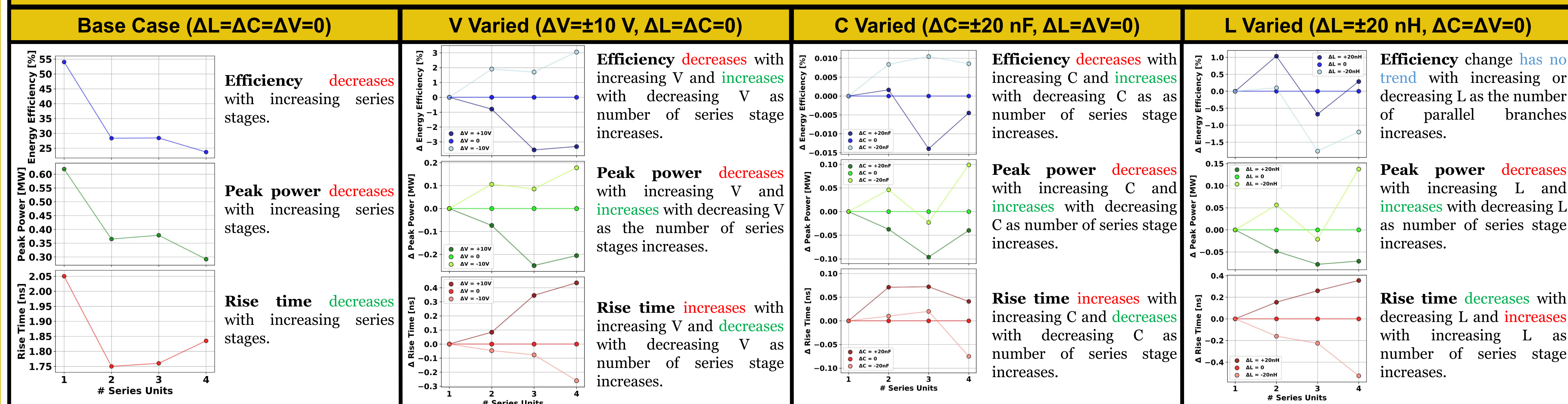
$$(3) \quad C_N = C_1 + \Delta C(N - 1)$$

Parameter	Steps
ΔC	± 20 nF
ΔL	± 20 nH
ΔV	± 10 V

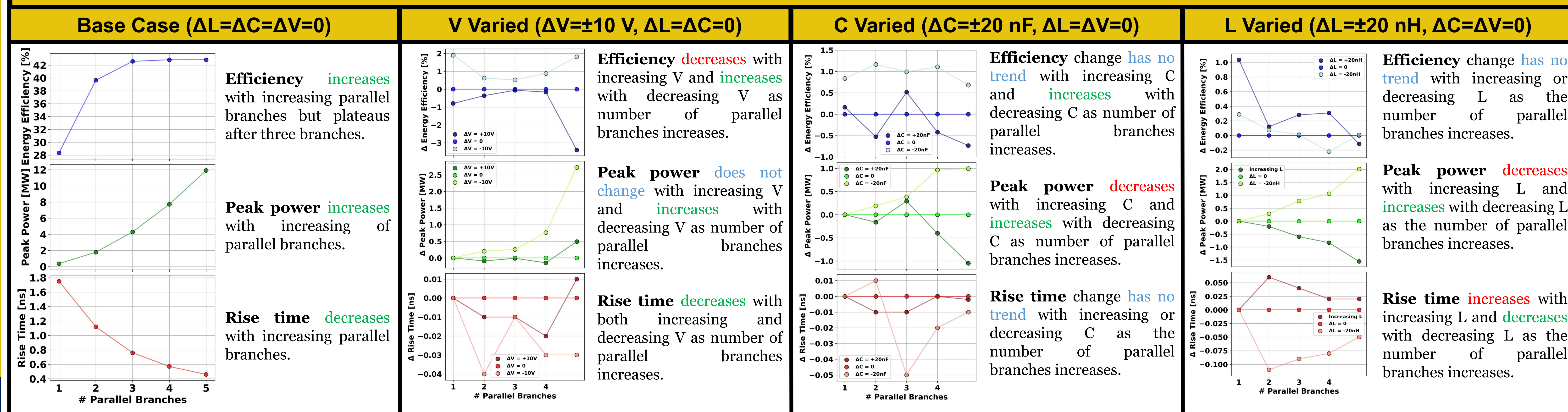
## Results

Influence of series and parallel unit along with the change in L, C, V on the output peak power, pulse rise time, and energy efficiency is shown below.

### Series Addition



### Parallel Addition



## Summary

Spice simulations were used to systematically identify the optimal trends in series-parallel topology and parameter choice for a SOS-IES type pulse generator circuit. The simulation results show:

- The peak power output positively correlates to increasing parallel branches, and negatively correlates to series addition of SOS-IES units. Furthermore, peak power showed positive correlation with the decreasing of all circuit parameters, L, C, and V.
- In both the series and parallel topologies, efficiency improved with the decreasing of circuit parameters C and V but did not correlate with L. Efficiency decreases with the increasing number of series stages and increases with the increasing number of parallel branches and then saturates around 43%.
- The amount of energy into the system is primarily a function of the number of parallel branches. Due to this phenomenon, the peak power improvement due to paralleling does not translate to improved efficiency and may cause the saturation seen in the efficiency (diminishing return) of the parallel base case.

## Future Work

Simulate permutations of the SOS-IES topology wherein more than one parameter (L, C, and V) is varied at a time to confirm the trends in the obtained results.

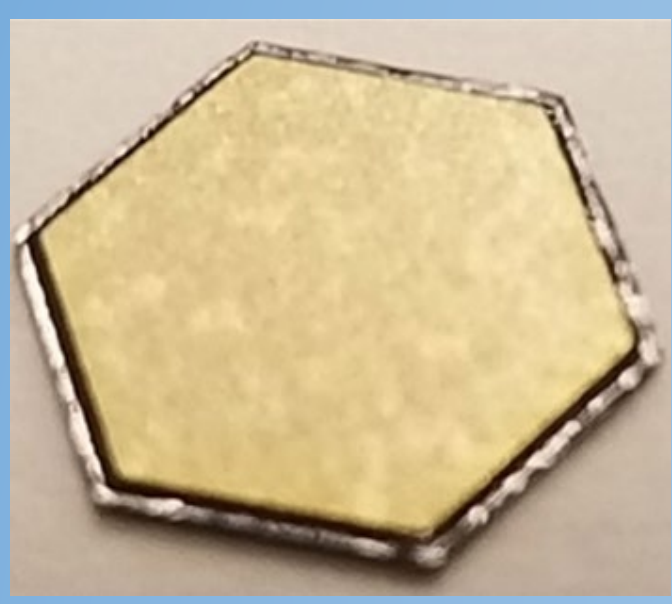
Generate an optimization algorithm such as genetic algorithm or machine learning algorithm to build a suitable predictive model for this SOS-IES topology.

The specific topology most worth prototyping is of the following form:

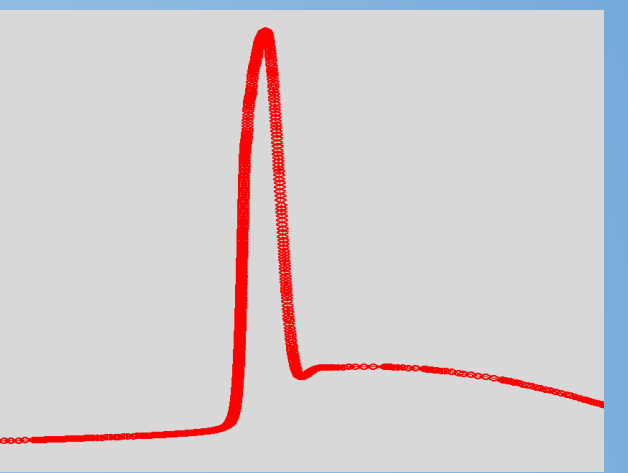
- Three or more parallel branches, and two or less series stages.
- Parameters L, C, and V should all be decreased as a function of the series stages.

## Reference

[1] T. Sugai *et al*, "Influence of forward pumping current on current interruption by semiconductor opening switch," in IEEE Transactions on Dielectrics and Electrical Insulation, vol. 22, no. 4, pp. 1971-1975, August 2015, doi: 10.1109/TDEI.2015.004989.



# TCAD Optimization of Drift-Step Recovery Diode (DSRD) Peak Power and Risetime



Jay Eifler<sup>1</sup>, Nick Flippin<sup>1</sup>, Dario Labrada<sup>1</sup>, Ron Focia<sup>2</sup>, Anthony Caruso<sup>1</sup>

1 - University of Missouri – Kansas City, Missouri Institute for Defense and Energy 2 - RF Engineering/Pulsed Power Laboratories, Inc.

## Objective

Drift-step recovery diodes (DSRDs) and DSRD-based pulsed power systems are competitive with PCS-based systems for HPM cUAS but do not require a laser. DSRD designs will be optimized to improve DSRD-based system performance for peak power, risetime, pulsewidth, compactness, low-jitter, cooling required, efficiency, additional pulse-sharpening, and for pulse repetition profiles.

## Background

DSRD are for fast current interruption of inductors to produce high-power, nanosecond-order pulses. Technology computer-aided Design (TCAD) software [1] can be used to model and simulate DSRD within an inductive pulser design. By calibrating the TCAD to experiment, simulation can be used for predictive optimization of the DSRD within an inductive pulser.

## Methods

The DSRD used is a p- $\pi$ -n diode shown in Figure 1. The DSRD thickness and junction placement have been optimized for peak power and risetime in prior art and are consistent with the published [2] state of the art.

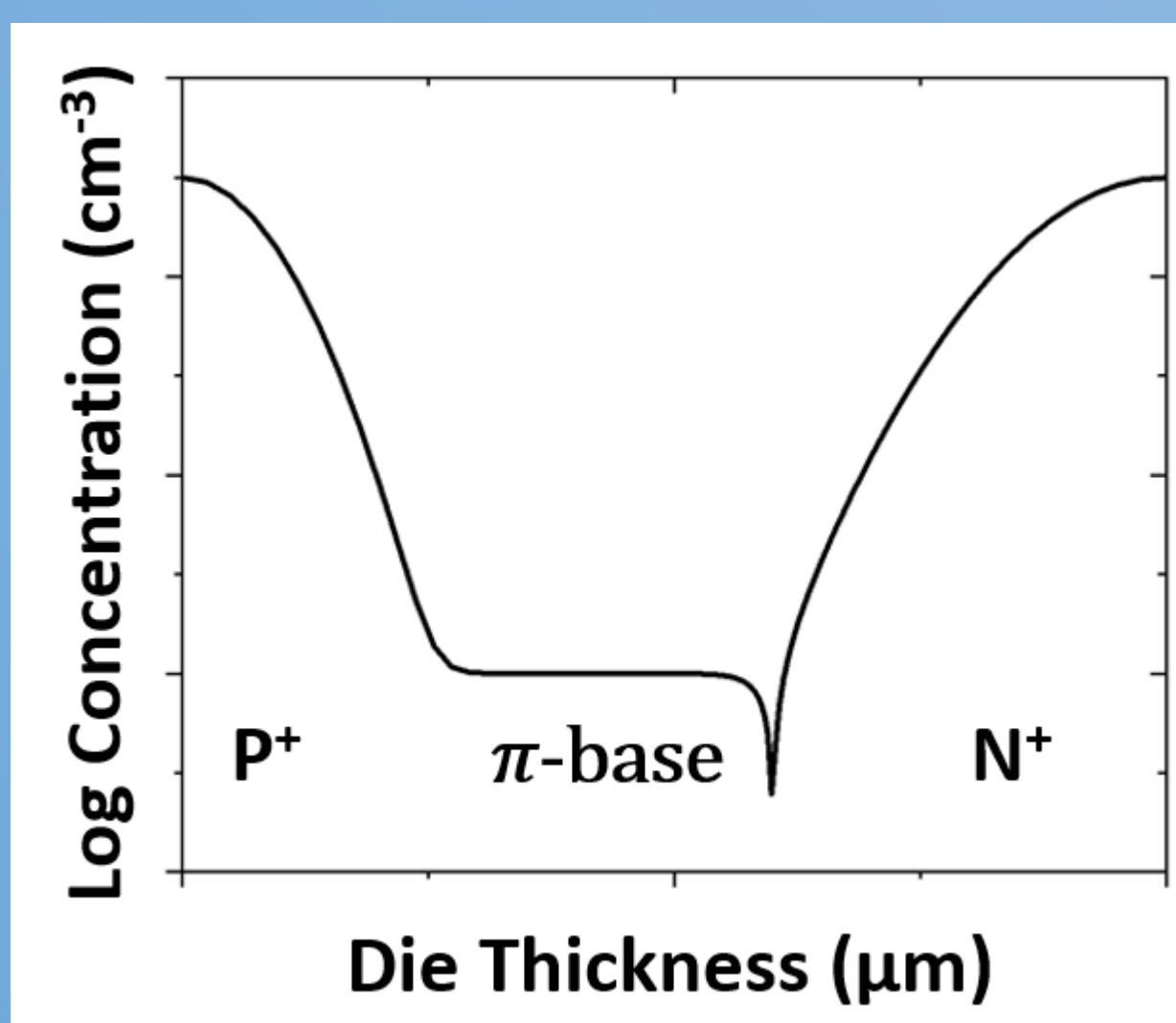


Figure 1. Doping profile for a p- $\pi$ -n diode.

The inductive pulser circuit used to characterize the DSRD pulse compression is shown in Figure 2. The inductive pulser primary pulse generation stage (not shown) is modeled as a sinewave pulse input to simplify the number of parameters in the circuit for the primary switch and driver. The voltage magnitude is 500 V and pulse period is 200 ns. On the 50  $\Omega$  load, the load voltage is used to determine the peak voltage and the risetime (10% to 90% of the peak voltage).

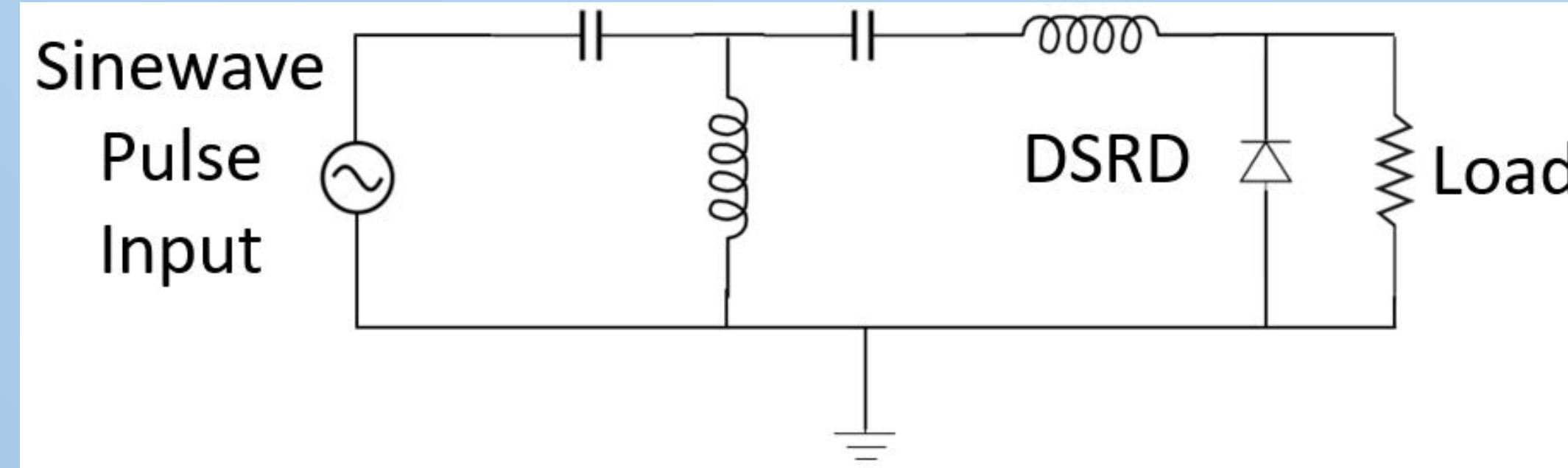


Figure 2. Inductive Pulser for characterization of DSRD

The operation of the circuit is: the DSRD (much lower resistance than the load) is forward pumped by an initial negative lobe of the sinewave pulse and then the current reverses direction quickly and in greater magnitude than the forward pumping current due to the capacitors and the grounded inductor. The DSRD interrupts the reverse current near its maximum and breaks the current in the inductor resulting in a voltage pulse at the load which the DSRD holds off.

To optimize the DSRD design for maximum peak power and minimum risetime considerations, TCAD is used to model and simulate the pulse operation (peak voltage, risetime, and riserate) from device parameters (junction placement, thickness, area, and stacking).

Models for carrier-carrier scattering mobility (used for high-power forward-biased devices) and avalanche generation (for static breakdown) have been used. A 2D parameter study of area and stack height for peak power, risetime and riserate has been performed. Additional studies for junction placement, series resistance and circuit parasitics are forthcoming to calibrate models used to experimental results.

## Results and Analysis

Device areas from 0.2-4 cm<sup>2</sup> and stack heights from 5-13 DSRD dies were simulated for peak voltage, risetime, and voltage riserate. For the following figures, the key is shown at the beginning and the open circles indicate results for including impact ionization (the selberherr model) and the closed circles for including only carrier-carrier scattering. The spreading resistance profile (SRP) for a DSRD is also used for comparison to the optimal doping profile.

Key for Figures 3-5.

- 5-stack
- SRP 5-stack
- 7-stack
- 13-stack
- 5-stack (impact)
- 7-stack (impact)

The main result demonstrates the correctness of the models for carrier-carrier scattering and impact ionization. In Figure 3, the peak voltage (5-stack (impact)) is close to the 4 kV peak voltage seen in experiment. A published result goes further using circuit parasitics to quantitatively and qualitatively match their experimental and simulation results using the same models [2].

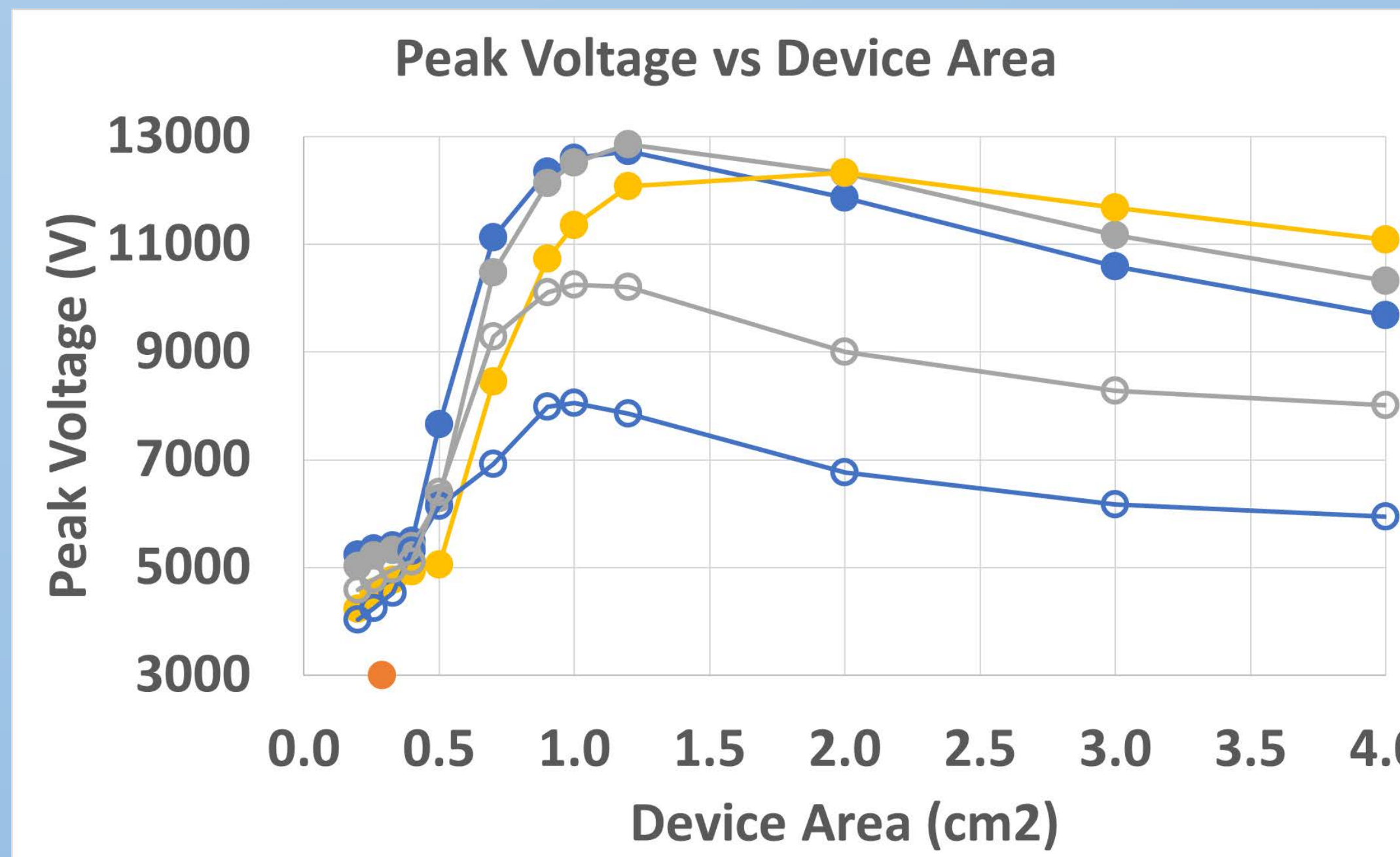


Figure 3. Peak voltage across stack and at load. Impact models (open circles) have peak voltage limited by breakdown.

The risetime results show a minimum risetime is achieved at 3 cm<sup>2</sup> area for the impact models (open circles). Avalanche has yet to be observed for pulse testing in-house and the results for both 5 and 7 stacks show considerable avalanche pulse distortion. This is likely due to doping variability and differences in the experimental setup and simulation (circuit component values and parasitics).

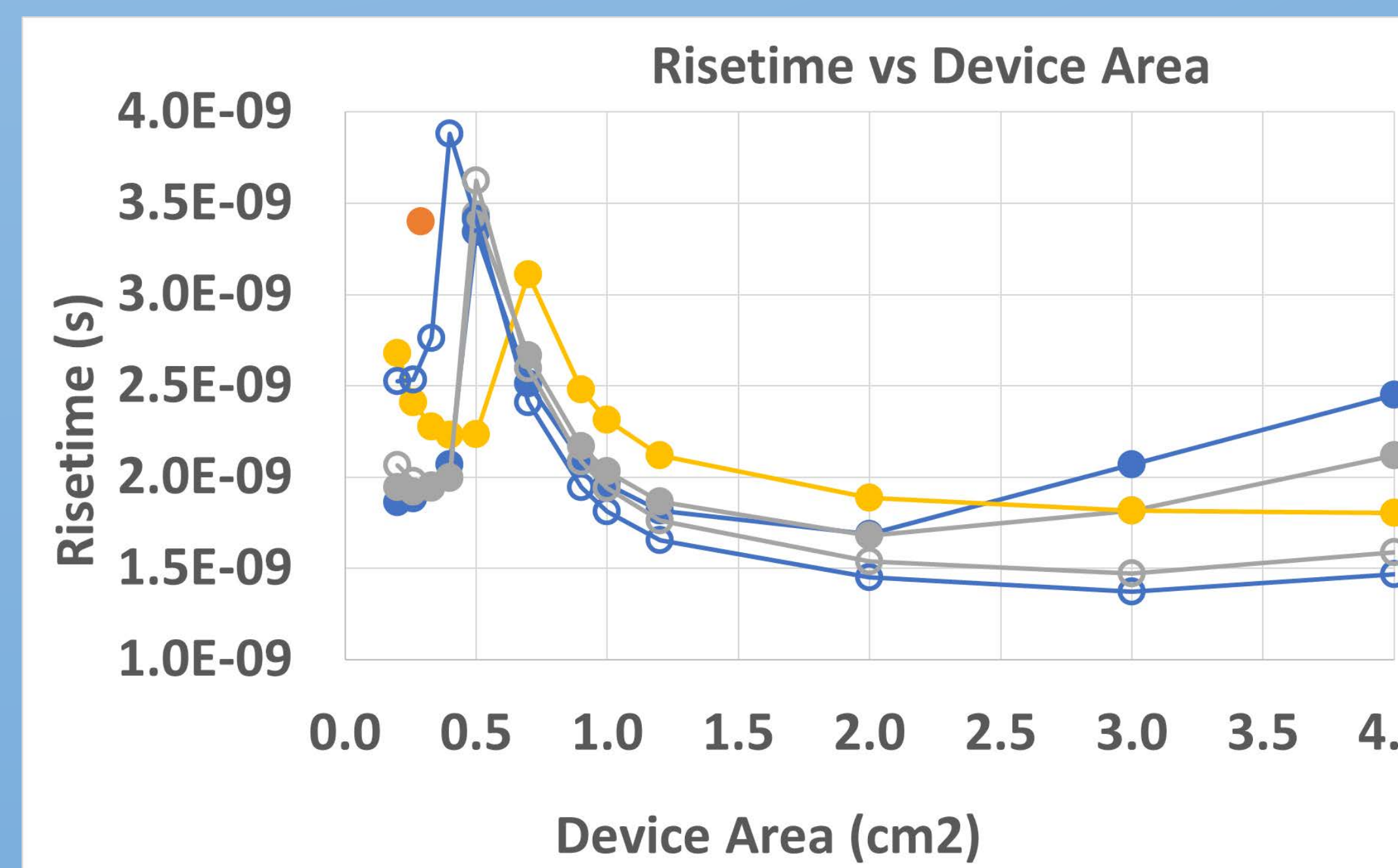


Figure 4. Risetime at load has different optimal area for impact models when considering risetime alone.

To verify that the breakdown models are correct the peak voltage per die (not shown) and voltage riserate per die were collected. In Figure 5, the impact models show riserates are below the  $1 \times 10^{12}$  V/s dynamic breakdown limit. Additionally, the breakdown voltage per die did not exceed 1600 V.

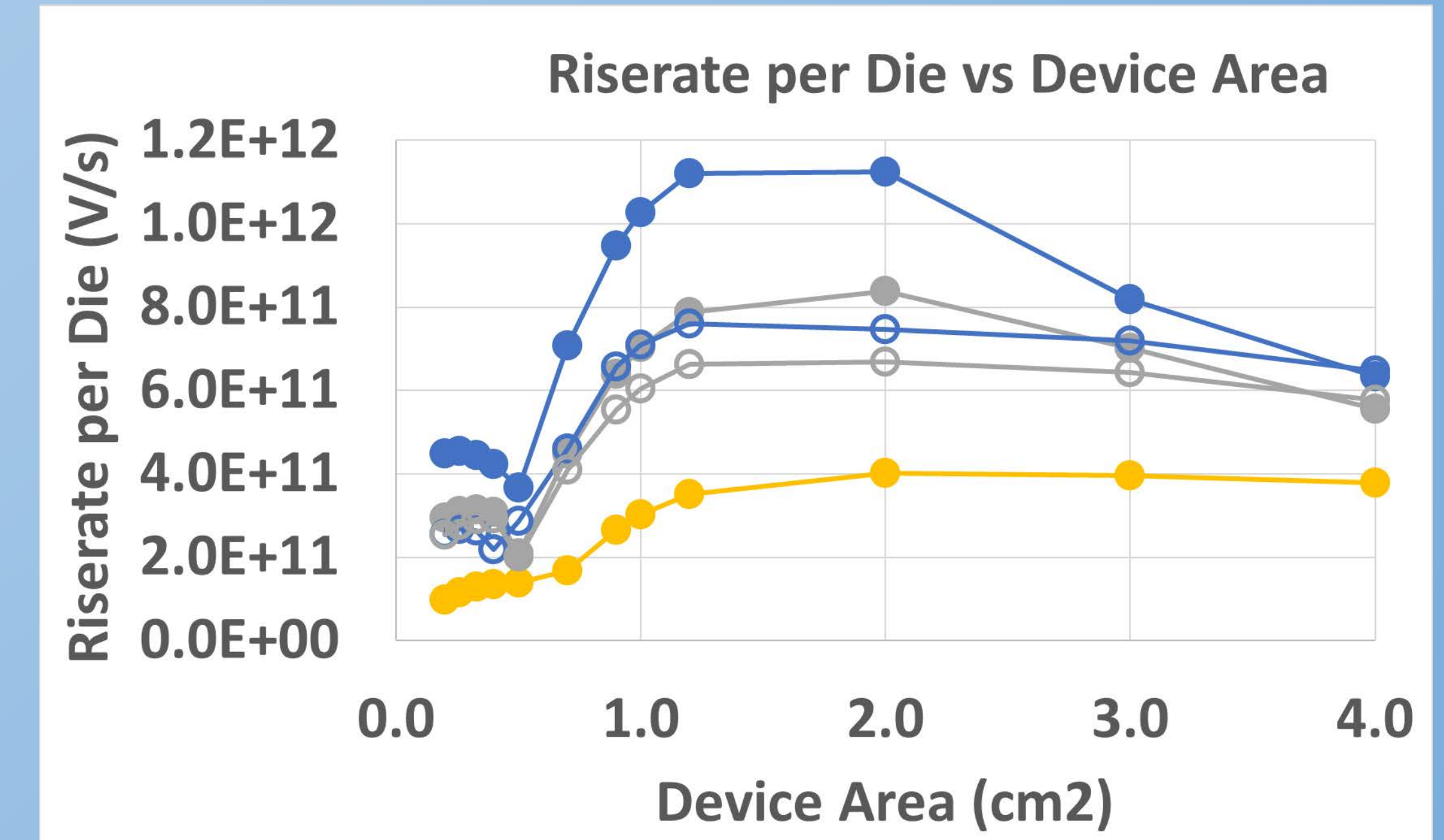


Figure 5. Voltage riserate per die of stacks. Impact model (open circles) limits riserates within conventional (non-dynamic) breakdown.

## Summary

- With TCAD simulations matched to experiment, DSRD/DSRD pulser system performance can and will be improved (difficult to quantify at this stage)
- 5-stack (impact) result is within the 4 kV peak voltage observed experimentally when accounting for series resistance, variation in doping profile, and avalanche pulse shapes
- Peak voltage and risetime are relatively flat from 1-4 cm<sup>2</sup> area (minimum at 3 cm<sup>2</sup>), peak voltage per die does not exceed  $\sim 1600$  V, voltage riserates are below  $1 \times 10^{12}$  V/s indicating static breakdown
- Future work is to calibrate the model to experiment by more exacting match and circuit parasitics (see [2])

## References

- [1] SILVACO Data Systems Inc., Silvaco ATLAS User's Manual, 2015.
- [2] Lyublinsky, A. G., E. I. Belyakova, and I. V. Grekhov. "Numerical and Experimental Study of an Optimized p-SOS Diode." *Technical Physics* 64, no. 3 (2019): 373-379.

## Acknowledgements

This work was supported by the Office of Naval Research, Award No. N00014-17-1-3016.



## Problem/Solution Space

**Primary Problem:** Need for a more compact, cost-effective RF pulse generation system for Navy afloat missions on smaller vessels and vehicles.

**Solution Space:** Improve efficiency and reduce necessary material, size, and thermal requirements by utilizing gallium nitride (GaN) in photo-conductive semiconductor switches (PCSS) through exploitation of its theoretical material properties which allow for higher operating voltages, frequencies, and temperatures, while also eliminating the need for pulse-shaping transmission lines through direct RF modulation using the laser/photon source driving the PCSS.

**Sub-Problem:** Lack of maturity in compensated gallium nitride semiconductor (i.e., GaN:X with X=C,Fe) PCSS manufacturing, development, and optimization.

**Solution Proposed:** Replace Si-PCSS device with GaN:C utilizing direct RF modulation — eliminating the need for a bulky pulse-forming transmission line (~3 ft long) — capable of handling >3 MW (peak power) with ~20 μJ of incident optical energy, device area <1 cm<sup>2</sup>, and operating temperature ~250-300°C (limited by circuit components and solder).

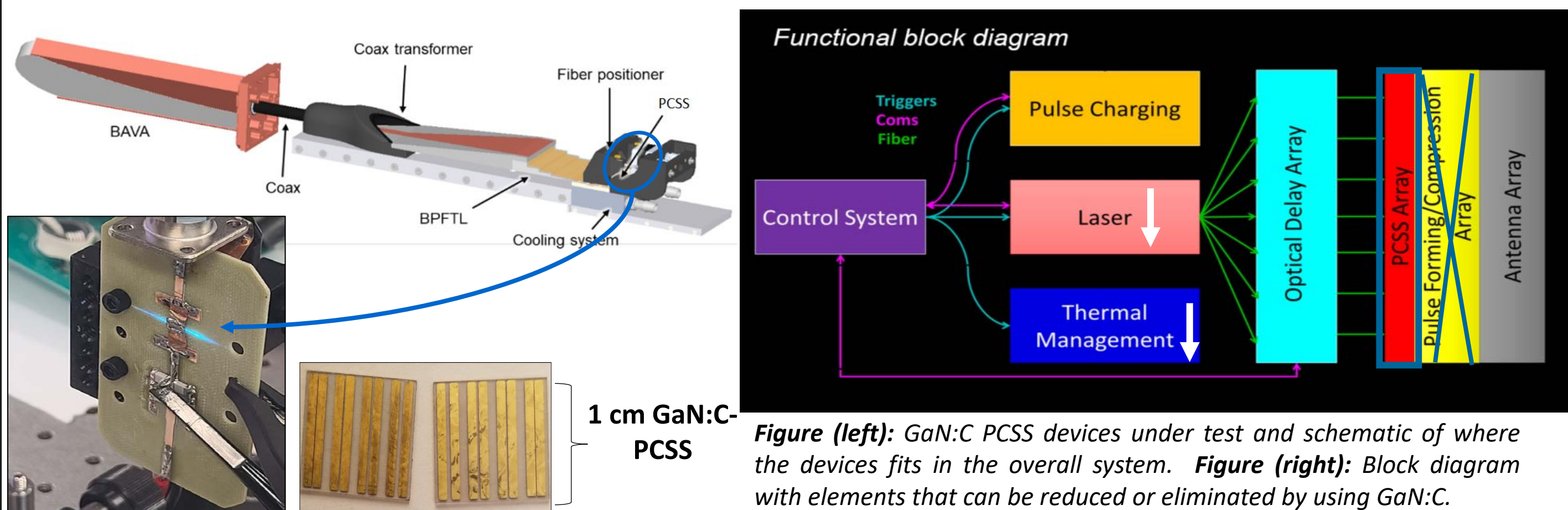


Figure (left): GaN:C PCSS devices under test and schematic of where the devices fits in the overall system. Figure (right): Block diagram with elements that can be reduced or eliminated by using GaN:C.

## Background

Silicon (Si) is commonly used in RF generation due to the maturity and low cost of material, but its short bandgap and material characteristics lead to deficiencies in performance that can be overcome by using a wide-bandgap material such as gallium nitride (GaN). The wider bandgap of GaN along with the higher melting point and faster saturation electron velocity and drift-velocity, allow for operation at higher operating voltages, frequencies, and temperatures, leading to an overall system that has a smaller form factor and increased SWAP-C<sup>2</sup> capabilities. Due to the increase in operating voltage, smaller PCSS devices can be used to achieve the same operating voltages seen in Si devices.

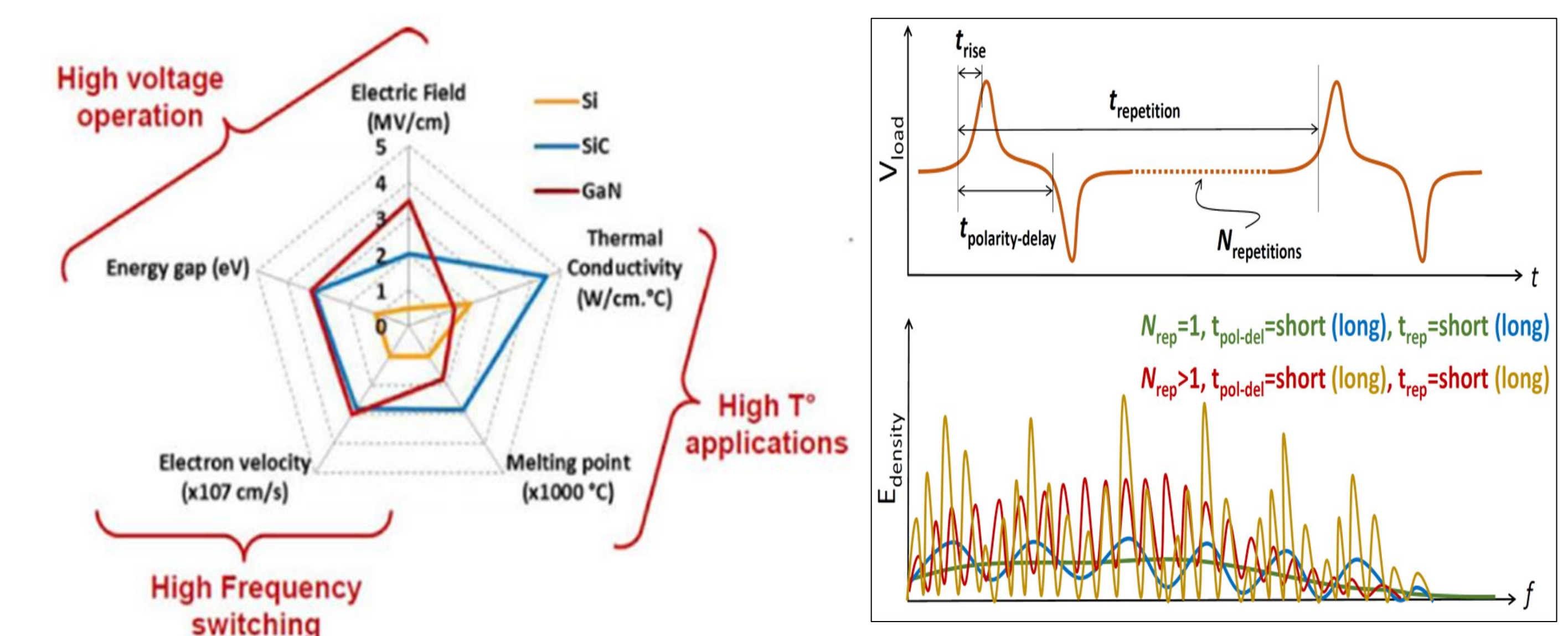
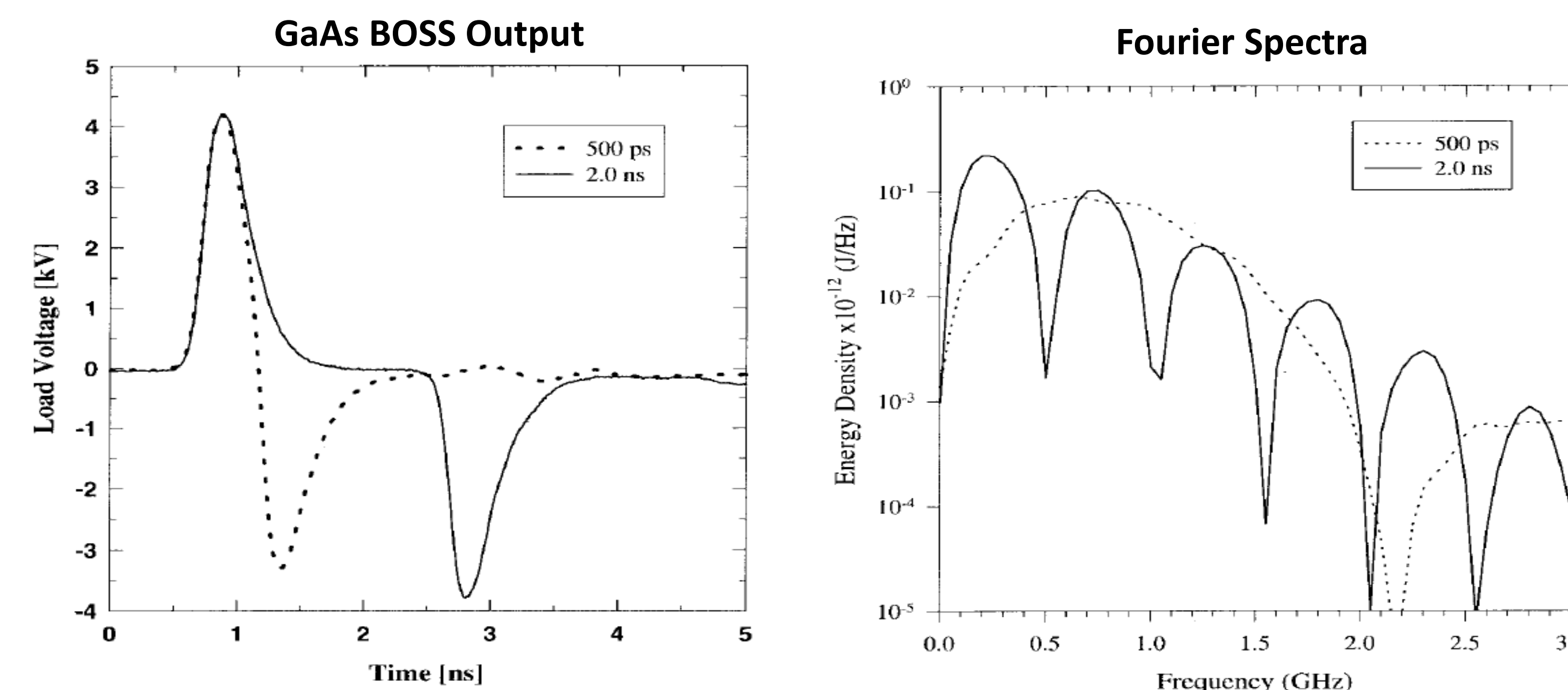


Figure: Material characteristics of commonly considered materials for PCSS applications.

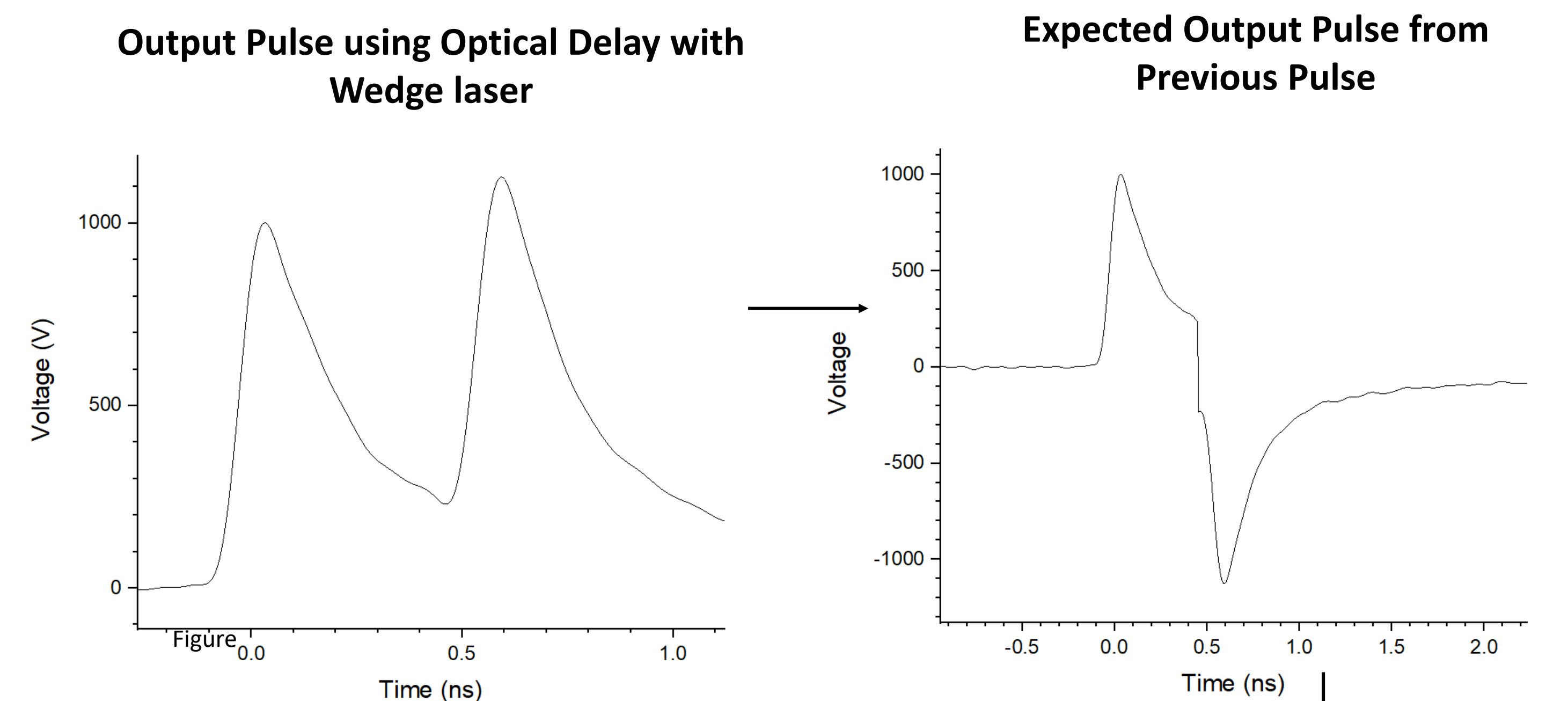
Due to the fast recombination in GaN:C, the output pulse of GaN:C PCSS is laser dependent (i.e., follows the characteristics of the incident laser/photon source), pulse-shaping and time separation of incident laser pulses can be used to vary frequency content. By changing the rise-time, pulse-width, pulse repetition rate, and delay between pulses, a GaN:C PCSS can be used as a frequency agile RF source that eliminates the need for bulky pulse-forming transmission lines.

## Direct RF Modulation Using GaAs

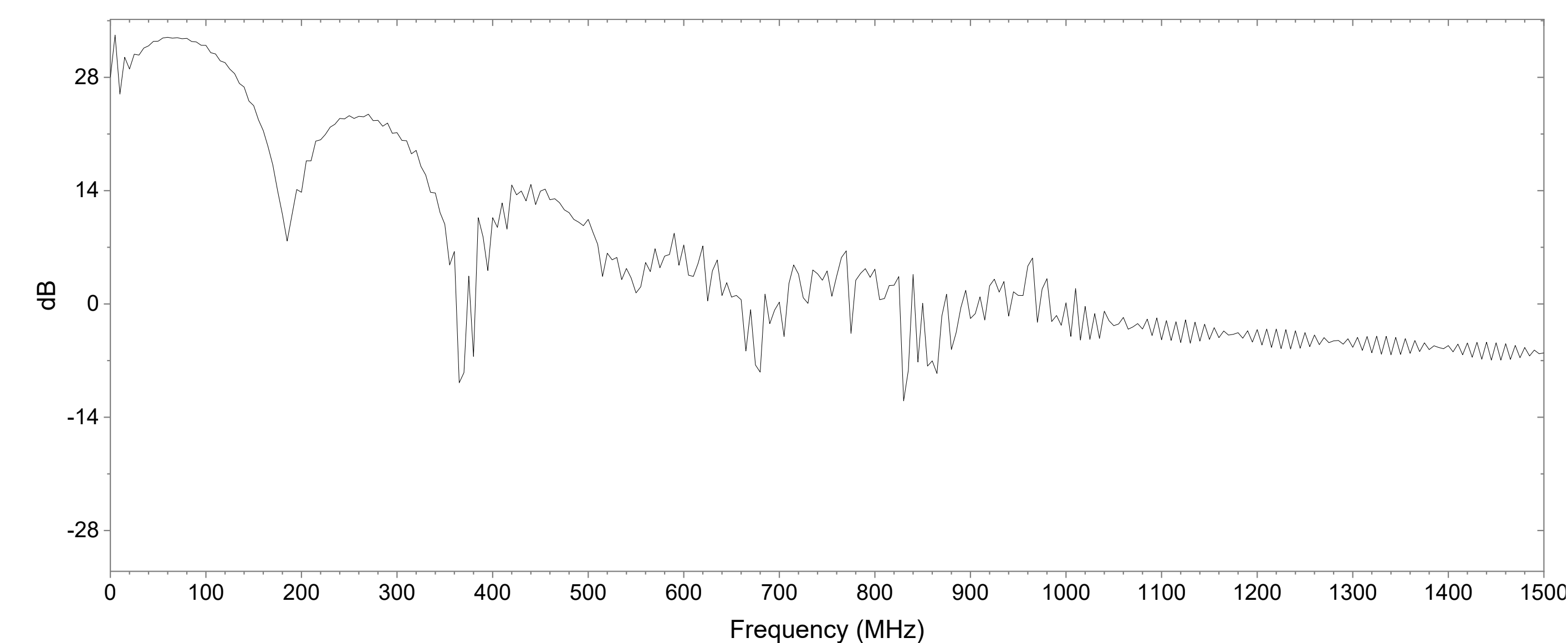


Direct RF modulation has been demonstrated using GaAs PCSSs, and the researchers were able to show that a frequency agile RF source was possible using a material with a fast recombination time and showed ones-of-GHz operation could be achievable [1].

## Expected Results – Using Initial Unipolar Modulation Results



## Expected FFT of Bipolar Output



Unipolar modulation using one GaN:C PCSS with the free-space optical delay has been demonstrated at <2 kV using the wedge laser (~1 ns rise-time). It is expected that by adding a second GaN:C PCSS, operating using negative bias, and adjusting the timing between the two pulses, will result in a decrease of the non-radiating DC output and allow for frequencies in the hundreds of MHz to ones of GHz to be achievable. The SHG/THG system has been setup with the neOLASE (70 ps vs ~1 ns pulse-width), so higher frequency content should be seen due to the quicker rise time and allow for higher pulse-repetition studies to be performed. Above is an example of the expected bipolar output and frequency content using the unipolar output measured using the wedge laser, which results in frequencies in the hundreds-of-MHz. This setup allows for RF output using a PCB based system instead of requiring the addition of pulse-forming transmission lines that can be ones-of-feet long.

## Experimental Setup

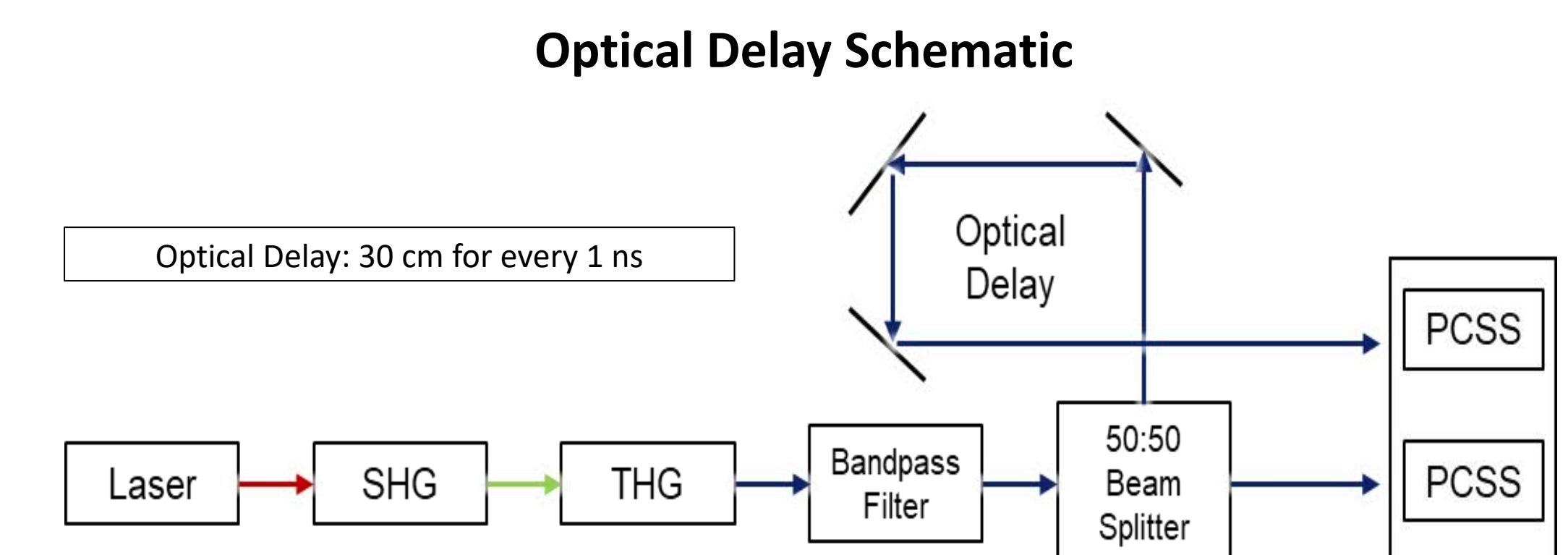


Figure: Schematic of the SHG/THG system

## GaN:C PCSS PCB for Bipolar Modulation

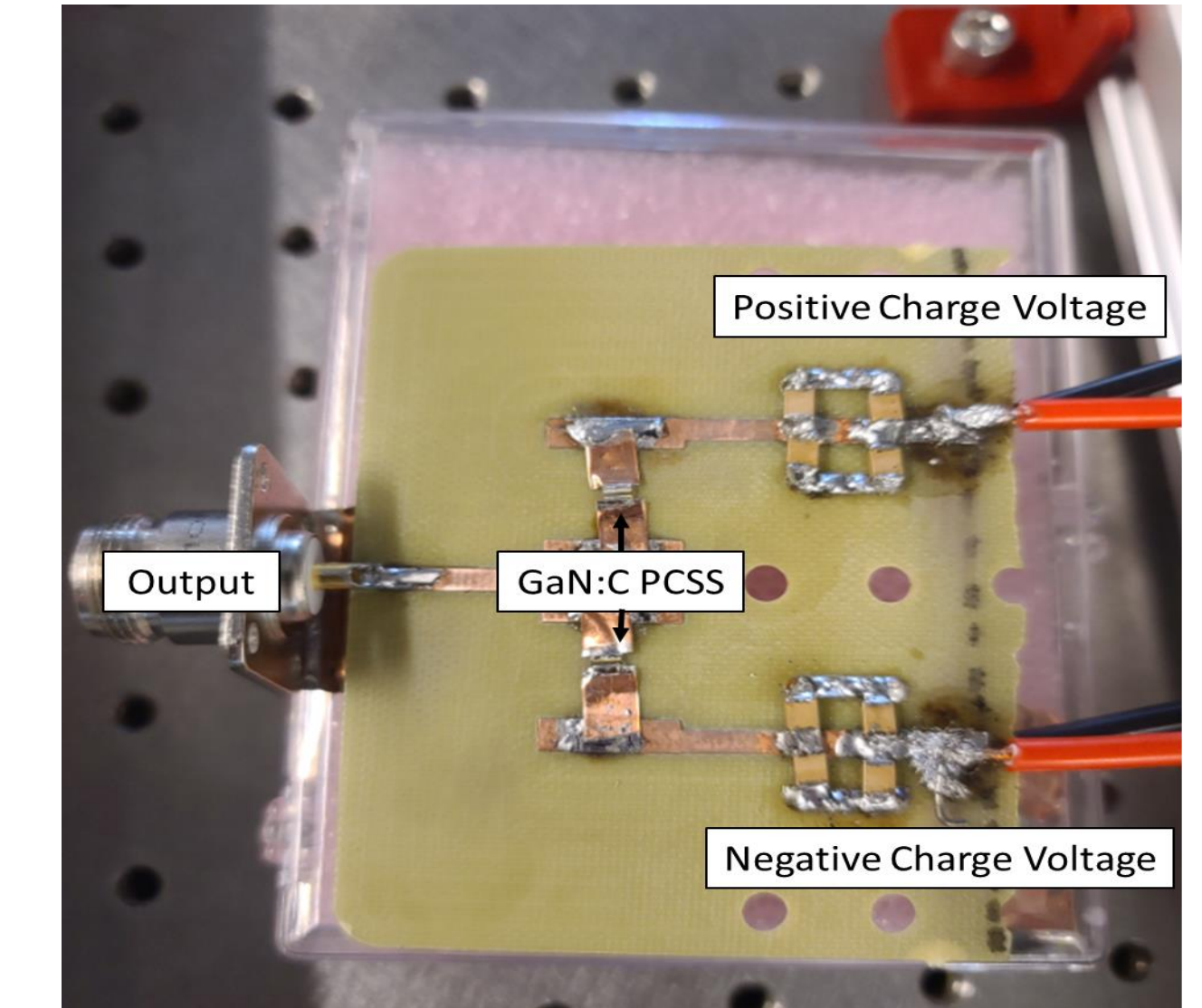


Figure: PCB being used for bipolar modulation of GaN:C PCSS.

Due to the wide bandgap of GaN:C, incident UVA light is necessary for device activation, so converting the IR source to UV using a second- and triple- harmonic generation (SHG/THG) setup is necessary. In order to manipulate the output, a free-space optical delay is set up that is adjustable to vary timing between pulses, affecting RF frequency output and allowing for some frequency agility.

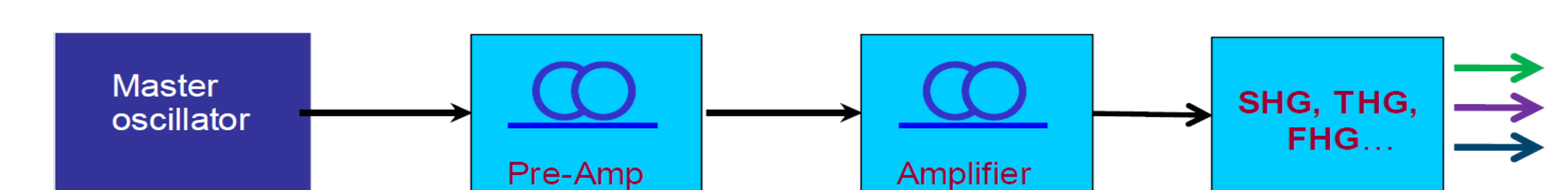
## Conclusion

Initial results using direct RF modulation with GaN:C PCSS have shown promising results that this will offer a viable solution for a frequency tunable RF source that is not reliant on pulse-forming transmission lines, making the overall system more compact. The next step in this work will be to demonstrate bipolar RF modulation using the neOLASE, allowing for higher frequency content and PRR studies.

## Future Work

To further reduce the form-factor of the system, future work will include using optical fiber amplification in conjunction with a SHG/THG system to activate GaN:C PCSS. This will allow for output modulation to occur by using the fiber for adjusting pulse-shape and time delay. Using fiber will also allow for set-up that doesn't require free-space time delay, allowing for safer operation while increasing conversion efficiency and ease of setup.

## Block diagram of a fiber master-oscillator power amplifier (MOPA) [2]



## References

- [1] Stoudt, D. C., Richardson, M. A., & Peterkin, F. E. (1997). Bistable optically controlled semiconductor switches in a frequency-agile RF source. *IEEE Transactions on Plasma Science*, 25(2), 131–137. <https://doi.org/10.1109/27.602483>
- [2] Starodoumov, A., & Hodgson, N. (2011). Harmonic generation with fiber MOPAs and solid-state lasers -- technical challenges, state-of-the-art comparison and future developments. *Solid State Lasers XX: Technology and Devices*, 7912(February), 79120H. <https://doi.org/10.1117/12.876873>

## Acknowledgement

This work was supported by the Office of Naval Research, Award No. N00014-17-1-3016.

## Objective and Motivation

**Primary Problem Space:** Decrease the size, weight, and cost of pulse forming networks (PFNs).

**Solution & Primary Objective:** Design a D-NLTL to function as a pulse shaping network capable of shifting spectral content up to the single GHz regime at single MW peak powers.

**Secondary Objective:** Demonstrate the ability to control the center frequency of the waveform through electrical or mechanical means.

**OSPRES Connection:** System volume, weight, and cost are limited resources aboard a naval vessel. A D-NLTL has the ability to optimize all three within the scope of a high-power microwave system.

## Diode-Based NLTL Background

**General:** Diode-based nonlinear transmission lines (D-NLTL) represent a class of transmission lines with a nonlinear dielectric provided by the reverse PN junction of a diode. D-NLTLs shift spectral content to higher frequencies by breaking a pulse into solitons, or disturbances, that propagate through a nonlinear medium with unchanging geometry.

The soliton generation is achieved through the phenomena of edge sharpening. The voltage-dependent nature of the diode capacitance causes high amplitude portions of the signal to propagate at a greater rate than small amplitude portions of the signal. The amount a given D-NLTL will reduce a rise time is determined by the chosen components and line geometry. If the rise time of the excitation pulse is small enough that the line would reduce the rising edge beyond zero, a shockwave is formed in the line. The shockwave is balanced by the dispersive nature of the lumped element structure and solitons form.

**Measurements:**

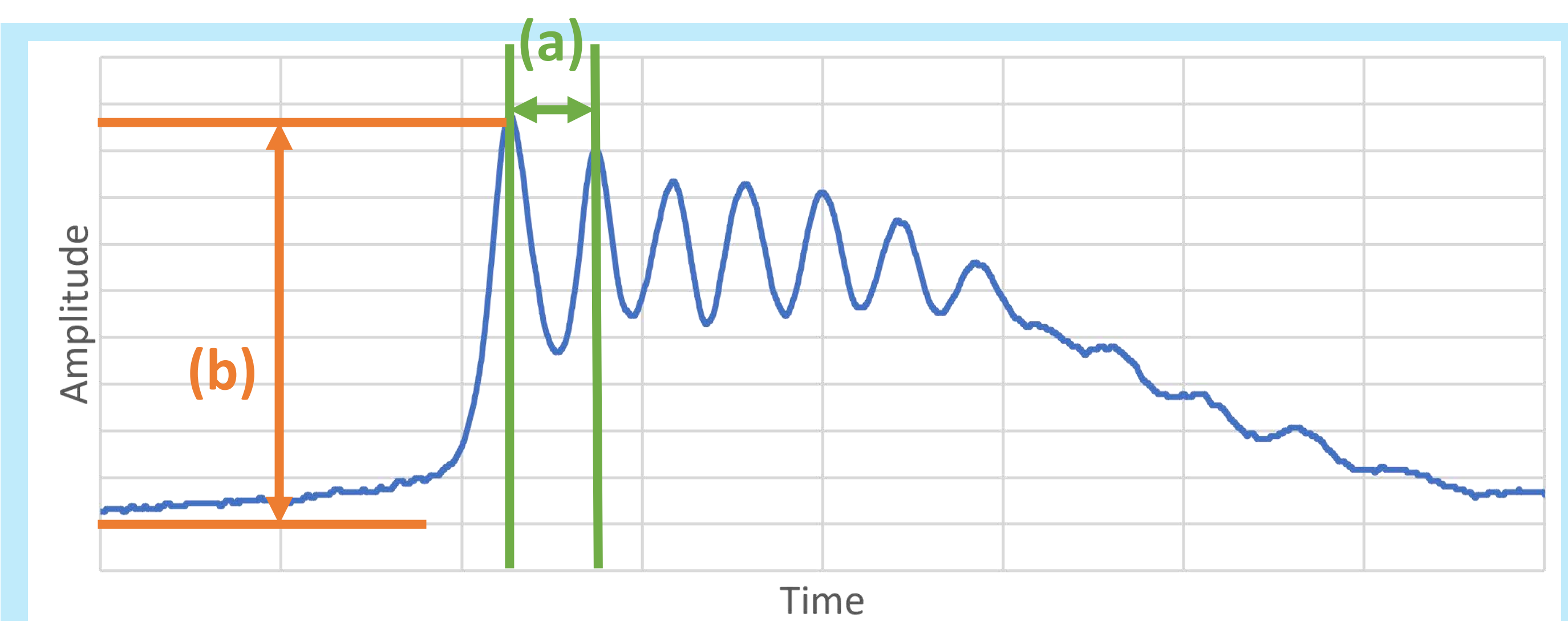


Figure 1: An example waveform generated by a D-NLTL. The center frequency measurement is marked by (a) and the amplitude measurement is marked by (b).

Figure 1 shows an example of a waveform generated by a D-NLTL. The three waveform characteristics of concern are:

- Center frequency: Represents the peak amplitude in frequency domain. Estimated by the inverse of the time between solitons (green above).
- Amplitude: Representative of the peak power generated, give by the height of first soliton (orange above).
- Max Frequency: The highest frequency generatable, measured as the inverse of the 10-90% rise time of the pulse (not shown above).

## GHz MW D-NLTL

**Background:** The primary barrier to D-NLTLs capable of MW powers is the reverse bias potential ( $V_R$ ) of the diode. A diode of model K100F was identified as having a large enough  $V_R$  and capacitance range capable of MW power generation at GHz frequencies.

**Set Up:** A 20 cell prototype with a 12 nH inductance per cell was excited using a half barrel DSRD (HB) source shown in Figure 2 (top).

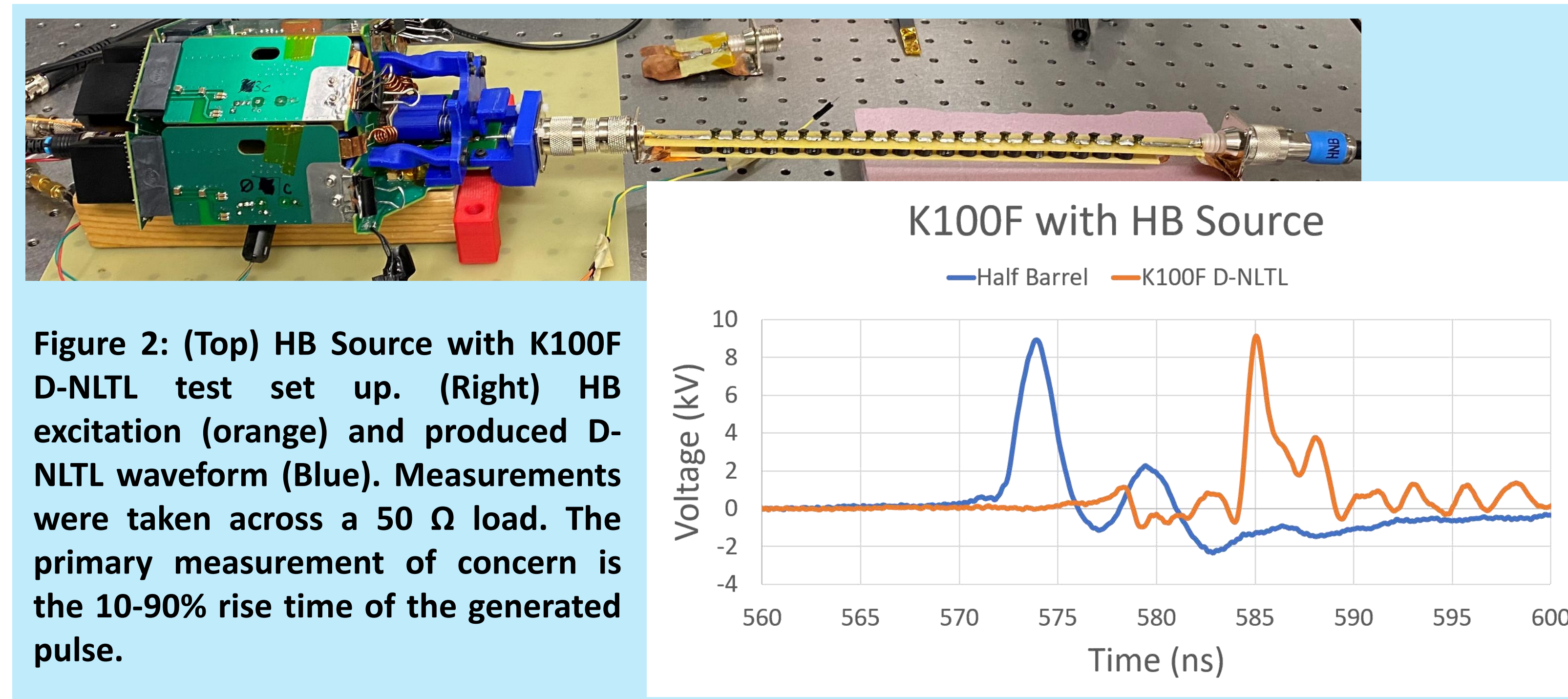


Figure 2: (Top) HB Source with K100F D-NLTL test set up. (Right) HB excitation (orange) and produced D-NLTL waveform (Blue). Measurements were taken across a 50  $\Omega$  load. The primary measurement of concern is the 10-90% rise time of the generated pulse.

**Results:** The K100F D-NLTL reduced the rising edge of the HB pulse from  $\sim 1$  ns to  $\sim 600$  ps, corresponding to a maximum produced frequency of 1.67 GHz. The peak amplitude of  $\sim 9$  kV corresponds to a power of 1.6 MW on a 50  $\Omega$  load.

## Diode Stacking

**Background:** Stacking diodes is a potential solution to the  $V_R$  limit. In a stack each diode would share a portion of the peak amplitude. A diode of model K50F was identified as a candidate as it possessed half the  $V_R$  and twice the low signal capacitance of the K100F diode; two K50F diodes in a stack should behave similarly to a single K100F diode.

**Set Up:** A 20 cell prototype was fabricated with a 12 nH inductance and 2 K50F diodes in series per cell.

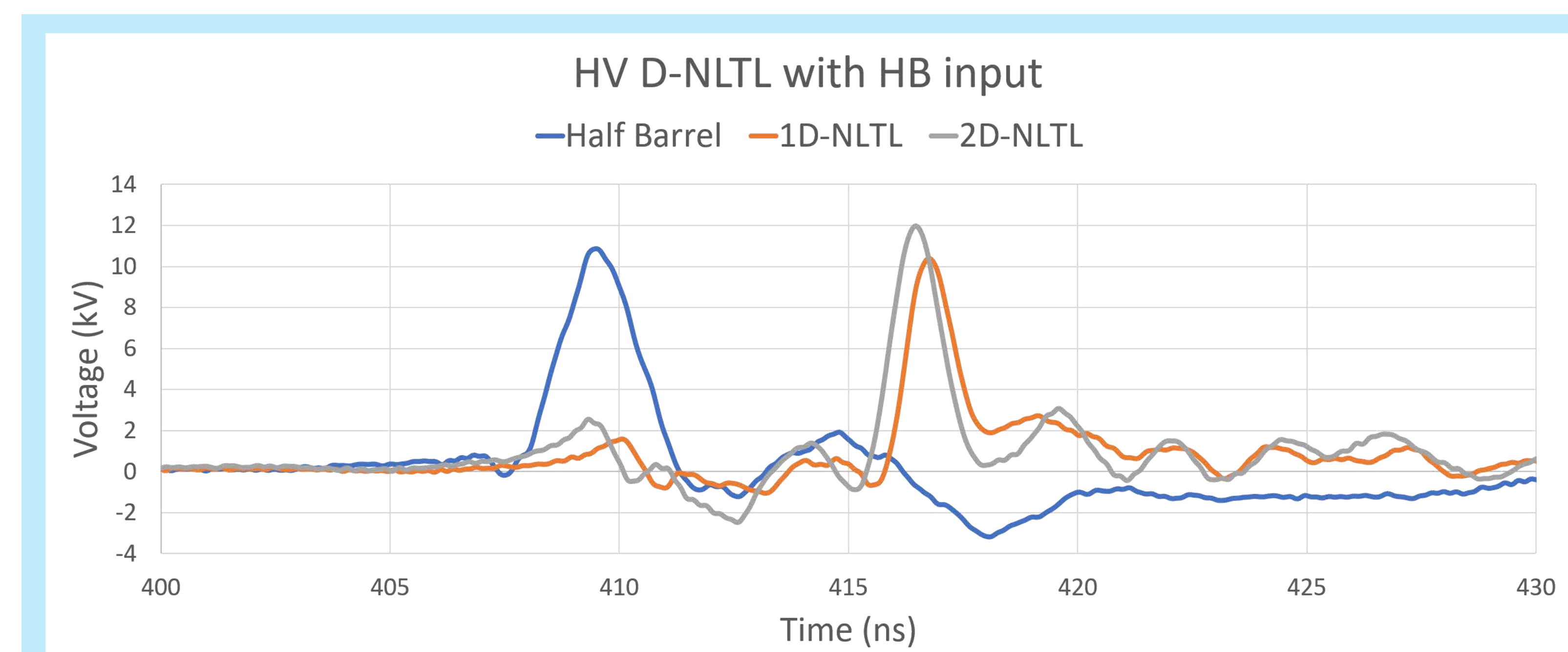


Figure 3: Comparison between the 1D and 2D NLTL. Each line had a similar effect on rise time and peak amplitude of the generated pulse with both generating GHz frequencies at single MW powers.

**Results:** The K50F line produced similar results to the K100F line with a rising edge of  $\sim 600$  ps. The difference in peak amplitude for each line could come from the re-soldering of connections at the source-line and line-load interfaces between tests affecting the impedance mismatch.

## Electrically Tunable D-NLTL

**Background:** The center frequency of a D-NLTL can be electrically altered by applying a DC bias to the cathode of the diodes utilized. The application of the bias effectively shifts the low signal capacitance with positive bias corresponding to an increased center frequency and a negative bias corresponding to decreased center frequency [1].

**Set Up:** A 40 cell prototype with a 22 nH inductance and diode model SMV1702 was constructed. A DC bias was applied to the cathode of each diode via a 1-k $\Omega$  resistance as shown in Figure 3 below.

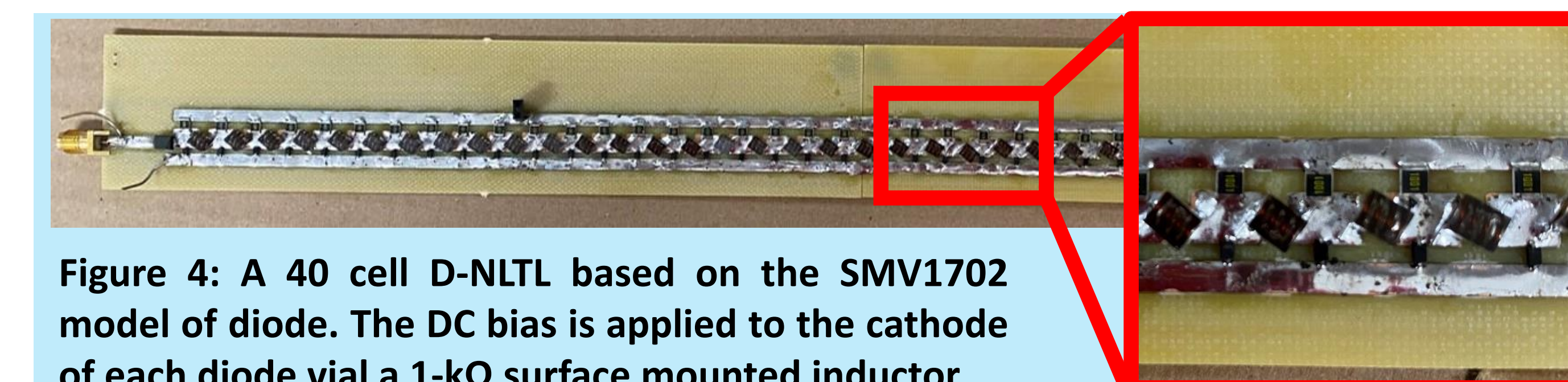


Figure 4: A 40 cell D-NLTL based on the SMV1702 model of diode. The DC bias is applied to the cathode of each diode vial a 1-k $\Omega$  surface mounted inductor.

**Results:** There exists a linear relationship between center frequency and DC bias up to a point where the diode saturates and increased bias no longer affects the center frequency.

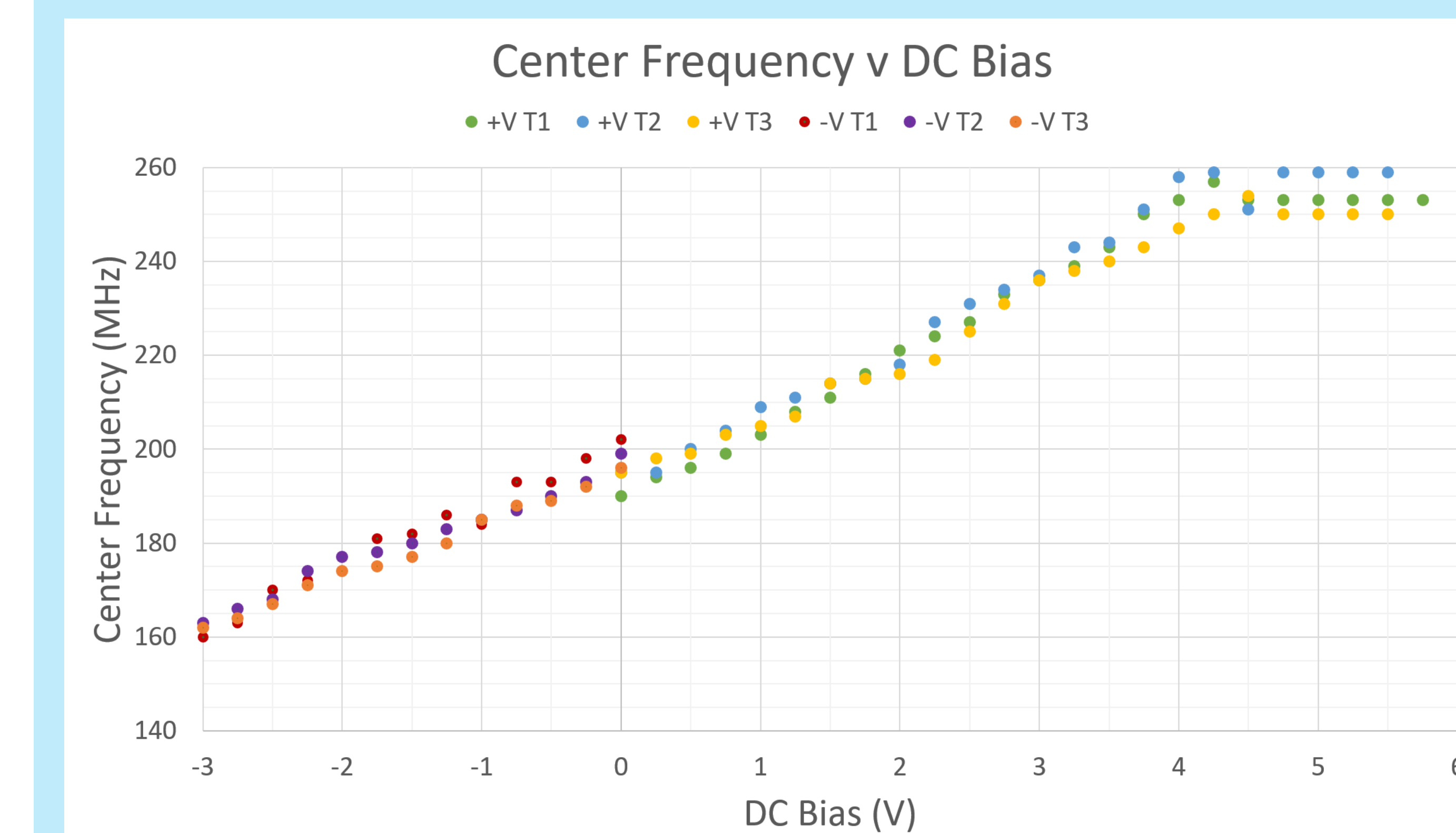


Figure 5: The dependency of the center frequency on the applied DC bias. Shown is a linear relationship up to an applied potential of  $\sim 4$ V after which the diode becomes saturated and little change occurs to the center frequency.

## Summary and Future Work

**Summary:** 3 key factors for D-NLTLs that have been demonstrated:

- GHz frequency generation at single MW peak powers are possible and have been achieved with prototype.
- The ability to achieve higher frequencies and peak powers through diode stacking has been demonstrated.
- It is possible to electrically tune the center frequency of a D-NLTL through the application of a DC bias potential to the diode

**Future Work:** Future research will progress on two fronts:

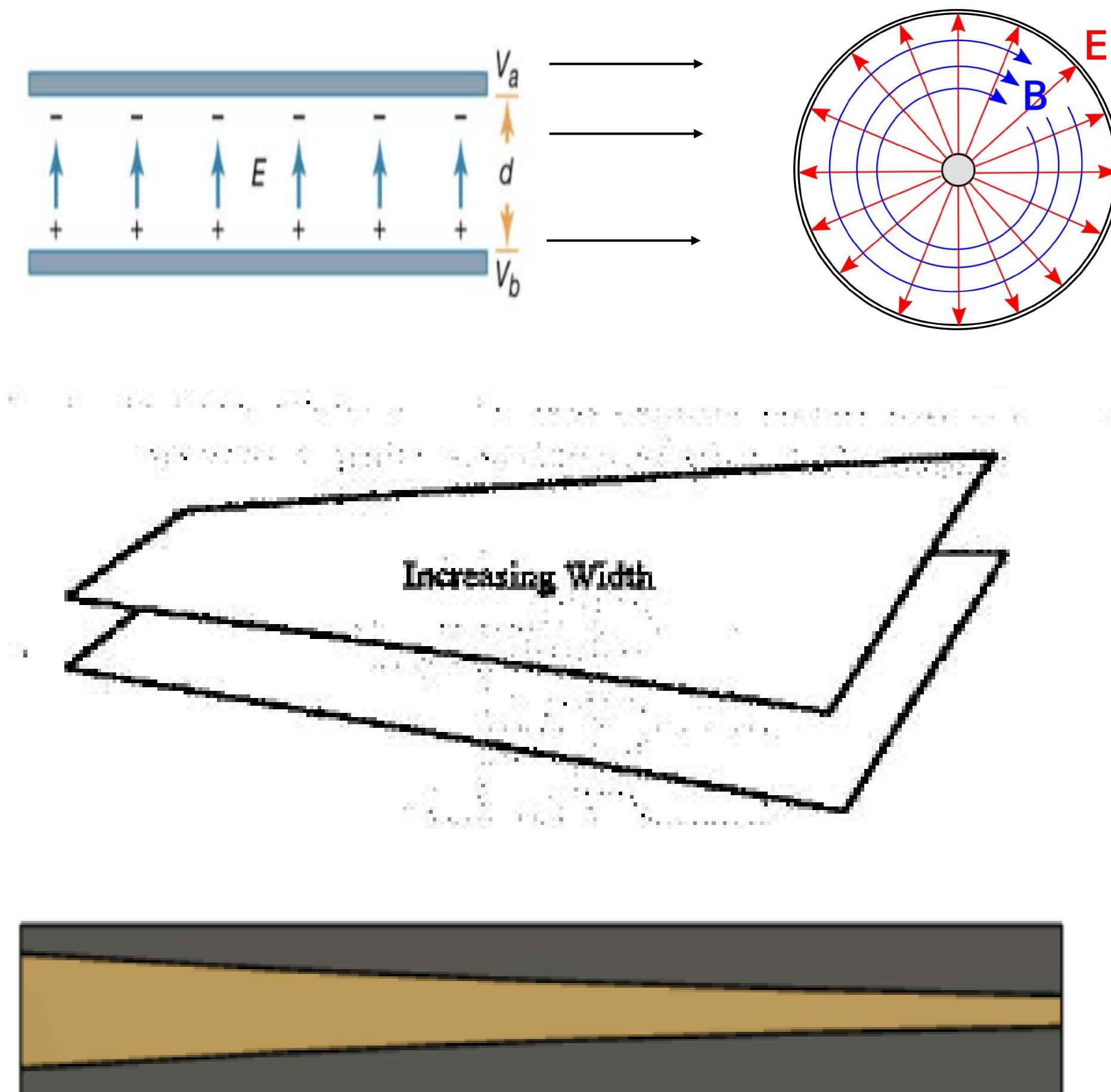
- Use the HV D-NLTLs to break a pulse into a sequence of solitons.
- Determine the sensitivity of the line to changes to determine feasibility of line parallelization for the purpose of power scaling.

### Introduction

Geometric unity-gain impedance matching transformers are used in electromagnetic (EM) signal transmission applications in which the signal driving elements and radiating elements are significantly different in physical cross section.

Tapered transmission line transformers are useful as geometric transformers and impedance transformers when transmitting pulses. They are primarily used for very short pulses on the order of <10 ns [1].

Tapered transmission line transformers can be configured with curved, linear, or flat active planes [2].



### Theory

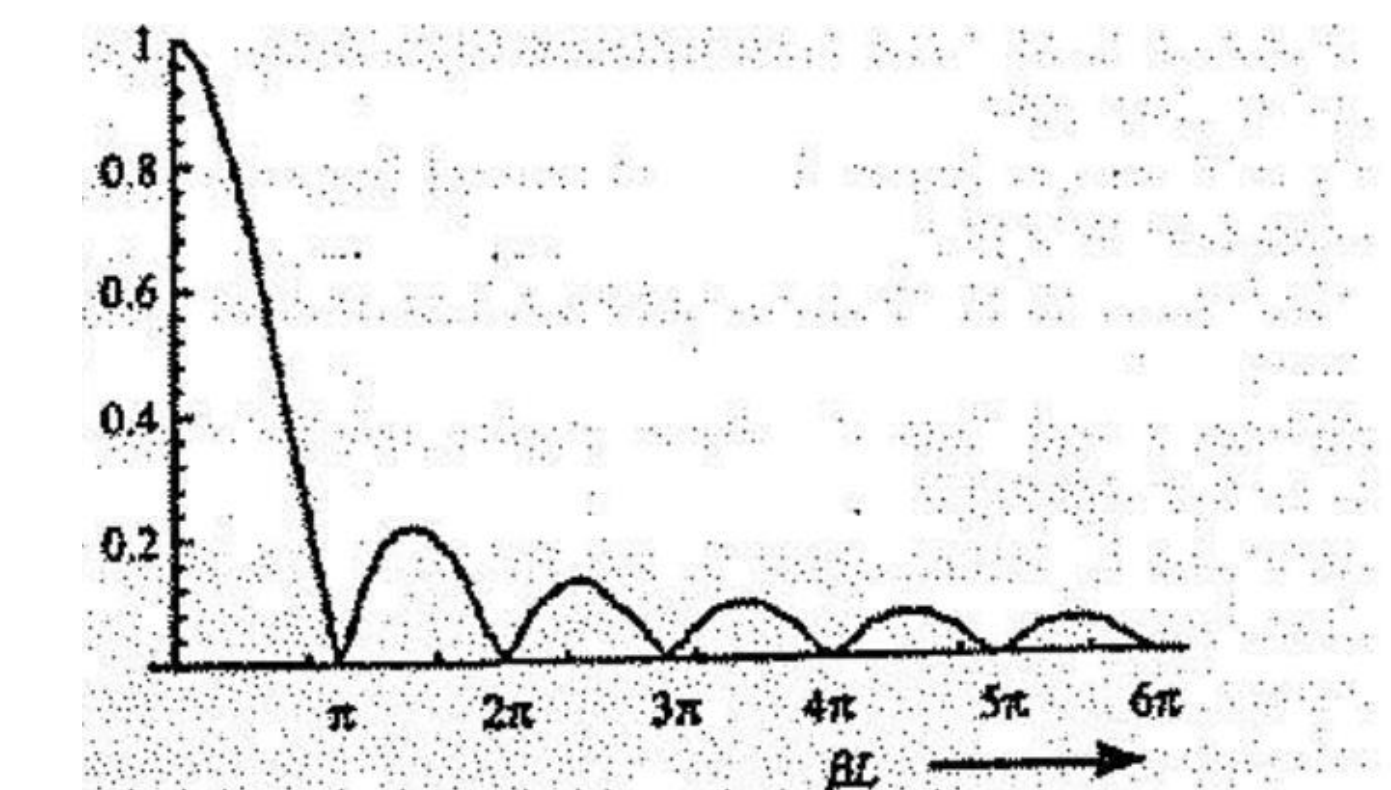
Tapered transmission line transformers are best used for short pulses because these transformers operate best at high frequencies. The wavelength of a transmitted frequency is assumed to be much smaller than a ~60% shift in impedance across the transformer [3].

The percentage of power transmitted is determined by factors such as the length of the transmitted pulse, the magnitude of impedance shift, the dielectric constant of the dielectric material, as well as the transformer's  $k$  factor, determined by the shape of the active plane [3].

A transformer with an exponential curve has the ideal  $k$  factor for transmitting a pulse across a high impedance shift. This is because transmission is tied to impedance shift relative to starting impedance, and an exponential curve keeps this percentage impedance shift constant. A graph of the performance of an exponential transmission line transformer can be seen to the right, detailing percentage transmission compared with wavelength relative to impedance shift.

$$\left| \frac{\lambda}{Z} \frac{dZ}{dX} \right| \ll 2\pi$$

$$P = \frac{\delta k^2 \tau}{8T(0)^2} * 100\%$$



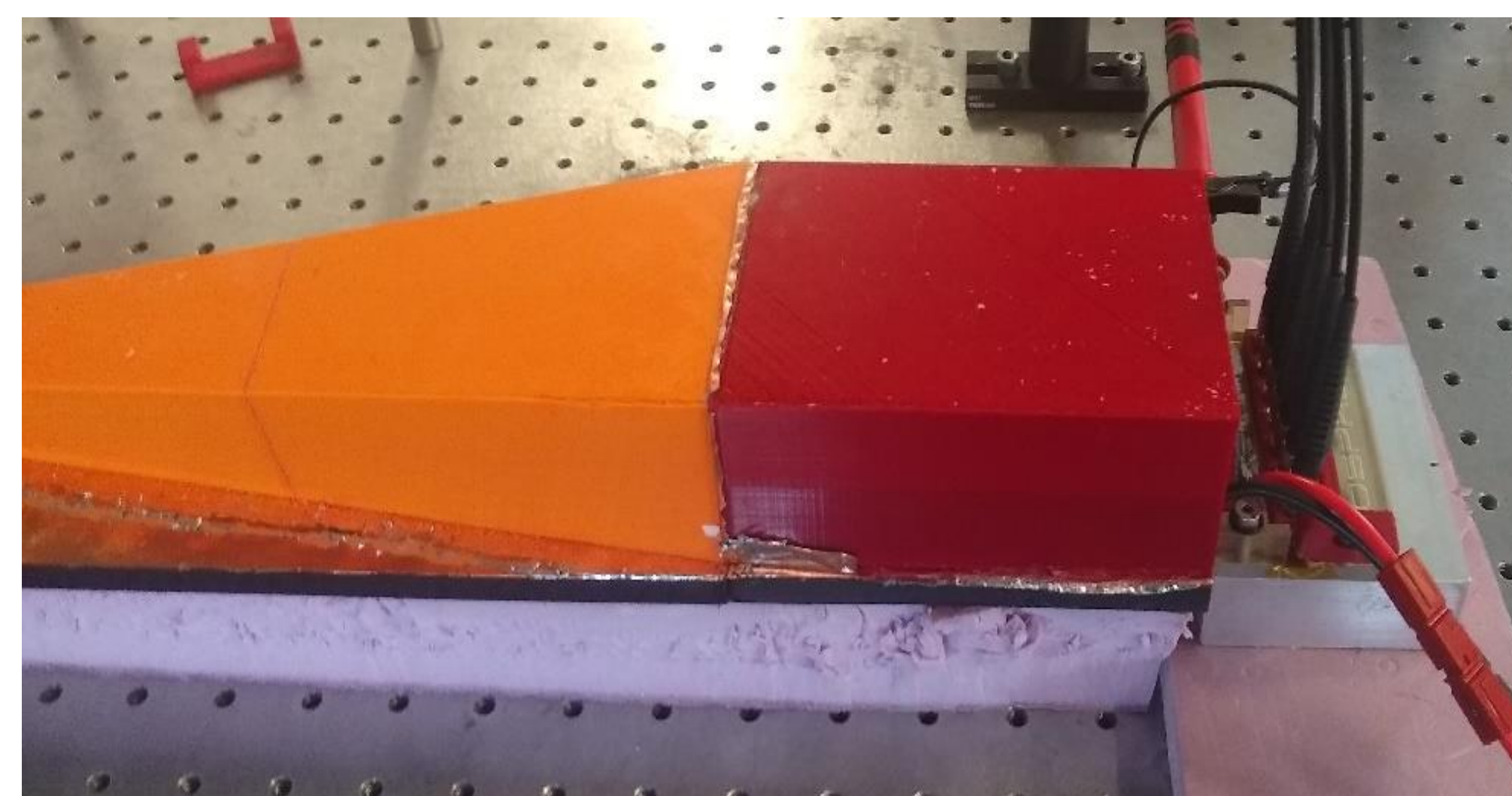
### Requirements

The design objectives are to create a high-power transition between the output of parallel plate radiating element and a coaxial element. The parallel plate output of the radiating element is 1.82cm tall and feed the pulse with a microstrip 4-cm wide. The coaxial input's inner cross-sectional dimensions are a1=3-mm, a2 = 7.75-mm. The resulting characteristic impedance for both input and output are 50-Ω. The maximum voltage handling capacity must be above 10-kV from a <100-ps pulse. The transmission of the component must fit the following criteria:

- Transmission should be below 1.5-dB power loss, or  $S_{21} > .9$ ;
- Wave shape, amplitude, and spectral content across 500-MHz to 2-GHz band should be maintained.

### Fabrication

Transmission line transformers operate very well under low impedance shift conditions as geometric transformers. In the image is an example of a geometric unity-gain impedance matching transformer fabricated with 3D printed parts.

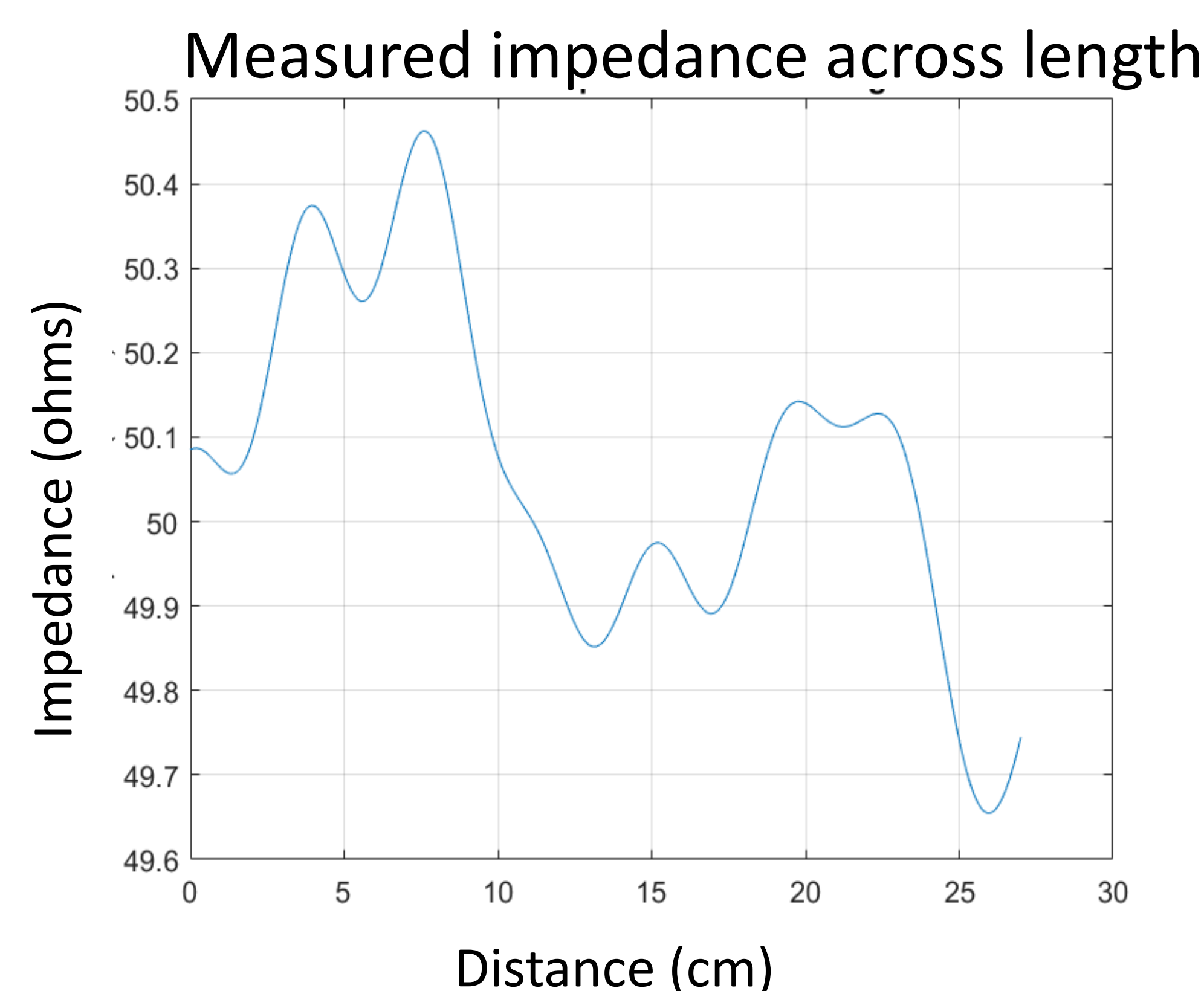


The active plane is linear, as can be seen in the simulated model. Linear transmission lines work optimally for geometric transformation with little to no impedance shifting. [4].

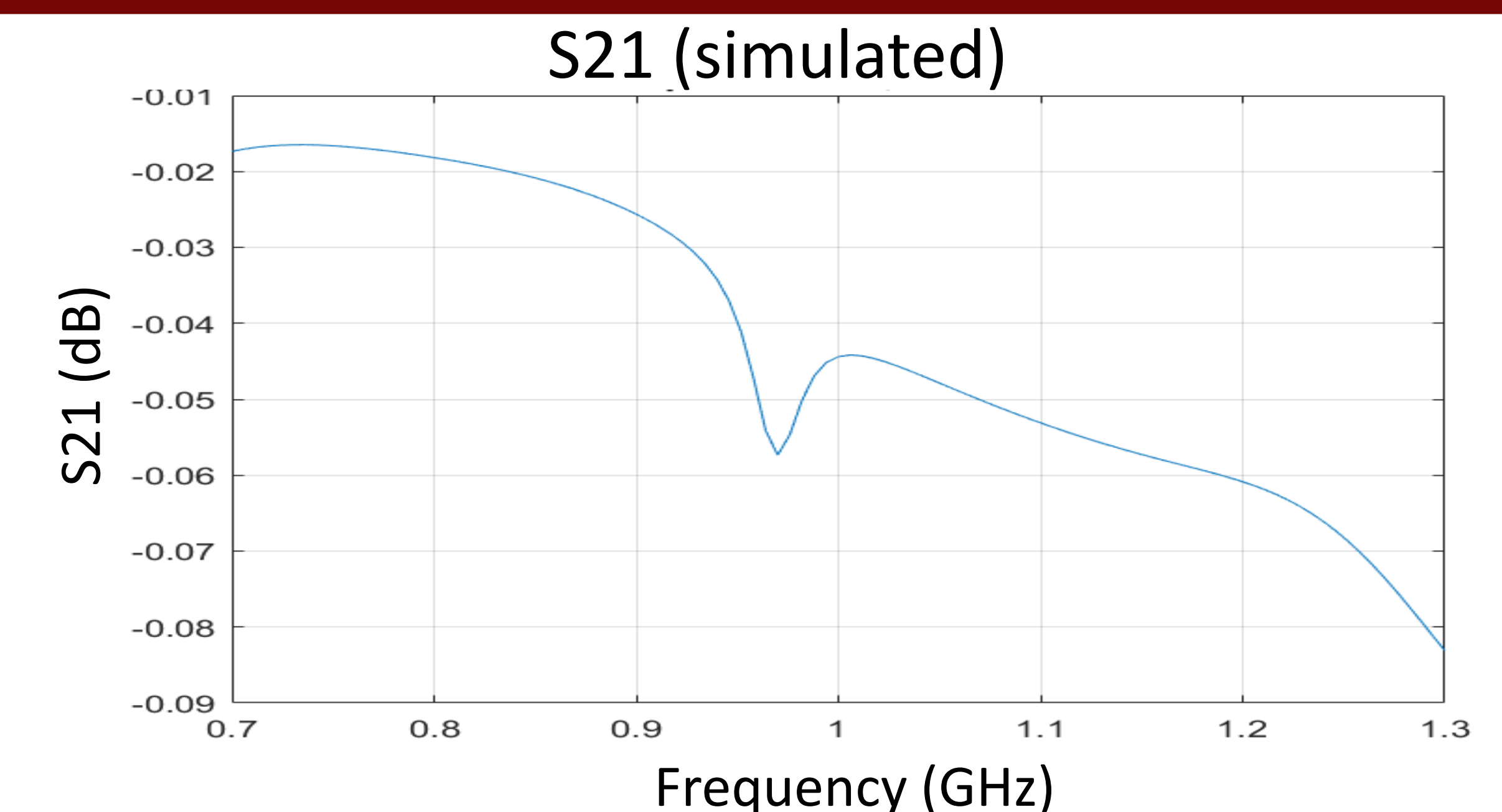


### Results

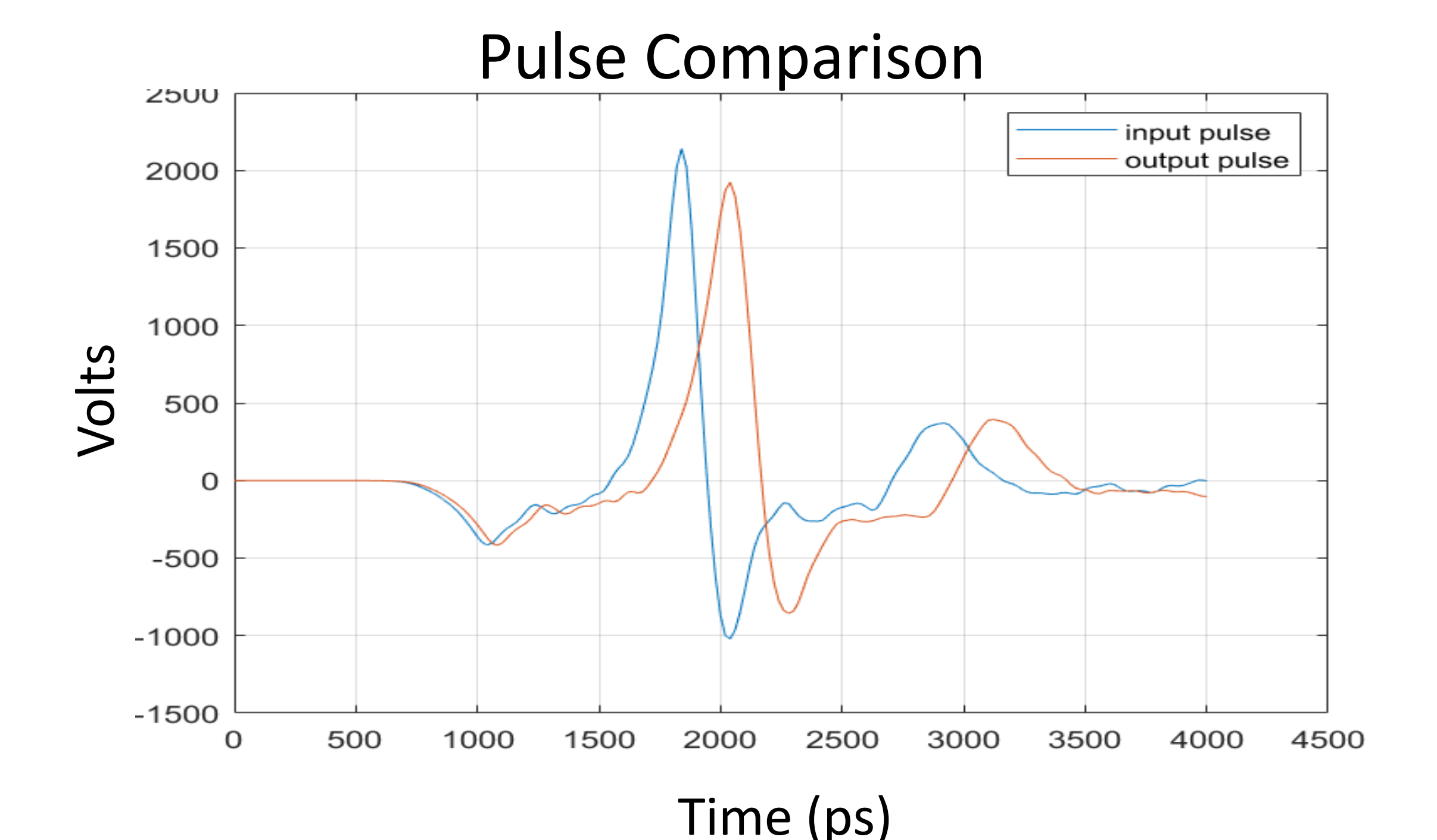
The linear tapered transmission line transformer is designed with as little impedance shift as possible, to facilitate optimal geometric transformation. The impedance measurement across the length of the transformer is obtained with time-domain reflectometry testing. The transformer contains less than 1% impedance shift across its length.



Here we see the scattering parameters of simulated linear tapered transmission line transformer, obtained through CADFEKO [5]. Very little attenuation occurs through this design across a wide bandwidth



Here we see a pulse transmitted through the fabricated linear tapered transmission line transformer. The output pulse is attenuated approximately 5%. The pulse is transmitted with no distortion of the pulse shape.



### References:

- [1] [19] A. O. Bah, Pei-Yuan Qin and Y. J. Guo, "An extremely wideband tapered balun for application in tightly coupled arrays," 2016 IEEE-APS Topical Conference on Antennas and Propagation in Wireless Communications (APWC), 2016, pp. 162-165, doi: 10.1109/APWC.2016.7738146
- [2] P. L. Carro, J. de Mingo, P. García-Dúcar and C. Sanchez, "Synthesis of Hecken-tapered microstrip to Paralell-Strip baluns for UHF frequency band," 2011 IEEE MTT-S International Microwave Symposium, 2011, pp. 1-4, doi: 10.1109/MWSYM.2011.5972676.
- [3] Paul. W. Smith "Transient Electronics – Pulsed Circuit Technology" Wiley, 2002
- [4] J. W. Duncan and V. P. Minerva, "100:1 Bandwidth Balun Transformer," in Proceedings of the IRE, vol. 48, no. 2, pp. 156-164, Feb. 1960, doi: 10.1109/JRPROC.1960.287458.
- [5] Altair FEKO CADFEKO version 2019 0.1-349439

# A Novel Method of Cooling a Semiconductor Device through a Jet Impingement Thermal Management System: CFD Modeling and Experimental Evaluation

Jordan N. Berg<sup>1</sup>, Roy C. Allen<sup>1,2</sup>, Sarvenaz Sobhansarbandi<sup>1</sup>

<sup>1</sup>Department of Civil and Mechanical Engineering  
<sup>2</sup>Missouri Institute for Defense and Energy (MIDE)  
 University of Missouri-Kansas City

## Objective and Motivation

**Primary Problem:** Laminar-flow-based cooling technologies are limited in their ability to compensate average-power dissipation  $>1 \text{ kW/cm}^2$  of the thermal load of high power density electronics.

**Sub-Problem:** An order-of-magnitude greater fluid flowrate and two orders greater pressure drop with jet impingement (JI) technique is required without increasing SWaP-cost.

**Relevance to OSPRES Grant Objective:** Increased cooling performance facilitates semiconductor devices to operate at higher average-power ( $>1 \text{ kW}$ ).

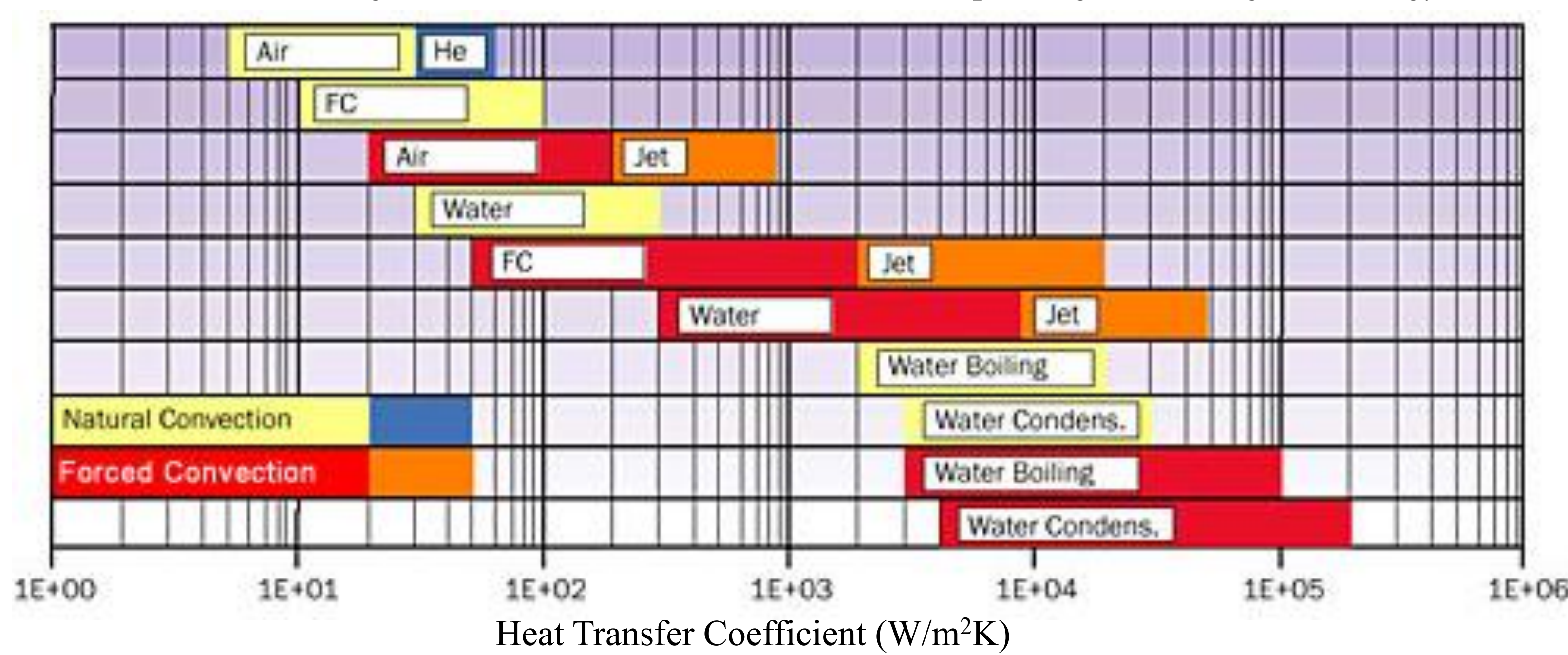
**State-of-the-Art (SOTA):** High power density electronics employing JI-TMS's have achieved 10's-of-kW of average power handling capabilities.

**Deficiency in the SOTA:** Chiller/pump systems consumption of power to produce thermal compensation, extreme pressures (100's-of-psi) to achieve optimal flow regime and cooling metrics.

**Solution Space:** Utilize novel cooling technologies which employ non-laminar flow regimes (i.e., JI-TMS). Develop a JI-TMS able to compensate average-power dissipation  $>1 \text{ kW}$  while maintaining the semiconductor temperature  $< 80 \text{ }^\circ\text{C}$ .

## Background

Order of Magnitude for Heat Transfer Coefficients Depending on Cooling Technology



## Methods and Analysis

- CFD modeling was performed with ANSYS Fluent 2020R2.
- The model was simulated under the transition SST viscous model.
- Mesh sizes of the model ranged from 181k nodes up to 1.639M nodes.

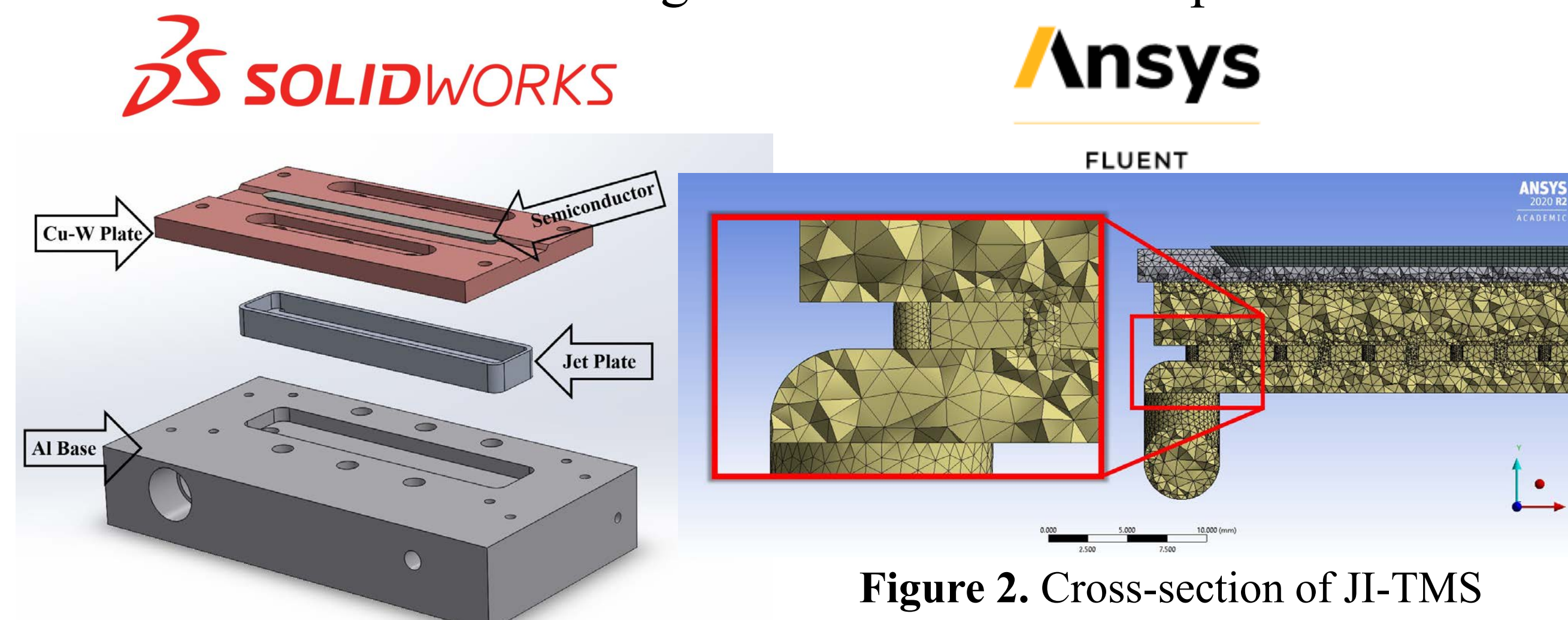


Figure 1. Staggered-nozzle Cooling System Prototype

Table 1. Boundary conditions

Properties	Values
Mass flow rate	0.06 kg/s
Heat flux	100 W, 200 W
Inlet temperature	10°C

- Experimental analysis was performed with chiller/pump connected to the JI-TMS and was filled with pure silicone fluid with the viscosity of 20 cSt (PSF-20cSt).
- The power supply was set to apply 100 W and 200 W to the device and thus induce the Joule heating effect.

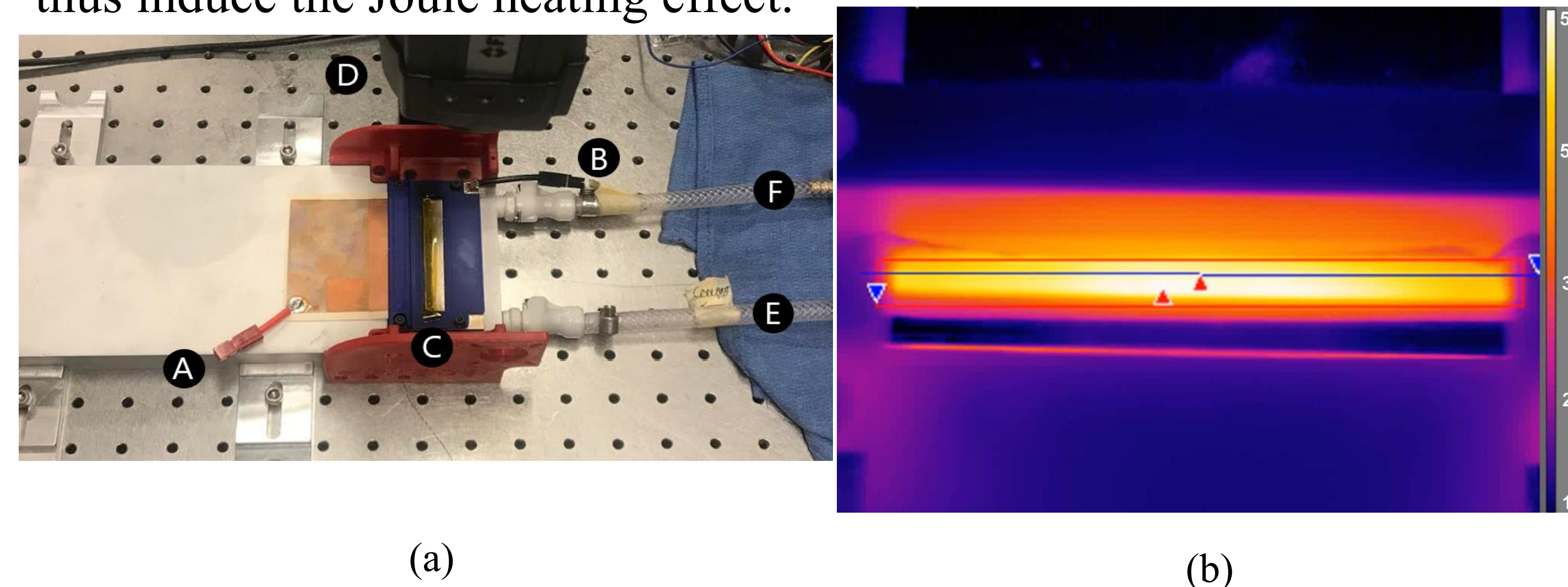


Figure 3. (a) Complete Test Setup. A-Power, B-Earthing, C-PCSS and TMS, D-FLIR Camera, E-Inlet, F-Outlet and (b) FLIR camera data of switch during 100W experimental test

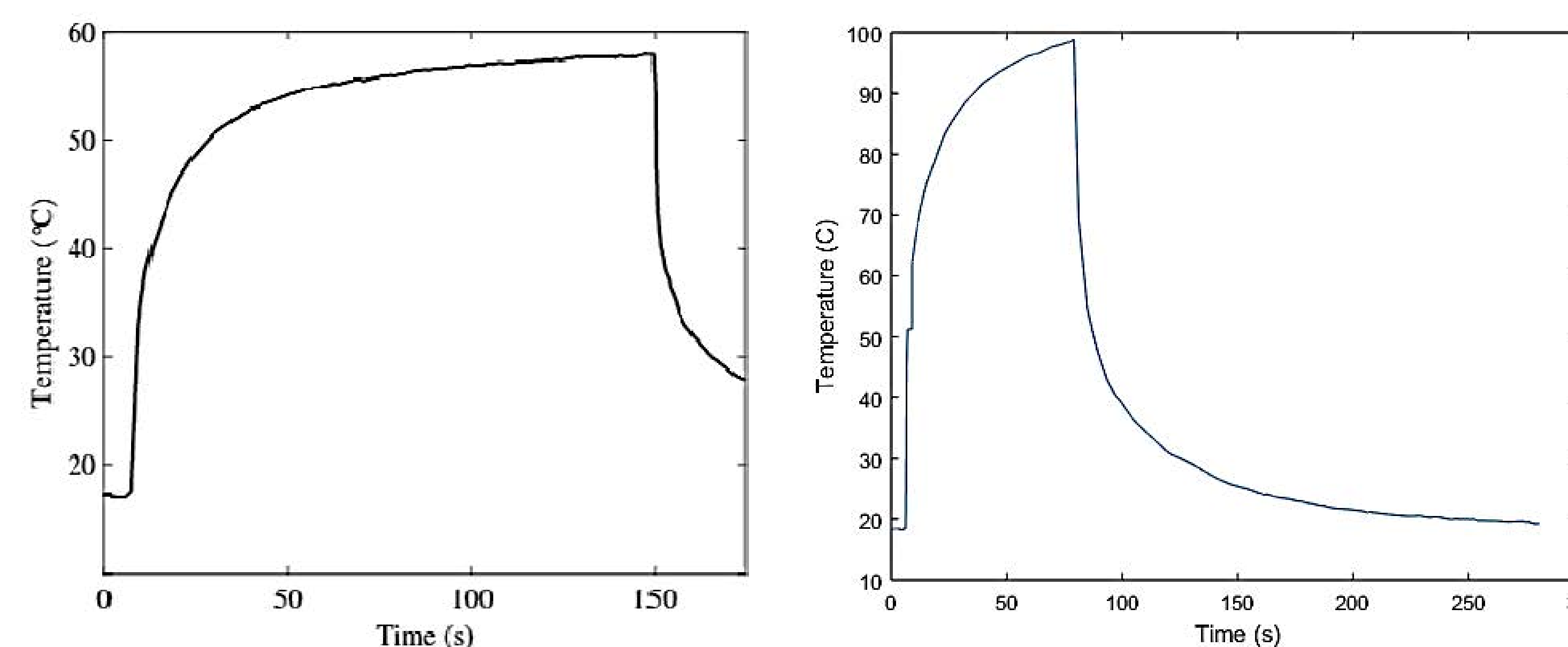


Figure 4. Temperature variation for 100 W (left) and 200 W (right) avg. power tests

## Results and Analysis

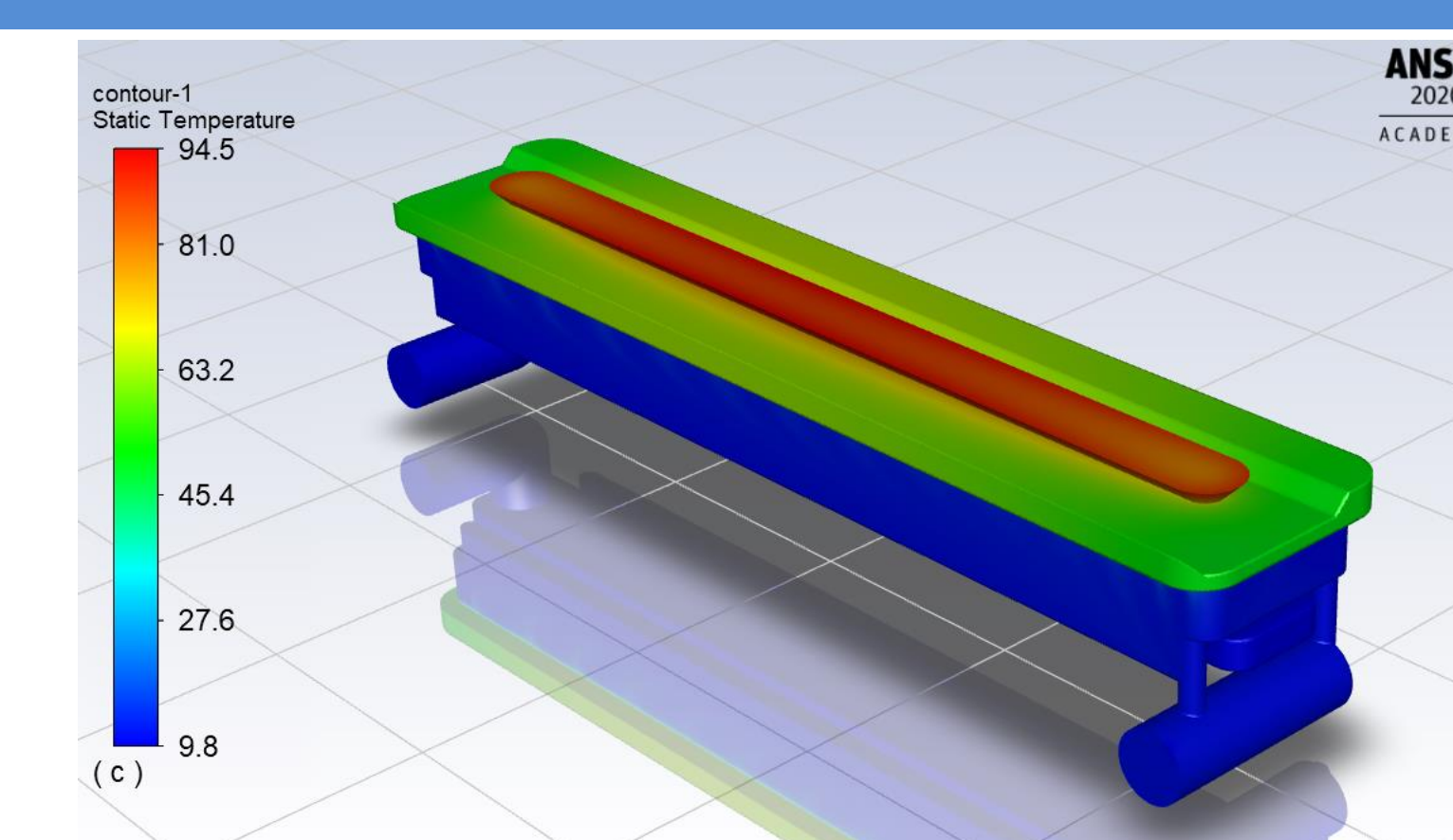


Figure 5. Temperature distribution of the JI-TMS at 200 W avg. power test : Uniform temperature distribution across the semiconductor, however, the temperature exceeds the threshold!

Figure 6. Spatial temperature distribution along semiconductor for 100 W avg. power test: The cross-validation results between CFD and experimental analysis show a good agreement with average error of 5.4%.

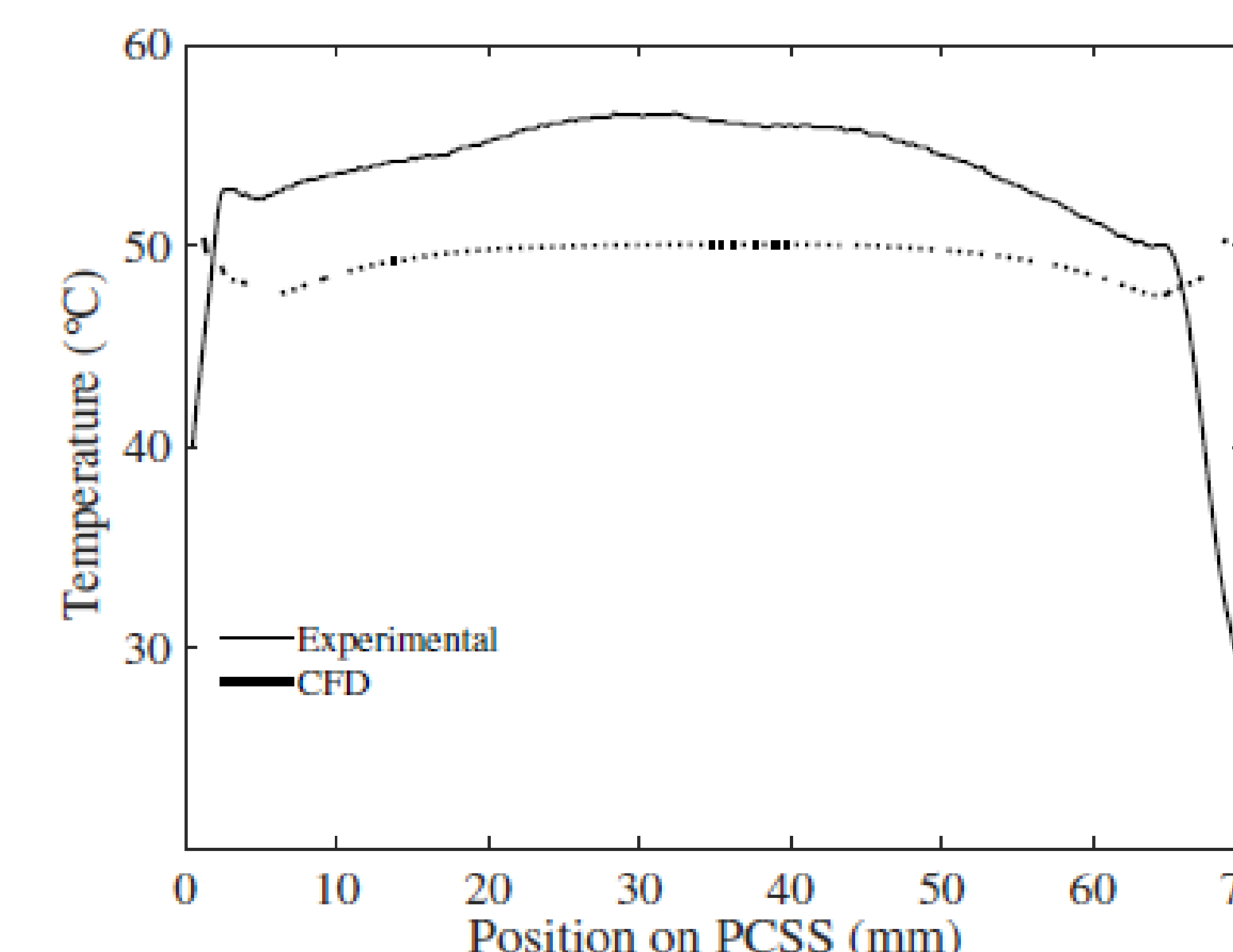


Table 2. Results of max switch temperature of the experiment and simulation

	Simulation	Experiment	Error
100 W Avg. Power	54.7	51.72	5.4%
200 W Avg. Power	95.48	98.87	3%

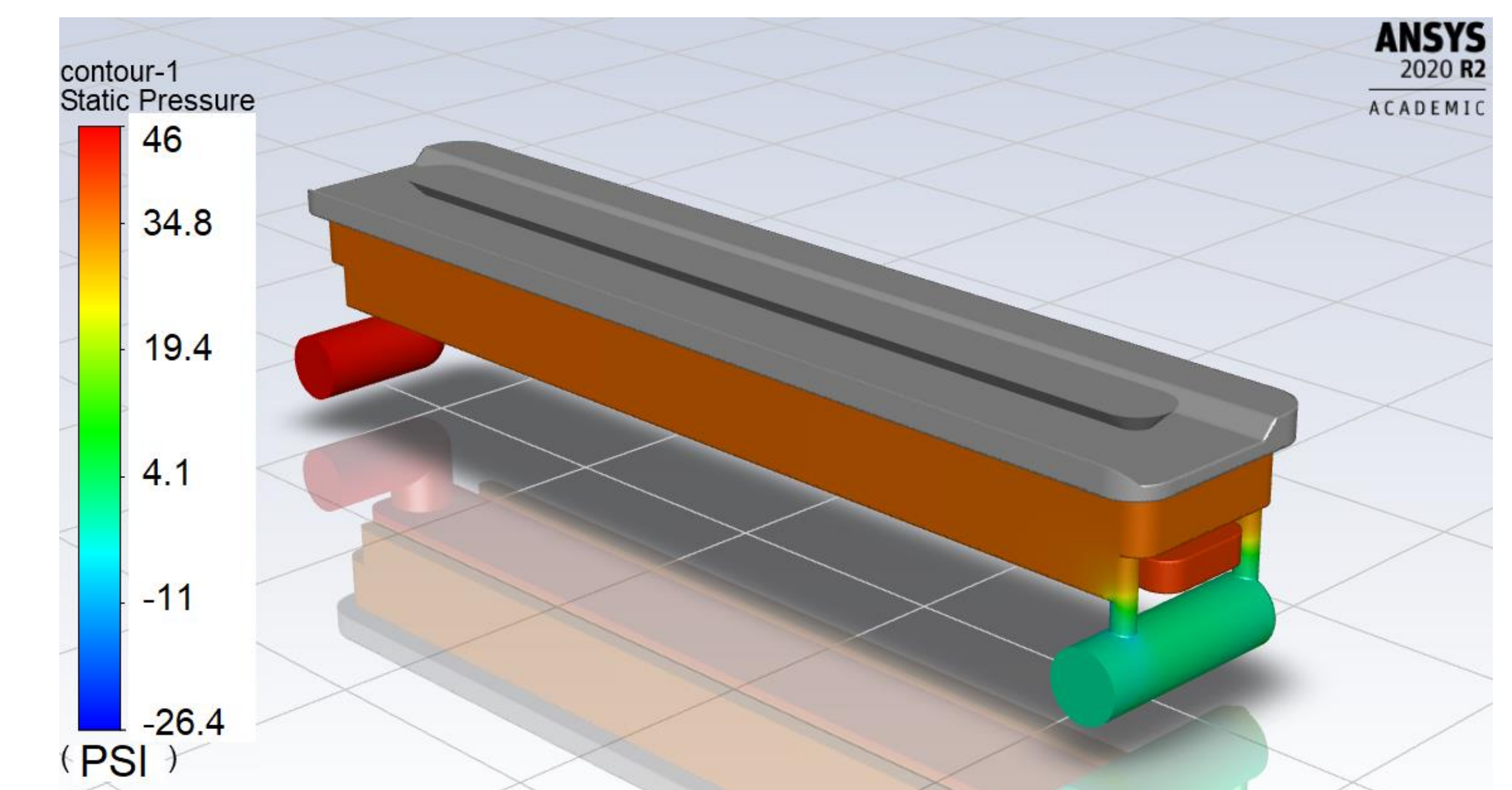


Figure 7. Pressure drop of 1 gpm flow shows 46 psi, yielding a laminar flow regime. To achieve the turbulence regime the flow rate needs to increase, therefore, drastically increasing the pressure requirement.

## Summary

- The results show that device temperature is well maintained below the desired operating temperature for 100 W of avg. power.
- The results for 200 W avg. power test show good agreement with the numerical data, however, the switch temperature exceeds the threshold temperature. For this reason, the current geometry will not be pursued.
- Based on the pressure drops incurred by the JI-TMS, the proposed cooling system is deemed unfeasible at this scale.



A more optimized cooling method is being considered as the on-going work of this study.

## References

- J. N. Berg, R. C. Allen, and S. Sobhansarbandi. "A Novel Method of Cooling a Semiconductor Device through a Jet Impingement Thermal Management System: CFD Modeling and Experimental Evaluation." International Journal of Thermal Sciences, 2021 (Under-review).
- M. Angioletti a , E. Nino a , G. Ruocco, 2004. "CFD turbulent modelling of jet impingement and its validation by particle image velocimetry and mass transfer measurements" . International Journal of Thermal Sciences 44 (2005) 349–356 .
- Bovo, Mirko, 2011. "On the numerical modelling of impinging jets heat transfer". Department of Applied Mechanics CHALMERS UNIVERSITY OF TECHNOLOGY.
- Hosain Lokman, 2013. "CFD Simulation of Jet Cooling and Implementation of Flow Solvers in GPU". Royal Institute of Technology School of Engineering Sciences.

## Acknowledgement

"The authors wish to thank the Office of Naval Research for their support of this work under Grant No. N00014-17-1-3016."

UMKC OSPRES Grant Biannual Review, Spring 2021



# Heat Transfer Enhancement of a Jet Impingement Thermal Management System: A Comparison of various Nanofluid Mixtures

Jordan N. Berg<sup>1</sup>, Roy C. Allen<sup>1,2</sup>, Sarvenaz Sobhansarbandi<sup>1</sup>  
<sup>1</sup>Department of Civil and Mechanical Engineering  
<sup>2</sup>Missouri Institute for Defense and Energy (MIDE)  
 University of Missouri-Kansas City

## Objective and Motivation

**Primary Problem:** Dielectric heat transfer fluids possess thermophysical fluid properties that inhibit their ability to achieve >1 GW/m<sup>3</sup> cooling densities.

**Sub-Problem:** Pure silicone fluid with viscosity of 20 cSt (PSF-20cSt) is ~15 times more viscous than water, and therefore requires increased pumping power within the TMS.

**Relevance to OSPRES Grant Objective:** Increased cooling performance facilitates semiconductor devices to operate at higher average-power (>1 kW).

**State-of-the-Art (SOTA):** Nanofluids have been shown to increase the thermal conductivity of base-fluids by 12% in comparison to the generic dielectric fluid alone; resulting in greater cooling density and decreased pumping power.

**Deficiency in the SOTA:** The addition of nanoparticles in base-fluids results in a tradeoff between thermophysical properties, i.e. the addition of nanoparticles can increase the thermal conductivity, while also increasing viscosity of the mixture.

**Solution Space:** Develop a nanofluid by entraining ceramic nanoparticles in the dielectric base-fluid to increase the nanofluid's thermal conductivity, thereby improving cooling density capabilities. Utilize a nanofluid with desirable thermal properties that can serve as a viable heat transfer fluid (HTF) for TMSs in high power density electronics.

## Background

**PSF-20cSt vs water**  
**4 times less heat capacity and thermal conductivity and 15 times more viscous!**

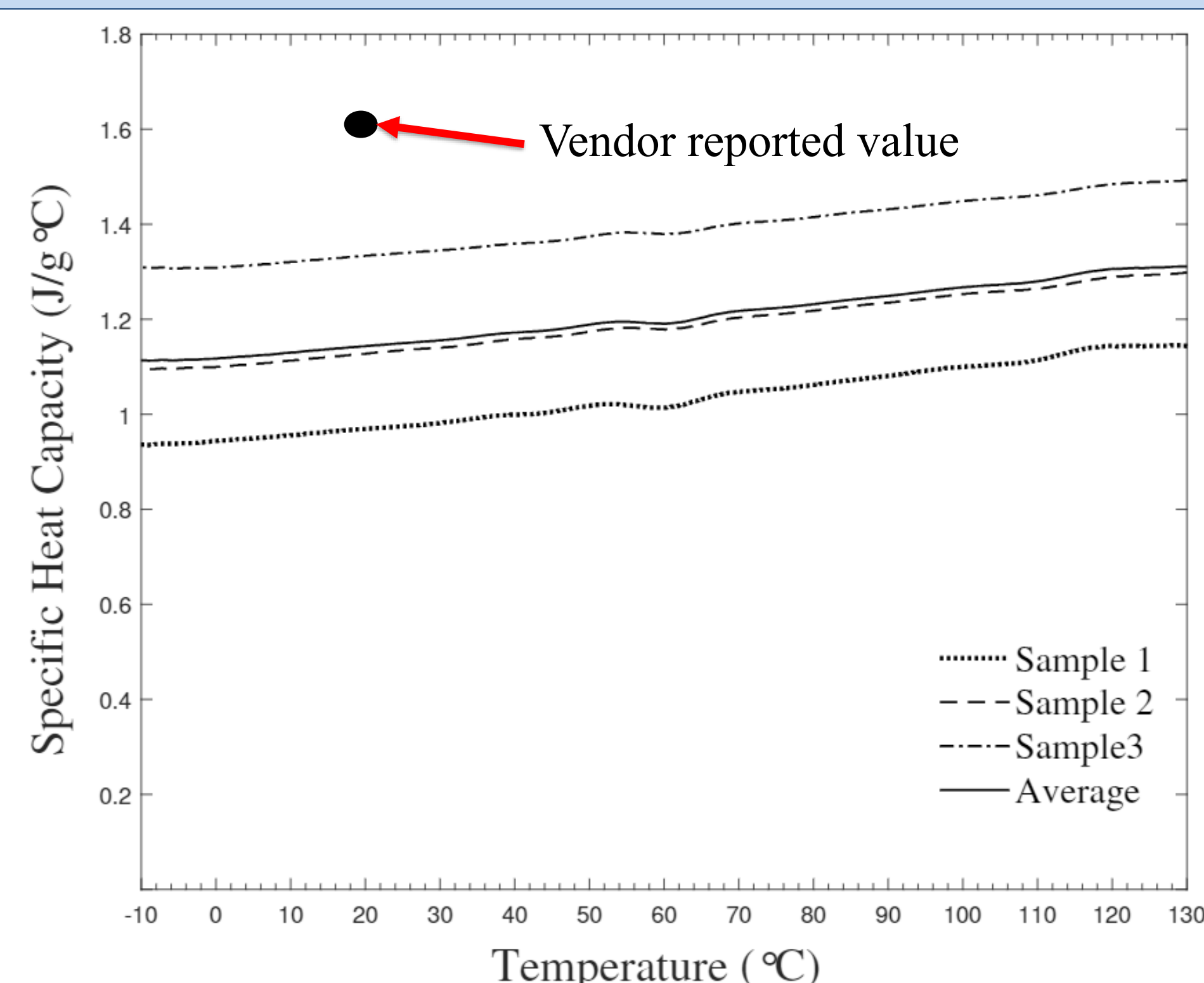
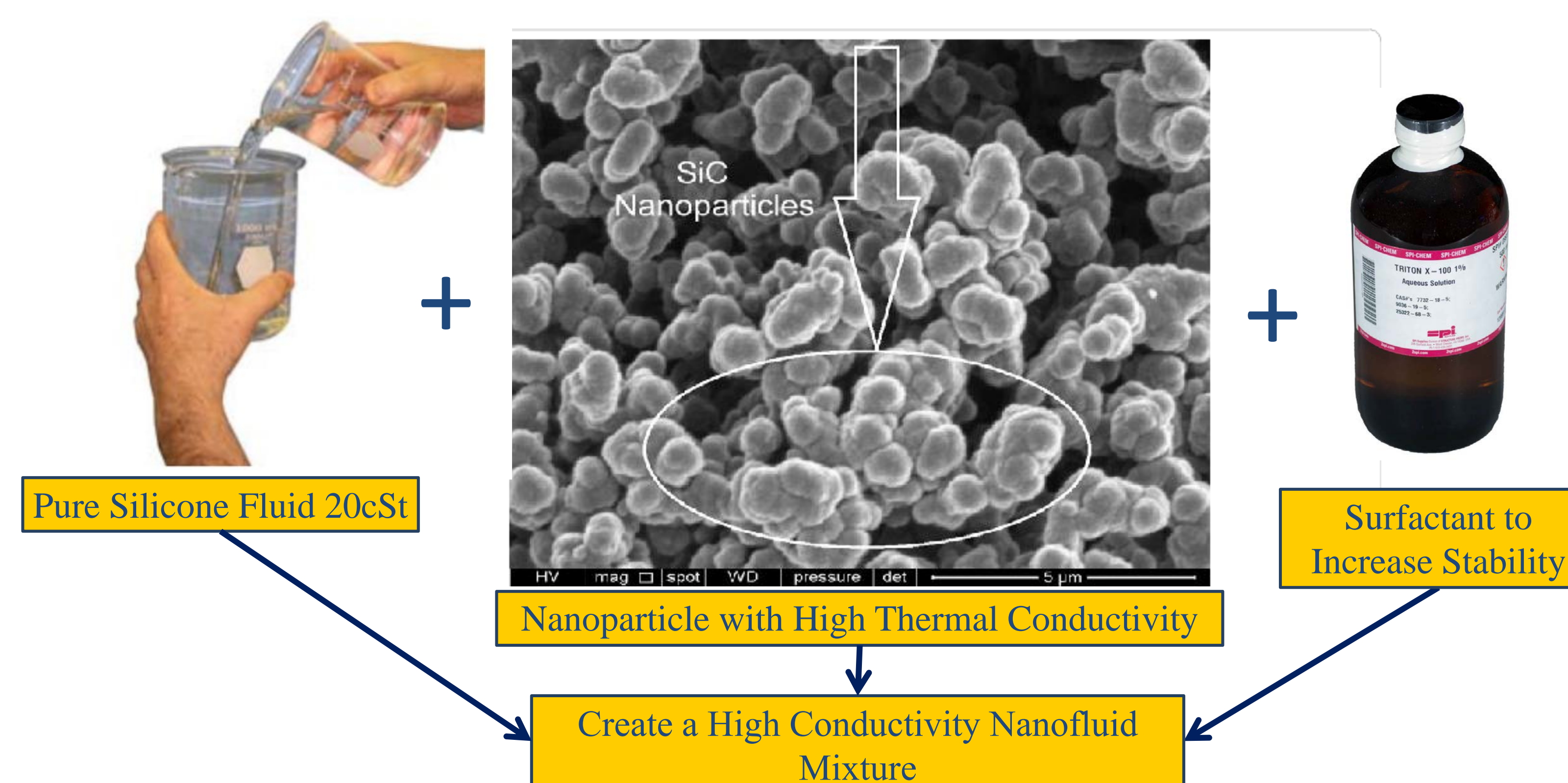


Figure 1. Heat capacity value from DSC testing vs. vendor value for 3 samples of PSF-20cSt

Table 1. Heat capacity deviation

Results	Avg. Heat Cap. (J/g°C)
DSC results	1.11
Vendor Values	1.60
Deviation percentage	30.65%

## How to increase thermophysical properties?



## Methods and Analysis

### Thermal Analysis Method

A DSC measures the difference in Heat Flow Rate between a sample and inert reference as a function of time and temperature

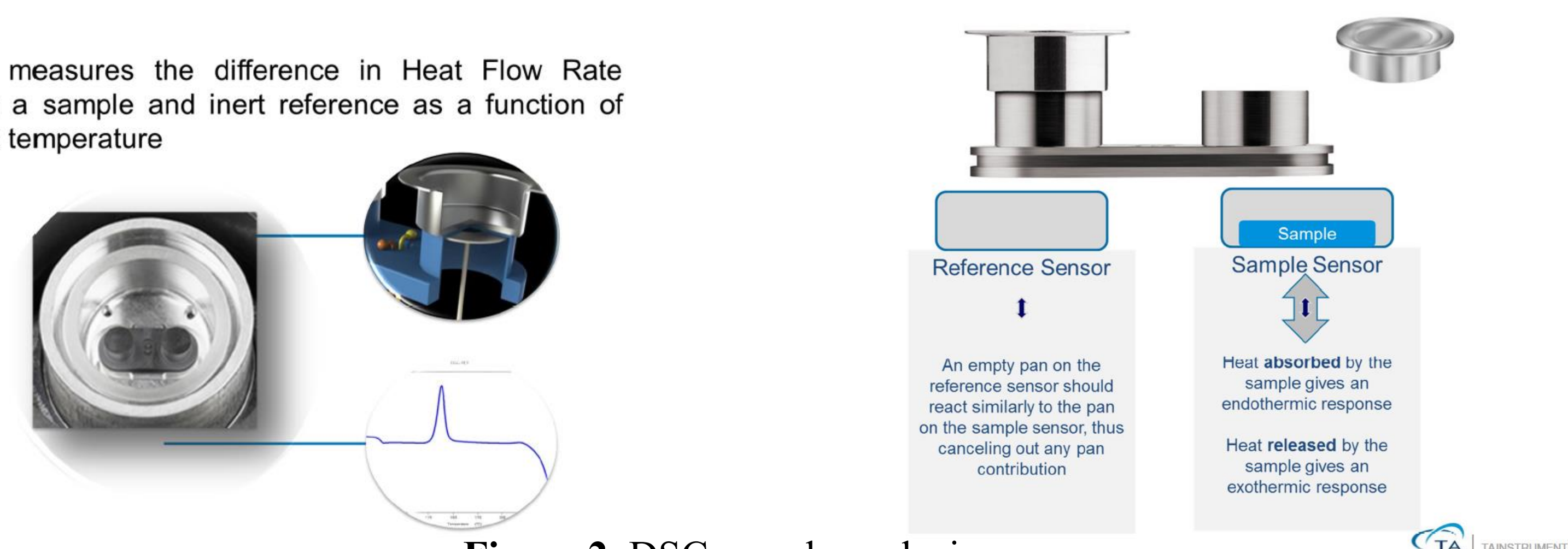


Figure 2. DSC sample analysis

### Samples Preparation and Testing

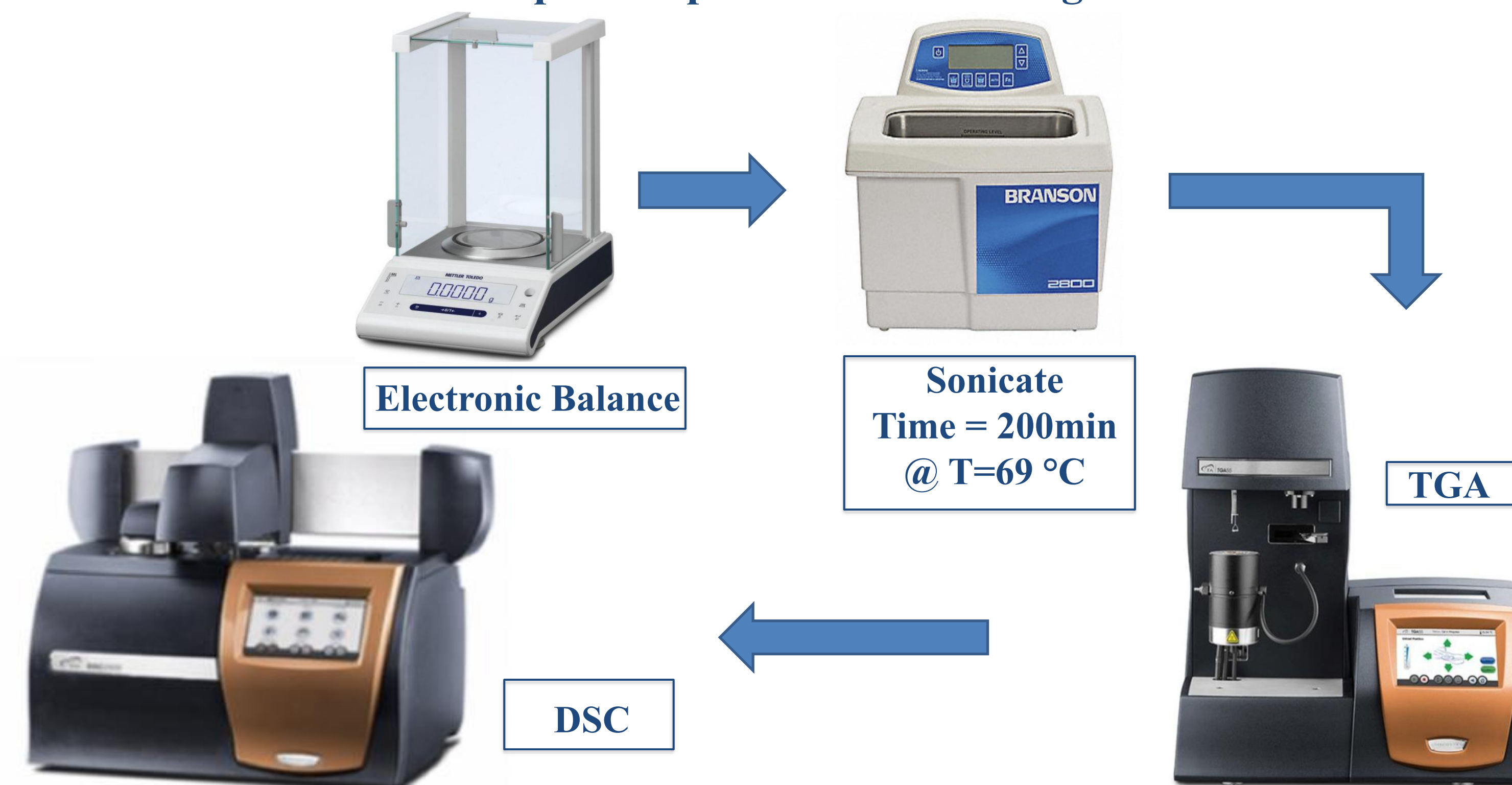


Figure 3. PSF-20cSt plus percentage variation of Alumina, Silicon Carbide and Iron (II,III) Oxide with and without surfactants

## Results and Analysis

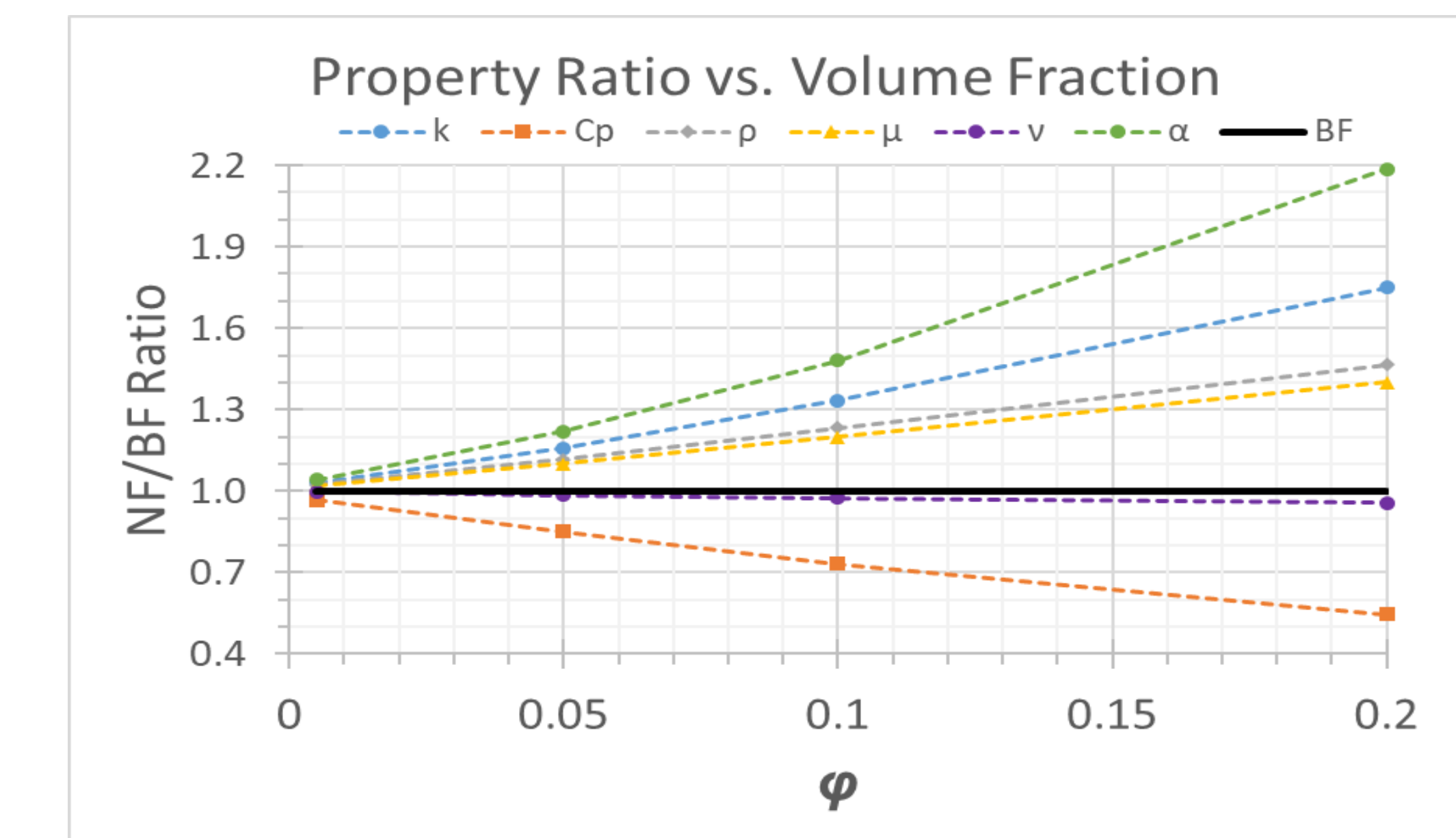


Figure 4. Thermophysical properties prediction of SiC-PSF-20cSt nanofluid vs base fluid at constant temperature for various volume fractions

- The thermal analysis of nanofluids with various nanoparticles combination have shown highest heat capacity enhancement of 15.2% and maximum heat capacity drop of 10.1% compared to pure PSF-20cSt.

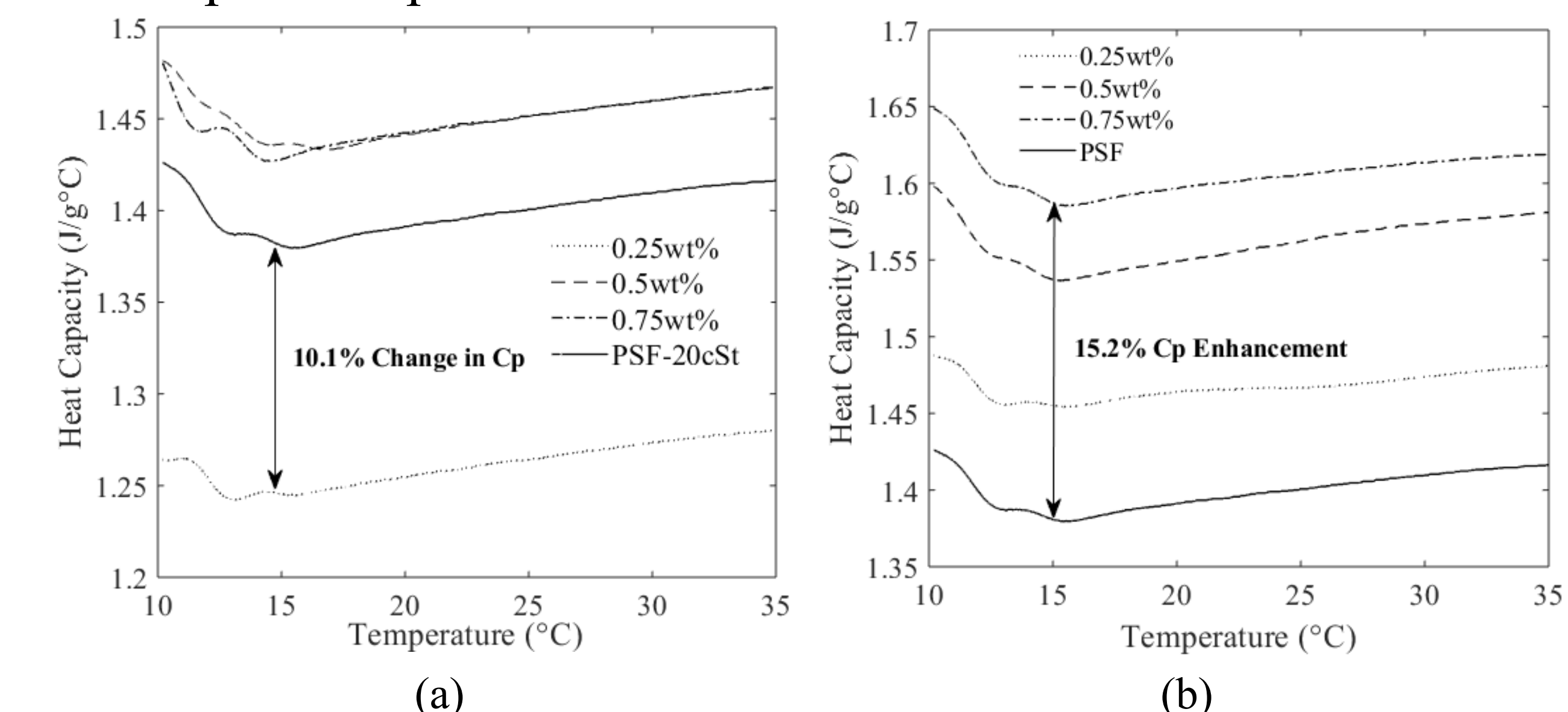


Figure 5. (a) SiC-PSF-20cSt nanofluid mixture, (b) Fe<sub>2</sub>O<sub>3</sub>-PSF-20cSt nanofluid mixture

## Summary

- The mixtures with highest and lowest heat capacity were selected to be tested for thermal conductivity.
- The enhancement in heat capacity results in high convective heat transfer, while enhancement in thermal conductivity results in conductive heat transfer enhancement.
- The enhancement in thermophysical properties of nanoparticle based PSF-20cSt will improve the performance of the high power density electronics.

## Acknowledgement

“The authors wish to thank the Office of Naval Research for their support of this work under Grant No. N00014-17-1-3016.”

UMKC OSPRES Grant Biannual Review, Spring 2021



## OBJECTIVE

Determining the extent to which the physical aperture size of an antenna array, composed of microstrip ESA elements, can be reduced, while maintaining performance in peak power density, bandwidth, and electronic beam steerability over the UHF range (0.4–1 GHz), compared with present-art high-power-microwave-capable antenna arrays.

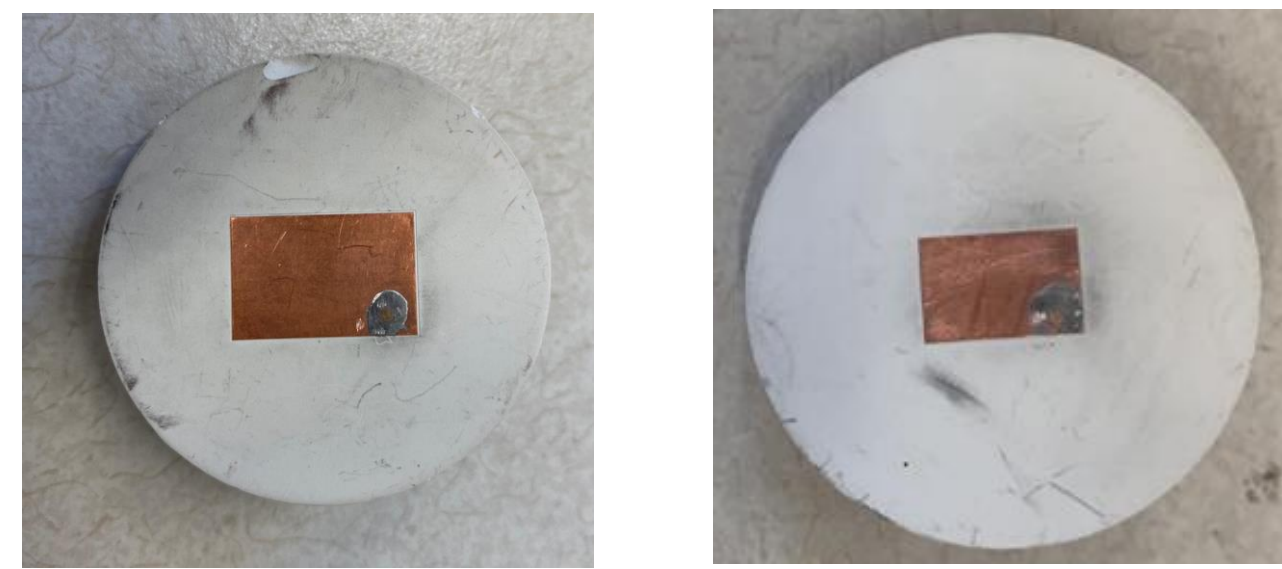
## STATE-OF-THE-ART (SOTA)

Horn, reflector, Vivaldi, valentine, etc. are commonly used ultra-wide-band antenna elements in a phased array for HPM transmissions. However, these antennas have the disadvantage of **large physical aperture size**.

## SOLUTION PROPOSED

1. Usage of wideband microstrip ESAs as array elements [1].
2. Performance optimization of antenna elements via multi-parameter D/Q (directivity/quality factor) technique.
3. Arrangement of ESAs in suitable lattice structures (preferably, hexagonal/triangular).

## MINIMUM VIABLE VALIDATION PROTOTYPES

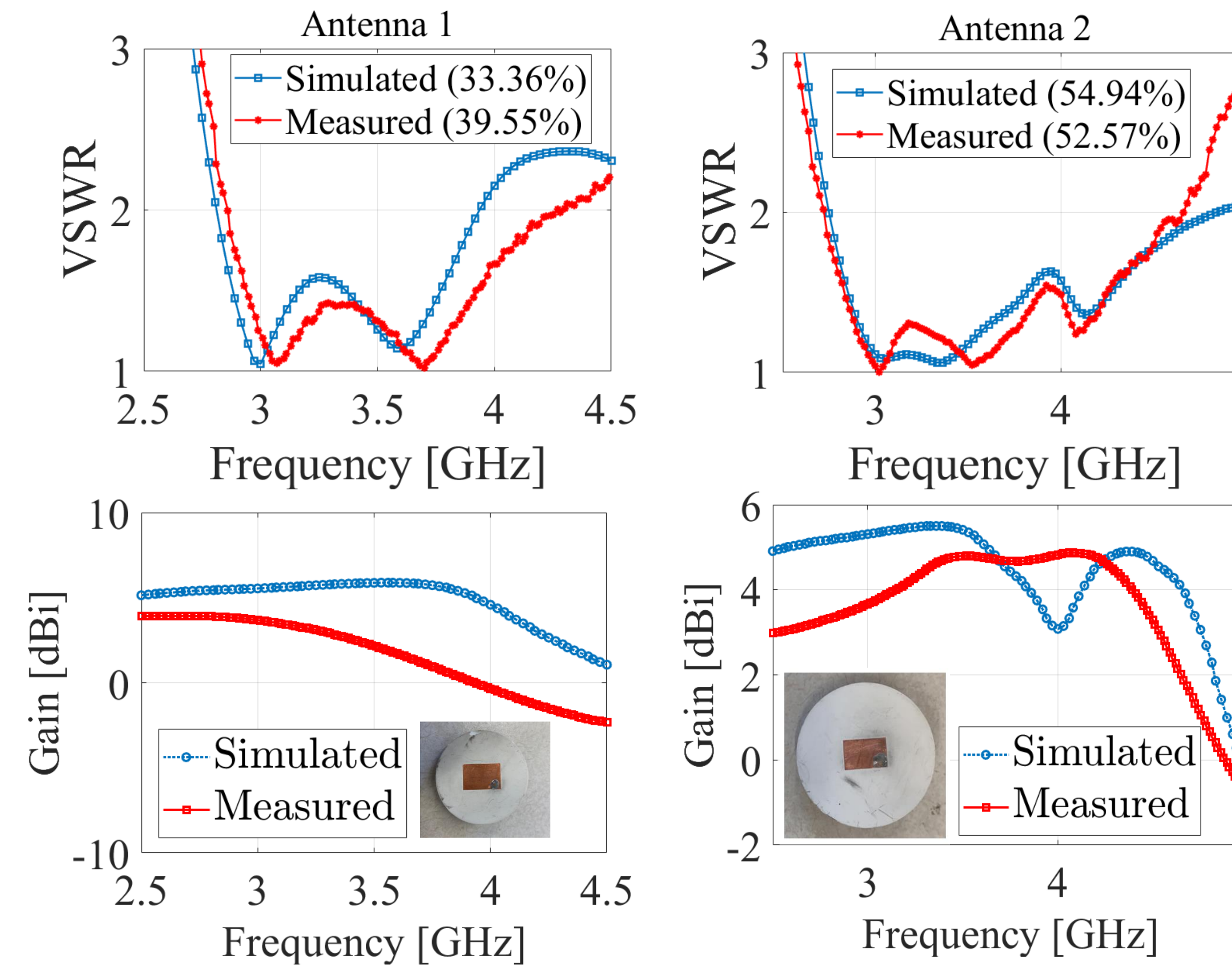


Antenna 1      Antenna 2

#	Patch Type	Substrate Used	Frequency Range (GHz)	Radiating Aperture Area (mm <sup>2</sup> )	rE/V (at 10 m)
1	Rectangular	TMM-6 ( $\epsilon_r = 6$ )	2.5 – 5	244.61	0.7902
2	Rectangular	TMM-10i ( $\epsilon_r = 9.8$ )	2.5 – 5	138.58	0.7855

- Due to unavailability of proper substrate panel sizes from the vendors required in the UHF region, the design methodology [1] is validated at 3.75 GHz, on TMM-6 and TMM-10i substrates.
- The rE/V value, in each case, has been computed via CST, by subjecting the elements to Gaussian pulse type voltage excitation.

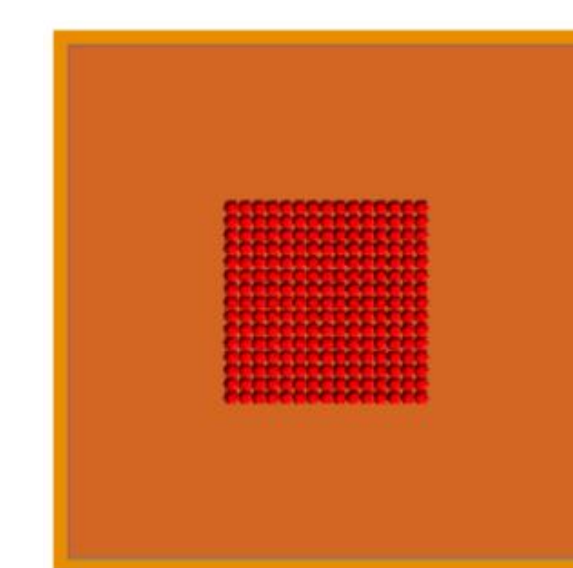
## EXPERIMENTAL RESULTS



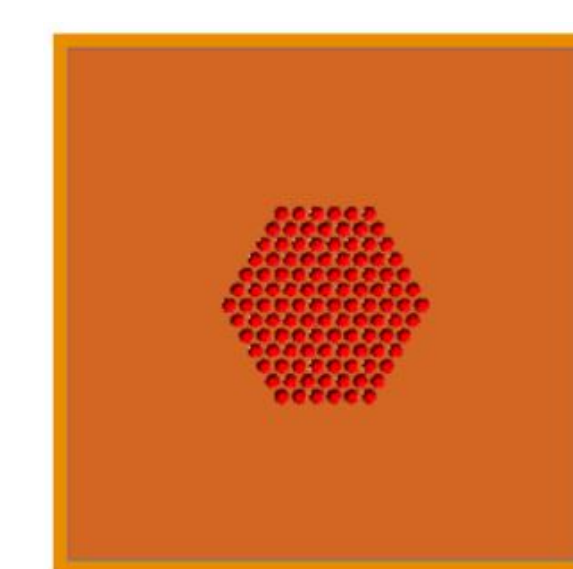
- For both antennas 1 and 2, good agreement has been achieved between the simulated and the measured VSWR data.
- Deviation in the measured gain results, from the corresponding simulated results, is primarily due to multiple reflections from surrounding metal objects.

## TRADESPLACE ANALYSIS OF ARRAYS OF ESA ELEMENTS

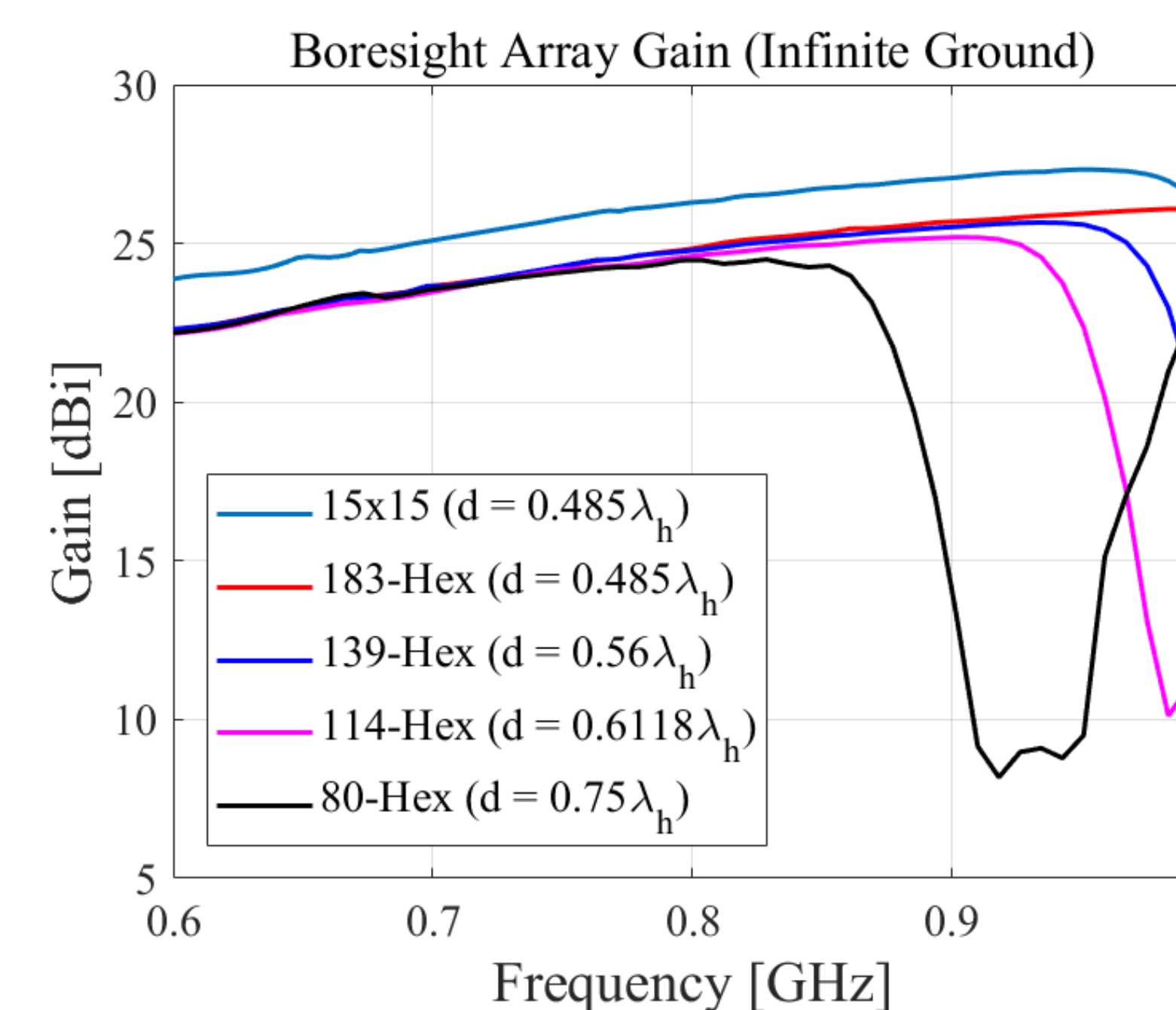
- Using the design approach [1], microstrip ESA element is designed in the UHF range (640 – 990 MHz) on a 1.05” thick TMM-10i substrate.
- Planar arrays, composed of these designed ESA elements, of various lattice formation and size, have been investigated.
- Transformation from square to hexagonal lattice resulted in 30% reduction in aperture area with < 3.5 dBi loss in gain.



Square Lattice



Hexagonal Lattice



## REFERENCES

- [1] B. Barman, K. C. Durbhakula, B. Bissen, D. Chatterjee and A. N. Caruso, "Performance Optimization of a Microstrip Patch Antenna using Characteristic Mode and D/Q Analysis," *2020 XXXIIIrd General Assembly and Scientific Symposium of the International Union of Radio Science*, 2020, pp. 1-4.
- [2] A. K. Shackelford, Kai-Fong Lee and K. M. Luk, "Design of small-size wide-bandwidth microstrip-patch antennas," *IEEE Antennas Propag. Mag.*, vol. 45, no. 1, pp. 75-83, Feb. 2003.
- [3] R. Garg, P. Bhartia, I. Bahl, and A. Ittipiboon, *Microstrip Antenna Design Handbook*, Boston, MA: Artech House, 2001, pp. 771 – 779.
- [4] Ming-Yao Xia, Chi Hou Chan, Yuan Xu and Weng Cho Chew, "Time-domain Green's functions for microstrip structures using Cagniard-de hoop method," *IEEE Trans. Antennas Propag.*, vol. 52, no. 6, pp. 1578-1585, Jun. 2004.

## SUMMARY

- A new method to design electrically small wideband (>30% 2:1 VSWR bandwidth) microstrip patch antenna elements is presented with supporting experimental data.

Comparative Analysis of Single Antenna Elements						
Antenna Type	Koshelev (Apr. 2021 MSR)	Shark (Apr. 2021 MSR)	U-slot Antenna [2]	Proposed Design 1 [1]	Proposed Design 2 [1]	
Substrate Used	-	-	Polyethylene ( $\epsilon_r = 2.33$ )	FR-4 ( $\epsilon_r = 4.5$ )	TMM-10i ( $\epsilon_r = 9.8$ )	
Operating frequency range ( $f_c \pm BW/2$ ) (MHz)	900 ± 180	-	900 ± 182.7	869.5 ± 162.5	899 ± 169	
Radiating Aperture Area (m <sup>2</sup> )	0.0076	0.0029	0.0129	0.0048	0.0019	
Volume (m <sup>3</sup> )	0.0017	3.05 × 10 <sup>-4</sup>	5.23 × 10 <sup>-4</sup>	1.5 × 10 <sup>-4</sup>	4.1 × 10 <sup>-5</sup>	
Gain (dBi) @ 900 MHz	4	2.72	~ 6 - 7	5.96	4.99	
HPBW (deg)	E-plane	83	119.6	Unknown	95.79	103.19
	H-plane	83	331.2	Unknown	82.78	102.62
rE/V at 10 m	1.39	Unknown	Unknown	0.9082	0.7333	
APHC @ 900 MHz (W) [3]	Unknown	Unknown	281.11	267.38	120.55	

APHC = Average Power Handling Capability ( $P_{av}$ ).

- Tradespace analysis of the arrays of designed microstrip ESA elements, of various size and lattice arrangements, show that with 30% reduction in the aperture area ( $\approx 50\%$  reduction in # of elements), the gain drops by < 3.5 dBi without any scan blindness spotted as the main beam is steered from boresight to  $\pm 60^\circ$  in the range 640 – 990 MHz.

## FUTURE WORK

- Optimization of the probe locations in the microstrip ESA elements using Genetic Algorithm optimizer in FEKO, along with supporting experimental data.
- Testing time-domain reflectometry for the designed ESA elements.
- Time-domain analysis of microstrip ESAs via [4] and its comparison with the FDTD solver in FEKO and CST (optional).

## ACKNOWLEDGEMENT

The authors would like to gratefully acknowledge Mr. Jeffery Newhook, for his contribution in antenna manufacturing; Mr. Benjamin Bissen and Dr. Kalyan C. Durbhakula, for their interest in and support with measurements; and Dr. Michelle Paquette, for taking her time out to review the document.

The authors wish to thank the Office of Naval Research for financially supporting this work under Grant No. N00014-17-1-3016.

### OBJECTIVE AND MOTIVATION

#### Problem Statement:

Determine the extent to which the physical aperture area of an antenna array, composed of antenna elements, can be reduced, while maintaining performance in peak power density, bandwidth, and electronic beam steerability over the UHF range (0.4–1 GHz), compared with present-art high-power-microwave-capable antenna arrays.

#### State-of-the-Art (SOTA):

The balanced antipodal Vivaldi antenna (BAVA) is the SOTA antenna element due to its exceptional 20:1 impedance bandwidth ratio as well as its ability to handle tens-of-MW input power.

#### Solution Proposed:

The Koshelev antenna has a unique design that generates an ultra-wide-band (UWB) response by effectively merging radiation characteristics from a transverse electromagnetic (TEM) horn antenna with exponentially tapered flares, an electric monopole, and magnetic dipoles over a wide frequency range [1]. This opens an opportunity to investigate the design parameter space and understand parameter effects on impedance bandwidth, radiation pattern, electric field distribution, and other metrics via a tradespace study.

#### Relevance to OSPRES Program:

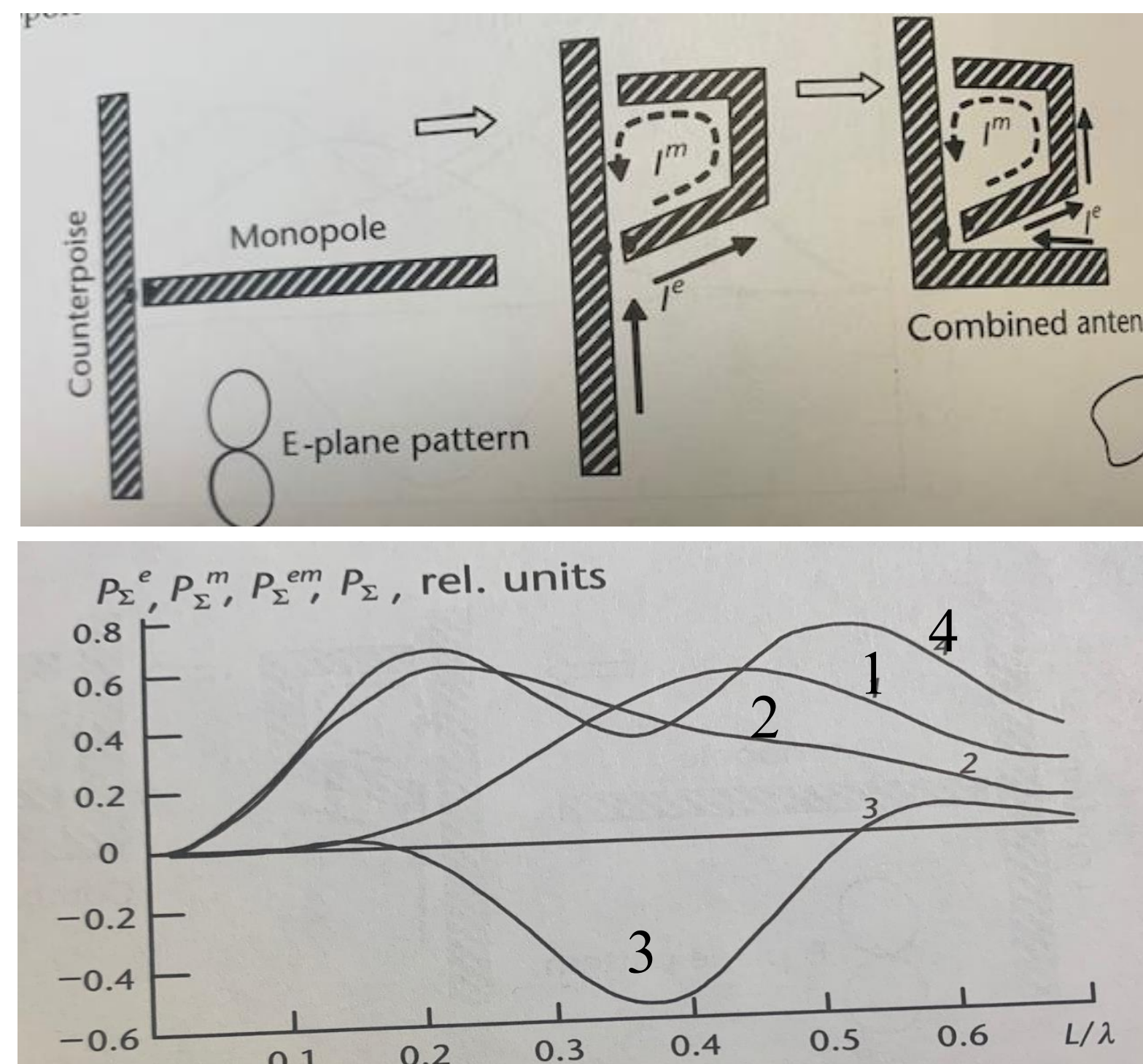
The Koshelev antenna has proven to withstand high input voltages (200 kV peak to peak bipolar pulses) which satisfies the specific OSPRES HPM radiator requirement. Furthermore, the Koshelev antenna was developed specifically for radiating short rise-time pulses over long distances with high transient gain, wide match band and wide beamwidth.

#### Target Metrics (Single Element):

Aperture size	$f_c \pm BW/2$	Peak Gain (900 MHz)	HPBW (900 MHz)	Aperture efficiency (900 MHz)	rE/V
$\leq 9 \text{ cm} \times 9 \text{ cm}$	900 MHz $\pm$ 200 MHz	$\geq 3 \text{ dBi}$	As wide as possible	$\geq 130\%$	$\geq 1$

### BACKGROUND

The Koshelev antenna belongs to the class of combined (electric radiator + magnetic radiator) antennas. Initially, a 2D flat combined antenna was prototyped and tested which suffered from pattern failure at upper bounds of their pass band. The 2D flat combined antenna is then replaced by 3D TEM horn based unbalanced combined antenna named after its creator V. I. Koshelev [2]. In short, the Koshelev antenna is made up of TEM horn with exponential profile, an electric monopole and two magnetic dipoles.

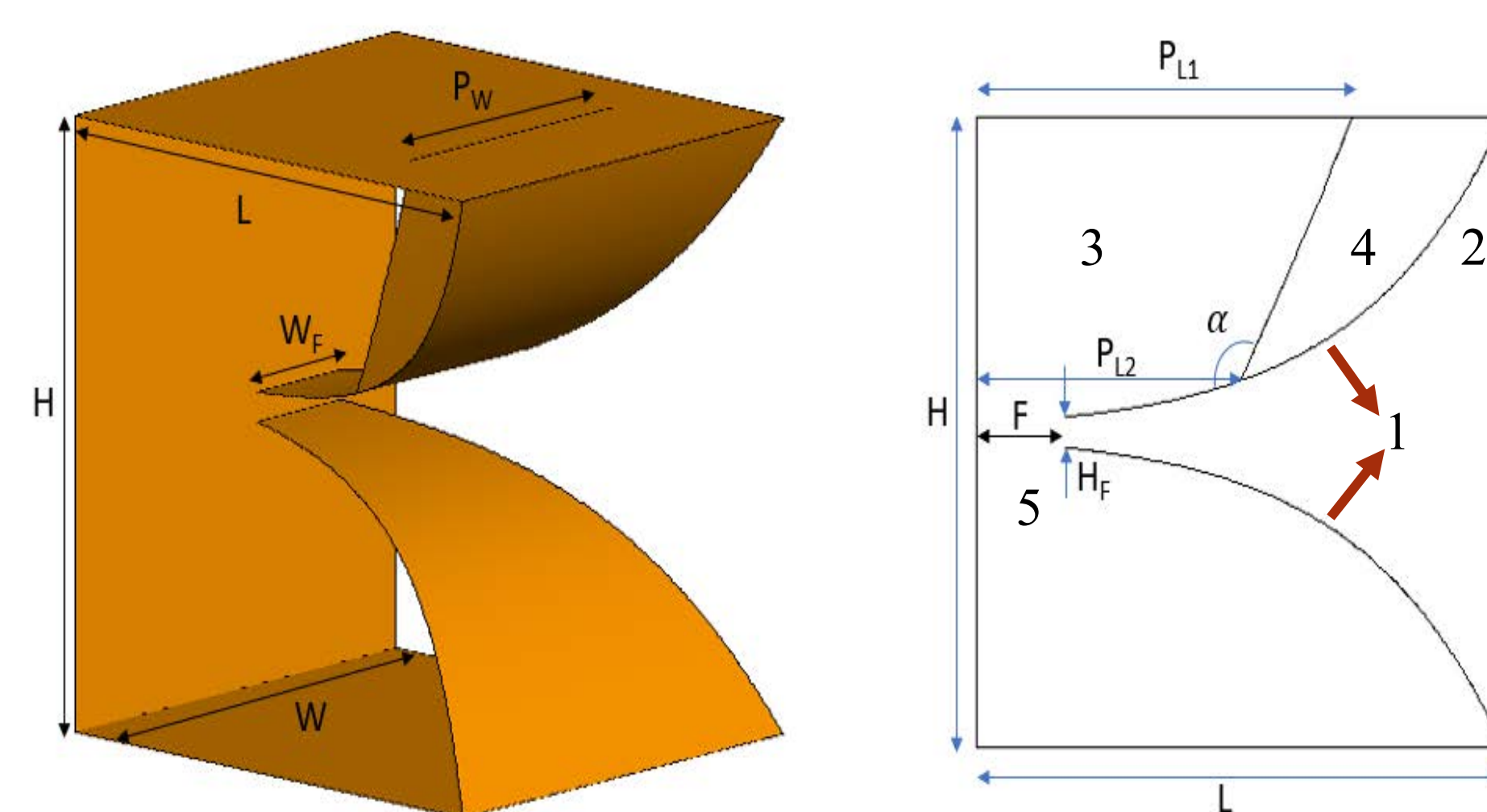


### METHODS

The computational design and electromagnetic (EM) simulations of the Koshelev antenna have been carried out using commercially available CST microwave studio software. For pulsed wave inputs, we have picked high-frequency time domain solver within CST as our choice of full-wave solver. The time domain solver is based on the Finite Integration Technique (FIT). The FIT method discretizes the structure into grids and uses the integral form of Maxwell's equations to calculate grid electric voltages. The default metrics such as reflection coefficient, far field electric field at 'x' meters distance, radiation pattern, directivity, peak gain over frequency obtained from CST are post-processed using MATLAB/Python to calculate auxiliary metrics such as aperture efficiency, transient gain (rE/V), impulse response, energy density, full-width half-maximum (FWHM), ringing etc.

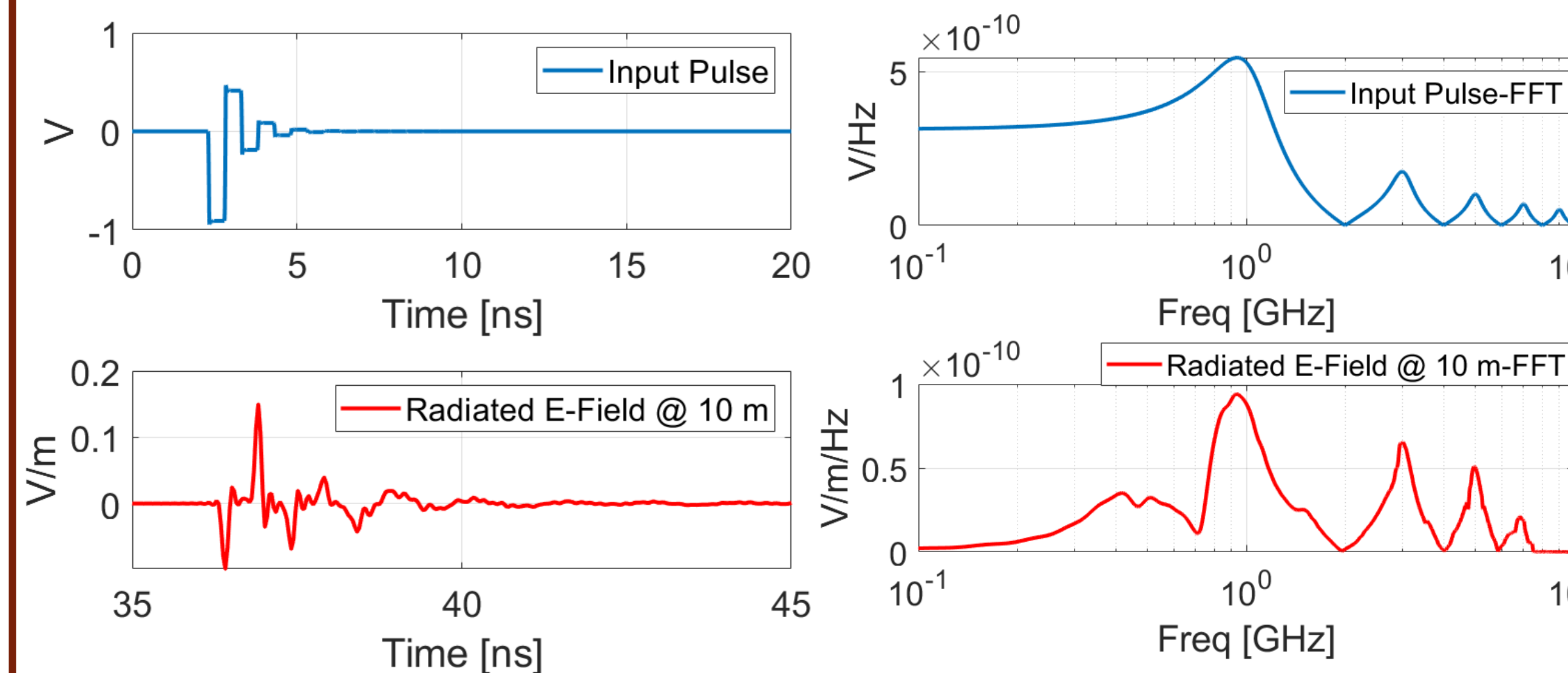
### RESULTS & ANALYSIS

Koshelev Antenna – Single Element



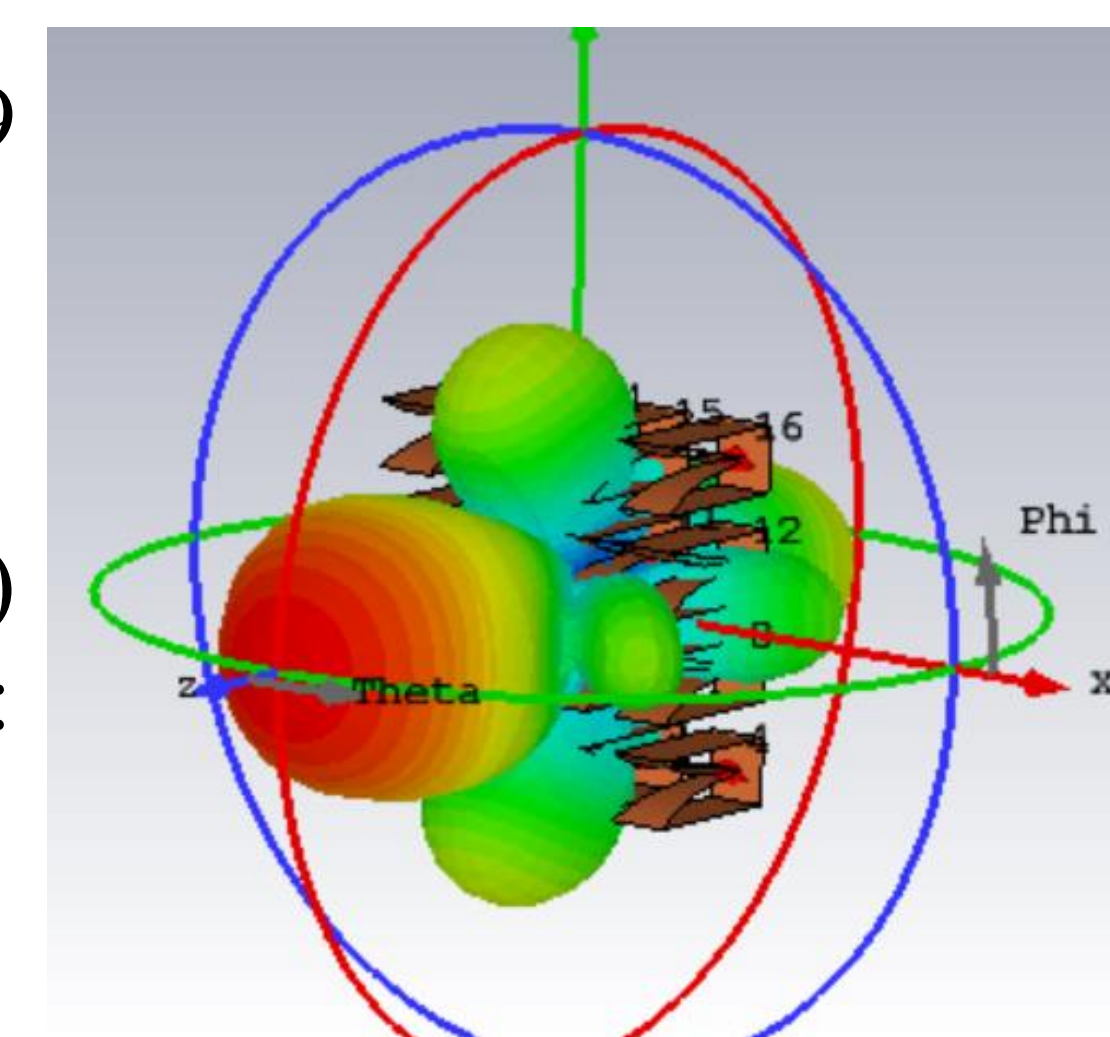
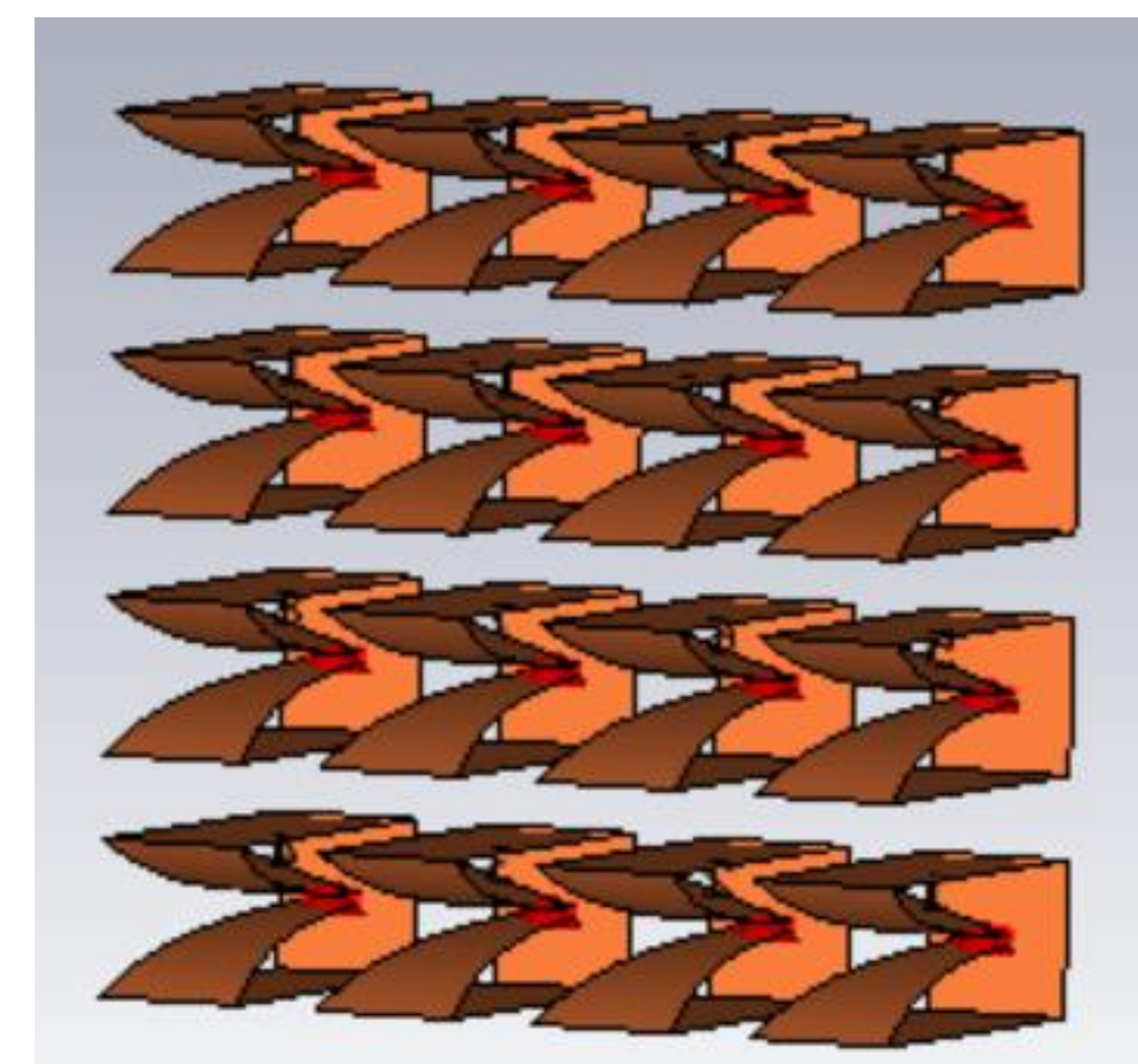
- 1 – TEM Horn
- 2 – Electric Monopole
- 3 – Active Magnetic Dipole
- 4 – Passive Magnetic Dipole
- 5 – Feed

Single element aperture size – **9.3 cm × 8.5 cm**  
 4 × 4 array aperture size with 50 mm spacing – **48 cm × 52 cm**  
 Transverse Length – **22 cm**



rE/V (SE) – 1.49  
 rE/V (4 × 4 Array) – 21.5  
 Rad Efficiency: -0.053 dB (98%)  
 Total Efficiency: -0.1671 dB (96%)

4 × 4 Koshelev Array Antenna

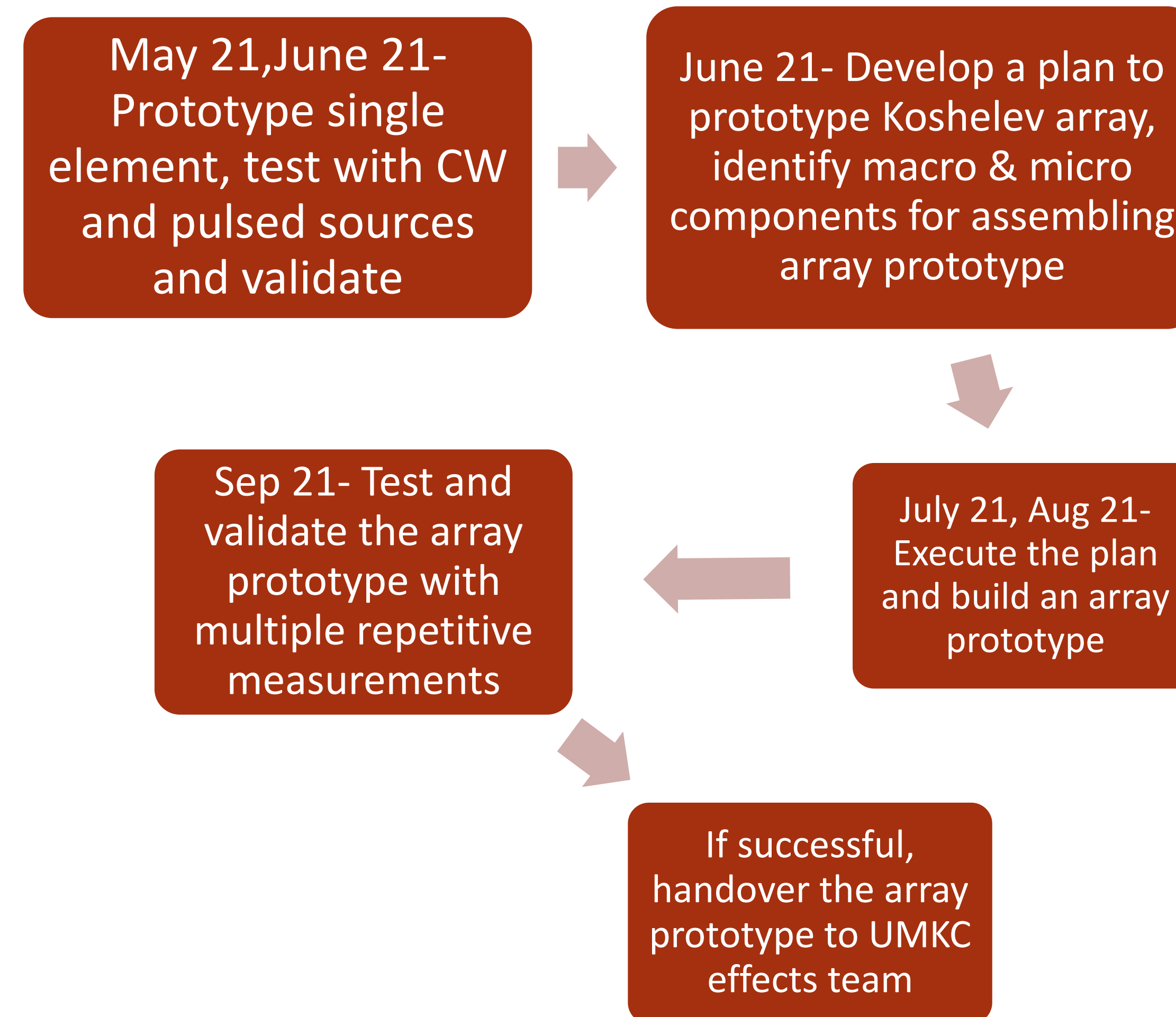


Antenna element type	BAVA [3] (Single Element)	Koshelev Antenna (Single Element)	Koshelev Antenna (4 × 4 Array)
Aperture size (H×W)	10 cm × 10 cm	9.3 cm × 8.5 cm	48 cm × 52 cm
Physical aperture area	0.001 m <sup>2</sup>	0.0076 m <sup>2</sup>	0.2496 m <sup>2</sup>
Operating frequency range (fc±BW/2)	900 MHz ± 100 MHz	900 MHz ± 180 MHz	900 MHz ± 100 MHz (Except few elements)
Peak gain (900 MHz)	1.3 dBi	4 dBi	15 dBi
HPBW (900 MHz)	E-plane	90°	30°
	H-plane	90°	30°
Aperture efficiency (900 MHz)	105%	303%	113%

### CONCLUSION

Antenna metrics comparison between Koshelev antenna and BAVA at desired operating frequency showed that the Koshelev antenna outperforms the SOTA BAVA [3] in terms of aperture area, peak gain, aperture efficiency and transient gain.

### FUTURE WORK



### REFERENCES

- Gubanov, V. P., et al. "Sources of high-power ultrawideband radiation pulses with a single antenna and a multielement array." *Instruments and Experimental Techniques* 48.3 (2005): 312-320.
- V. I. Koshelev et al., "Ultrawideband Short-Pulse Radio Systems," Artech House, Boston, 2017.
- Zhang, Jian, Xiaoxing Zhang, and Song Xiao. "Antipodal Vivaldi antenna to detect UHF signals that leaked out of the joint of a transformer." *International Journal of Antennas and Propagation* 2017 (2017).

### ACKNOWLEDGMENTS

The authors wish to thank the Office of Naval Research for their support of this work under Grant No. N00014-17-1-3016

### OBJECTIVES and MOTIVATION

#### Objective:

Determine the extent to which the physical aperture area of a Shark antenna can be reduced, while maintaining performance in peak gain, bandwidth, and half power beamwidth (HPBW) over the ultra high frequency (UHF) range (0.4–1 GHz) with respect to the prior state of the art balanced antipodal Vivaldi antenna (BAVA).

#### State of the Art and Deficiencies:

The BAVA design parameter space has been exhausted over the past couple of decades. The physical aperture area remains very large and there is no viable path through tradespace study for further physical aperture area reduction.

#### Relevance to OSPRES Program:

The design parameter space of the Shark antenna has not been studied rigorously in the literature. Therefore, the tradespace study will provide novel antenna information to the OSPRES program. The Shark antenna also has aperture efficiencies exceeding 100% in the UHF range. Improved aperture efficiencies are of high interest, as they allow for a smaller physical areas of antennas while maintaining peak performance.

### BACKGROUND

The design of the Shark antenna is based on that of the well known bi-cone antenna. The bi-cone antenna is of interest to high power microwave (HPM) applications due to its impressive impedance matching over a wide bandwidth of frequencies. To focus electromagnetic (EM) radiation towards the front of the antenna, the bi-cone design is truncated at the back and top, and tilted forward. A backplane is also incorporated to reflect backwards radiation.

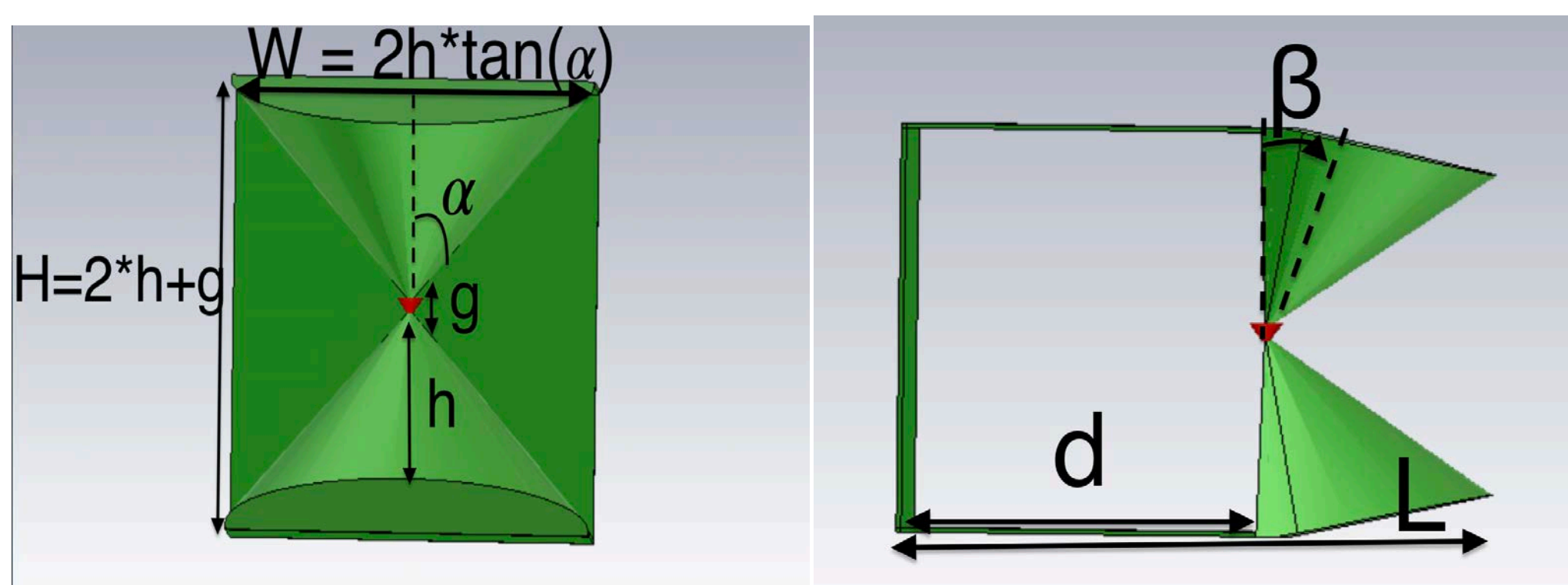


Figure 1: Shark Antenna Design Parameters

### METHODS

To explore the design space of the Shark antenna, a tradespace study has been performed with a focus on improving impedance matching in the 0.7–1.2 GHz range with minimal increase in size. The following design cases have been simulated using CST Microwave Studio and FEKO

$h$ (mm)	$d$ (mm)	$\alpha$ (°)	$h$ (mm)	$d$ (mm)	$\alpha$ (°)
30	75	20	40	75	15
		45			
		70			
60	75	20	45	100	20
		45			
		70			
30	45	20	40	100	20
		45			
		70			
60	45	20	45	100	20
		45			
		70			

Table 1: Initial Tradespace Study

Table 2: Refined Tradespace Study

The first tradespace study outlined in Table 1 gave general insight into how the cone height ( $h$ ), distance to backplanes ( $d$ ), and flare angle ( $\alpha$ ) affect important antenna metrics such as impedance bandwidth, gain, rE/V, and aperture efficiency. This preliminary study along with known OSPRES requirements was used to inform the cases chosen in Table 2.

### RESULTS

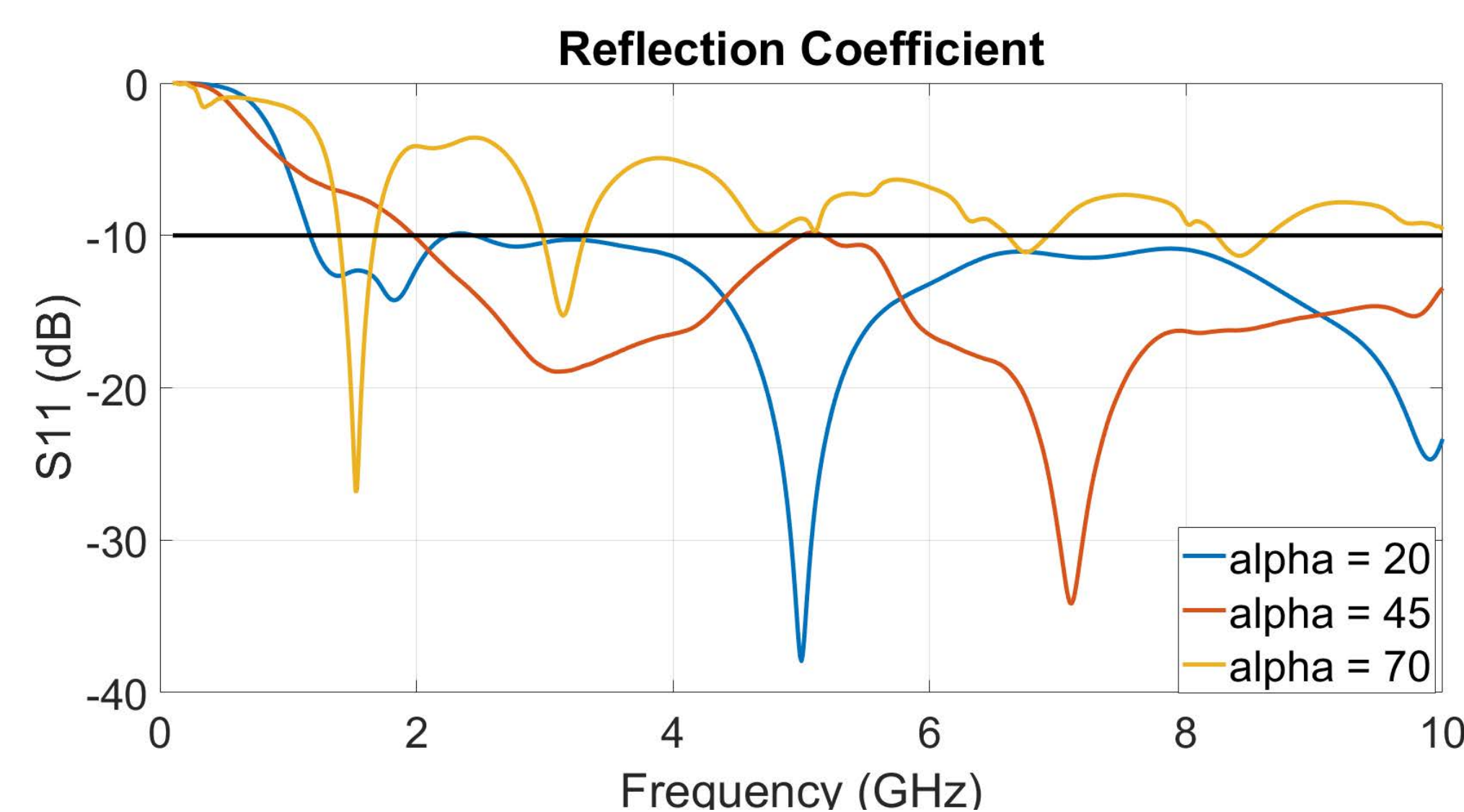


Figure 2: S11  $h = 30$  mm,  $d = 75$  mm,  $\alpha = 20^\circ$  (blue),  $\alpha = 45^\circ$  (red),  $\alpha = 70^\circ$  (yellow)

From Figure 2 it was determined that for large flare angles such as  $75^\circ$  the S11 performance is degraded. It can also be seen that the smaller flare angle case of  $20^\circ$  has a lower initial -10dB crossing frequency.

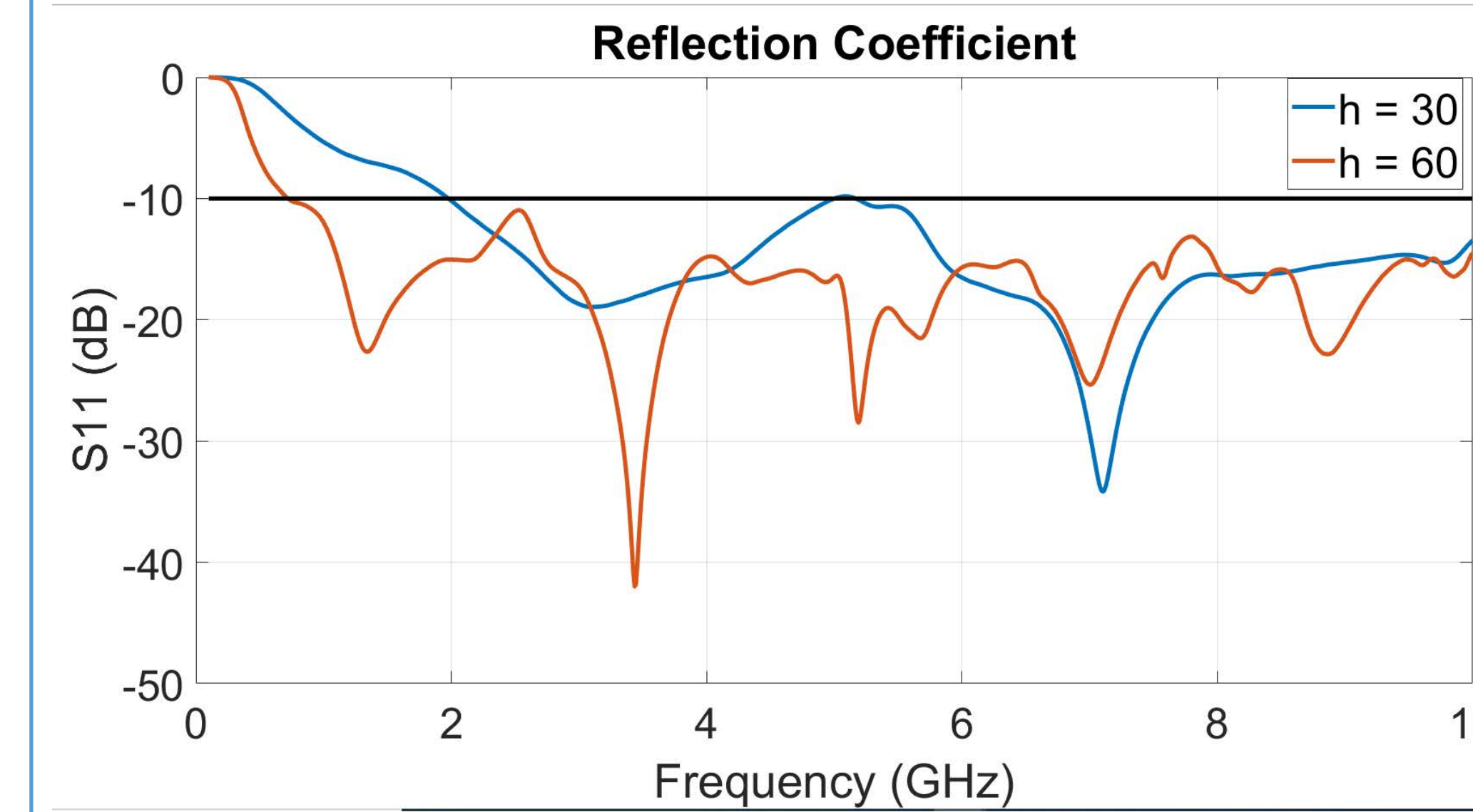


Figure 3: S11  $d = 75$  mm,  $\alpha = 45^\circ$ ,  $h = 30$  (red),  $h = 60$  (blue)

From Figure 3 it has been found that the cone height has a significant effect on the low operating frequency. Increasing the cone height shifts the lowest -10dB operating frequency down. It has also been found that increasing the distance to backplanes from 75 mm to 100 mm has a minimal effect on shifting the the lowest -10dB operating frequency.

$h$ (mm)	$d$ (mm)	$\alpha$ (°)	rE/V	
			$r = 1$ m	$r = 2$ m
40	75	20	0.734	0.734
45	75	20	0.932	0.906
40	100	20	0.7	0.736
45	100	20	0.694	0.713

Table 3: rE/V Transient Gain

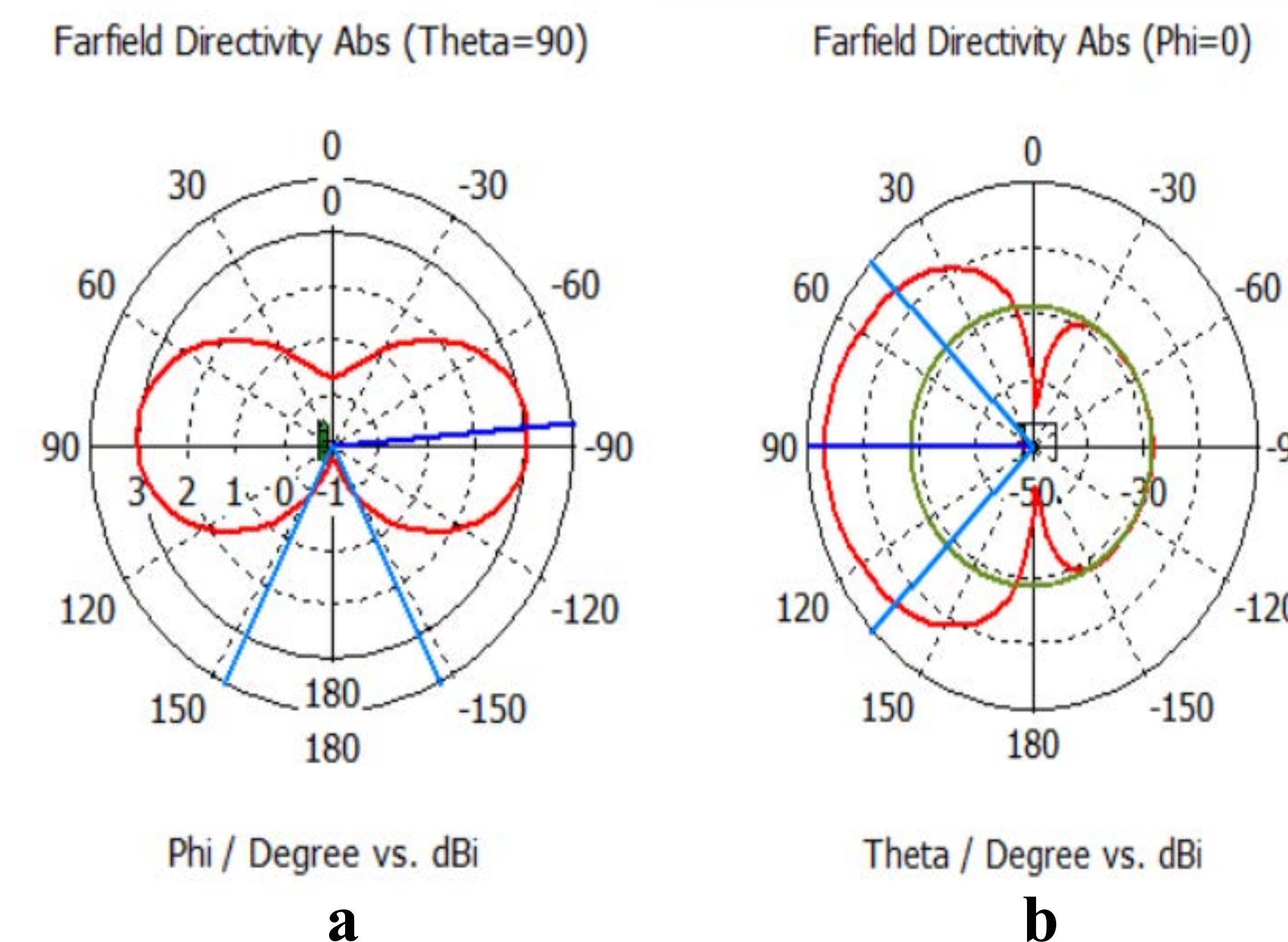


Figure 4: Radiation Pattern 1 GHz - (a) H-Plane HPBW =  $306.1^\circ$ - (b) E-Plane HPBW =  $134.5^\circ$

$h$ (mm)	$d$ (mm)	$\alpha$ (°)	Physical Aperture Area (mm <sup>2</sup> )	Peak Gain (dBi) (900 MHz)	Aperture Efficiency (900 MHz)
40	75	20	30 X 82	2.73	670%
45	75	20	32 X 92	2.72	560%
40	100	20	30 X 82	3.48	1000%
45	100	20	32 X 92	3.48	1000%

Table 4: Tradespace Study Aperture Efficiency Results

### CONCLUSIONS

Overall, the tradespace study has informed how the Shark antenna design parameter space affects low frequency performance. Metrics such as gain and aperture efficiency follow the expected trend of increased size leading to an increase in performance. The optimal values for  $h$ ,  $d$ , and  $\alpha$  are 45 mm, 75 mm, and  $20^\circ$  respectively. With this design a reasonable peak gain in the range of 2.7 dBi is achievable, and the aperture efficiency at the target frequency of 900 MHz is well exceeding 100%.

### FUTURE WORK

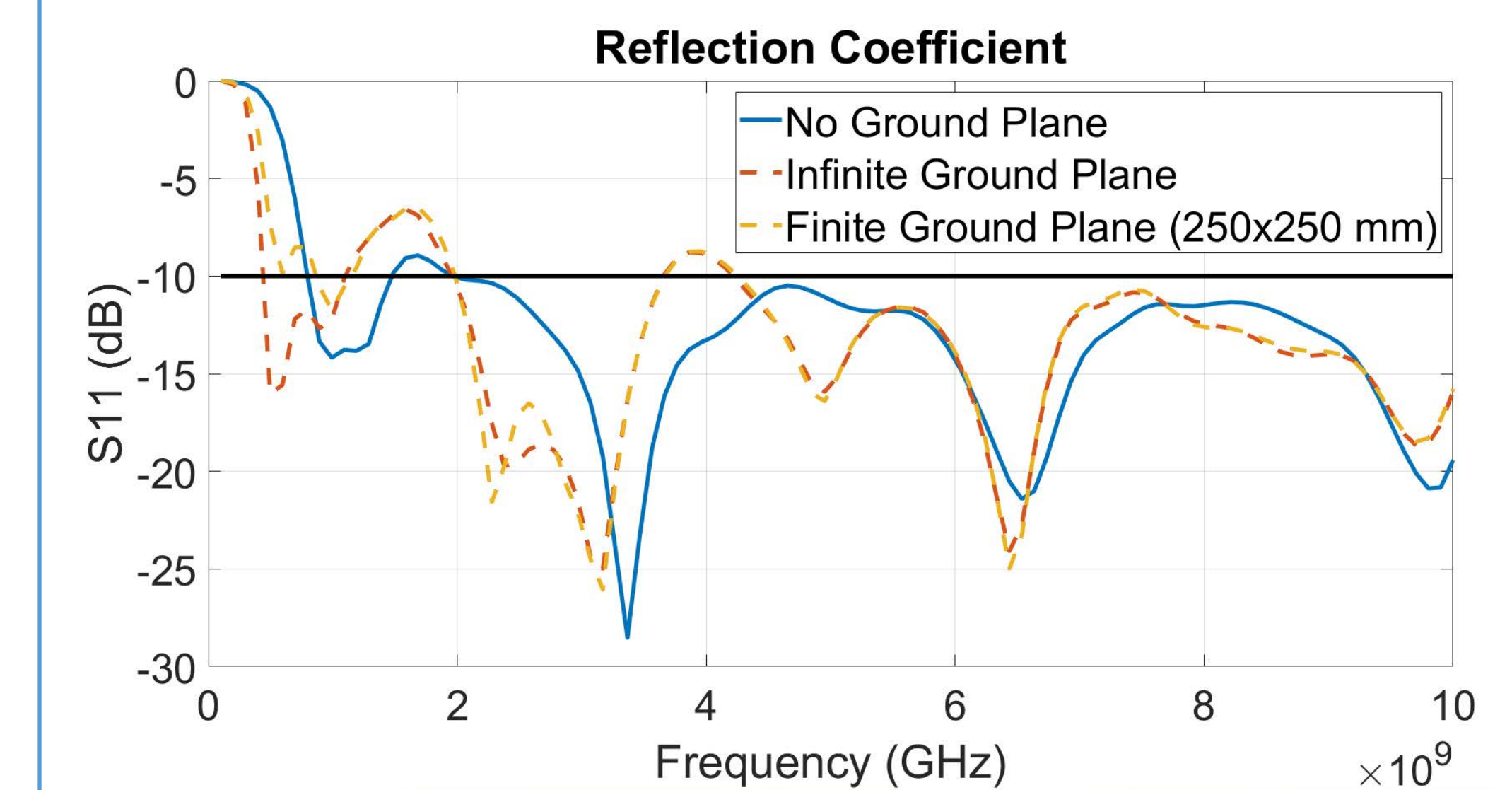


Figure 5: S11  $d = 100$  mm,  $\alpha = 20^\circ$ ,  $h = 45$  mm, ground plane study

To further reduce the lowest operating frequency, special EM techniques will be applied such as the inclusion of a ground plane, dielectric loading, and capacitive loading. Figure 5 shows preliminary results of including a ground plane. With the infinite ground plane, the lowest operating frequency has been shifted all the way to 0.4 GHz.

### Acknowledgments

The authors wish to thank the Office of Naval Research for their support of this work under Grant No. N00014-17-1-3016.

## Objective and Motivation

**Problem statement:** Determine the extent to which Machine Learning (ML) algorithms/models can be applied to evaluate and optimize the performance of antenna geometries with faster turnaround time while maintaining the accuracy levels of traditional electromagnetic (EM) wave solvers.

### Relevance to the OSPRES objective:

Application of existing ML models on ultra-wide-band (UWB) antenna geometries checks the high-risk high-payoff effort box by directly reducing the computational time in the process of optimizing or predicting an antenna response/metrics.

**State-of-the-art (SOTA):** Conventional full-wave solvers such as method of moments (MoM), multi-level fast multipole method (MLFMM), finite element method (FEM), and finite difference time domain (FDTD) method.

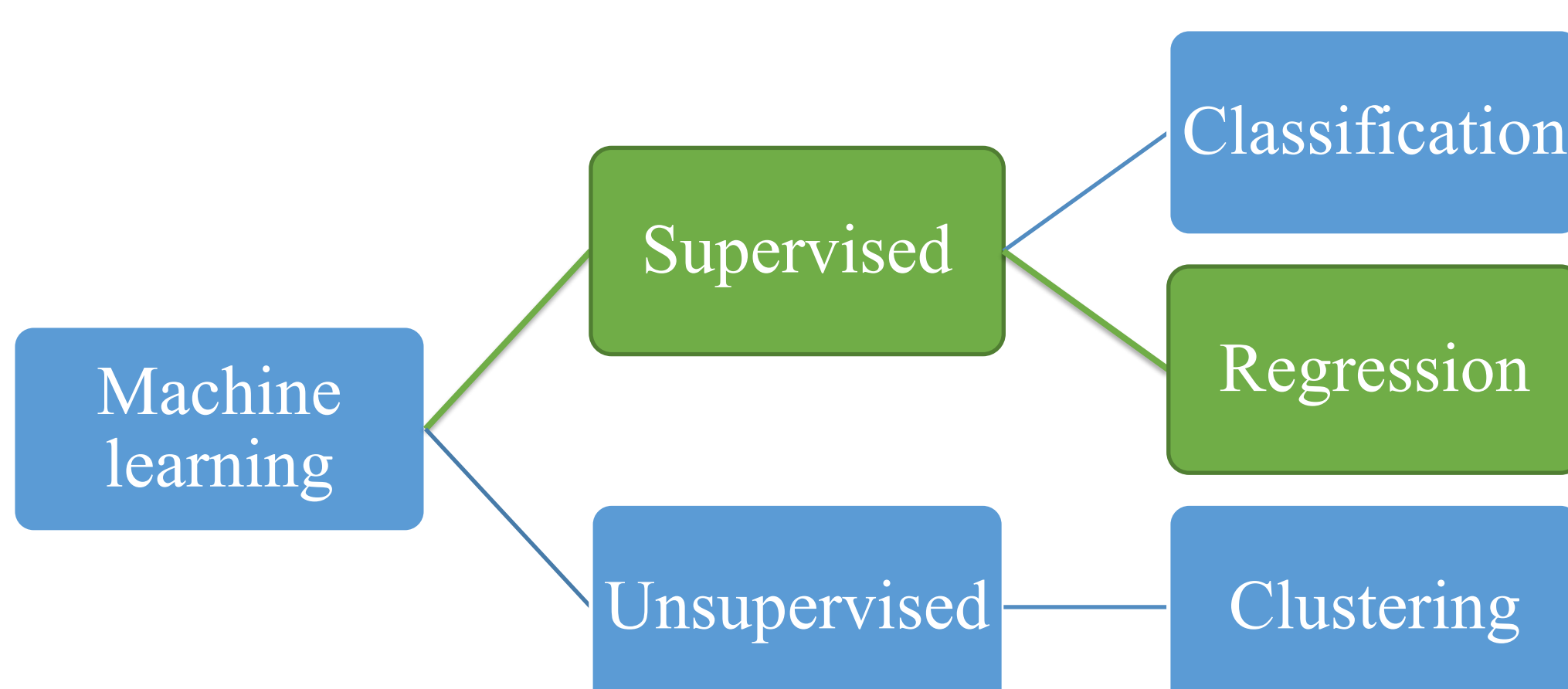
**Deficiency in SOTA:** Optimization approaches in traditional EM solvers such as parametric sweep, and different stochastic algorithms take significant computational time and memory.

**Solution:** Apply ML models available in Altair Hyperstudy on a specific antenna geometry to study and understand the limitations, and accuracy levels of these ML models.

### Objective:

To implement, improvise and/or apply existing ML models on UWB antenna geometries for fast and efficient antenna response/metrics prediction or optimization.

## Background



## Antenna Geometry

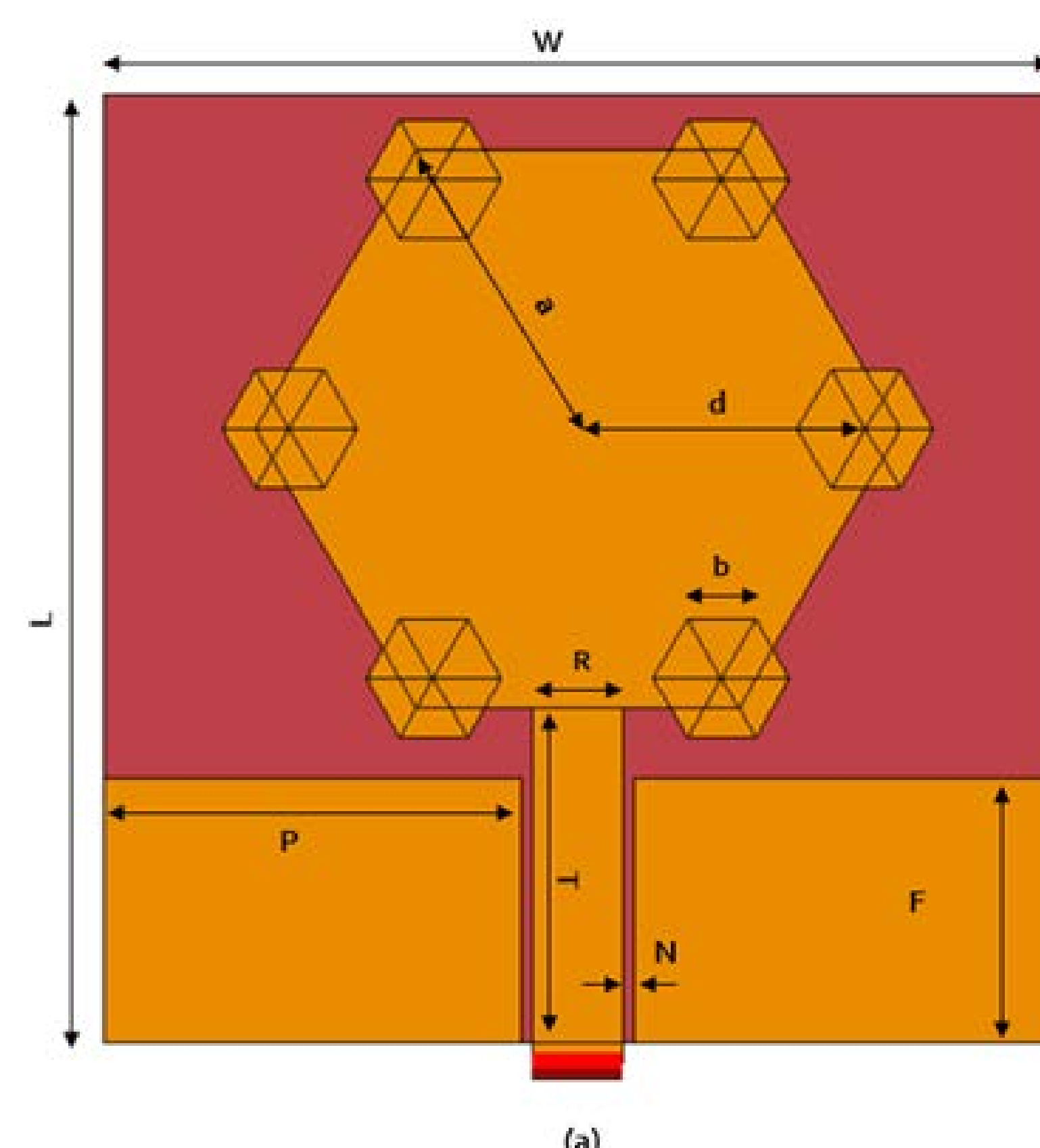
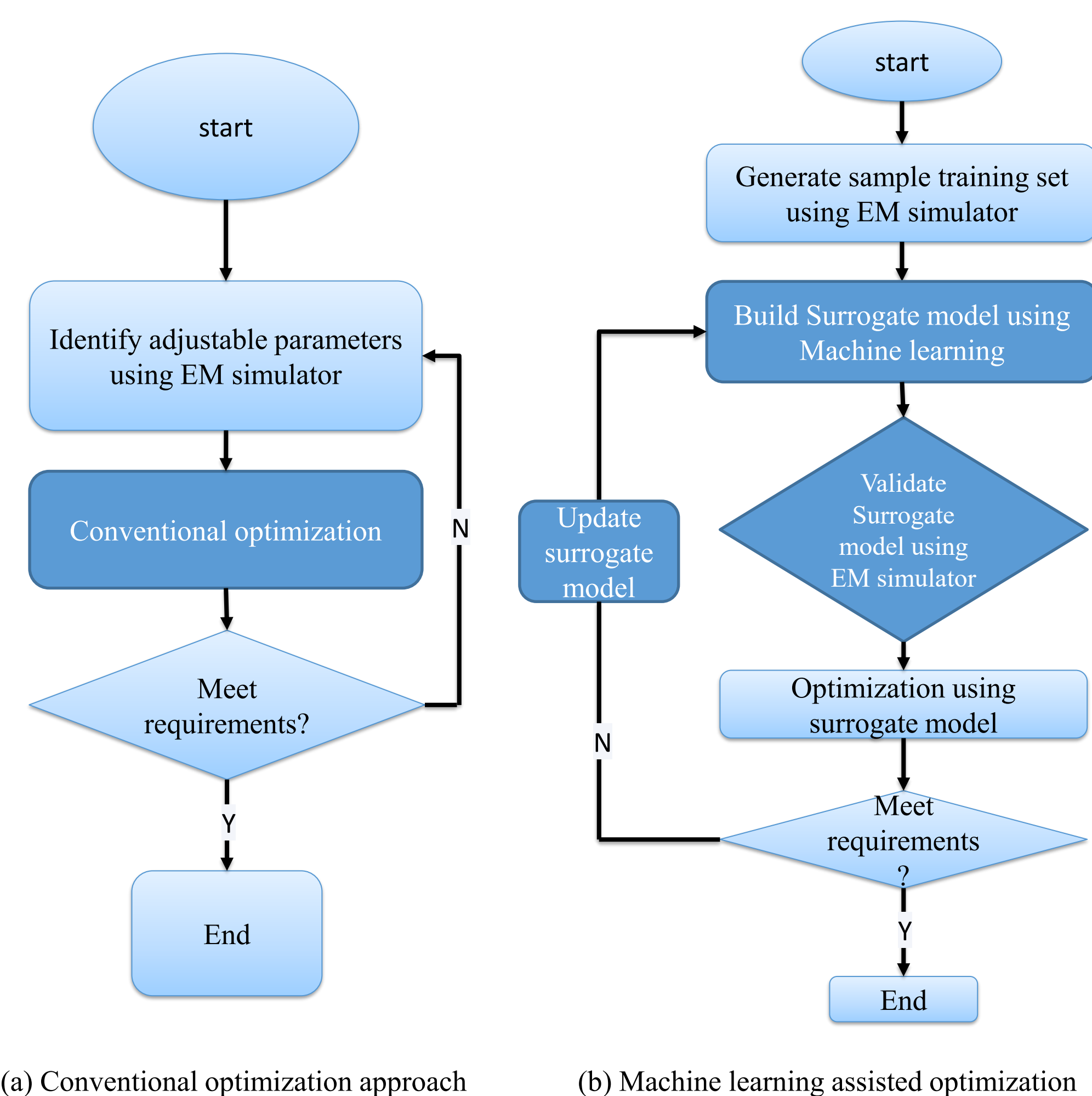


Fig. 1 Top view of the hexagon patch antenna with hexagon fractal elements.

## Methodology

Workflow for different optimization approaches



(a) Conventional optimization approach

(b) Machine learning assisted optimization

The conventional optimization method uses traditional full-wave solvers for every iteration, which in turn requires large computational resources to simulate the design and to save the data. Whereas ML approach trains a surrogate model using the training data obtained from preliminary FEKO/CST simulations.

## Results

Selected antenna geometry has 12 different adjustable design variables as shown in figure 1. Two variables, Hexagon patch radius 'a' and Fractal element radius 'b' are down selected to generate the training dataset.

### Steps followed:

- Generated 5 different pairs of input ('a' and 'b') and corresponding output (S11 response) for 30 different discrete frequency point over a range of 100MHz to 3GHz.
- Trained radial basis function (RBF) ML model on the given dataset.
- The reflection coefficient (S11) output from ML model is compared against FEKO and CST output (EM simulator), which is shown in figure 2.

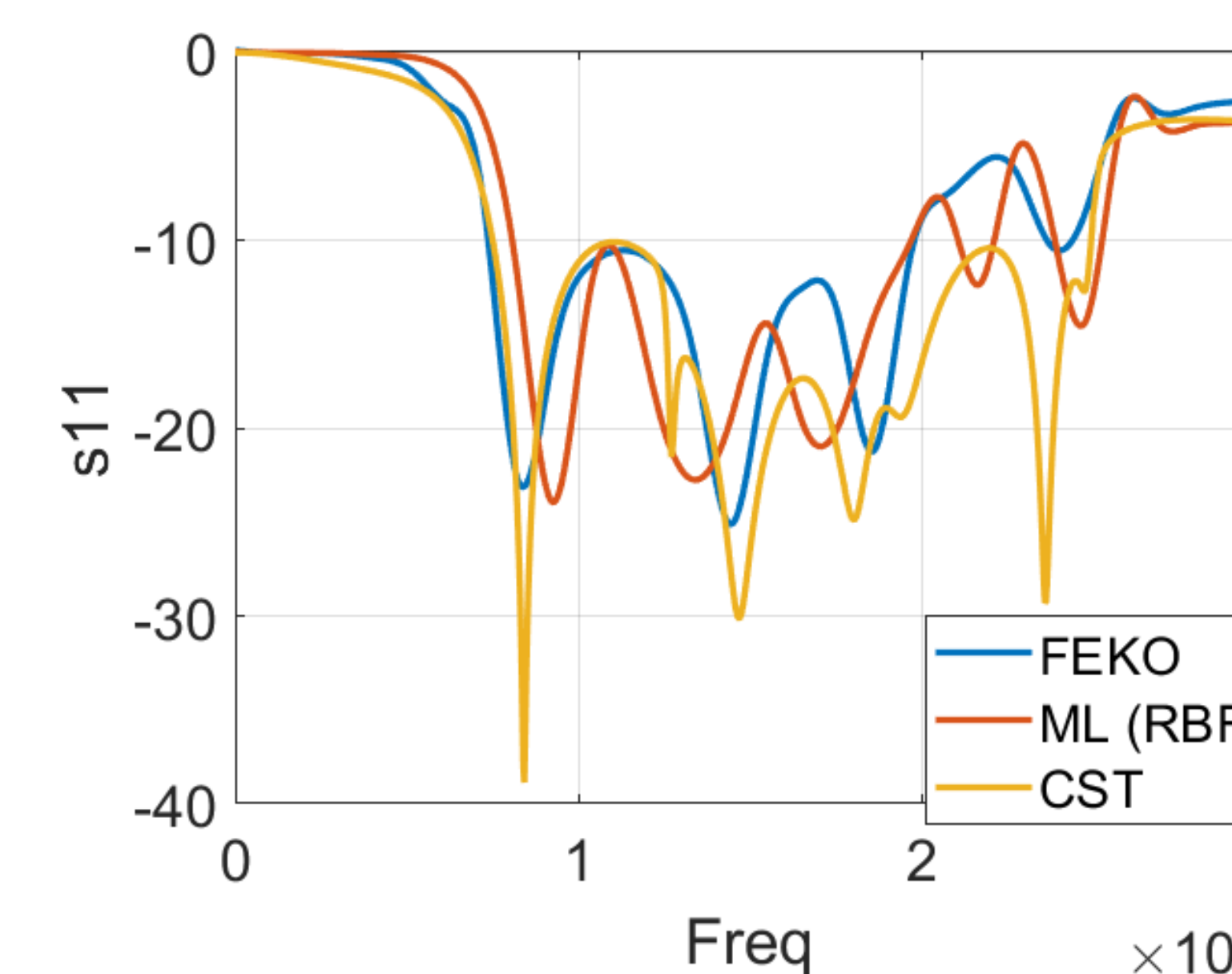


Fig. 2. Reflection coefficient (S11) comparison between FEKO, CST and ML model.

Table 1: Computational Time

Approach	Time	Memory
MoM solver - FEKO	1:40 hours	1.5 GB
Finite Integration Method - CST	40 mins	694 MB
RBF - ML	< 5 secs	< 10 MB

Table 1 shows computational time and memory utilized by three different methods to complete a parametric sweep.

## Conclusion

Fractal antenna design has 12 adjustable features and from the initial parametric study two features ('a' and 'b') have been identified to have significant impact on the antenna response. New machine learning approach has been applied to try and predict the antenna response to reduce computational time and memory consumption. Machine learning model is trained with sample training dataset size of 5. Antenna responses from trained machine learning model and the convectional EM simulator (FEKO and CST) are compared and illustrated. From the results it is evident that antenna response from machine learning model and EM simulator are in good agreement with each other.

## Future Work

- Future studies will be extended to find and include other machine learning algorithms and to find best algorithm suitable to the given requirement/objective.
- Stochastic optimization techniques will be applied on trained machine learning model as an additional optimization tool.
- Sample training dataset size will be slightly increased to get a closer agreement between traditional methods and ML models.
- Extend ML model to predict other antenna metrics such as realized gain and electric field.

## Acknowledgement

The authors wish to thank the Office of Naval Research for their support of this work under Grant no. N00014-17-1-3016.

## References

- [1] M. Aneesh, J. A. Ansari, A. Singh, Kamakshi and S. Verma, "RBF Neural Network Modeling of Rectangular Microstrip Patch Antenna," 2012 Third International Conference on Computer and Communication Technology, 2012, pp. 241-244, doi: 10.1109/ICCCT.2012.56.
- [2] H. Fallahi and Z. Atlasbaf, "Study of a Class of UWB CPW-Fed Monopole Antenna With Fractal Elements," in IEEE Antennas and Wireless Propagation Letters, vol. 12, pp. 1484-1487, 2013, doi: 10.1109/LAWP.2013.2289868.

# Modeling and Verification of High-Power Electromagnetic Coupling to Nonlinear Electronic Systems using the Equivalent Circuit Approach

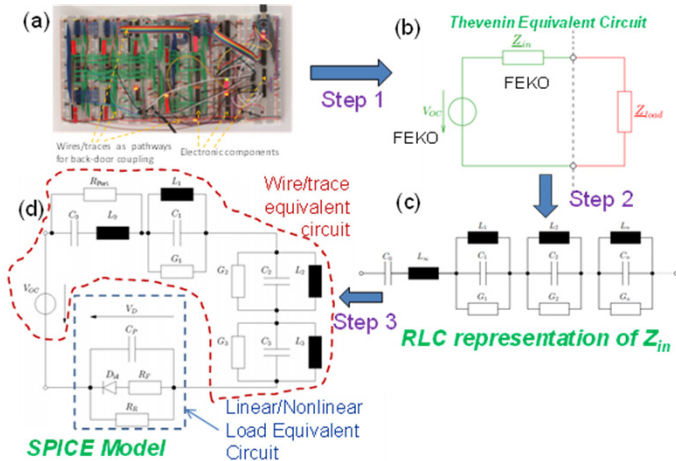
Mohamed Z. M. Hamdalla<sup>1</sup>, Benjamin Bissen<sup>2</sup>, Thomas Ory<sup>2</sup>, Anthony N. Caruso<sup>2</sup>, Ahmed M. Hassan<sup>1</sup>  
<sup>1</sup>Computer Science Electrical Engineering Department, UMKC <sup>2</sup>Missouri Institute for Defense & Energy, UMKC

## Objective and Motivation:

- Predict RF coupling to a complex system of wires with nonlinear loads and develop RF guidelines
- Predict the optimum incident waveform properties to maximize the coupled voltage/currents to a nonlinear load of interest
- OSPERES Relevance:** Provide explanation to experimental results, Predict RF coupling results to guide experimental measurements, provide guidance to minimum properties of the incident waveforms to generate the desired effects.

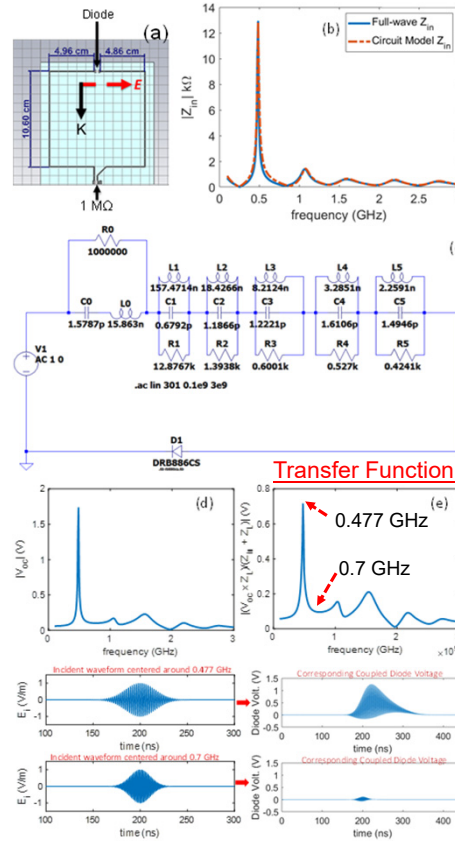
## Equivalent Circuit Approach (ECA):

- The Equivalent Circuit Approach (ECA) has been commonly used for quantifying coupling to receiving antennas and wire systems.
- The ECA is based on developing a Thevenin equivalent circuit for the wiring system that involves 3 main components:
  - Open-circuit voltage,  $V_{oc}$ .
  - Input impedance,  $Z_{in}$ , of the wiring/trace system.
  - Load impedance,  $Z_L$ , of the load of interest which can be linear or nonlinear based on the electronic component of interest [1].
- Full-wave electromagnetic solvers are used to calculate (1) & (2).
- A SPICE solver can be used to simulate the entire wire system at a fraction of the computational time with no loss in accuracy.
- The ECA provides physical insight into RF coupling problems



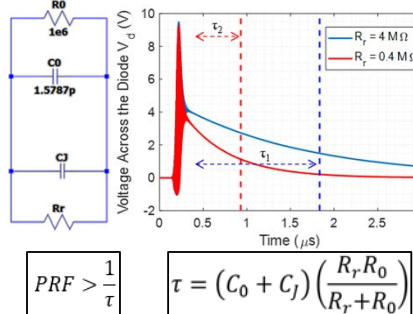
## Representative Example:

- A 10.5 cm by 10.5 cm square trace was on FR4 substrate with a 1 MΩ resistor and an **RB886CST2R Schottky diode**. Trace 1 mm thick. FR4 substrate was 1.7 mm thick,  $\epsilon_r = 4.8$ ,  $\tan(\delta) = 0.017$ .
- A transfer function can be developed to identify the optimum frequency to couple to the load of interest.
- Two 1 V/m Gaussian Sinusoidal pulses with 5% BW centered around: (i) 0.477 GHz and (ii) 0.7 GHz.
- Knowledge of the transfer function can save 20 dB in the power of the incident waveform to create the same coupled voltage across the diode.



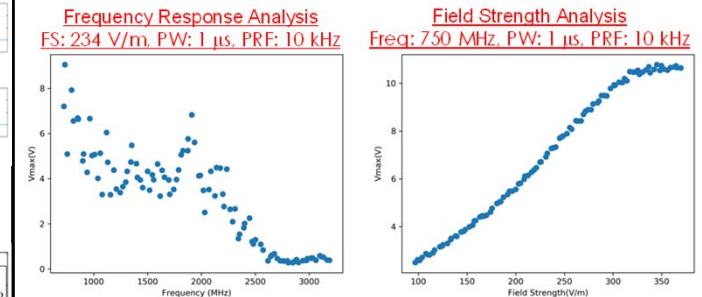
## Voltage Buildup and Pulse Repetition Frequency:

- In between pulses, equivalent circuit can be simplified into  $C_j$  (junction capacitance),  $R_r$  (reverse resistance),  $C_0$  and  $R_0$  the low-frequency limit of the capacitance resistance of square trace.



## Experimental Validation:

- Arbitrary Waveform Generator → Broadband Amplifier → GTEM → Diode → Wire loop → Oscilloscope
- We increased the amplitude of the incident field and the PRF until the diode was affected
- The diode was characterized as affected because its behavior changed between the 50 kHz 1<sup>st</sup> measurement and the second one.
- Data collection automated to test arbitrary incident waveforms with variable center frequency, PRF, field strength, pulse width



## Summary:

- Close correlation between measurements and ECA results show its capability in predicting the optimum properties of the incident waveform to maximize coupling.

**References:**  
 R. Michels et al., "Modeling and Verification of a Parasitic Nonlinear Energy Storage Effect Due To High-Power Electromagnetic Excitation," *IEEE Trans. Electromagn. Compat.*, vol. 62, no. 6, pp. 2468–2475, Dec. 2020.

**ACKNOWLEDGMENTS:** This work was supported by ONR grant # N00014-17-1-2932 and ONR grant # N00014-17-1-3016

# Predicting Electromagnetic Coupling to UAV Models

Mohamed Z. M. Hamdalla<sup>1</sup>, Anthony N. Caruso<sup>2</sup>, Ahmed M. Hassan<sup>1</sup>

<sup>1</sup>Computer Science Electrical Engineering Department, UMKC

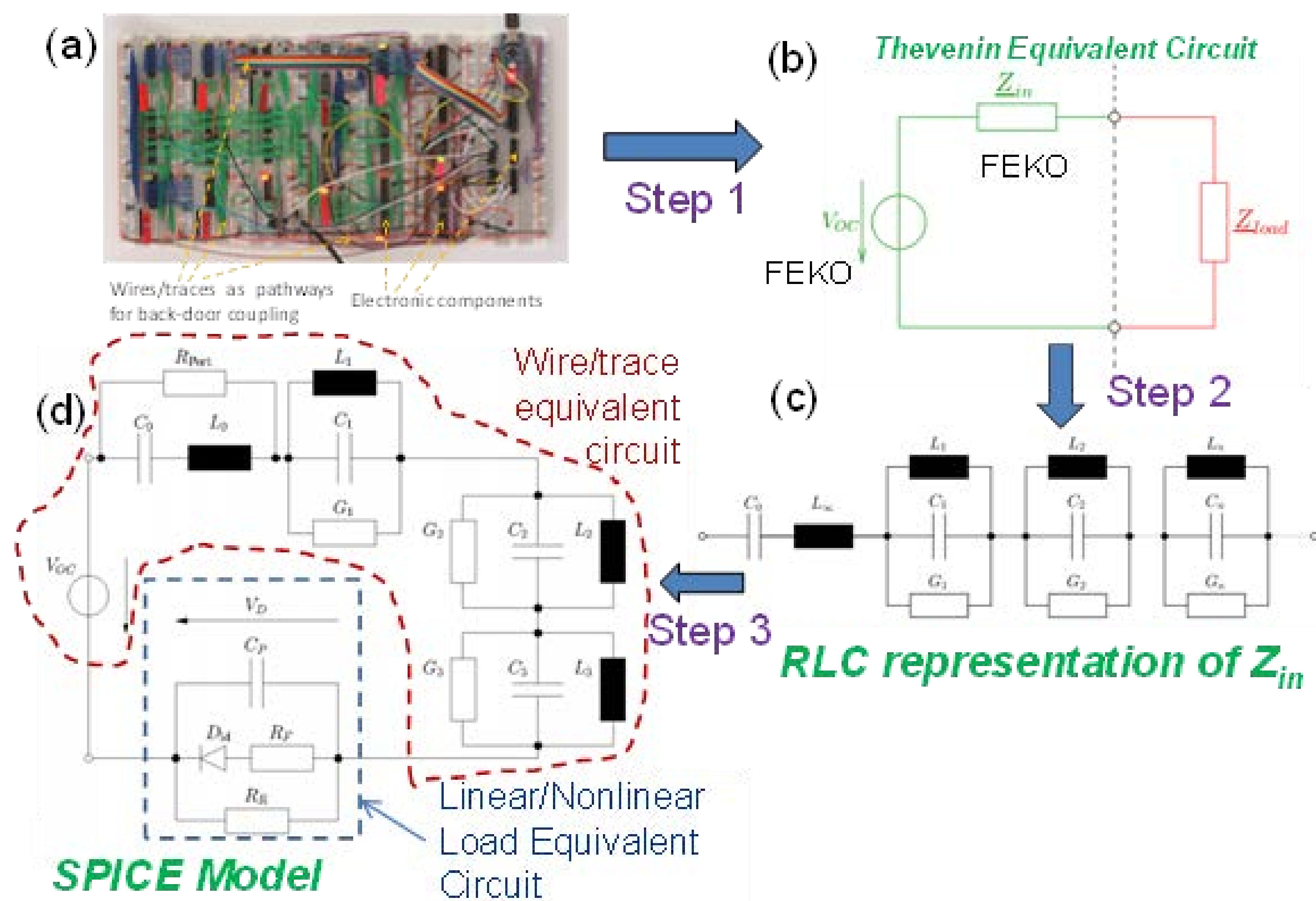
<sup>2</sup>Missouri Institute for Defense & Energy, UMKC

## Objective and Motivation:

- Develop an accurate UAV model with all the wires and all the IC components to act as a numerical platform to study effects and guide/validate experimental measurements.
- Investigate UAV model simplifications that will not reduce accuracy.
- **Show that the Equivalent Circuit Approach can predict coupling to a complex system of wires and loads**
- **OSPRES Relevance:** Provide explanation to experimental results, Predict RF coupling results to guide experimental measurements, provide guidance to minimum properties of HPM sources to generate the desired effects

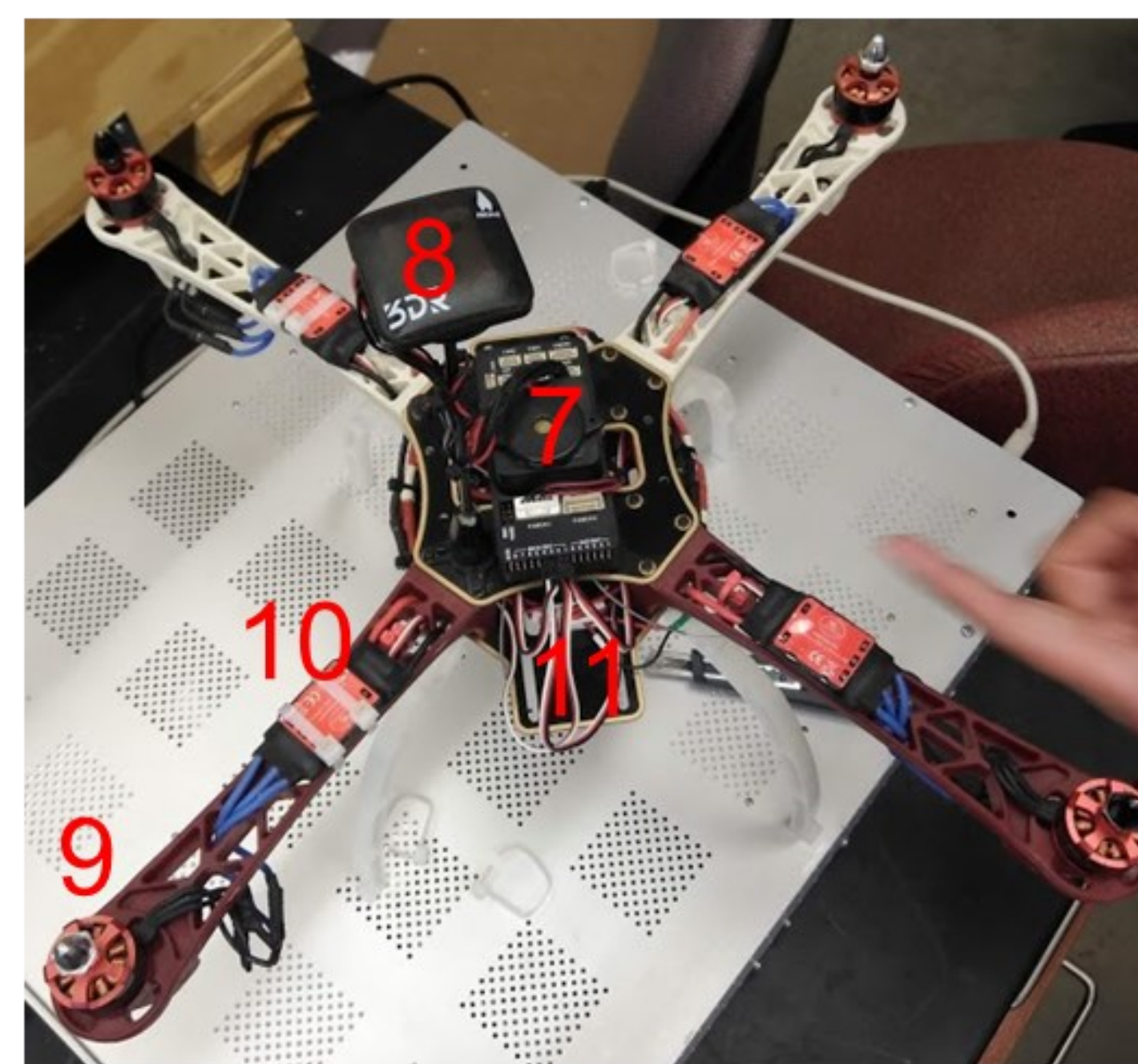
## Equivalent Circuit Approach (ECA):

- The ECA is based on developing a Thevenin equivalent circuit for the wiring system that involves 3 main components:
  - 1) Open-circuit voltage,  $V_{oc}$ .
  - 2) Input impedance,  $Z_{in}$ , of the wiring/trace system.
  - 3) Load impedance,  $Z_L$ , of the load of interest which can be linear or nonlinear based on the electronic component of interest [1].
- Full-wave electromagnetic solvers are used to calculate (1) & (2).
- A SPICE solver can be used to simulate the entire wire system at a fraction of the computational time with no loss in accuracy.
- The ECA provides physical insight into RF coupling problems

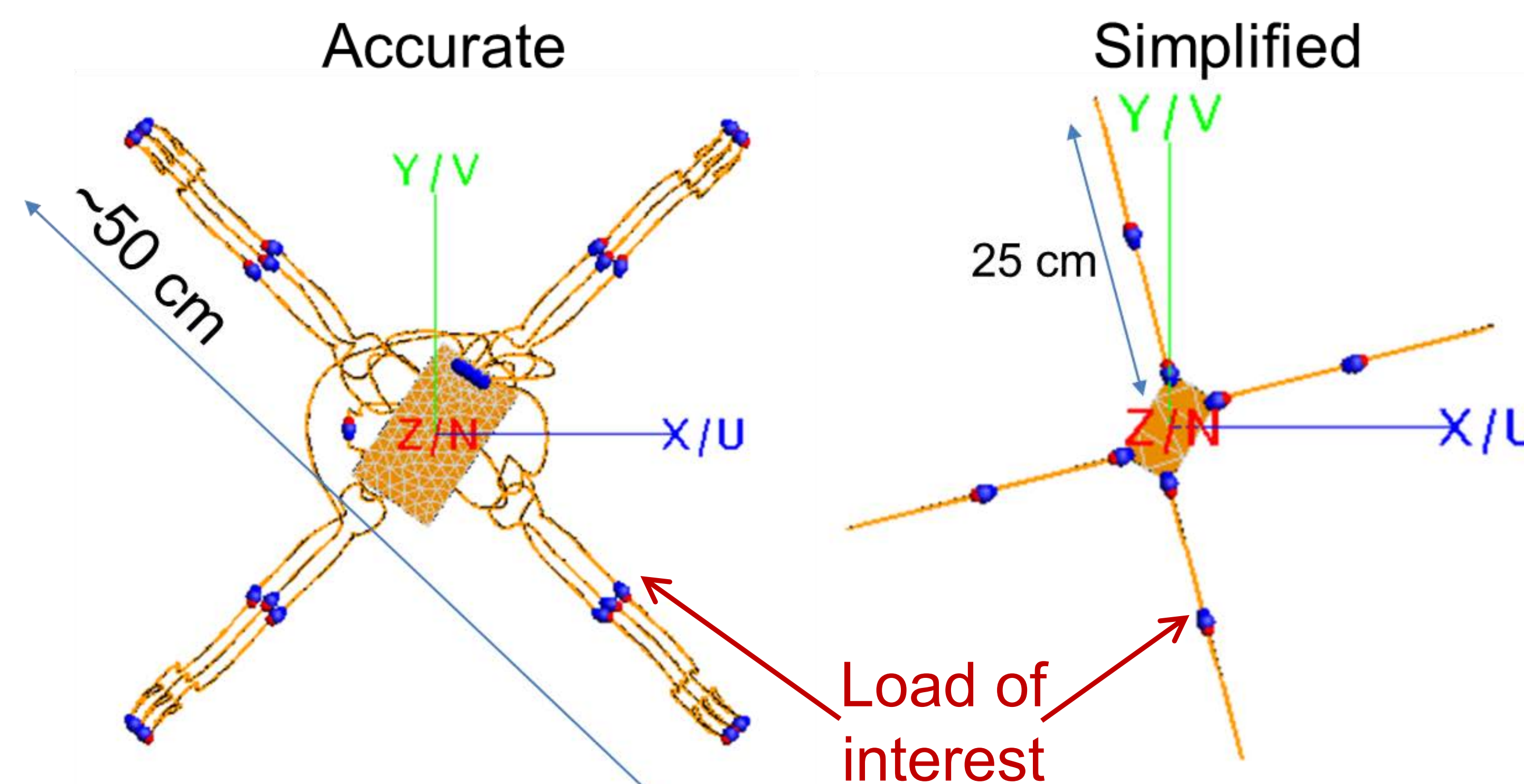


**DISTRIBUTION STATEMENT A.** Approved for public release: distribution unlimited.

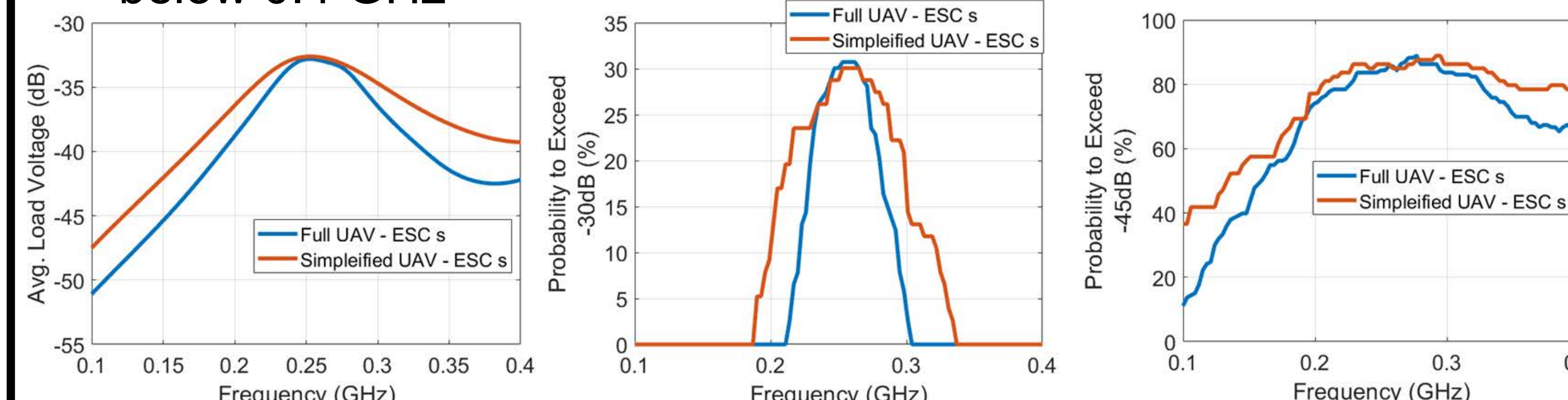
## UAV Wiring System and Circuitry Representations:



Build Computational Model

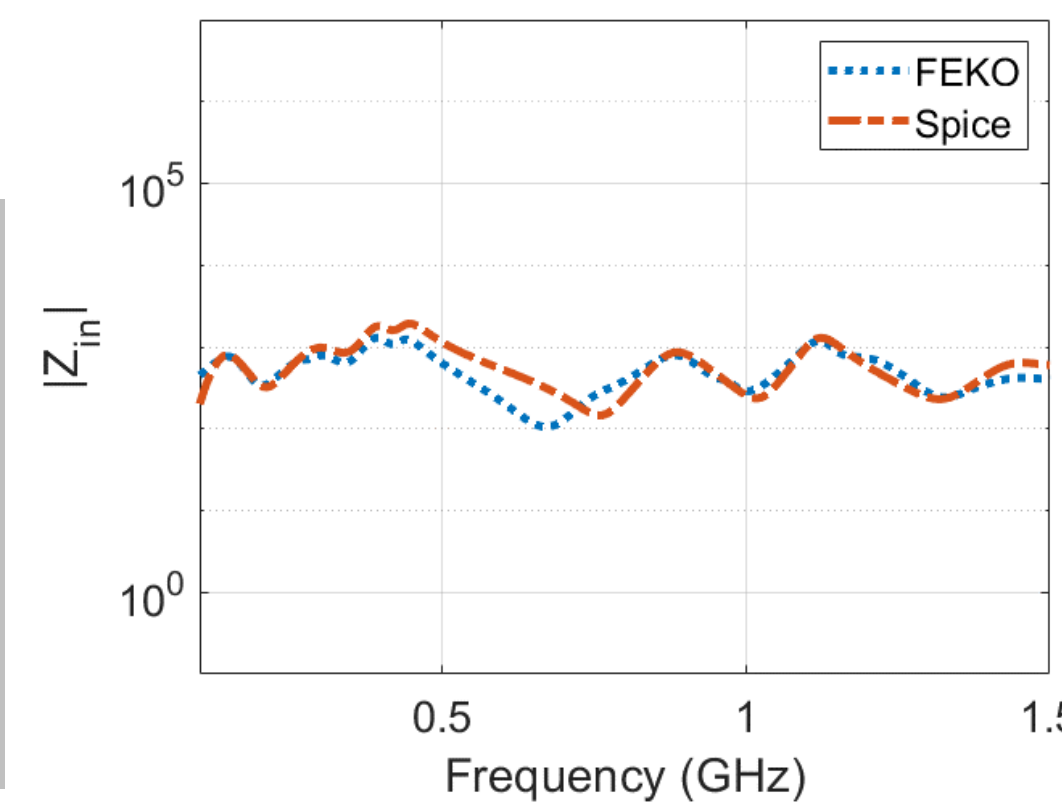
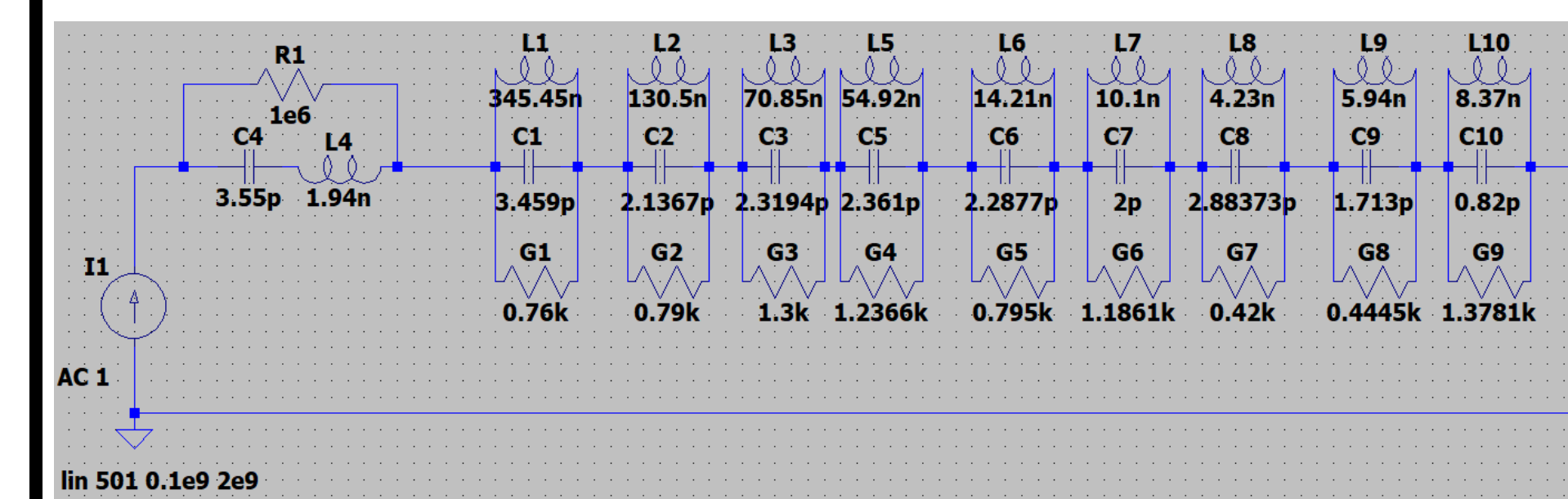


- All loads were assumed 50  $\Omega$  and will be updated in the future to include the experimentally measured impedance of chip/component
- We modeled the coupled voltage to the load of interest at multiple angles of incidence and calculated the probability that the coupled voltage will exceed a certain threshold
- Both models generated accurate results in the frequency range below 0.4 GHz

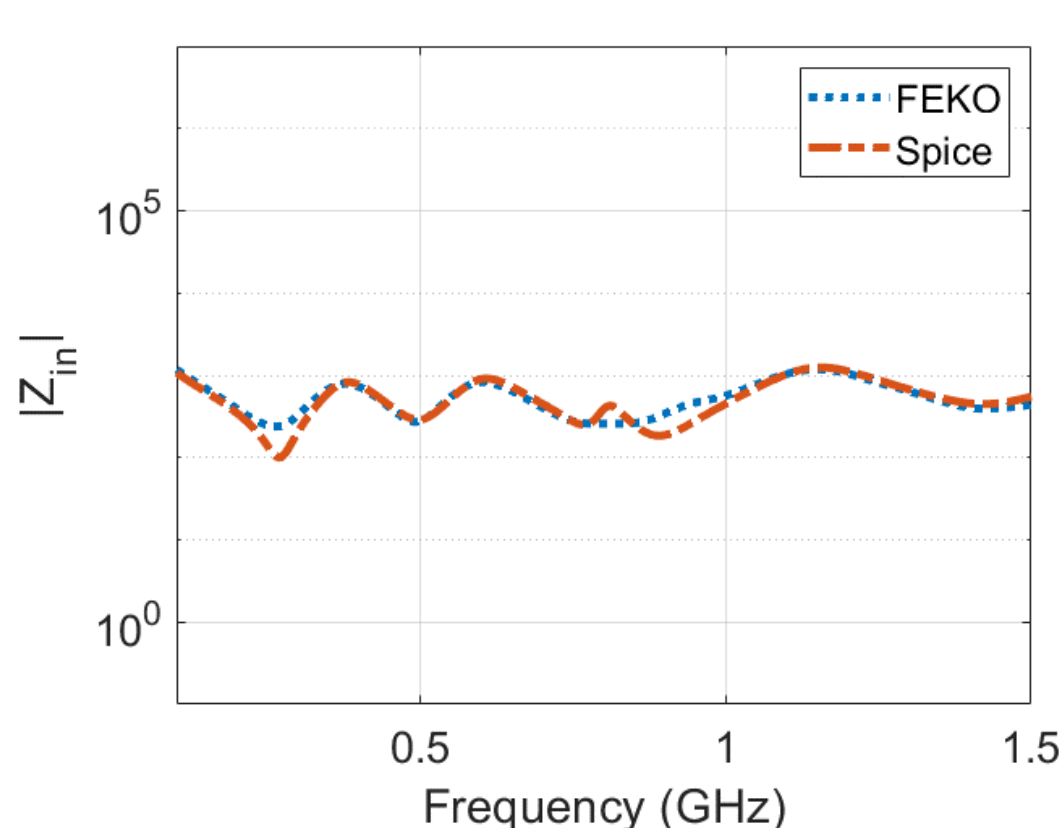
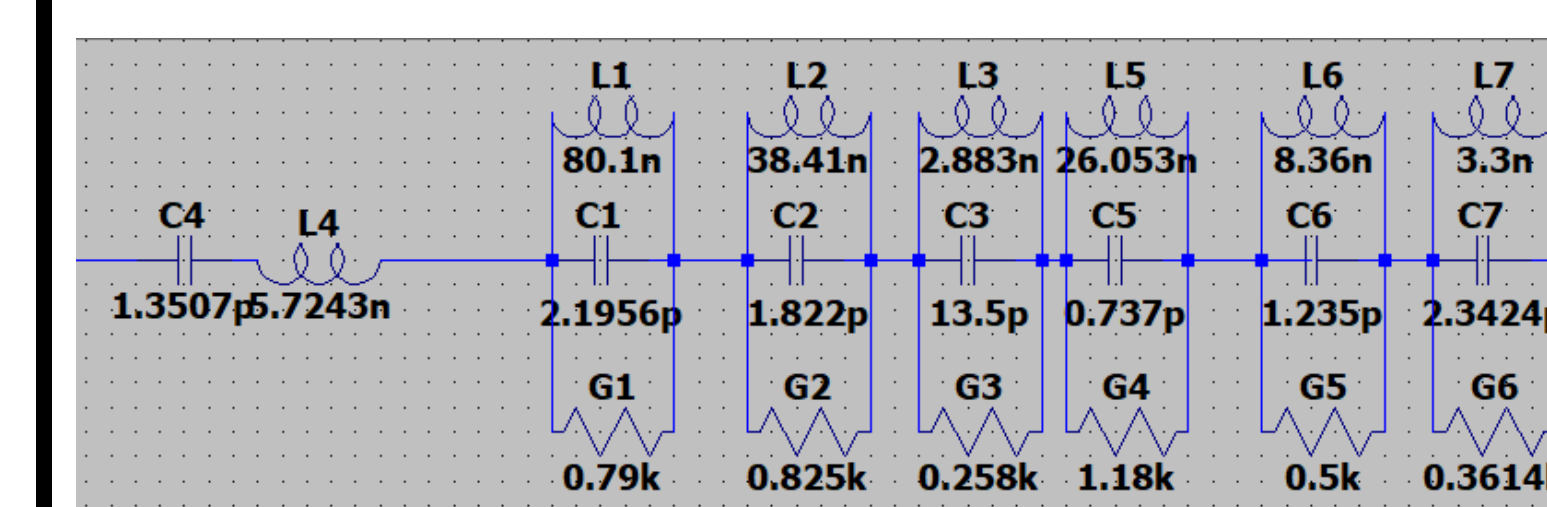


## Equivalent Circuit Approach of UAV Model:

### Accurate Model

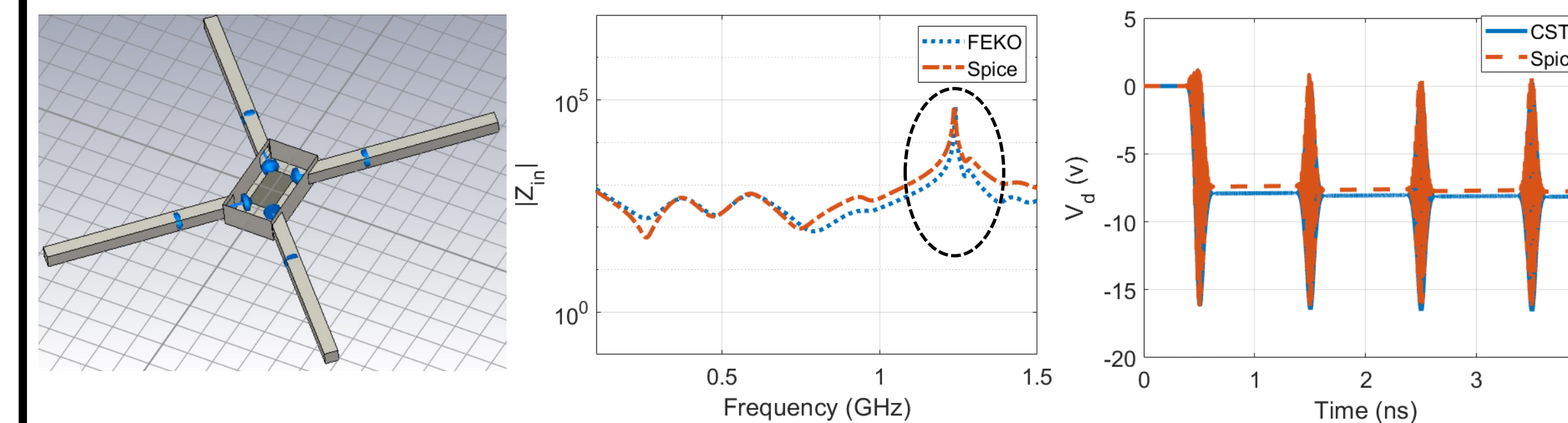


### Simplified Model

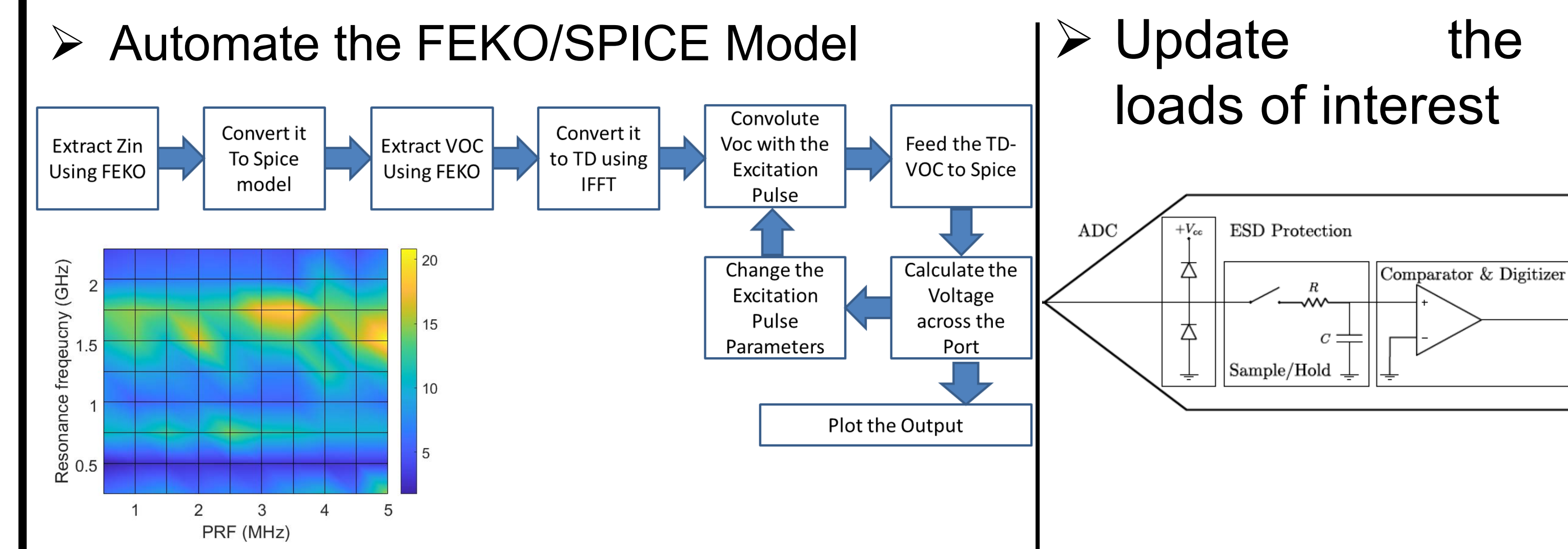


## Full-Wave Simulation Versus SPICE Model:

- A nonlinear diode was placed at load of interest; simplified UAV model was excited by a train of Gaussian Sinusoidal pulses
- Simplified model was placed in an open enclosure; equivalent circuit was updated to account for extra resonance
- **SPICE simulation required seconds/minutes versus hours for the full-wave CST solver, achieving excellent accuracy even for a complex wire system in a complex environment.**



## Future Work:



### References:

- R. Michels et al., *IEEE Trans. Electromagn. Compat.*, vol. 62, no. 6, pp. 2468–2475, Dec. 2020.
- I. Giechaskiel et al., *IEEE Communications Surveys & Tutorials*, vol. 22, no. 1, pp. 645-670, 2020,

**ACKNOWLEDGMENTS:** This work was supported by ONR grants: # N00014-17-1-2932 and ONR grant # N00014-17-1-3016

## Objective / Motivation

- Need for the development of a target assignment framework for incoming aerial hostile agents
  - Effective target assignment is defined by the minimization of “leaker” agents followed by mission-specific criteria (e.g., closest agent, fastest agent, etc.)
- Applicable for ground-based defense systems, aerial-based defense systems, or layered defense systems (combination of defense system types)
- These types of problem are commonly handled through path planning algorithms like the Traveling Salesman Problem (TSP) and the Vehicle Routing Problem (VRP).

## Background

### Classical Traveling Salesman Problem (TSP)

- Aimed at determining the shortest path for a single ‘salesman’ to visit a series of ‘cities’, which measures the distance between any two cities by the Euclidean Distance between the two.

### Traveling Salesman Problem with Neighborhoods (TSPN)

- Extension of the TSP, but with the addition of ‘neighborhoods’ where the salesman is only required to reach a singular point within a region around the city.

### Dynamic Traveling Salesman Problem (DTSP)

- Generalization of the TSP but with moving cities

### Dubin’s Curves

- Shortest path between two points with a constraints on the curvature of the path with prescribed initial and terminal headings
- Used by many non-holonomic vehicles

### Vehicle Routing Problem (VRP)

- Generalization of the TSP but with multiple salesman

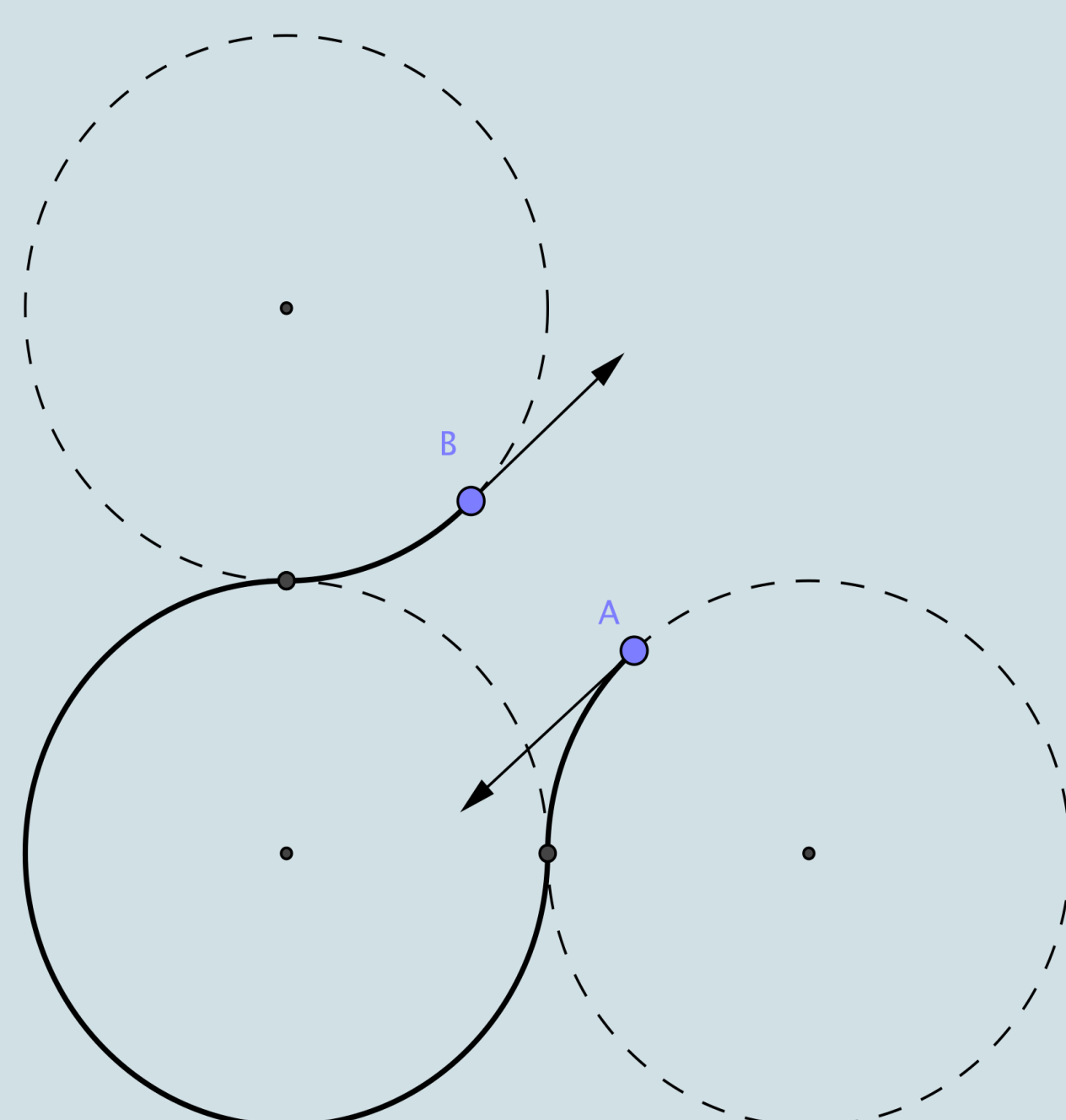


Figure 3: Dubin's Path Example [1]

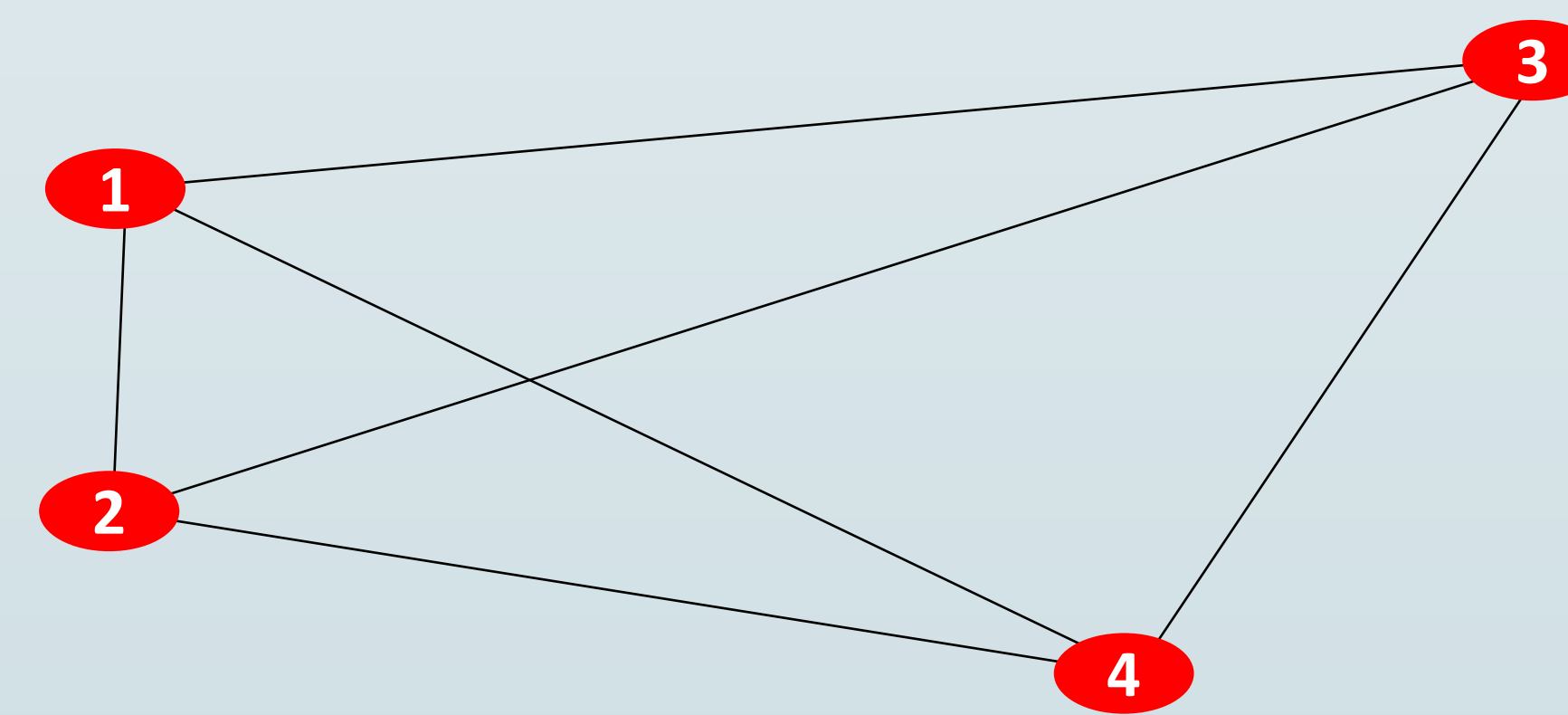


Figure 1: Path Solutions for the Classical Traveling Salesman Problem (TSP)

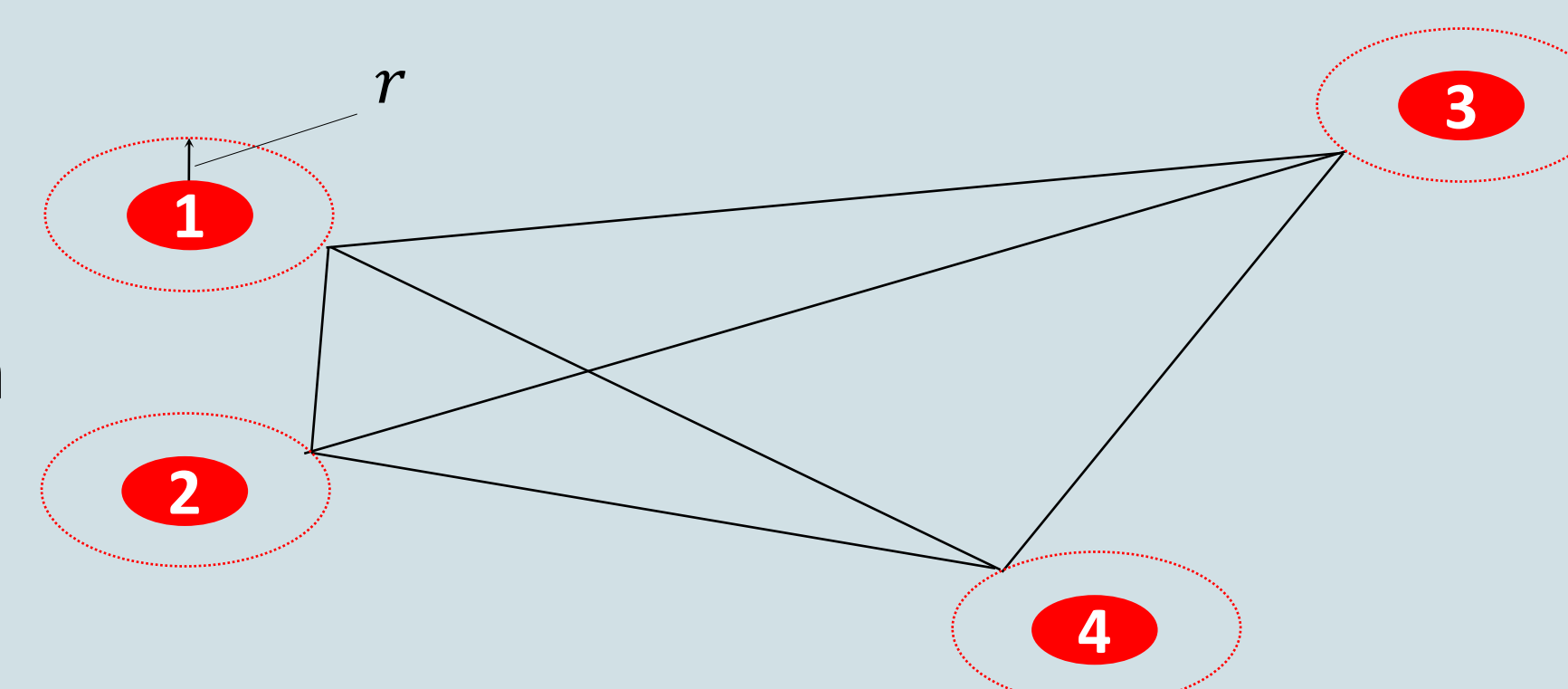


Figure 2: Path Solutions for the Classical Traveling Salesman Problem with Neighborhoods (TSPN)

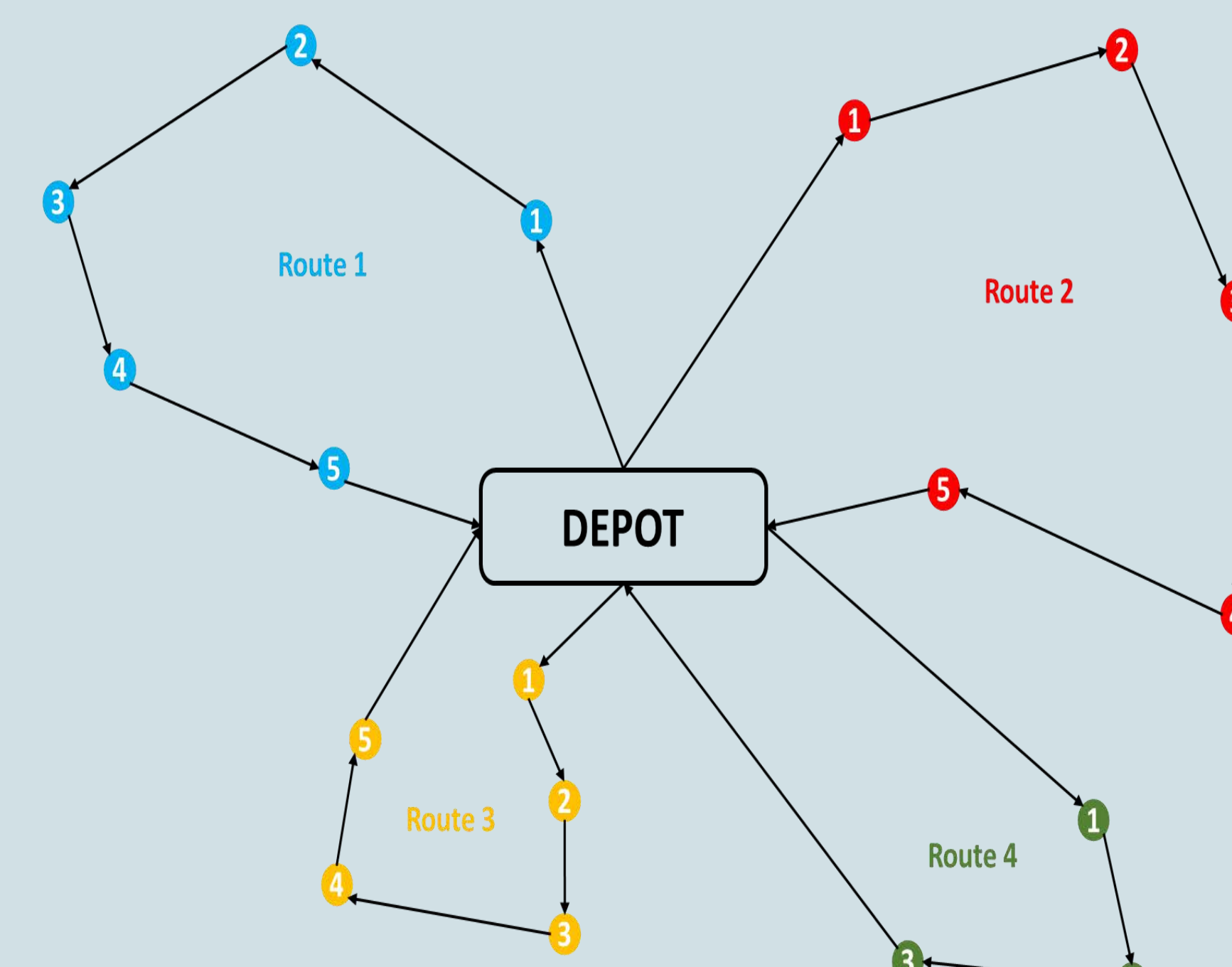


Figure 4: A Path Solution for the Vehicle Routing Problem (VRP)

## Current Study

The development of an effective target assignment framework requires a combination of features from several path planning algorithms. For this study, multiple core assumptions must be made about the engagement scenario.

### Engagement Scenario Assumptions

1. Multiple constant linearly moving hostile agents
2. Multiple dynamic friendly agents
3. Non-Holonomic friendly agents
4. Hostile agents pursuing a single location
5. Constant friendly and hostile agent velocities

Termed “Coordinated Dynamic Traveling Salesman Problem with Neighborhoods” (CDTSPN), CDTSPN handles mission requirements for the assumed engagement scenario by combining features of other algorithms.

### Key Features:

1. Classical TSP combinatorial optimization
2. Neighborhoods (constant radius)
3. Multi-Agent Path Planning (see VRP)
4. Dubin’s Path lengths for cost function calculation

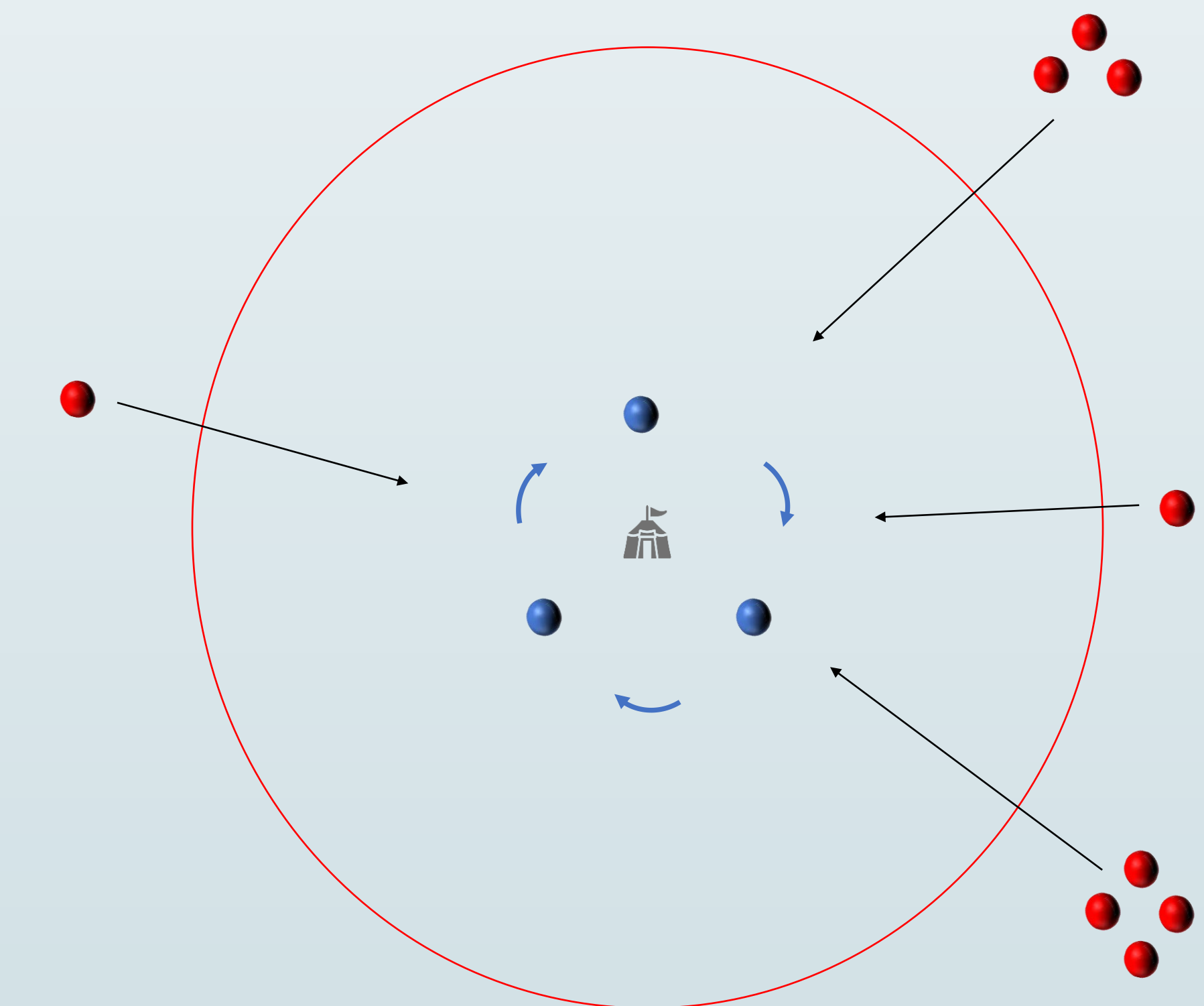


Figure 5: Example Engagement Scenario

## Methodology

By assuming constant velocities for both friendly and hostile agents, positions for each hostile agent are calculated for each combination of potential assignments / path solution. Once a path solution and its associated agent positions are calculated, a cost function is used to determine the cost between each assignment. The cost function can be developed from various parameters such as, Dubin’s Path length, Euclidean distance, time, energy, payload, etc. Furthermore, weights can be added to parameters to customize the cost function to meet desired target assignment performance. Path optimization is then performed by minimizing the total path cost using TSPN with multiple friendly agents.

## Future Work

- Reduction of engagement scenario assumptions (e.g., constant agent velocities, dynamic constraints, etc.)
- Integrating ground-based and aerial-based defense systems into a single target assignment problem
- Dynamic Path Updating

## References

[1] File:Dubins1.svg (2020, October 4). Wikimedia Commons, the free media repository

# Evaluation of Localization Uncertainty and Its Effect on Vehicle Intercept

Paul Klappa and Travis Fields

University of Missouri – Kansas City and Missouri Institute for Defense & Energy

## Motivation

Ground-based defense systems rely on range dependence which constrain engagement scenarios. Furthermore, ground-based defense systems rely on target tracking uncertainty. In order to mitigate the range dependence, an aerial-based defense system was considered. Although the range constraint is mitigated with an air-based system, tracking uncertainty is still an issue and was the subject of this research effort. Thus, a simulation was designed using MATLAB® to assess the endgame portion of a pursuer-evader scenario.

### Endgame Evaluated:

- Non-Kalman Filter estimation vs Kalman Filter estimation
- Five pursuer positions
- Four tracking sensor uncertainties
- Pursuer-evader miss distance

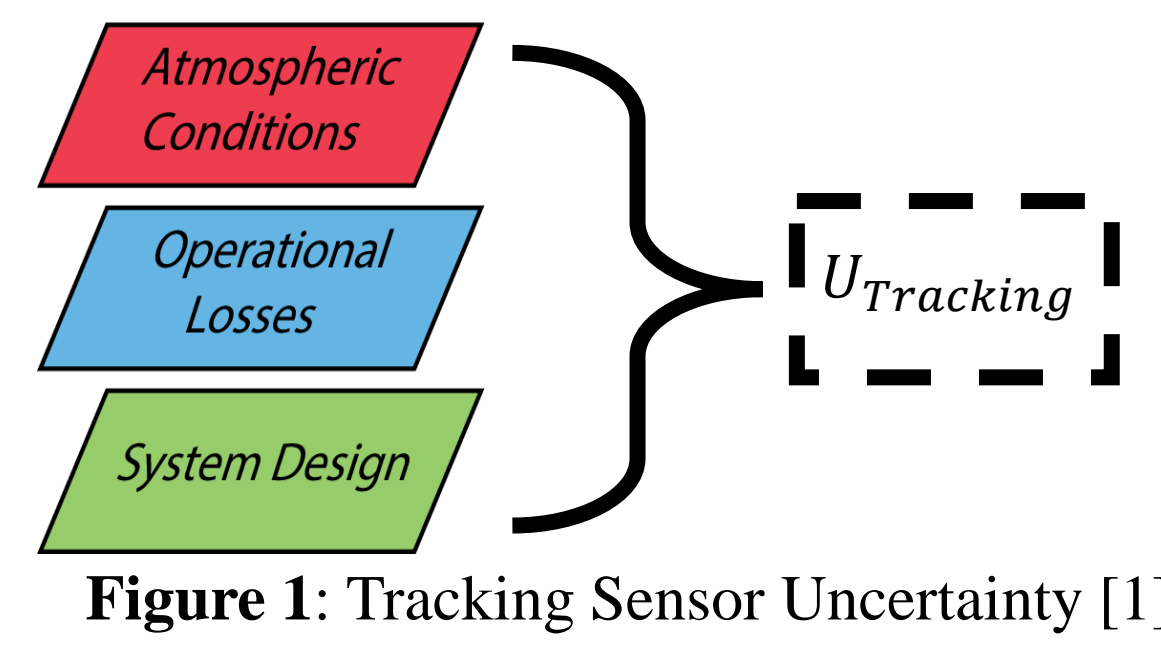


Figure 1: Tracking Sensor Uncertainty [1]

## Background

### Pursuer Endgame

Defined as the last 20 seconds of the pursuer and evader engagement before intercept occurs. However, the 20 seconds assumes there is no noise associated with the evader's position; thus, engagements may last longer.

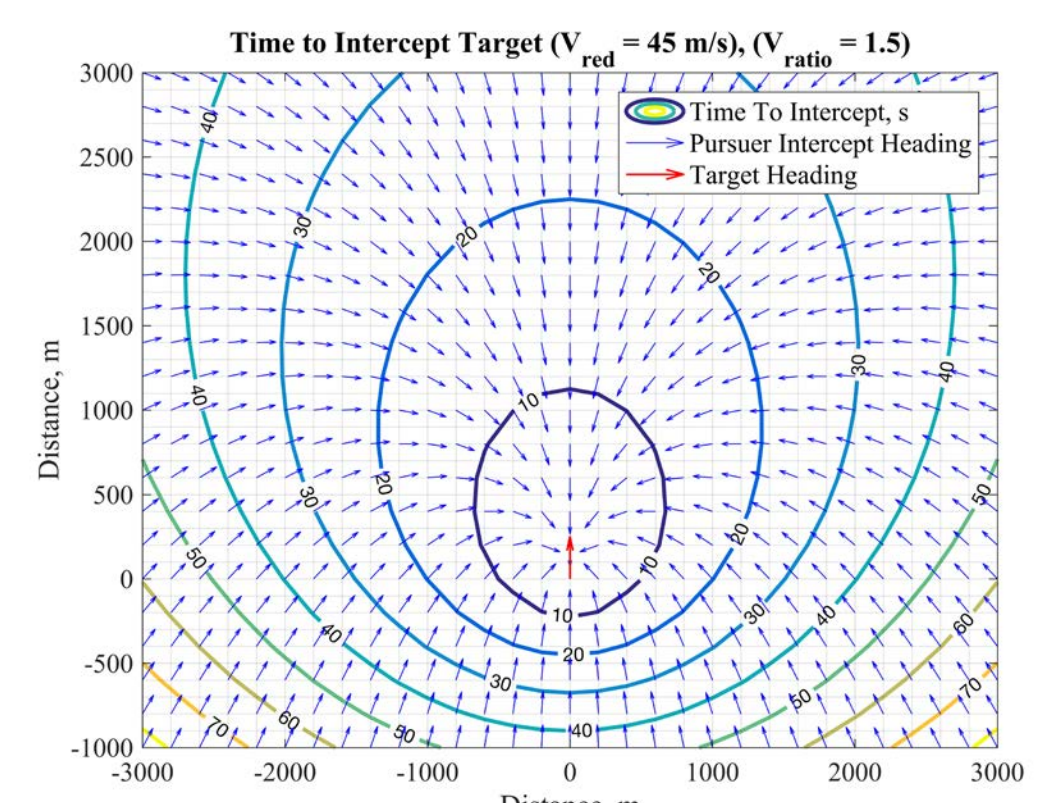


Figure 2: Time and Heading to Intercept

### Proportional Navigation (PN)

Navigation logic that was used for the pursuer. Relies on the derivative of the line of sight ( $\frac{d\theta}{dt}$ ) angle between the pursuer and evader along with a PN gain ( $N=3$  was used) [2]. The commanded turn rate ( $\frac{d\gamma}{dt}$ ) is used to modify the heading of the pursuer.

$$\frac{d\gamma}{dt} = N \frac{d\theta}{dt} \quad \text{Eq. (1)}$$

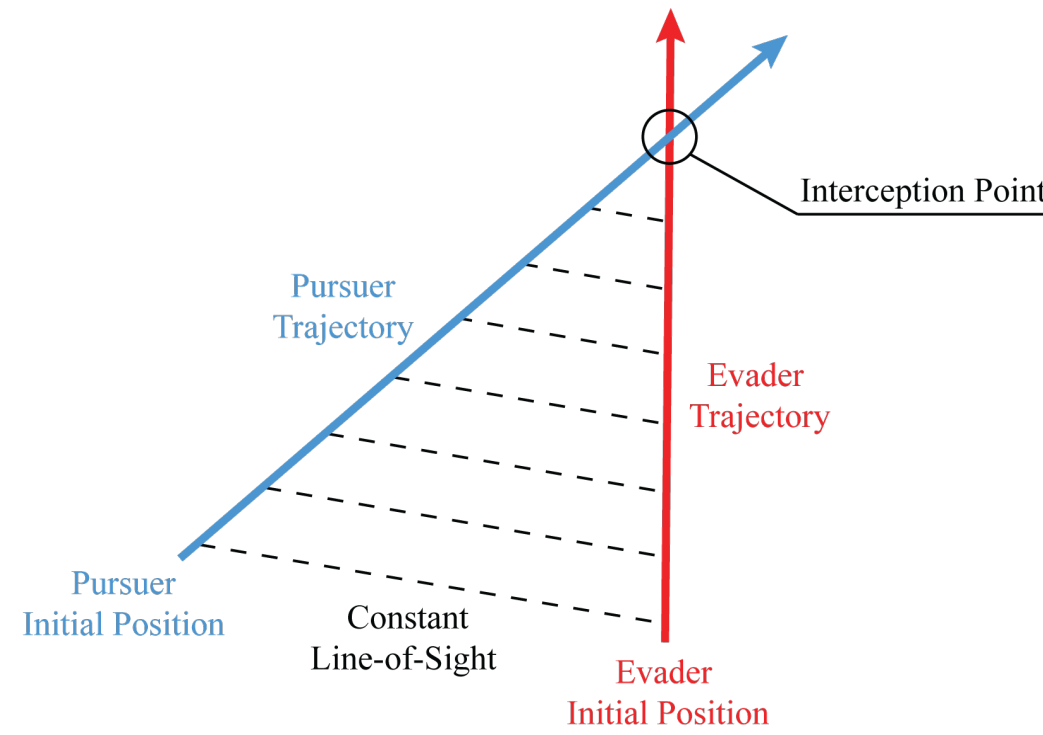


Figure 3: Straight path pursuit using PN

### Kalman Filtering (KF)

A Kalman Filter was used to provide position estimates of the evader. The KF uses a cyclic structure to propagate and correct the evader's state estimates. The propagation phase uses a process dynamics model, defined by kinematics, and the correction phase uses tracking sensor measurements [3].

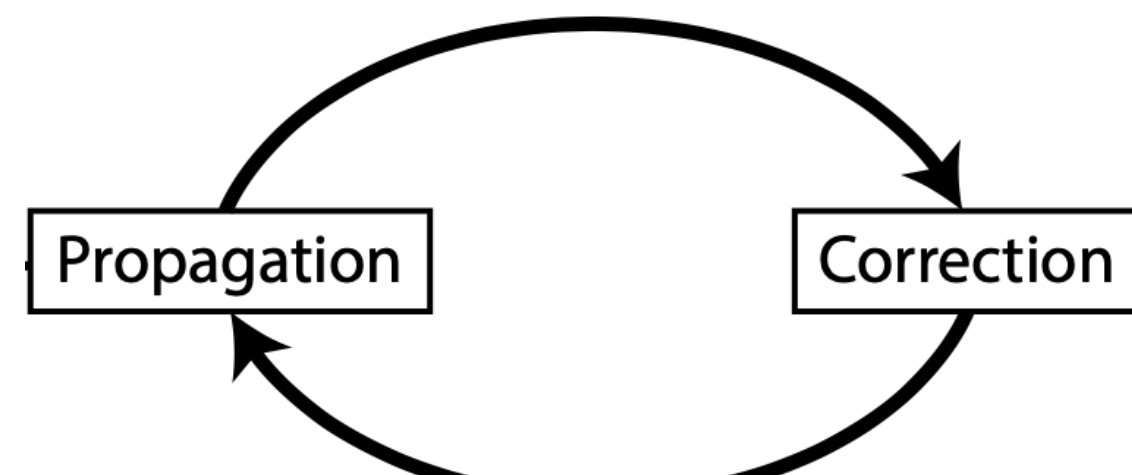


Figure 4: Kalman Filter Phases [4]

## Simulation Methodology

A MATLAB® simulation was designed for the pursuer-evader endgame. Five initial starting position for the pursuer were considered and four different tracking uncertainty values were used. The evader's position was estimated using two methods: raw tracking sensor measurements and a KF estimation approach. Each initial position was replicated 100 times per uncertainty level.

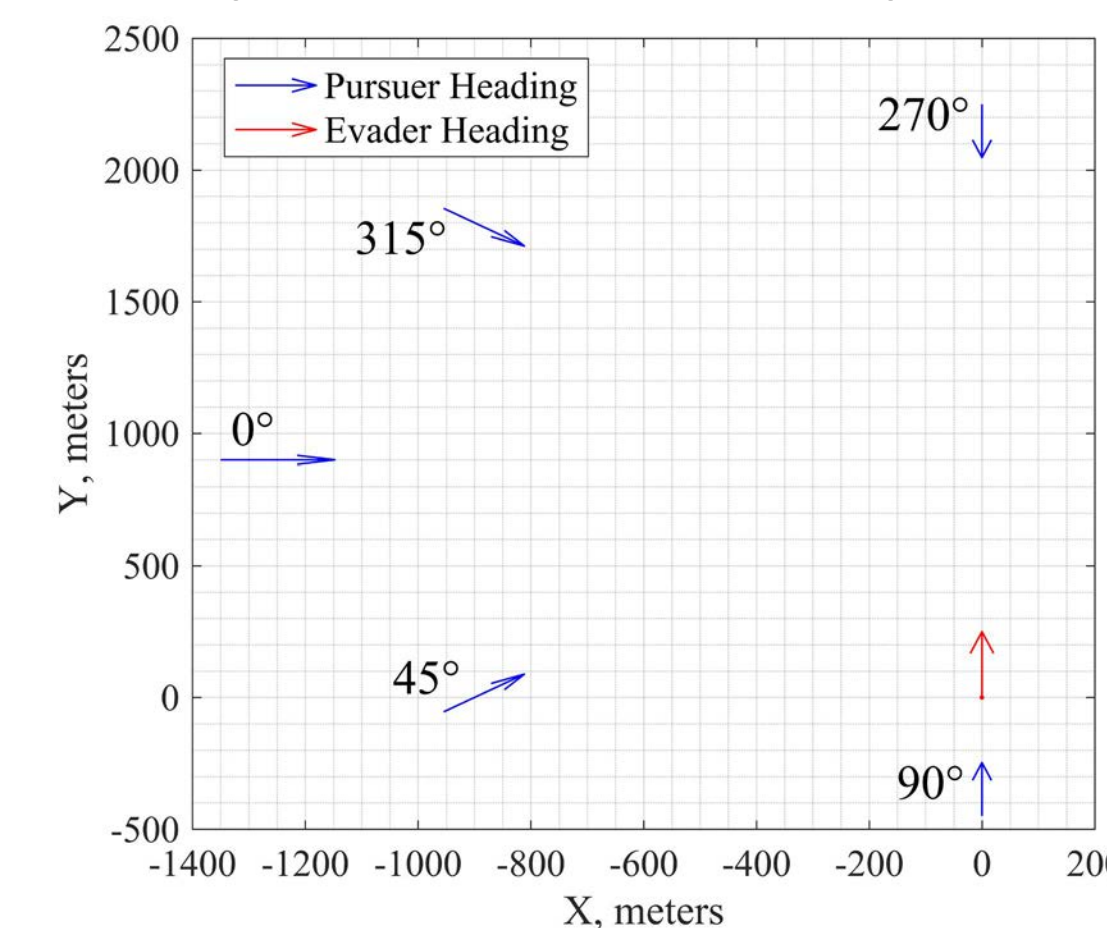


Figure 5: Simulation starting positions and headings

Table 1: Simulation Parameters

Simulation Parameter	Value	Units
Simulation Frequency	450	Hz
Tracking Update Frequency	10	Hz
Evader Speed	45	m/s
Evader Size	0.1	m
Pursuer G-Limit	5	g
Pursuer-Evader Speed Ratio	1.5	NA
Proportional Navigation Gain	3	NA

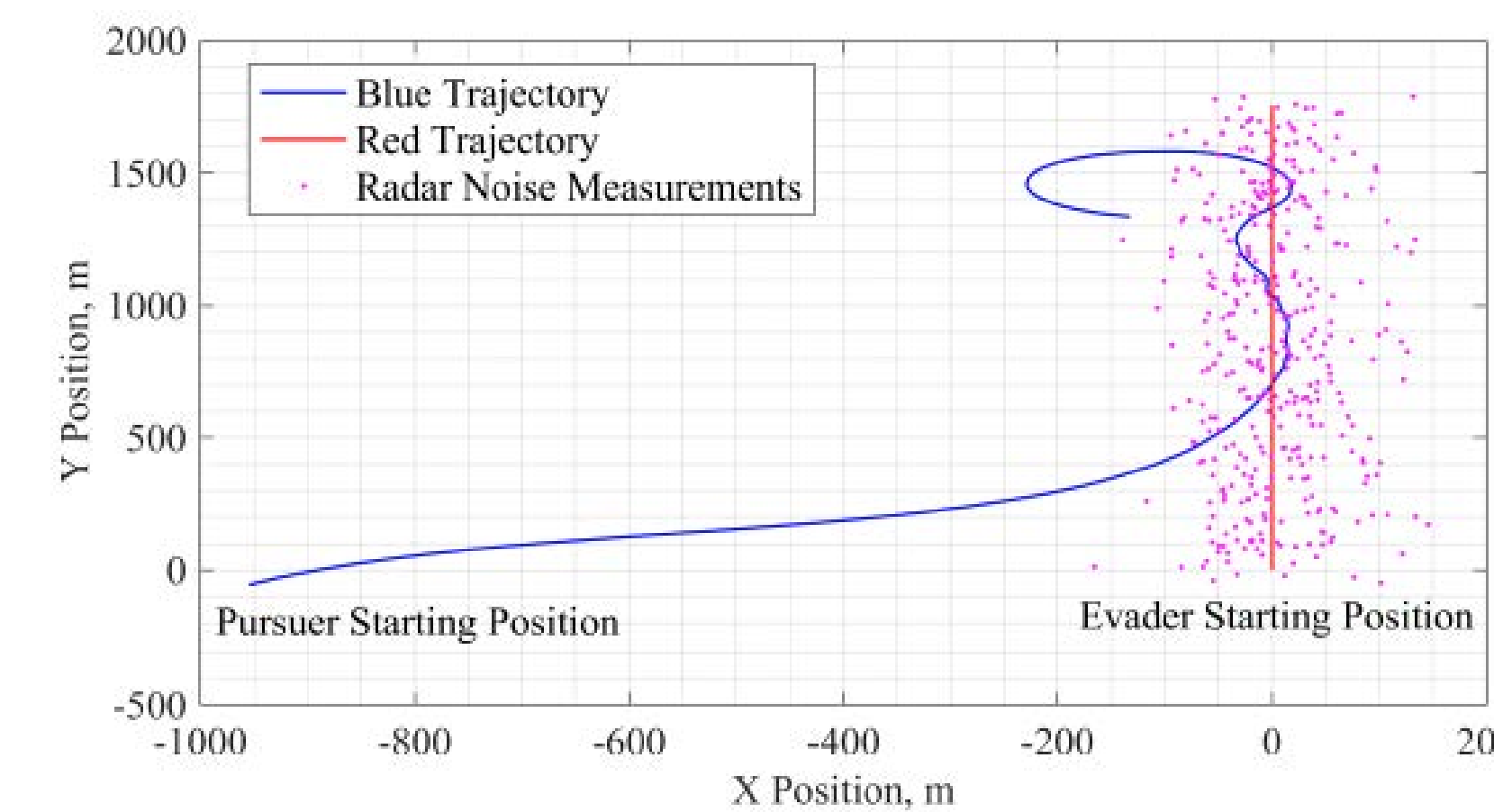


Figure 6: Representative pursuer-evader engagement.

## Results & Analysis

Miss distance was defined as minimum Euclidean distance between the pursuer and true evader position. Miss distance results were compared between the non-KF approach and the KF estimation approach. In most engagements, the miss distance was minimized by using a KF. Furthermore, the KF estimation expanded the modeling capabilities of the evader.

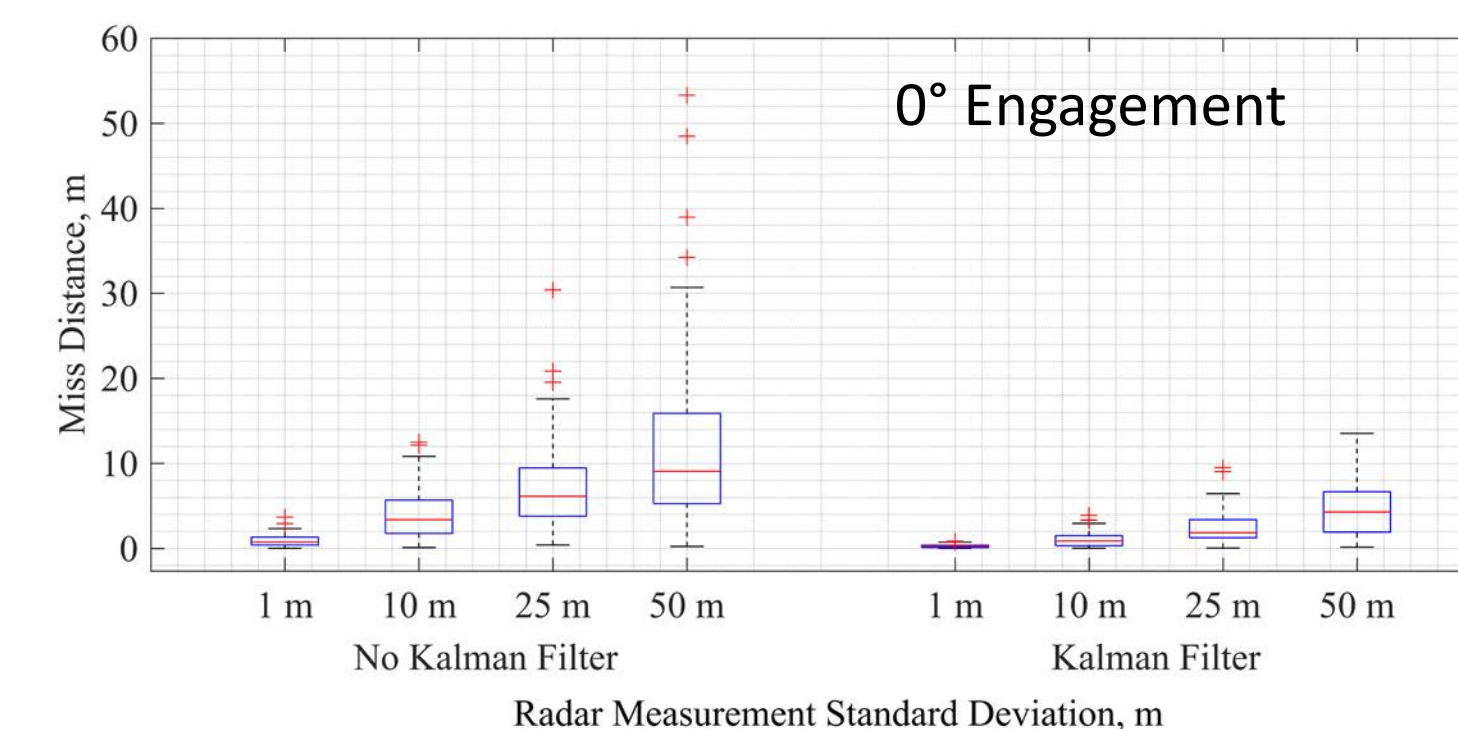


Figure 7: Miss distance vs estimation method (0° engagement).

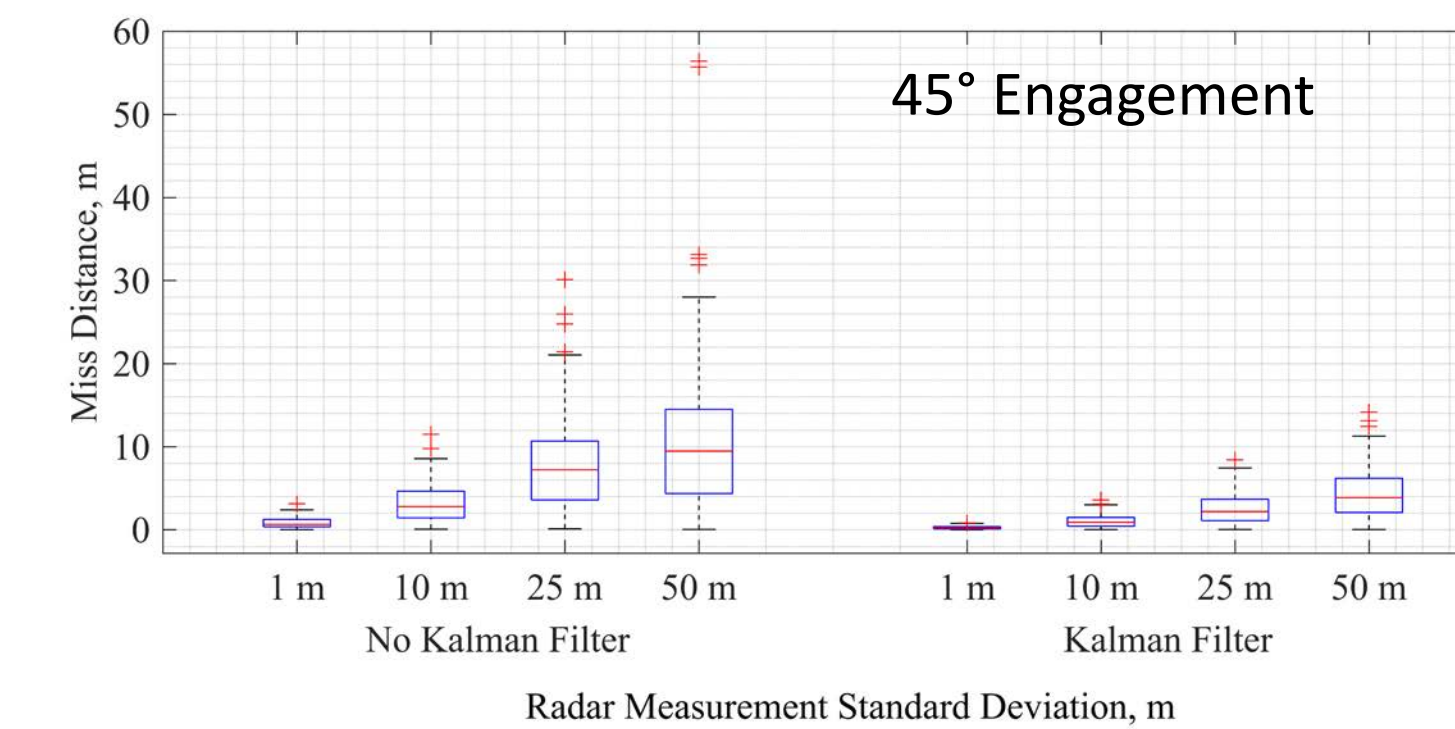


Figure 8: Miss distance vs estimation method (45° engagement).

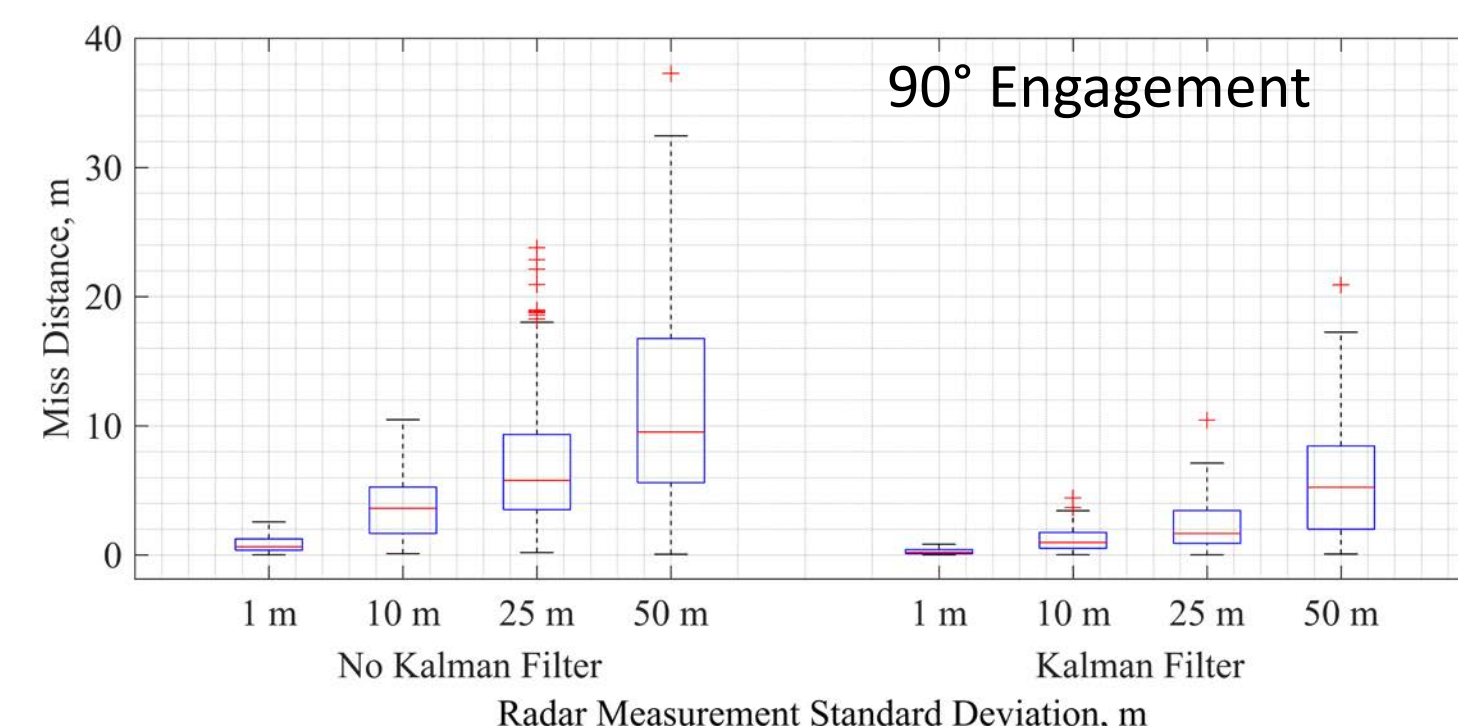


Figure 9: Miss distance vs estimation method (90° engagement).

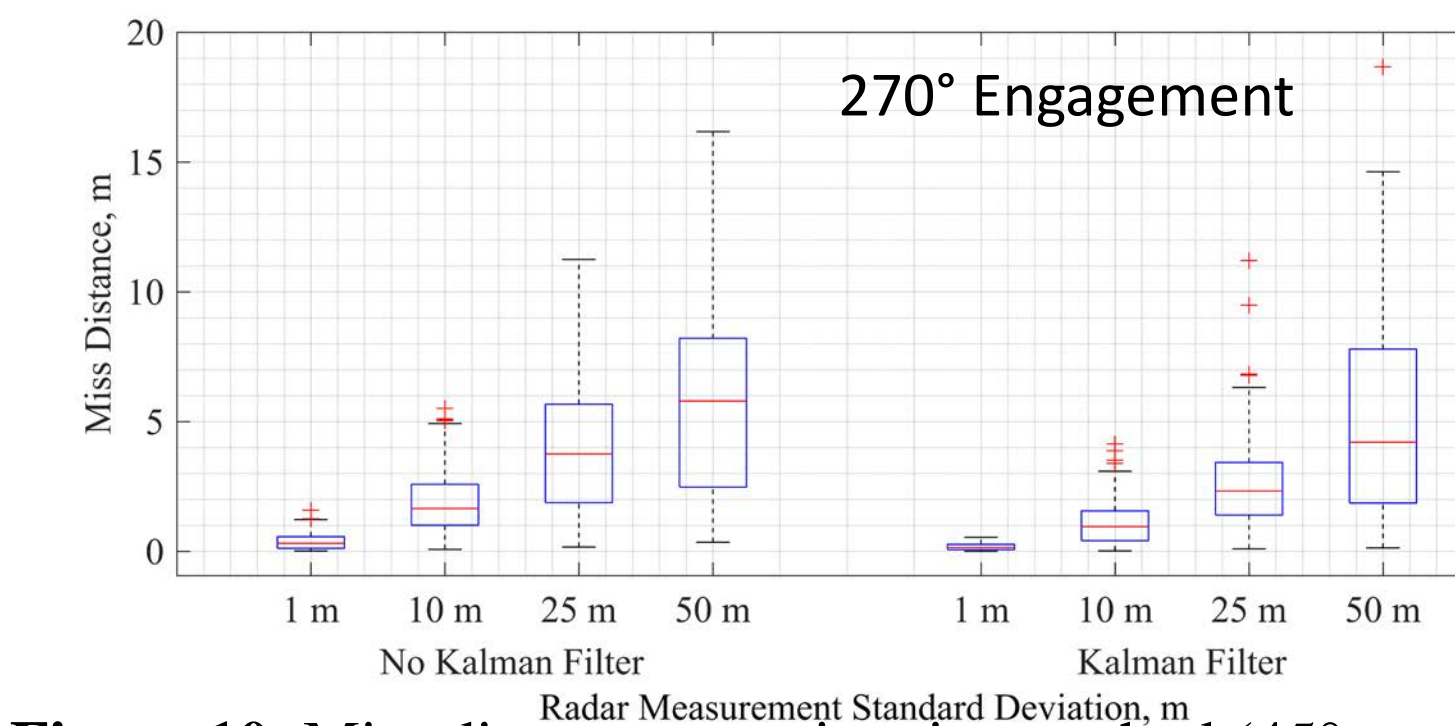


Figure 10: Miss distance vs estimation method (270° engagement).

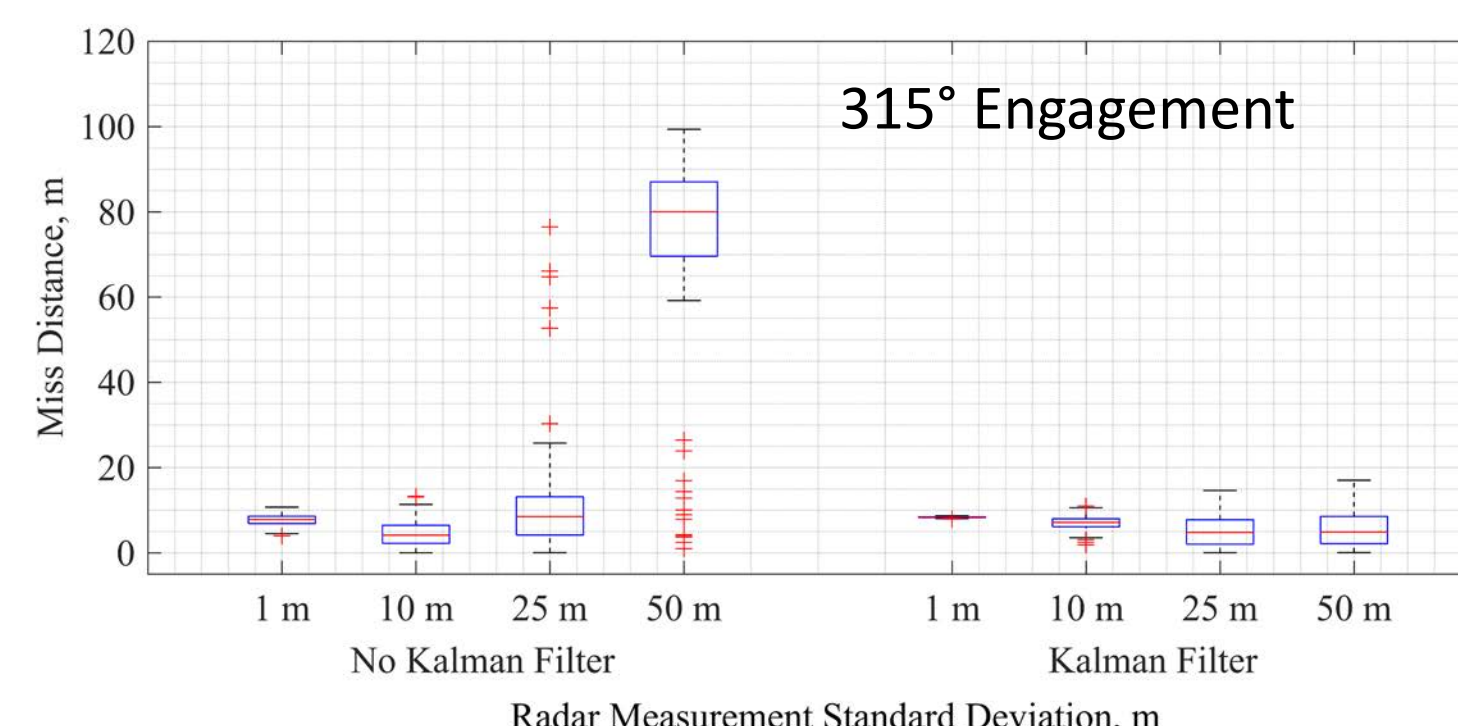


Figure 11: Miss distance vs estimation method (315° engagement).

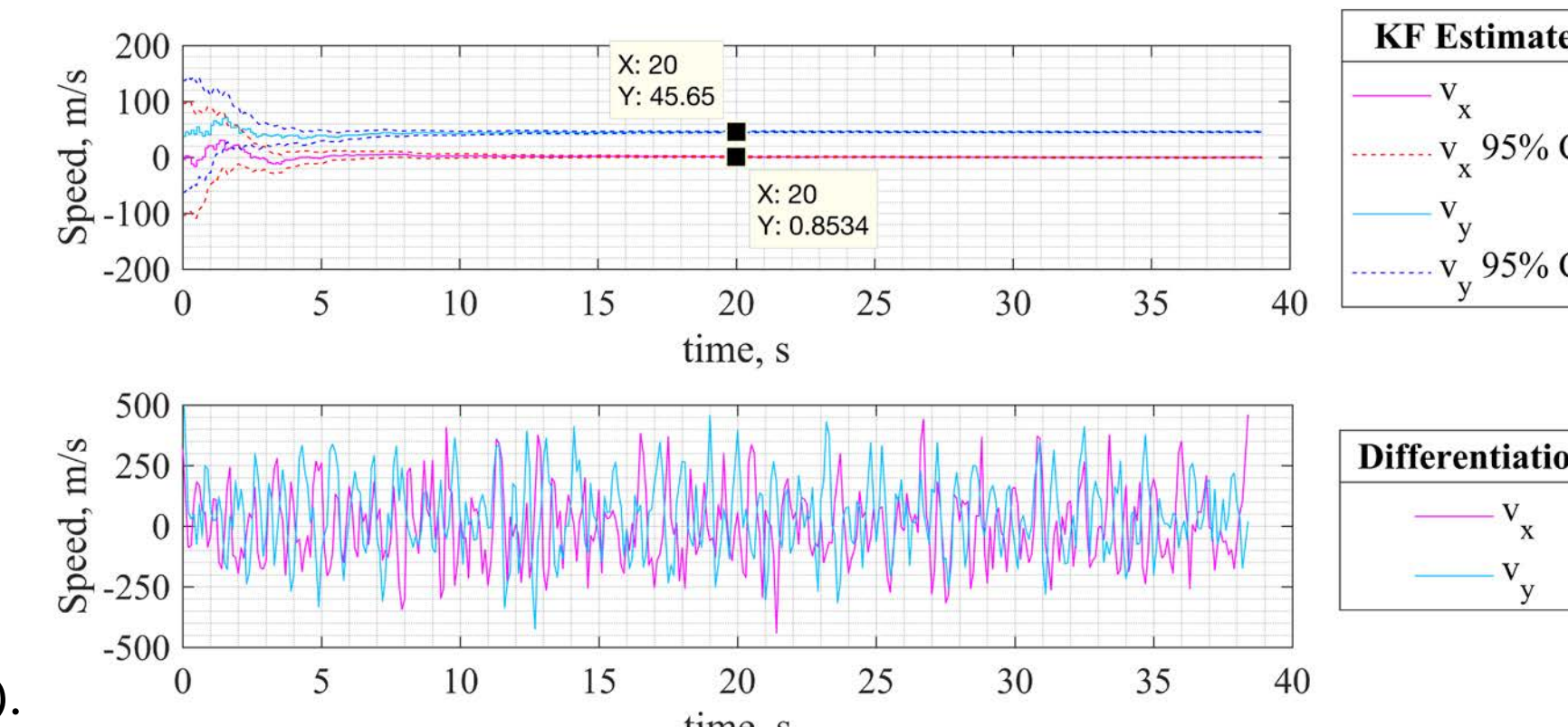


Figure 12: Kalman Filter Additional Estimation

## Summary & Conclusion

Table 1: Miss distance and time of intercept summary table.

State Estimator	Initial Heading	Mean Miss Distance, m				Mean Intercept Time, s			
		1 m	10 m	25 m	50 m	1 m	10 m	25 m	50 m
Non-Kalman Filter	0°	0.92	3.99	7.18	11.79	26.78	27.81	28.06	28.20
	45°	0.87	3.36	7.86	11.47	25.92	26.47	26.51	26.64
	90°	0.82	3.78	7.43	11.82	20.00	20.01	20.00	20.05
	270°	0.39	1.86	4.01	5.78	20.00	20.00	20.00	20.00
Kalman Filter	315°	7.67	4.64	11.63	71.27	23.37	23.98	24.37	21.65
	0°	0.26	1.06	2.35	4.65	26.76	26.77	26.89	27.15
	45°	0.25	1.06	2.61	4.43	25.90	25.91	25.98	26.12
	90°	0.26	1.19	2.25	5.91	20.00	20.00	20.01	20.02
	270°	0.17	1.09	2.74	4.98	20.00	20.00	20.00	20.00
	315°	8.32	6.95	4.86	5.67	23.26	23.28	23.38	23.42

The KF estimation method improved the miss distance in most engagements. Tracking uncertainty for the evader's states improved throughout the duration of the engagement when using a KF. Modeling capabilities of the evader were expanded by implementing the KF.

When considering scenarios that use ground-based defense and aerial-based defense systems, a state estimation algorithms in conjunction with a tracking sensor can improve the state estimation of a target.

## Future Work

- Conduct tracking system flight tests to aid in tracking-based modeling.
- Assess Kalman Filter performance on a maneuvering evader.
- Implement nonlinear estimation algorithms that account for nonlinear error (Extended Kalman Filter).

## References

- [1] Rahman, H. *Fundamental Principles of Radar*, 1<sup>st</sup> ed., CRC Press, 2019, Chap. 4, pp. 70-72.
- [2] Nahin, P. *Chases and Escapes: The Mathematics of Pursuit and Evasion, Paradoxes, perplexities, and mathematical conundrums for the serious head scratcher*, Princeton University Press, 2012.
- [3] Brown, R. G., and Hwang, P. Y., *Introduction to Random Signals and Applied Kalman Filtering: with MATLAB Exercises and Solutions*, 4th ed., Wiley, 2012, Vol. 1, Chaps. 4,7, pp. 143-147, 257-260.
- [4] Klappa, P. J., and Fields, T., "Assessment of Fixed-Wing UAV System Identification Models During Actuator and Payload Drop Failures," *AIAA SciTech 2021 Forum*, 2021. doi:10.2514/6.2021-1529.

## Acknowledgements

The authors wish to thank the Office of Naval Research for their support of this work under Grant No. N00014-17-1-3016